Faculty of Materials, Metallurgy and Recycling
Technical University of Košice

METALLURGY JUNIOR 2018

Proceedings

The conference is held under the aegis
of assoc. prof. Iveta Vasková, PhD., dean of FMMR TUKE

Faculty of Materials, Metallurgy and Recycling Technical University of Košice

METALLURGY JUNIOR 2018

Proceedings

10. - 11. May 2018
Herľany, Slovak Republic

Contributions did not pass through language correction of editors.
The contributions were reviewed.

Title**:**	**Metallurgy Junior 2018 , Proceedings**
Editors:	**Pikna Ľubomír, Heželová Mária**
Publisher:	**Technical University of Košice**
Year:	**2018**
Issue:	**first**
Number of copies:	**50**
Number of pages:	**142**
ISBN:	**978-80-553-2971-0**

CONTENT

The evaluating methods of corrosion resistance of automotive sheets with zinc-based coatings

Gabriela Baranová, Mária Hagarová

Institute of Materials and Quality Engineering, Faculty of Material, Metallurgy and Recycling, Technical University of Kosice, Park Komenského 11, 042 00 Košice

Abstract

The article deals with evaluating methods of increased corrosion resistance of steel sheets by metal coat application on their surface. Nowadays, the most used coats are those based on zinc, for the reason there is an optimal ratio between its qualities and its price. The qualities of the coat can be improved by modifications of its chemical composition therefore new researches can be carried out in this field of study.

Introduction

Steel sheets have an important function in automobile industry; therefore demands for their qualities are very high. These sheets are expected to be well compressible, weldable, varnishable [1] and last but not least their corrosion resistance is very important. A vehicle life-time is to a considerable extent limited by durability of a bodyshell; that is often limited by its corrosion resistance. The extent of a corrosion attack depends on material composition, quality of material surface, characteristics of an external environment, but also other influences such as aggressive contaminats in the atmosphere, contact of dissimilar noble metals, solid particles residuals, dust, etc.[2] New kinds of coating sheets have been developed to restrict formation of diverse corrosion damages of steel mouldings (as a part of body shell) but mainly to increase their life-time.

Zinc-basedCoatings

Currently, galvanized steel sheets have the largest participation in the field of coated sheets, due their rentability regarded quality-cost ratio[1]. Galvanized coatings offer anticorrosive protection to steel substrate in two ways: barrier effect (prevents intrusion of oxygen and atmosphere humidity) and cathodic protection in the defect. Protective features of a coating depend, to a large extent, on its thickness, compactibility and adhesion to substrate.

A zinc coating can be deposited by hot-dip galvanization (HDG) or electro galvanizing (EG). A commonly used coat based on the zinc basis is so-called „galvannealed (GA), which is not built up only by zinc, but it contains also compounds of Fe-Zn. It's an annealed zinc coating. The differences in these coatings are presented in Tab. 1.

Table 1 *Advantages and disadvantages of certain kinds of galvanized coatings [3-4]*

Type of coating	**Thickness (µm)**	**Advantages**	**Disadvantages**
„galvanneal“	6	formability, weldability, price	flaking by plastic deformation
hot-dip galvanize	7-20	ductility, price	abrasion of electrodes in resistance spot welding
electrolytic galvanized	7.5	ductility, formability	high price (+10% compared to hot dip galvanized)

Defining the nature of products formed during corrosion process with different kinds of coatings and different exposition conditions can be the key to make protective layers with higher quality. Improving anticorrosive properties of zinc layer can be arrived by adjusting chemical composition. The coatings based on the Zn-Al-Mg alloys seem to be very perspective,

investigated in various publications [5-7] which demonstrate their higher corrosion resistance. Mg and Al create a passive layer on a coating surface and therefore they decrease electrochemical activity of zinc, perhaps even its corrosion products, by which a natural protection of coated material is facilitated. [8-10]. The influence of magnesium on the corrosion resistance of a galvanized coating is presented in Figures 1 and 2. With the higher concentration of Mg and Al increase the life-time of a coating in corrosive environment of salt spray was observed.

The corrosion resistance rises with higher weight of coatings [10]. The authors used cyclic corrosion tests in a salt spray test chamber for the testing of durability of these coated sheets.

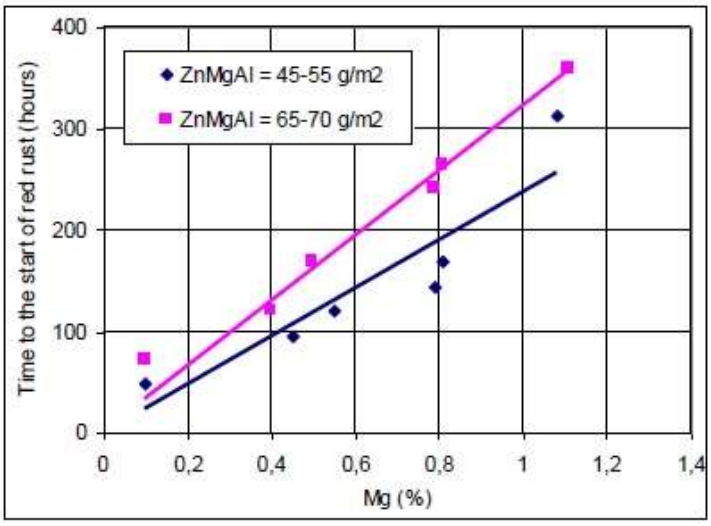

Figure 1 The influence of Mg content (%) on the start of corrosion process of coatings [10]

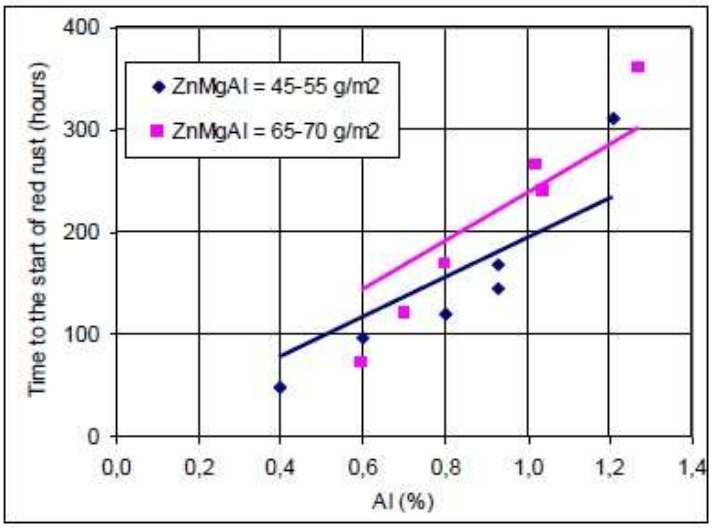

Figure 2 The influence of Al content (%) on the start of corrosion process of coatings [10]

In comparison with pure zinc coatings the Zn-Al-Mg coatings have better mechanical properties, better weldability, compressibility, and ultimately they reduce zinc consumption. [9].

The determination methods of corrosion resistance

For determining the corrosion characteristics of coated steel the laboratory corrosion tests were used, which complement each other and therefore more complex corrosive characteristics of the samples can be reached[4]:

- Measuring the open corrosion potential OCP of the samples during the period of exposition in corrosive environment;
- determining the corrosion rate of exposed samples according to Tafel and Stern. The kinetics of overall reaction depends on the kinetics of anodic and cathodic reactions, and it's determined on the basis of potentiodynamic polarization curves
- determining the corrosion potential and current density of bimetallic cell by Evans polarization diagrams. The change of the corrosion rate in a bimetallic joint can be predicted by variation of ratio anode to cathode surface.

The author [4,11] studied possibilities of usage the bimetallic couples of metal materials under real conditions. The resistance against the degradation by differently electrochemical noble material couples is determined by "anodic index", which represents a potential difference ΔE of single materials, from which the bimetallic couple is built. The particular outcomes are demonstrated in Tab. 2. On this basis the bimetallic joint, which was a galvanized coating - IF (Interstitial Free) steel, was suitable even for more aggressive environment.

Table 2 *The criteria of suitability of bimetallic joint placement in environment on the basis of „anodic index."[11]*

Anodic index	**Environment**
$\Delta E < 500$ mV	non-aggressive environment
$\Delta E < 250$ mV	more aggressive environment
$\Delta E < 150$ mV	aggressive environment

The author [4] dealt with the determining of corrosion characteristics, e.g. bimetallic couple – zinc coating and IF steel or another couples of metals exposed in different model environments, which represented operating conditions: 3% NaCl, SARS as simulated acid rain solution. From the results of open corrosion potential (OCP) measurement in the work listed above was clear that zinc coating on the steel had highly corrosion resistance and therefore it seemed as more likely to be used in more aggressive corrosion environments (Fig. 3).

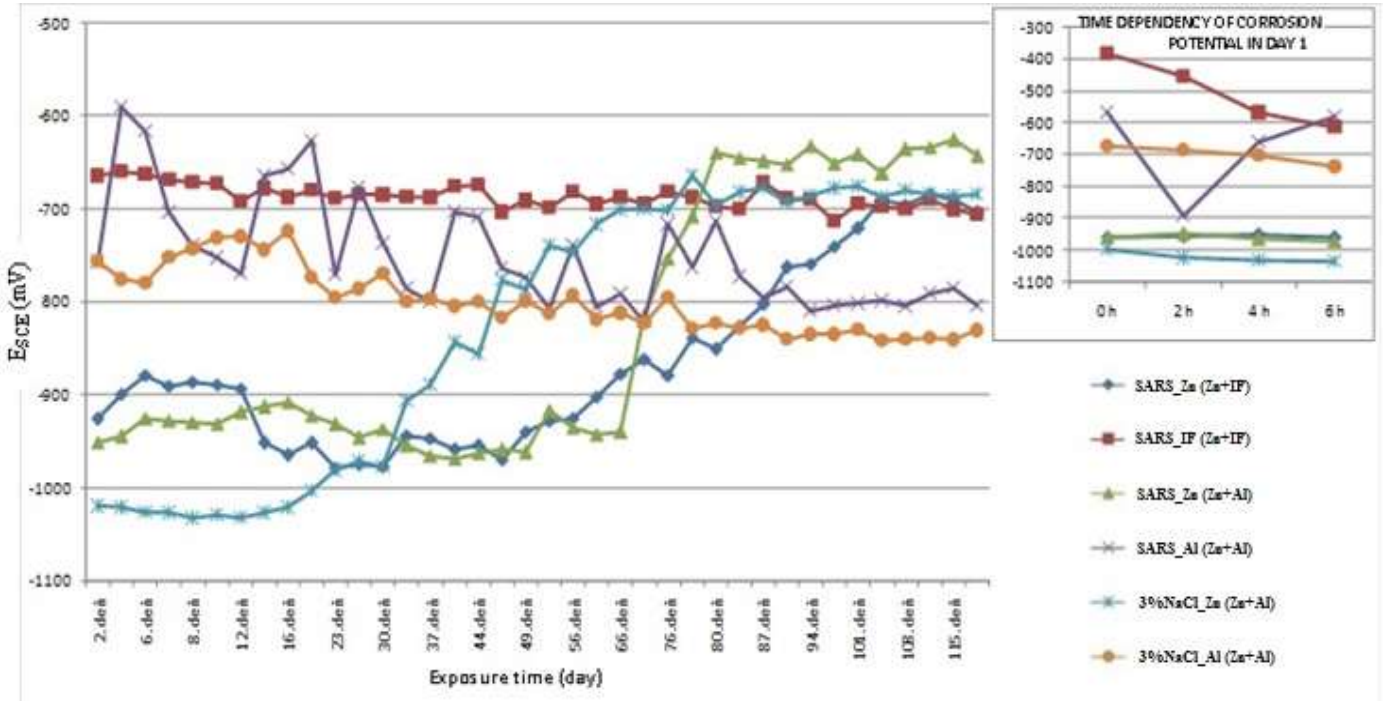

Figure 3 The results of measuring E_{SCE} for couples: Zn+IFsteel(SARS); Zn + Al (SARS); Zn + Al (3%NaCl) [4]

The „anodic index“ was estimated by measured OCP values of tested bimetallic couples during exposition time under simulated corrosive environments. The specific outcomes of measurements are presented in Tab. 3 together with suitability of usage of these couples in differently aggressive environments.

Table 3 *"Anodic index" for the tested material couples [4]*

"Anodic index" according to references	**Environment**	**"Anodic index" according to measuring E_{SCE}**	**Tested couples**
Δ E < 250 mV	more aggressive environment	ΔE = 161 mV	Zn + Al (solution SARS)
Δ E < 150 mV	aggressive environment	ΔE = 147 mV	Zn + Al (3% NaCl)
		ΔE = 2 mV	Zn + IF (solution SARS)

Sykes and Xu [12] dedicated their work to studying of electrochemical reactions of bimetallic couple Fe-Zn (galvanized steel), which is coated by paint with high ionic resistance and exposed to NaCl solution for 12 days. Their aim was to create well defined galvanic cell between iron and zinc (simulation of real damage of zinc coating on the steel). They used a combination of various methods of corrosion resistance (EIS, OCP, potentiostatic measuring). In separate measurements changes in the coating above anode and cathode were assessed by EIS, and the anodic polarization of the zinc and cathodic polarization of the steel were measured potentiostatically. Evans diagrams were carried out from real data after corrections, from these combinations of measurements. (Figures 4-5).

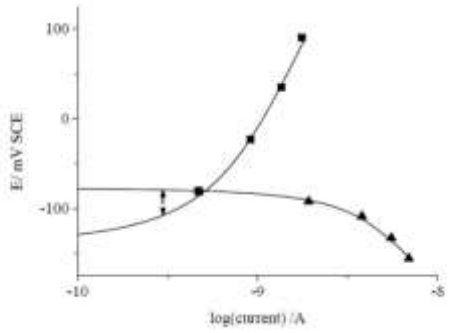

Figure 4 Evans diagram for zinc and steel (day 4), with potential drop (dash line). Cathodic curve (steel): ▲; anodic curve (Zn): ■.[12]

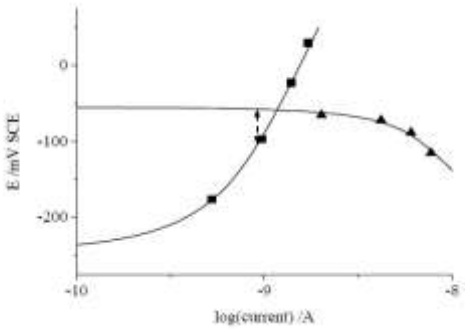

Figure 5 Evans diagram for zinc and steel (day 12), with potential drop (dash line). Cathodic curve (steel): ▲; anodic curve (Zn): ■.[12]

In the both graphs there is a little polarization of the steel cathode. After four days of sample exposition, OCP of zinc is high so the zinc polarization is yet low. However, after 12 days exposition, the zinc polarization is clearer than after 4days exposition and OCP is moving downwards, what authors ascribe to the coating's ability to exclude chlorine. Chlorine would, otherwise, initiate active zinc dissolution.

Conclusion

Surface treatment of metallic materials is being applied in order to improve their qualities. Increased corrosion resistance is showed up on increased reliability and life-time of overall coated system. The methods of evaluation of corrosive resistance coated materials conduce to define their suitability for usage under both simulated and real operating conditions.

References

[1] Výboch J. et al.: Štatistická analýza kvality Fe-Znpovlakovaných plechov pre automobilový priemysel. In Strojírenská technologie Plzeň 2011: sborník abstraktů: IV. ročník mezinárodníkonference konané vednech 25.- 26.1.2011 v Plzni. Vyd. 1. ISBN 978-80-7043-934-0

[2] Kačmárová, A., Kačmár, M.: Trendy vo vývoji protikoróznej ochrany dutín karosérií automobilov. In: Tribotechnika,TechPark, o.z., 2012,Vol. 4, ISSN: 1338-0524

[3] Davies, G.: Materials for automobile bodies. Butterworth-Heinemann, 2012, 1st ed., ISBN 978-0-08-096979-4

[4] Šimko R., Možnosti riešenia korózie v automobiloch. Diplomová práca, 2016, Technická univerzita v Košiciach, Hutnícka fakulta

[5] Volopich P. et al.: Understanding corrosion via corrosion product characterization: II. Role of alloying elements in improving the corrosion resistance of Zn–Al–Mg coatingson steel. In: Corrosion Science. 2011,Vol.53, p. 2437–2445

[6] Yao C. et al.: Effectof Mg content on microstructure and corrosionbehaviorof hot dipped Zn-Al-Mgcoatings. In: Journal of Alloys and Compounds, 2016, Vol. 670, p. 239-248

[7] Prosek T. et al.: Improving corrosion stability of Zn—Al—Mg by alloying for protection of carbodies. In: Surf. Coat. Technol., 2016, Vol. 306, p. 439–447

[8] Schuerz S. et al.: Corrosion behaviour of Zn–Al–Mg coated steel sheet in sodium chloride-containing environment. In: Corrosion Science, 2009, Vol. 51, p. 2355–2363

[9] Evin E. et al.: Analýza odolnosti pozinkovaných plechov proti korózii po plastickej deformácii. In: Koroze a ochrana materiálu, 2016,Vol. 60, No. 4, p. 114-121

[10] Graban J. et al.: Influence of coating´s chemical composition on corrosion resistance of galvanized steel. Metal 2013,15. - 17. 5. 2013, Brno, Czech Republic, EU

[11] Halama M.: Bimetalická korózia konštrukčných kovových materiálov pri atmosférických podmienkach, Dizertačná práca, 2006, Technická univerzita v Košiciach, Hutnícka fakulta

[12] Sykesj. M., Xuy.: Investigation of Electrochemical Reactions beneath Paint using a Combination of Methods. In ECS Transactions, 2010, Vol. 24, No.1, p.137-146

Autotrophic growth and CO_2 fixation of iron oxidizing bacteria

Zuzana Bártová, Daniel Kupka

Institute of Geotechnics, Slovak Academy of Sciences, Watsonova 45, 040 01 Košice, Slovak Republic, bartova@saske.sk, dankup@saske.sk

Introduction

Iron oxidizing bacteria were among the first groups of microbes to be recognized for carrying out a fundamental geological process. Because of difficulties in culturing important community members and many questions about their metabolism, studies of Fe-oxidizing bacteria have lagged behind the other important lithotrophic bacteria. Nowadays, research on lithotrophic, oxygen-dependent iron oxidizing bacteria that grow at low pH (less than 3) is accelerating [1].

There has been a great increase in our knowledge and understanding of microbiology diversity of biomining environments and mutual microbial interactions. The results from laboratory experiments (stirred tank and heap bioreactor systems simulations) have shown that microbial communities are more wholesome than pure cultures of mineral oxidizing acidophiles. They also tend to be more effective at bioleaching and bio oxidizing ores and these might be adapted to meet future challenges in biomining operations [2].

Iron-oxidizing bacteria

The iron-oxidizing acidophilic bacteria may be chemoautotrophs that assimilate CO_2 by using the energy derived from the ferrous iron oxidation [3] or mixotrophs and heterotrophs that metabolize organic carbon. They are though to play an important role in generating leach liquors by converting hardly soluble metal sulfides via biochemical oxidation reactions into water soluble metal sulfates and maintaining robust bioleaching microbial communities [2, 4].

Ferrous iron is not the only energy source for acidophilic bacteria. Substrates like reduced inorganic Sulphur compounds (RISC), such as hydrogen sulfide, elemental sulfur, thiosulfate, or tetrathionate, and also some metal sulfides can be used as sources of energy [5]. Moreover, it has been shown that *A. ferrooxidans* can use hydrogen as sole source of energy with oxygen as terminal electron acceptor [6].

For our purpose we were dealing with acidophilic iron-oxidizing bacteria. Good example of such a bacterium is model organism *Acidithiobacillus ferrooxidans*. It is a chemolithoautrophic, γ-proteobacterium which thrives at low pH (1–2). It solubilizes copper and other metals from sulphide minerals and plays an important role in nutrient and metal biogeochemical cycling in acid environments [7]. As it is considered to be a model organism, the whole genome was sequenced and important genes needed for its chemolithoautorophic lifestyle were identified by Valdes et al.[7].

Those finding we can apply also on other acidophilic, iron-oxidizing bacteria such as *Acidithiobacillus ferrivorans* that we used in our experiments. In particular, we were using strain SS3 purified by colony isolation from a Norilsk mining region [8]. Using this culture, we were focusing on ferrous ion oxidation, O_2 consumption, CO_2 fixation and bacterial growth under CO_2 and O_2 limited conditions.

CO_2 fixation

Autotrophic fixation of carbon dioxide into cellular carbon occurs via several pathways but quantitatively, the Calvin cycle is the most important [9].

Primary reaction in Calvin cycle is the addition of CO_2 molecule to the molecule of ribulose bisphosphate. This reaction is catalyzed by the enzyme called (ribulose-1,5-bisphosphate-karboxylase/oxygenase) [10].

Naturally, there are 4 forms of the RuBisCO enzyme. Three of them (RuBisCO I, II, III) catalyzes the carboxylation and oxygenation of ribulose -1,5-bisphosphate and the forth one (RuBisCO IV) is so called RuBisCO like enzyme and it doesn't possess any catalytic activity [11].

Type I RuBisCO has been considered the most abundant enzyme on Earth, being present in plants and algae as a chloroplast protein. Type II RuBisCO is found primarily in the Proteobacteria [12] suggested that the type II is the ancestral form of RuBisCO because of its relatively poor affinity for carbon dioxide. Type II RuBisCO functions best under environmental conditions with high concentrations of carbon dioxide, and low oxygen levels, a situation reminiscent of early Earth's atmosphere [13].

The two types differ structurally, with type I RuBisCO containing eight large and eight small subunits; whereas type II RuBisCO has only large subunits which are also structurally different from the large subunits of type I RuBisCO [14].

It is proposed that all the genes of Calvin cycle are composed of five gene clusters that are predicted to encode all the enzymes involved in the Calvin cycle and also associated so called carboxysome formation [15].

Carboxysomes are intracellular compartments found in cyanobacteria and some chemoautotrophs. They encapsulate the enzymes carbonic anhydrase and ribulose-1,5-bisphosphate carboxylase/oxygenase (RuBisCO). Its function is to concentrate CO_2 around RuBisCO eliminating the competitive reaction with oxygen [16].

Bacterial cultivation in mineral, liquid medium with ferrous iron

We cultivate A. *ferrivorans* SS3 at low temperatures (5°C) and we focus on Fe^{2+} oxidation rate and also on the rate of CO_2 and O_2 consumption.

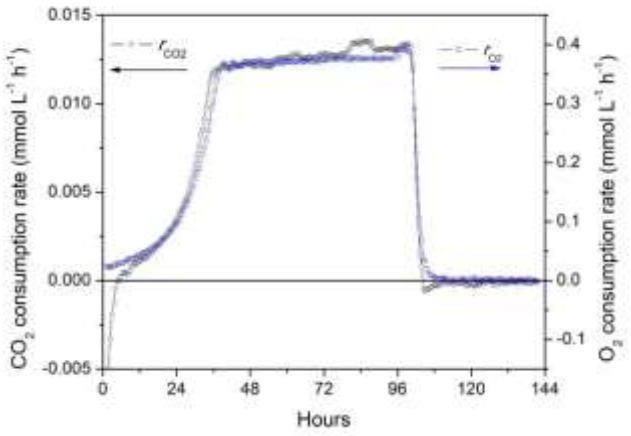

Figure 1 CO_2 and O_2 consumption rate and CO_2 and O_2 limitation after the exponential phase during bacterial growth with limited aeration

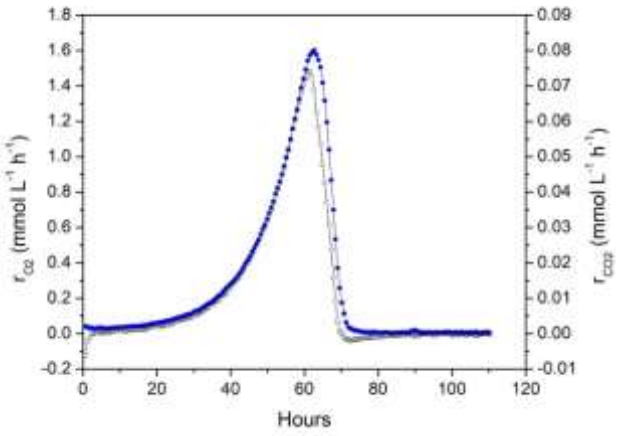

Figure 2 CO_2 and O_2 consumption rate during unlimited bacterial growth. The culture was incubated without gas limitation.

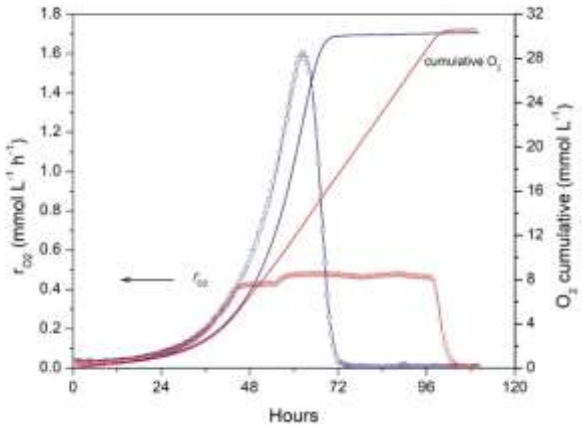

Figure 3 Comparison of O_2 consumption rate during limited and unlimited growth. Cumulative oxygen consumption is the same in both cases

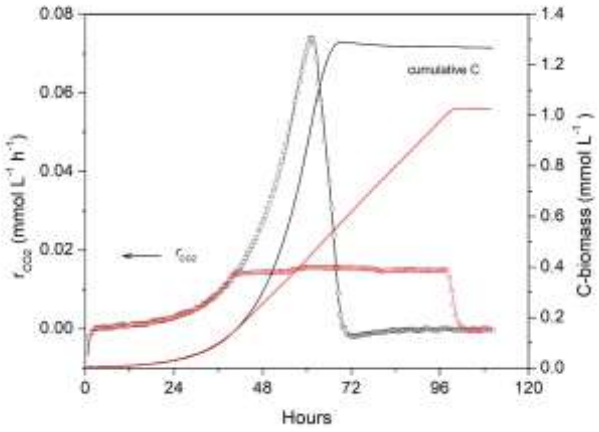

Figure 4 Comparison of CO_2 consumption rate during limited and unlimited growth. Cumulative CO_2 consumption is higher in the case of unlimited growth (higher yield)

Results and discussion

For our purpose we used small reaction flasks, with magnetic stirring set at 350 rpm. During the incubation CO_2 and O_2 consumption rates were measured on-line by gas analysis. Bacterial culture *A. ferrivorans* SS3 originating from Norilsk mining region was used in the experiments.

In Fig. 1 we can notice plateau region of growth curve which represents gas limitation for bacterial culture. It means that after initial exponential phase the growth rate had been limited by gas transfer rate and afterwards the bacterial culture grew linearly. After (Fe^{2+}) depletion the growth rate decreased to zero. In addition, we can notice small value of CO_2 release which can be explained by the carboxysomes presence in the bacterial cell.

In the Fig. 2 we can see unlimited growth of the bacterial culture in the same medium with Fe^{2+}. There is no gas limitation and just after the energy source (Fe^{2+}) had been depleted from the medium, culture growth rate decreased.

In the Fig. 3 and 4 we can see comparison of O_2 (Fig. 3) and CO_2 (Fig. 4) consumption rate during limited and unlimited growth. Notice, that cumulative oxygen consumption is the same in both cases where approx. 30 mM of consumed oxygen correspond to ¼ of initial $FeSO_4$ concentration, which is 120 mM. It is according to following formula 1.:

$$4\ Fe^{2+} + 4\ H^{+} + O_2 \rightarrow 4\ Fe^{3+} + 2\ H_2O \qquad (1)$$

Cumulative CO_2 consumption is higher in the case of unlimited growth, which means higher yield. It means, that understanding the mechanisms and kinetics of bacterial growth and ensuring appropriate incubation conditions can lead to more efficient growth of bacteria and accordingly to better yield of their metabolites and oxidation activity.

Conclusions

Many mining companies have become aware of the microbiological approaches potential for recovering base and precious metals from low-grade ores, and also for remediation of acidic, metal-rich wastewaters. Biological systems offer a number of environmental and also economic advantages over conventional approaches, even though their application is not convenient in every kind of situation. Many people speculate that bio mining will increase significantly in terms of the range of mineral ores and concentrates processed and the scale of metal produced, in the 21st century [2].

Acknowledgement
This work has been supported by the Marie Curie Programme FP7-People-2013-IAAP-WaSClean project No 612250, the Slovak Grant Agency VEGA, project No 2/0145/15, and the Operational Programme Research and Development through the project: Centre of Excellence for Integrated Research of the Earth's Geosphere (ITMS: 26220120064)

References

[1] Emerson D., E.J. Fleming and J.M. McBeth: Iron-oxidizing bacteria: an environmental and genomic perspective. Annu Rev Microbiol, 2010. 64: p. 561-83
[2] Johnson D.B.: Biodiversity and interactions of acidophiles: Key to understanding and optimizing microbial processing of ores and concentrates. Transactions of Nonferrous Metals Society of China, 2008. 18(6): p. 1367-1373
[3] Noike T., K. Nakamura and J.I. Matsumoto: Oxidation of ferrous iron by acidophilic iron-oxidizing bacteria from a stream receiving acid mine drainage. Water Research, 1983. 17(1): p. 21-27
[4] Bosecker K.: Bioleaching: metal solubilization by microorganisms. FEMS Microbiology Reviews, 1997. 20(3): p. 591-604
[5] Kappler A. et al.: Geomicrobiology of iron. 2015. 343-399
[6] Drobner E., H. Huber and K.O. Stetter: Thiobacillus ferrooxidans, a facultative hydrogen oxidizer. Applied and Environmental Microbiology, 1990. 56(9): p. 2922-2923
[7] Valdes J. et al.: Acidithiobacillus ferrooxidans metabolism: from genome sequence to industrial applications. BMC Genomics, 2008. 9: p. 597
[8] Kupka D., et al.: Bacterial oxidation of ferrous iron at low temperatures. Biotechnol Bioeng, 2007. 97(6): p. 1470-8
[9] Esparza M. et al.: Expression and activity of the Calvin-Benson-Bassham cycle transcriptional regulator CbbR from Acidithiobacillus ferrooxidans in Ralstonia eutropha. FEMS Microbiol Lett, 2015. 362(15): p. fnv108
[10] Berg I.A., Ecological Aspects of the Distribution of Different Autotrophic CO(2) Fixation Pathways. Applied and Environmental Microbiology, 2011. 77(6): p. 1925-1936
[11] Tabita F.R. et al.: Distinct form I, II, III, and IV Rubisco proteins from the three kingdoms of life provide clues about Rubisco evolution and structure/function relationships. J Exp Bot, 2008. 59(7): p. 1515-24
[12] Ogunseitan O.: Microbial Diversity: Form and Function in Prokaryotes. 2004
[13] Jordan D.B. and W.L. Ogren: Species variation in the specificity of ribulose biphosphate carboxylase/oxygenase. Nature, 1981. 291: p. 513
[14] Watson G.M. and F.R. Tabita: Microbial ribulose 1,5-bisphosphate carboxylase/oxygenase: a molecule for phylogenetic and enzymological investigation. FEMS Microbiol Lett, 1997. 146(1): p. 13-22
[15] Esparza M., et al.: Gene Organization and CO2-Responsive Expression of Four cbb Operons in the Biomining Bacterium Acidithiobacillus Ferrooxidans. Advanced Materials Research, 2009. 71-73: p. 207-210
[16] Blanchard J. and F. Abdul-Rahman: Carboxysomes, Structure and Function, in Encyclopedia of Astrobiology, R. Amils, et al., Editors. 2014, Springer Berlin Heidelberg: Berlin, Heidelberg. p. 1-3

Synthesis and characterization of graphene oxide material and their application in the environment

Dominika Behunová[1], George Gallios[2], Miroslava Václavíková[1]

[1] Institute of Geotechnics SAS, Watsonova 45, 040 01 Košice, Slovakia
[2] Aristotle University of Thessaloniki, School of Chemistry, Lab. General & Inorganic Chemical Technology, 54124 Thessaloniki, Greece
vaclavik@saske.sk

Abstract

Water pollution is worldwide environmental concern. The effective strategies of water treatment inpure by pollutants (mainly heavy metal ions and organic dyes) can be treated with adsorption using graphene oxide-based composites, which shows strong binding with these pollutant species. Graphene is a single-atomic layered material, made by the powerful oxidation of graphite, which is cheap and generous. Graphene oxide is an oxidized form of graphene, laced with oxygen-containing groups. In this paper, a Hummers and Improved methods for preparation of graphene oxide are described. An electroplating method will be used to synthesize graphene oxide architectures, exhibing ultrahigh capacitance as electrodes and more active surface area for adsorbing chargers.

Introduction

Graphene is an exciting material of the 21st century, as a single-atomic layered material of sp2 bonded carbon atoms in honeycomb crystal lattice is interesting for researchers over the world [1]. Graphene oxide (GO), the functionalized graphene containing epoxy and hydroxyl chemical groups, has a superior properties such as large surface area, mechanical stability, tunable optical, thermal and excellent electrical properties [2]. Nowadays, graphene can be produced by micromechanical exfoliation of highly oriented pyrolytic graphite (HOPG), epitaxial growth, electrochemical exfoliation, chemical vapor deposition (CVD) and different chemical method [3]. Usually, GO is made by the powerful oxidation of graphite using Brodie method, Staudenmaier method, Hofmann method and Hummers-Offeman method and also their modified and improved forms [4]. In these methods, initially graphite powder is chemically reacted with acids (HCl, H_2SO_4 and HNO_3 etc.) followed by the intercalation of alkali metals (alkali metal compounds $KClO_3$, $KMnO_4$, $NaNO_3$ etc.) into the graphitic layers [5]. Brodie first demonstrated the synthesis of GO in 1859 by adding a portion of potassium chlorate to a slurry of graphite in fuming nitric acid [6]. In 1898, Staudenmaier improved on this protocol by using concentrated sulfuric acid as well as fuming nitric acid and adding the chlorate in multiple aliquots over the course of the reaction. This small change in the procedure made the production of highly oxidized GO in a single reaction vessel significantly more practical [7]. In 1928, Hofmann used combination with concentrated nitric acid and potassium chlorate. In 1958, Hummers reported the method most commonly used today, the graphite is oxidized by treatment with potassium permanganate and sodium nitrate in concentrated sulfuric acid [8].
However, in this paper, both the modified Hummers and the Improved method, more eco-friendly method without using $NaNO_3$ was employed. This improved method can produce a greater amount of hydrophilic oxidized graphene material and eliminates toxic gases [3].

Hummers method

GO was prepared by oxidizing the natural flake graphite with a mixture of concentrated H_2SO_4, $NaNO_3$ and $KMnO_4$ by a modified Hummers method. First graphite powder and sodium nitrate were stirred in sulfuric acid and cooled to 0°C in ice bath. The reaction takes place when a mixture of potassium permanganate as strong oxidizing agent is combined with a concentrated sulfuric acid (Eq. (1)). In terms of the permanganate used as an oxidizing agent, it is generally accepted that the main reactive specie in oxidation of graphite is the dimanganese heptoxide (Mn_2O_7) as can been seen in Eq. (2), not taking into

account the changes in the method. Mn_2O_7 can react explosively as long as the temperature raise above 55°C or to come into contact with organic compounds [9]. During the stirring, the suspension becomes thick and was then further diluted using water and treated with H_2O_2 (3%) to reduce the residual permanganate and manganese dioxide to colorless soluble manganese sulfate. Finally, the diluted suspension was filtered and washed several times with water to remove the soluble salt [5]. The dry form of GO was obtained by centrifugation followed by dehydration at room temperature in vacuum.

$$KMnO_4 + 3H_2SO_4 \rightarrow K^+ + MnO_3^- + H_3O^+ + 3HSO_4^- \quad (1)$$

$$MnO_3^+ + MnO_4^- \rightarrow Mn_2O_7 \quad (2)$$

Chemical species involved in the synthesis of graphene oxide [9].

Improved method

Afterwards, more eco-friendly method without using $NaNO_3$ was employed, which can produce a greater amount of hydrophilic oxidized GO material. This method eliminates toxic gases and simplifying the disposal of waste waters. Increasing the amount of $KMnO_4$, and performing the reaction in a 9:1 ratio the mixture of H_2SO_4/H_3PO_4 improves the efficiency of the oxidation process. The effectiveness of an oxidation process of the GO is often evaluated by the carbon/oxygen ratios [3].

Electrophoretic deposition

lectrophoretic deposition (EPD) is a two-step process in which charged particles in suspension move toward an electrode of opposite charge due to the influence of an electric field and then deposit to form a compact film at the surface [10]. The formation of a homogeneous, closely packed deposit requires the use of a stable suspension in which the particles are dispersed with minimal aggregation. Stable suspensions of a wide assortment of materials can be prepared by tuning the particle-particle interactions, foremost of which are attractive van der Waals forces and repulsive electrostatic forces. EPD can deposit multiple layers of colloidal graphene and may improve the conductivity of previously oxidized graphene through reduction electrochemistry [12].

SEM measurement

Surface morphology of stainless steel plates were measured by field emission scannig electron microscopy MIRA 3 FE-SEM microscope (TESCAN, Czech Republic). Measurment has been applied for the surface examination. The SEM images of stainless steel plates are shown in Fig. 1, displays thickness of graphene oxide layers on stainless steel plate. EPD produce thin films, which usually exhibit agglomerated and wrinkled architectures.

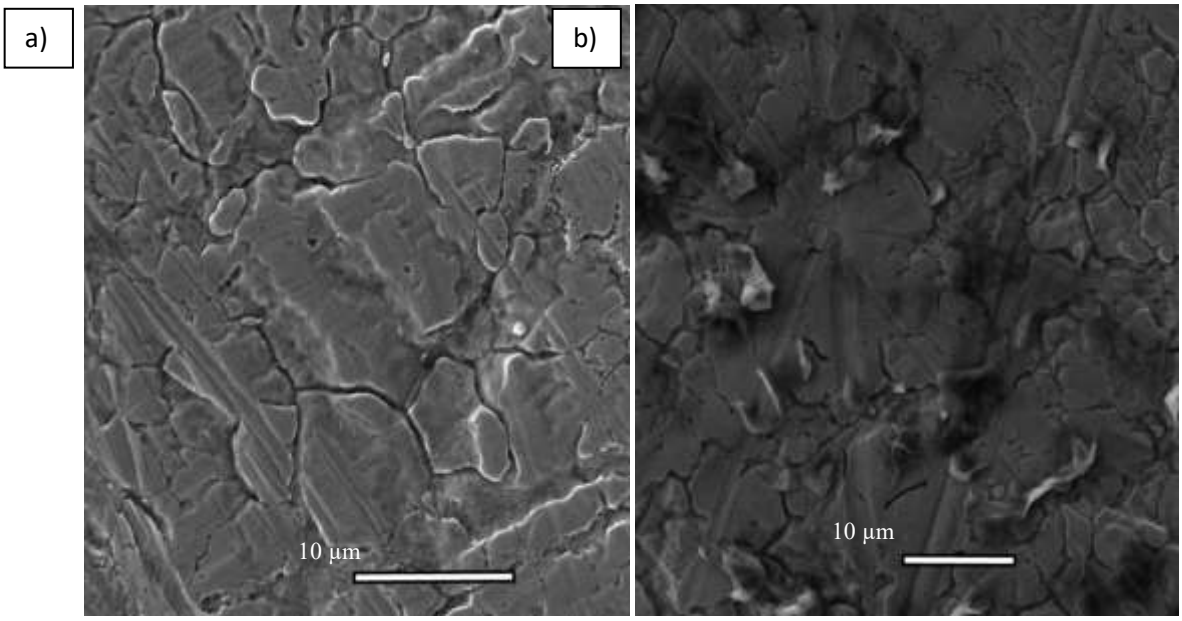

Figure 1 a) SEM picture of stainless steel, **b)** SEM picture of stainless steel after EPD with graphene oxide

Applications

Graphene and its derivatives are very attractive for constructing membranes for high-efficiency separation applications including water purification and desalination. GO-polymer membrane shows excellent water flux and salt rejection (a NaCl rejection of 99.9%), alongside excellent mechanical stability and chlorine tolerance for the osmosis process [11]. In our study, GO will be employed for the electroplating/surface covering of the stainless steel electrode. Electroplating method will be used to synthesize 3D porous GO architectures, exhibiting ultrahigh capacitance and energy density as electrodes. Electrochemical oxidation technique is simple and effective for treatment of various wastewaters. Oxidants are produced during the process directly at the electrode surface or indirectly from chemical compounds in the treated water [13]. It is expected that surface covering of the stainless steel electrode by GO will provide more active surface area for adsorbing chargers and thus increase efficiency of electrochemical oxidation technique in wastewater treatment.

Conclusions

It is widely recognized that nanotechnology and applications may play an important role resolving issues related to water and soil clean-up. Due to their large surface areas and their size and shape dependent catalytic properties, considerable efforts are given to explore uses of nanomaterials in application such as sorption. In the polluted water, various GO composites not only display strong affinity for the adsorption of heavy metal ion and organic contaminants but also function as efficient chemical and photo catalysts in converting the toxic metal ions and organic contaminants in to the harmless products.

Acknowledgements

This work has been supported by the Marie Curie Programme FP7-People-2013-IAAP-WaSClean project No 612250 as well as H2020-MSCA-RISE-2016-NANOMED project No 734641. The support of Slovak R&D Agency project No APVV-10-0252-WATRIP, Science and Scientific Grant Agency VEGA project No. 2/0158/15, Greek national support project No 40124 and R&D support project (MVTS) of Slovak Academy of Sciences are greatly acknowledged as well.

References

[1] Geim A.K, Novoselov K.S.: The rise of graphene, Nature Materials 6 (2007), 183–191

[2] Novoselov K.S., Geim A.K., Morozov S.V. et al.: (2004) Electric Field Effect in Atomically Thin Carbon Films. Science , 306, 666-669

[3] Marcano D.C., Kosynkin D.V., Berlin J.M. et al.: Improved synthesis of graphene oxide. ACS Nano (2010); 4(8):4806–4814
[4] CHen J., Yao, B., Li Ch. Et al.: An improved Hummers method for eco-friendly synthesis of graphene oxide. CARBON 64 (2013), 225 –229
[5] Singh R.K., Kumar R., Singh D.P.: Graphene oxide: strategies for synthesis, reduction and frontier applications. RSC Advances (2016), 6, 64993
[6] Brodie B.C.: On the atomic weight of graphite. Philosophical Transactions of the Royal Society of London (1859); 14:249–59
[7] Staudenmaier L.: Verfahren zur Darstellung der Graphitsaure. Ber Dtsch Chem Ges (1898); 31(2):1481–1487
[8] Hummers W.S., Offeman R.E.: Preparation of graphitic oxide. Journal of the American Chemical Society. (1958) 80(6):1339
[9] Amieva E.J-C., Lopez-Barossi J., et al.: Chapter from the book: Recent Advances in Graphene Research, InTech, Chapters published October 12, (2016) under CC BY 3.0 license
[10] Chavez-Valdez A., SHaffer M.S.P., Boccaccini A.R.: Applications of Graphene Electrophoretic Deposition. A Review, The Journal of Physical Chemistry, B (2013), 117: 1502-1515
[11] Kim S., Lin X., Ou R. et al.: Highly crosslinked, chlorine tolerant polymer network entwined graphene oxide membrane for water desalination, Journal of Materials Chemistry A ,4, (2017)
[12] Hasan A., Rigueur J. L., Harl R. R. et al.: ACS Nano 2010, 4 (12), 7367−7372
[13] Jager D., Kupka D., Vaclavikova M.: Degradation of Reactive Black 5 by electrochemical oxidation. Chemosphere 190 (2018) 405-41

Electrochemical Oxidation of Atrazine

Gergő Bodnár, Daniel Kupka, Dávid Jáger, Miroslava Václavíková

Institute of Geotechnics, Slovak Academy of Sciences, Watsonova 45, 040 01 Košice, Slovak Republic, bodnar@saske.sk

Introduction

Atrazine is a commonly used selective herbicide of the triazine class. It has been widely used in the world. Atrazine was banned in the European Union in 2004, because of its endocrine disruptor effects, possible carcinogenic effect, and negative environmental impact when the contamination in groundwater exceeds the safety levels stated by the EU.

Atrazine

Atarzine ($C_8H_{14}ClN_5$) was developed by Geigy laboratories in 1958 in a series of triazine herbicides. Atrazine is an organic compound consisting of an s-triazine-ring. Its main role is to eliminate the broadleaf weed and increase the agricultural output of crops. The effectiveness of atrazine is based on blocking the plastoqiunone-binding protein in photosystem II and to accelerate the oxidative damage by breaking down the electron transport system [1].

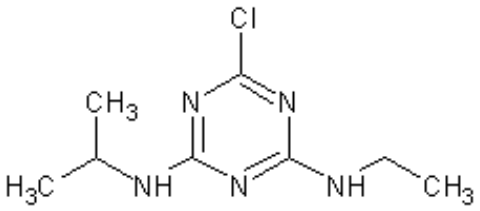

Figure 1: The structural formula of Atrazine

The effects of atrazine on human health and environment were studied for decades. Wide-spread and repeated usage of triazine class pesticides can cause disruption of endocrine system, low birth weight, risk of preterm delivery and malformation of an embryo (teratogen effects) [2], [3], [4].
The negative effect of atrazine contamination can be represented on amphibians. Teratogenic effect on population of frogs causes demasculinization on males and disruption of endocrine system. Even at low concentrations of atrazine male tadpoles turned into hermaphrodites and had both male and female characteristics [5]. Degradation of atrazine is accelerated in soil by the action of bacteria, although in fresh water and ground water the breakdown of atrazine is slower. Because of this persistence, atrazine can accumulate in drinking water and cause severe, long term health problems [6].
Advanced oxidation processes (AOPs) have been widely used to improve biodegradability of many xenobiotic compounds. The use of AOPs as a pre-treatment for the enhancement of the biodegradability can be justified if the intermediate products resulting from the reaction can be used by microorganisms.

Electrochemical oxidation

Electrochemical oxidation (EO) is the most popular procedure among the electrochemical advanced oxidation processes (EAOPs) for removing organic pollutants from wastewater. The basic principle of electrolytic oxidation of persistent organic compounds is oxidation of the primary molecules to smaller degradable molecules or to fully oxidize to CO_2 inorganic ions. This oxidation can be achieved by two ways:

- Direct anodic oxidation, which is based on the direct transfer of electrons to the anode.
- Mediate reaction of hydroxyl radicals (·OH), which are produced by the electrolysis of water.

The action produced radicals can achieve partial or full degradation of pollutants. These types of chemical radicals enable the full oxidizing of pollutants to CO_2 inorganic ions, or production of carboxyl acids, which are biodegradable [7].

$$2\ H_2O \rightarrow 2\ OH\cdot + 2\ H^+ + 2e^-$$
$$OH^- \rightarrow OH\cdot + e^-$$

We can differentiate between "active" and "non-active" electrodes.
Active electrodes are produced from precious metals Au, Pt; and metallic oxides TiO2, IrO_2, RuO_2. On the surface of the electrode active centers M are located, which reacts whit OH· radicals and form MO centers. These MO^- centers react with organic compounds and educates to the basic state.

$$M + \cdot OH \rightarrow MO + H^+ e^-$$

Non-active electrodes are BDD – Boron doped diamond electrodes, metallic oxides of PbO_2, SnO_2. On these electrodes active centers are not being formed by chemical sorption but with physical formation of M(OH)· centers.

$$M + \cdot OH \rightarrow M(OH)\cdot$$

The selection of the anode material plays a key role in the effectiveness of the degradation of organic pollutants [8].

Materials and methods

Synthetic aqueous solution of atrazine was prepared by dissolving 20 mg L^{-1} analytical standard grade atrazine (PESTANAL® Sigma Aldrich) in 8 mM NaCl electrolyte. The acidity of the solution was adjusted at pH 4 with hydrochloric acid.
Electrolysis of the atrazine solution was performed under galvanostatic conditions in an undivided electrochemical cell. Two different anodic materials were used in the tests. Titanium mesh coated with mixed oxides of $RuO_2/IrO_2/TiO_2$ i.e. dimensionally stable mixed metal oxide anode (DSA® anode) and niobium mesh coated with a boron doped diamond layer (BDD anode) respectively. Stainless steel plates were used as cathode material. The electrolysis was carried out at room temperature in a batch mode at current density 100 A m^2. The solution was mixed by up-flow gas lifting (Fig. 2).

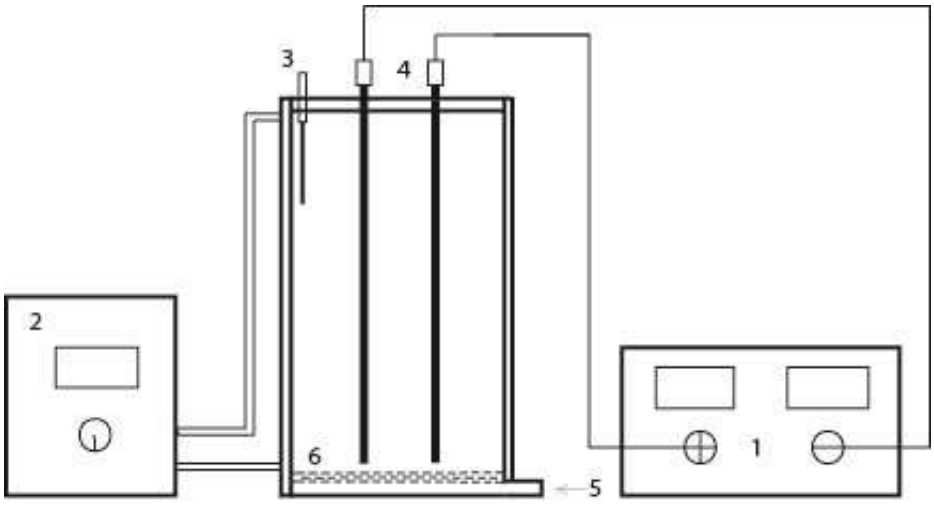

Figure 2 Electrochemical cell; 1 – DC power supply, 2 – thermostat, 3 – gas sampler, 4 – electrodes, 5 –air input, 6 – fritted glass sparger

The reaction cell was gas tight sealed by the lid with openings for excurrent gas sampling and occasional withdrawal of liquid samples. The cell gas was analyzed on-line for oxygen and carbon dioxide. Pure nitrogen was directed to electrolytic cell at the bottom and sparged by porous glass frit. Before the start of electrolysis, the electrolyte was made free of oxygen and carbon dioxide by passing N_2 gas through the electrolytic cell for about 20 min. When current was applied the gases (O_2, CO_2) produced in the electrochemical reactor yielded an upward-going signal from the zero (baseline) value.
During electrochemical treatment, the liquid samples were withdrawn from the electrolytic cell at regular intervals for chromatographic and mass spectrometric analyses. The products of electrochemical degradation of atrazine were separated using high performance liquid chromatography (HPLC) on reversed phase. The separated species were detected by diode array detector (DAD) and electrospray ionization mass spectrometry (ESI-MS).

Results and discussion

The extent of atrazine mineralization was evaluated on-line by monitoring the amount of CO_2 liberated in the course of electrolysis. The amount of carbon dioxide produced during the electrochemical oxidation of atrazine corresponds to the TOC decrease (Fig. 3).

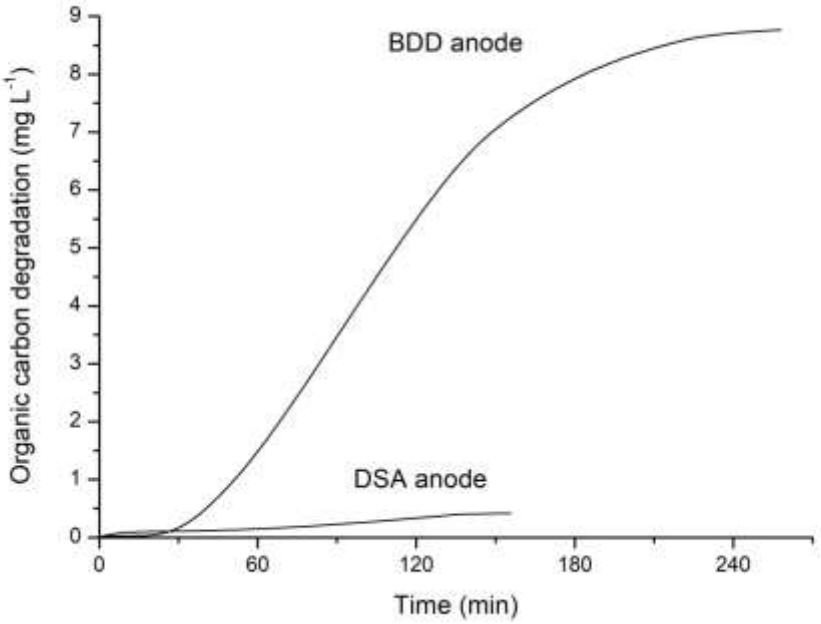

Figure 3 Degradation of organic carbon calculated from CO_2 production during electrochemical oxidation of atrazine with BDD and DSA anode respectively.

The carbon mass balance was calculated from the initial organic carbon concentration of the atrazine solution and the amount of carbon released as CO_2 in the off gas. The molecular formula of atrazine $C_8H_{14}ClN_5$ comprises eight atoms of carbon which accounts for 44.55% of the molecular mass of atrazine. Accordingly, complete mineralization of 20 mg atrazine yields 8.91 mg of carbon in the form of CO_2.

The results obtained at electrochemical treatment with BDD and DSA anode revealed differences among the electrochemical processes which implies different degradation mechanisms. The oxidation of organic compounds occurs primarily through reactions with hydroxyl radicals. In general, the effectiveness of an electrochemical oxidation is proportional to the ability of anode material to generate hydroxyl radicals.

The high overpotential for oxygen evolution and the low adsorption density of OH radicals onto the BDD anode surface, allow favorable conditions for effective oxidation of organic matter. During electrochemical oxidation with BDD anode very high concentration of OH radicals can be reached in a thin liquid film near the electrode surface where the organic compounds are mineralized with high faradaic yield.

Titanium-based mixed metal oxides are good catalysts for chlorine evolution. However, using these anode materials, organic oxidation yields low current efficiency for complete combustion, since they favor the secondary reaction of oxygen evolution. No full mineralization to CO_2, nor complete TOC removal, could be obtained with mixed metal oxide anodes. The production of CO_2 at the initial stage of electrolysis with DSA anode might be the result of the mineralization of small aliphatic parts of the compound ($-CH_2-CH_2-$) whereas the aromatic ring of the atrazine molecule stayed intact.

Conclusions

Electrochemical oxidation is an emerging technology for cleaning up wastewater contaminated with various organic compounds. Our experiments have demonstrated effective decomposition of the pesticide atrazine by anodic oxidation in electrochemical cell. The complete mineralization of the organics to CO_2 and good Faradic efficiency can be obtained using "non-active" electrodes with high oxygen overpotential, such as BDD, because these electrodes involve the production of hydroxyl radicals, that non-selectively oxidize the organic pollutants and their intermediates.

On the other hand, the mineralization of organic carbon in the electrochemical cell with "active" type anode was low. CO_2 formed during the electrochemical reaction with the DSA anode was the product of the incineration of the side chains of the atrazine molecule without opening the triazine aromatic ring.

A low oxidation power anode is characterized by a strong electrode–hydroxyl radical interaction resulting in a high electrochemical activity for the oxygen evolution reaction and to a low chemical reactivity for organics oxidation. Several authors have reported that DSA-type anodes coated with mixed metal oxide layer can be used efficiently for organic disposal by indirect electrolysis generating in situ active chlorine by the oxidation of chloride ions present in the solution.

Electrochemical oxidation can be used as pre-treatment step to enhance biodegradability of the refractory xenobiotic compounds. Although a complete mineralization of the pollutants by electrochemical treatment is usually not economically feasible, the combination of both electrochemical and biological technologies is widely reported to reduce operational costs.

Acknowledgement

This work has been supported by the Marie Curie Programme FP7-People-2013-IAAP-WaSClean project No 612250, the Slovak Grant Agency VEGA, project No 2/0145/15, and the Operational Programme Research and Development through the project: Centre of Excellence for Integrated Research of the Earth's Geosphere (ITMS: 26220120064)

References

[1] Appleby Arnold P., F. Müller, and S. Carpy, Weed Control.
[2] Kucka M. et al.: Atrazine acts as an endocrine disrupter by inhibiting cAMP-specific phosphodiesterase-4. Toxicology and Applied Pharmacology, 2012. 265(1): p. 19-26
[3] Stayner L.T. et al.: Atrazine and nitrate in drinking water and the risk of preterm delivery and low birth weight in four Midwestern states. Environmental Research, 2017. 152: p. 294-303
[4] Wirbisky S.E. et al.: Embryonic atrazine exposure alters zebrafish and human miRNAs associated with angiogenesis, cancer, and neurodevelopment. Food and Chemical Toxicology, 2016. 98: p. 25-33
[5] Hayes T.B. et al.: Demasculinization and feminization of male gonads by atrazine: Consistent effects across vertebrate classes. The Journal of Steroid Biochemistry and Molecular Biology, 2011. 127(1): p. 64-73
[6] Rohr J.R. and K.A. McCoy: A qualitative meta-analysis reveals consistent effects of atrazine on freshwater fish and amphibians. Environ Health Perspect, 2010. 118(1): p. 20-32
[7] Martínez-Huitle C.A. and E. Brillas: Decontamination of wastewaters containing synthetic organic dyes by electrochemical methods: A general review. Applied Catalysis B: Environmental, 2009. 87(3): p. 105-145
[8] Gernátová M., J. Pavel: Elektrochemická degradácia chlórfenolov. Chem. Listy, 2006. 100(10): p. 5

Evaluation of shake-out properties of new hot cured inorganic binders

Martin Conev, Iveta Vasková

Technical University of Košice, Faculty of Materials, Metallurgy and Recycling, Institute of Metallurgy, Letná 9, 042 00 Košice, Slovakia
martin.conev@tuke.sk

Abstract

Automotive industry is one of the largest customers for aluminium castings. Casted parts of engine blocks and heads are one of the most demanding areas of casting process. New generations of engine blocks and cylinder heads are designed to keep or even increase performance, while decreasing fuel consumption and emissions. This means increased geometrical complexity of inner channels. Additionally, last decade is characterised by an effort in using ecologically friendly inorganic binder systems in core making process, which brings along well known technological challenges such as decreased knock-out properties compared to organic binders. This paper deals with knock-out properties evaluation by method of abrasion resistance measurement on test bars after thermal load of 400 °C for 10 minutes. Mixtures with different composition were tested for knock-out properties, selected mixtures were then used for core production in order to confirm laboratory trials in real production of aluminium cylinder head casting. Results showed, that evaluation of shake-out properties by described method correspond well with the production trials. Mixtures with 30% addition of fine sand exhibited decreased shake-out properties as well as mixture containing different type of powder additive.

Introduction

Nowadays, sand cores are most often produced from resin-bonded silica sands, which release emissions and related odour not only during casting but also during core production process. Constant pressure of increasing environmental requirements and safety regulations resulted into development of new hot cured two component inorganic binder systems [1-2]. Managing the demanding technological requirements of organic binder systems which result from the increasing demands on castings quality represents grand challenges for inorganic binder systems developers [3]. Inorganic binders based on modified silicate or water glass solutions as new binder systems, which are cured by heat were presented at GIFA 2003 by leading binder system producers and suppliers. The fact, that moulding materials with "classic" water glass binder can reach significantly higher strengths by drying when using heated tools was the main idea of development [4,5,6]. Depending to the nature of hardening process, different character of gel is reached. Result of chemical way of curing is a gel disrupted by crystalline formations, which are causing internal stress in gel (Fig. 1 a). Gel is then brittle and cohesive forces as well as compression strength are low. On the other hand, gel created via physical way of curing is creating intact and coherent layer which results in higher strength properties and cohesive forces (Fig. 1 b) [7].

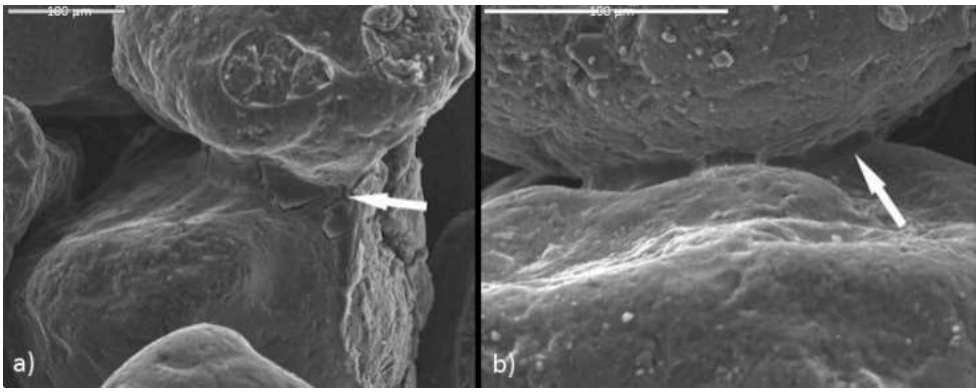

Figure 1 SEM image of binder bridge created by a) chemical reaction, b) physical curing [7]

Principle of hot-curing process with inorganic binder systems consists of blowing moulding material into a heated core box on commercial core blowing machines. Core box is usually heated between 100 - 200°C depending mainly on core geometry, but also on binder system used [5,9,10]. When the moulding mixture is in the core box, due to a heat a shell along the outer contour of the core is being formed. Whole process is ideally accelerated by purge of the hot air, which improves heating of moulding material and at the same time efficiently drains off the water expulsed during curing. Curing process has mainly physical basis - drying of solvent water, but also chemical reaction can be triggered depending on binder system used [5]. During curing process, dehydration of alkali silicate solution occurs, which leads to a poly-condensation reaction and crosslinking of silicate particles, through a reactive groups of powder additive particles silicate networked is created (Fig. 2) [11].

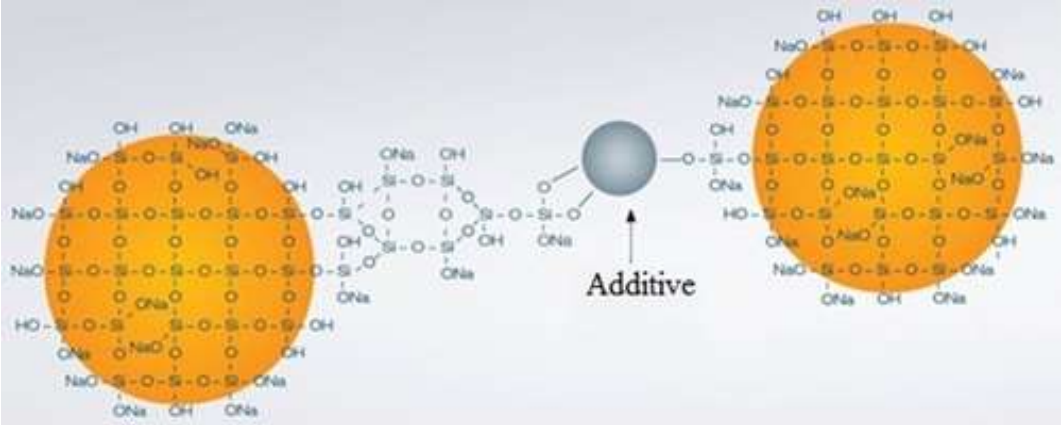

Figure 2 Effect of additive on silicate network creation [11]

Additives are blend of natural and synthetic compounds, their main function in the binder system is to accelerate curing reaction, increase immediate and final strength, increase humidity resistance and improve knock-out properties. Additionally, additives can improve other properties such as surface of the casting, depending on their composition. Although, developers of inorganic binder systems significantly improved binder systems for aluminium castings for automotive industry, there is still a connection to technological problems compared to resin-bonded sands such as lower knock-out properties, low ability to reclaim [8] and limited storage of cores [3].

Materials and methods

Shake-out properties (de-coring ability, knock-out properties) can be defined as ability of sand mould or sand core to disintegrate after casting (thermal load) and cooling down to knocking-out (de-coring) temperature [12]. The de-coring is usually carried out by machine, whereby the steps are subdivided into pre-de-coring and the actual de-coring and shaking out. In principle, the core is broken by introducing impact energy (using a hammer or vibration/swinging energy) and the broken mould material can trickle out of the core holes of the casting - often aided by a simultaneous turning movement. Lower knock-out properties of alkali silicate based binders in combination with geometrically more complex cores for engine block and cylinder head castings often lead to a remaining sand in the small cross-sections of the casting channels (e.g. water jacket cooling system). This research work is focused on dealing with such a problem in specific cylinder head casting. Mixtures presented in Table 1 were tested for knock-out properties evaluation in laboratory conditions by method described below [13]. After collecting data of knock-out behaviour, castings were produced with selected mixtures and after de-coring controlled by X-Ray method for remaining sand in the water jacket channels.

Table 1 *Overview of tested mixtures*

Mixture	Sand		Binder amount [%]	Additive	
	Coarse [%]	Fine [%]		Type	Amount [%]
No. 1	70	30	2,30	A	1,20
No. 2	70	30	2,40	A	1,10
No. 3	100	-	2,40	A	1,10
No. 4	100	-	2,30	B	1,30
No. 5	100	-	2,20	A	0,80

Method of abrasion resistance measurement on test bars

Test bars were produced on Benetlab laboratory core blower with blowing and curing described in [14]. Test bars, after cooling to the ambient temperature, were placed in the furnace heated to the 400 °C for 10 minutes in order to simulate thermal load during casting process. After 10 minutes, test bars were removed from the furnace and cooled down to the ambient temperature. Next step was measurement of the abrasion resistance using +GF+ device (Fig. 3) for 60 seconds. Measure of knock-out properties is then calculated using equation (1).

$$D = \frac{m_b - m_a}{m_b} . 100\% \qquad (1)$$

where: D – decoring ability [%], m_b – weight of the sample before test [g], m_a – weight of the sample after test [g].

The higher percentage mixture has, the better knock-out properties. This method provides only relative value of knock-out properties of tested mixture and cannot consider geometrical complexity of the core itself. On the other hand, after collection of sufficient data, man can decide whether it is needed to use mixture with better knock-out properties and choose other recipe with higher percentage value obtained by this method.

Figure 3 +GF+ device for measurement of abrasion resistance

Results and discussion

Figure 4 shows results of evaluation of de-coring ability of tested mixtures in laboratory conditions according to the method of abrasion resistance measurement on test bars after thermal load. From the results it can be seen that each tested mixture has different knock-out properties. Lowest value had mixture No. 4 with 45,59%, highest de-coring ability showed mixture No. 5 with 100%.

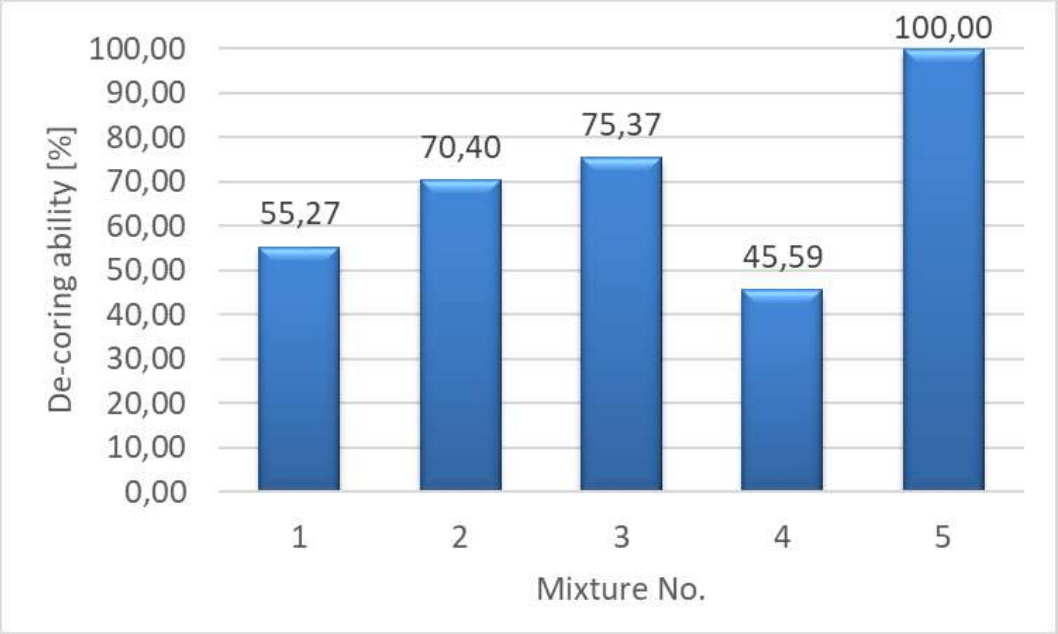

Figure 4 De-coring ability of tested mixtures

After laboratory evaluation of shake-out properties, cores from tested mixtures were prepared and casted. Shake-out of castings with all mixtures was performed under constant conditions of time and pressure of hammers. Blockage of the water jacket channels was controlled by X-Ray method, figure 5 shows channels free of residual sand (a) and channels blocked with sand (b).

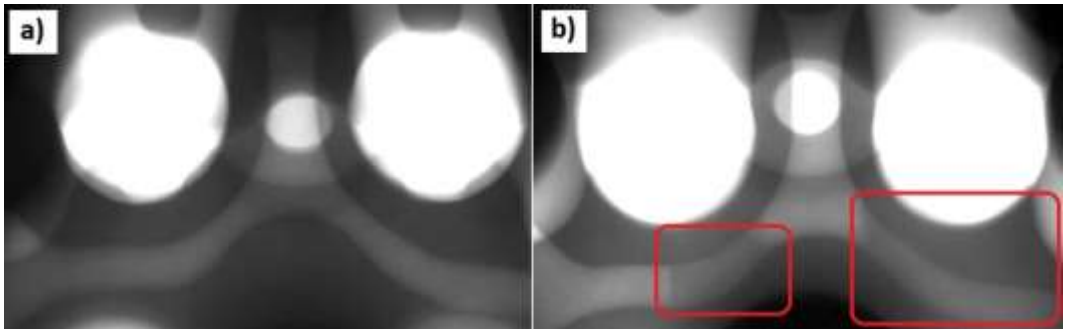

Figure 5 X-Ray pictures: a) casting with free channel, b) casting with blocked channel

Figure 6 represents percentage values of castings with residual sand inside of water jacket channels. From the results it can be seen that laboratory results correspond well with production trials. Cores from mixtures 3 and 5 with 75,37% and 100% de-coring ability were successfully removed from casting. Cores produced from mixtures 1 and 2 with 55,27 and 70,40% of de-coring ability had some castings with blocked water jacket channels and mixture 4 with lowest de-coring ability of 45,59% could not be removed from any casting. Mixture 1 contained lower binder amount and higher powder additive amount, which did not result into better knock-out properties than by mixture 2. Mixtures 2 and 3 differed only with 30% of fine sand addition, which is increasing compaction of core, but at the same time decreasing knock-out properties. Mixture 4 contained different type of powder additive, which resulted in lowest de-coring ability, that points on very high impact on powder additive composition. Mixture 5 had lowest binder and powder additive amount, which results in lower strength and at the same time in excellent knock-out properties.

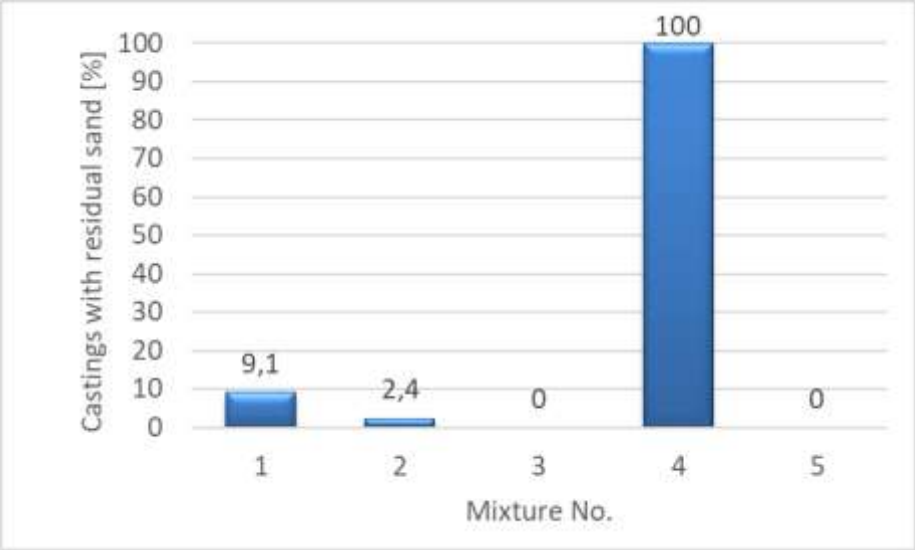

Figure 6 Evaluation of de-coring ability in production trial

Conclusions

This paper dealt with knock-out properties of two component inorganic binder systems cured by heat. In first step, 5 mixtures were tested in laboratory conditions by method of abrasion resistance on test bars after thermal load for de-coring ability. After collecting values of de-coring ability, castings were made using cores produced with the same mixtures. Blockage of the channels inside the casting was evaluated using X-Ray control. From the obtained results it can be stated that evaluation of de-coring ability of mixtures by described method corresponds well with the results of practical trials. Mixtures 3 and 5 can be used for core production for this specific casting, since their removal from the casting was fully successful. Additionally, it could be seen on mixtures 1 and 2, that addition of fine sand into coarse is decreasing knock-out properties and on mixture 1 that lower binder amount and higher powder additive amount did not lead to better shake-out of the cores in this case. Use of different type of powder additive resulted in the significant decrease of knock-out properties, which means composition of the additive used significantly influences cores disintegration after casting. For this specific water jacket core, it can be also stated that critical/minimal needed de-coring ability value is between 70,40 and 75,37% evaluated by method used in this investigation.

References

[1] Wang J. et al., China Foundry. Vol.4, No.1, 026-030 (2007)
[2] Loechte K., Boehm R., Casting plant + Technology International. 3/2005, 6-11 (2005)
[3] Müller J. et al, Slévárenství. No. 7-8, 235-240 (2015)
[4] Franken M., Giesserei. 90 Nr. 6, 182–184 (2003)
[5] Polzin H.: Inorganic binders for mould and core production in the foundry, 2014 Schiele&Schön GmbH, Berlin
[6] Škuta R.: Dehydration processes of alkaline silicates hardening, 2014 TU v Košiciach, Slovakia
[7] Stachowicz M. et al. Archives of Foundry engineering. Vol. 10, No. 3, 123 – 128 (2010)
[8] Dobosz S. M., Jelínek P., Major-Gabryś K., China Foundry. Vol.8 No.4, 438-446 (2011)
[9] Mueller J., Weicker G., Koerschgen J., Giesserei-Praxis. 05/2007, 192-194 (2007)
[10] Zaretskiy L., International Journal of Metalcasting. Vol.10 Issue 1, 88-99 (2016)
[11] Wallenhorst C., Giesserei-Praxis. No. 6, 181 – 184 (2010)
[12] Lewandowski J. L., Tworzywanaformyodlewnicze, 1997 Kraków
[13] Conev M. et al., Archives of Metallurgy and Materials, Vol. 62, No. 2, 703 – 706 (2017)
[14] Conev M. et al., Manufacturing Technology. Vol. 16, No. 2. 327-334 (2016)

Improving of Fe6.8Si powder alloy compressibility

Michaela Dilýová, Radovan Bureš

Institute of materials research of SAS, Watsonova 47, 040 01 Košice Slovakia,
mdilyova@saske.sk

Introduction

Fe6,8Si alloy continue to find more and more electromagnetic applications in industrial practice, due its excellent soft magnetic properties, such as high relative permeability, low magnetocrystalline anisotropy, and almost zero magnetostriction. Owing to the relatively high Si content, that greatly increase the brittleness at room temperature and make the alloy very difficult to be processed into thin sheets by the conventional rolling processes. [1] Cold pressing of this material by uniaxial press is also very difficult due to its spherical shape of particles, their rigidity and plasticity and limited plastic deformation. [2] The aim of this study was not to change the phase or chemical composition of powder but to change morphology of powder by milling to improve its compressibility.

Experimental, Methods and Material

Commercial alloy FESI68HQ-355µm was supplied by Höganäs. This FeSi powder has sieve cut 355µm and average particle size 150µm, its particle size distribution is showed in Figure 1.

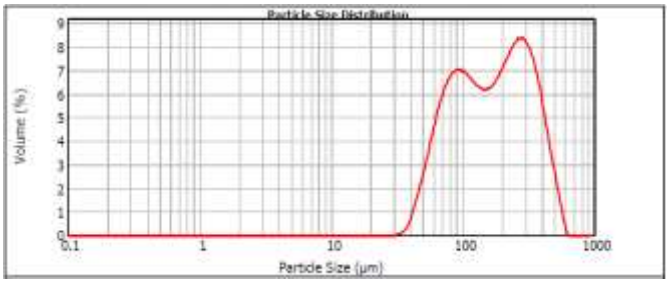

Figure1 Particle size distribution of Fe6,8Si

FeSi powder was mixed in vibration ball mill LAARMANN LMLW - 320/2 Milling jar from abrasion resistant steel and 5 grinding balls from stainless steel was used and the temperature during the whole milling process was controlled by thermo cam Optris PI. Temperature was scanned on surface of drum and on the powder inside drum after every minute of milling to prevent overheating of powder and possible recrystallization and oxidation. The process of milling was discontinuous, the mill was paused for at least 2minutes after every one minute of milling for material to cool down to temperature below 32°C. To set an optimal ball to powder weight ratio, 50g of FeSi powder was discontinuously milled on frequency 12Hz for 15minutes. Weight of the milling balls was 68,130g (b:p = 1,36:1). Samples were observed with optical (OM) and electron (SEM) microscopes. This b:p ratio was too high, and the milling was not efficient, therefore for further experiments was the weight of milled powder reduced to 10g so the b:p ratio was 6,8:1.

In vibrating milling it is possible that very high frequencies can by less effective therefore was the powder milled on frequencies 12Hz, 15Hz, 20Hz and 0Hz (maximum possible frequency for this mill) for 3minutes. Samples of the powder were observed with optical Nikon SMZ 18 and Nikon ECLYPCE LVDIA - N and electron C SEM EVO MA 15 microscope, and also were measured for density, with He pycnometry by AccuPic1340. FeSi alloy is soft magnetic compound therefore measuring of and coercive field by COERCIVE FORCE METER ATS320 was used for milling process monitoring. Coercivity Measurement Instrument meets the standards of IEC 60404-7 (Method of measurement of the coercivity of magnetic materials in an open magnetic circuit). Frequency for further experiments was set to 30Hz.

For selecting the optimal time of the milling was powder milled on frequency 30Hz for 3, 5, 6, 7, 8, 10 and 15minutes and the samples were observed with OM and SEM, and were measured for density, coercive field and also the relative compression was calculated from compression curves. Sample with volume 1ml (constant volume pressing) from every time of milling on frequency 30Hz was compressed with uniaxial pressing device LabTest 5.600 ZL. The force and the shift of punch were obtained from continuous compression curve of pressures up to 1000MPa with sampling frequency of 0.02s. Decrease in volume was calculated from track and compression pressure from the force. From the above mentioned parameters was selected the optimal milling time 15min on frequency 30Hz. For this particular powder was measured size of the particles by laser diffraction analyzer Mastersizer 2000M and bulk flow properties (apparent density, flowability, tap density and friction index) in accordance with the standard STN EN 23 923 - 1 and STN EN 42 0890.

Powder was annealed in singlemode microwave cavity size of diameter 28mm and height 80 mm. Nominal maximum magnetron power was 750W. The powder was annealed in the argon atmosphere with dwell of 20min at temperature 500°C and the cooling rate was 10°C/min. Temperature was measured by optical pyrometer Optris CT series. During annealing was monitored the absorbed microwave energy by microwave impedance analyzer HiPOM. Temperature of annealing was driven by change of sample position in cavity, respectively by moving sample to the place with higher or lower density of microwave energy.

Cylindrical (diameter 10mm), prism (20x5mm) and ring (17,85x23,85mm) samples were compacted and sintered in laboratory chamber furnace Carbolite in Ar+10%H atmosphere with dwell of 60 min. at temperature 1200°C with cooling rate 5°C/min.

Results and discussion

In the process of selecting optimal frequency of milling, an effort was made to find one that at shortest time achieved the better properties. From the morphology of the particles (Figure 2) is clear that on frequency 30Hz particles started to have lace surface structure that helps compressibility. Another reason for selecting frequency 30Hz was that density of the material was increasing with the time of milling (Figure 3). As expected with the supply of mechanical energy by milling was increasing the coercive field (Figure 4) due to tensions and lattice defects in the crystallographic lattice of the material.

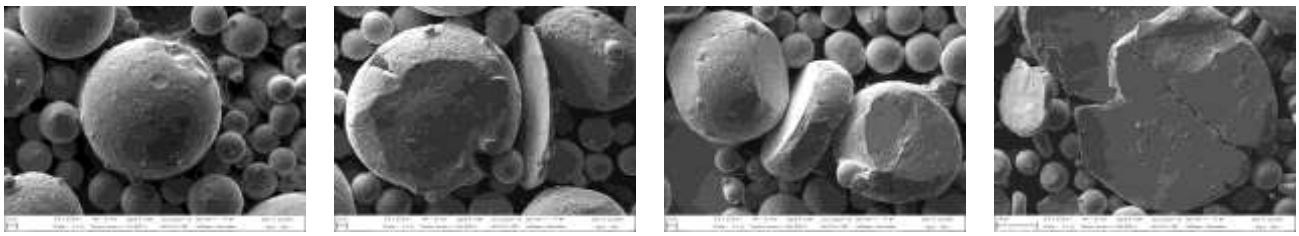

12 Hz 15 Hz 20 Hz 30 Hz

Figure 2 Morphology of particles after milling on different frequencies, SEM

Milling process was documented by OM and SEM, on the (Figure 5) is shown that firstly was changed the shape of larger particles, than smaller particles, the larger particles started to disintegrate, then around 6^{th} minute has even the small particles disintegrated and from the 7^{th} minute they started agglomerate to larger particles of flaky shape. In 15^{th} minute was the flake shaped particles largest (Figure 6). With the next continuation of milling would the particles re-agglomerate and disintegrate due to complete depletion of plastic deformation. The peak of agglomeration was in the 15^{th} minute.

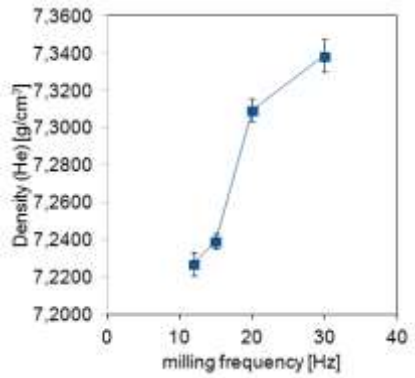

Figure 3 Density (He) to milling frequency dependence

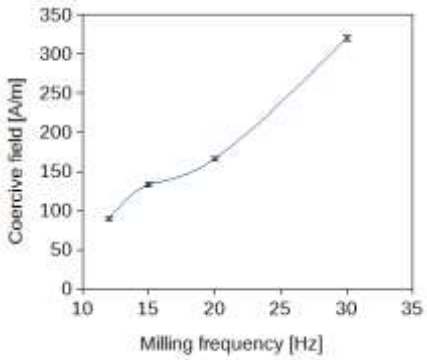

Figure 4 Coercive field to milling frequency dependence

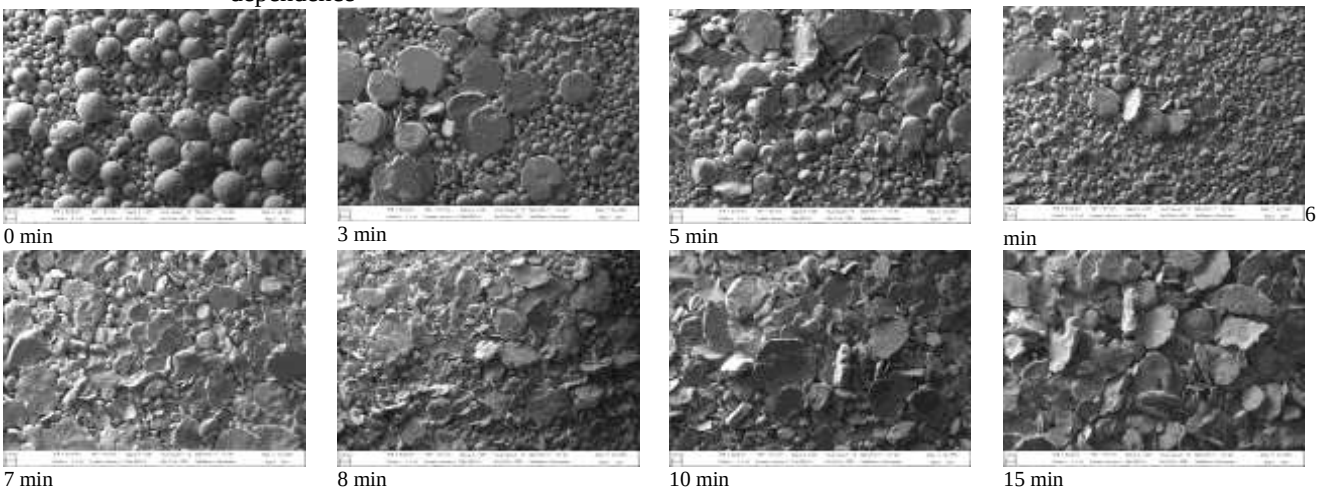

Figure 5 Milling process documented by SEM

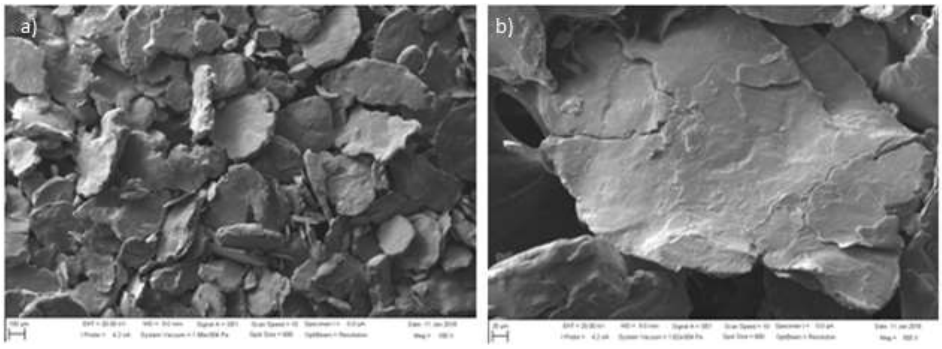

Figure 6 Powder after milling for 15 min/ 30 Hz (a) and close-up of the surface of particle (b), SEM

With prolongation of the time of milling density of the milled material was decreasing (Fig. 7) and coercive field was increasing (Fig. 8), this event was caused by the increase of lattice defect in the crystallographic lattice of material due to milling. On the (Fig.8) is observable that the rapid rise of coercive field ended around 10th minute of milling and the curve started to settle around 565 A/m. Technological powder properties of powder as received and powder after 15 min of milling are shown in Table 1 and particle size distribution for powder after milling for 15 min/30 Hz is shown in Fig. 9.

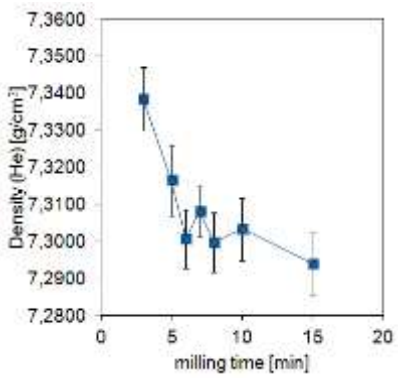

Figure 7 Density (He) to milling time dependence

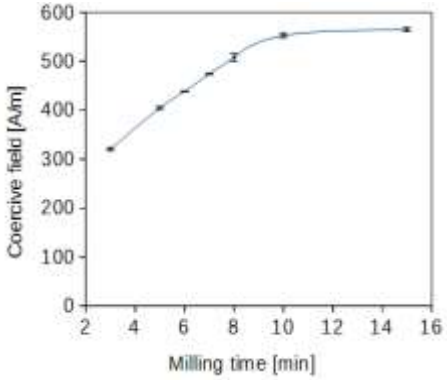

Figure 8 Coercive field to milling time dependence

Table 1 *Technological powder properties*

Milling time	Aparent density [g/cm^3]	Flowability [s/50g]	Tap density [g/cm^3]	Frictional index
0 min	4,62	16,2	5	1,08
15 min	2,67	40,05	3,77	1,41

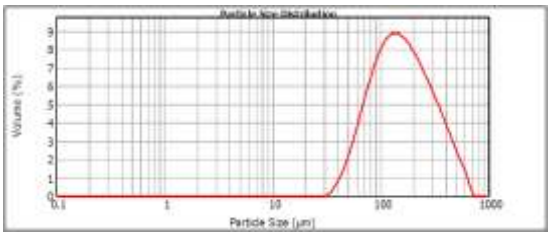

Figure 9 Particle size distribution

The aim of this study was to change particle morphology of powder in order to be able to obtain green compact with manipulative strength, therefore the relative compression as the indicator of compressibility was very important calculate from compression curves. In the Figure 10 were documented dependences of volume of the powder to pressure during compression and relief. In 1 was presented the dependence of relative compression to time of milling. The upper curve represents relative compression in the die without releasing of the powder and the curve below considers spring-back of the powder.

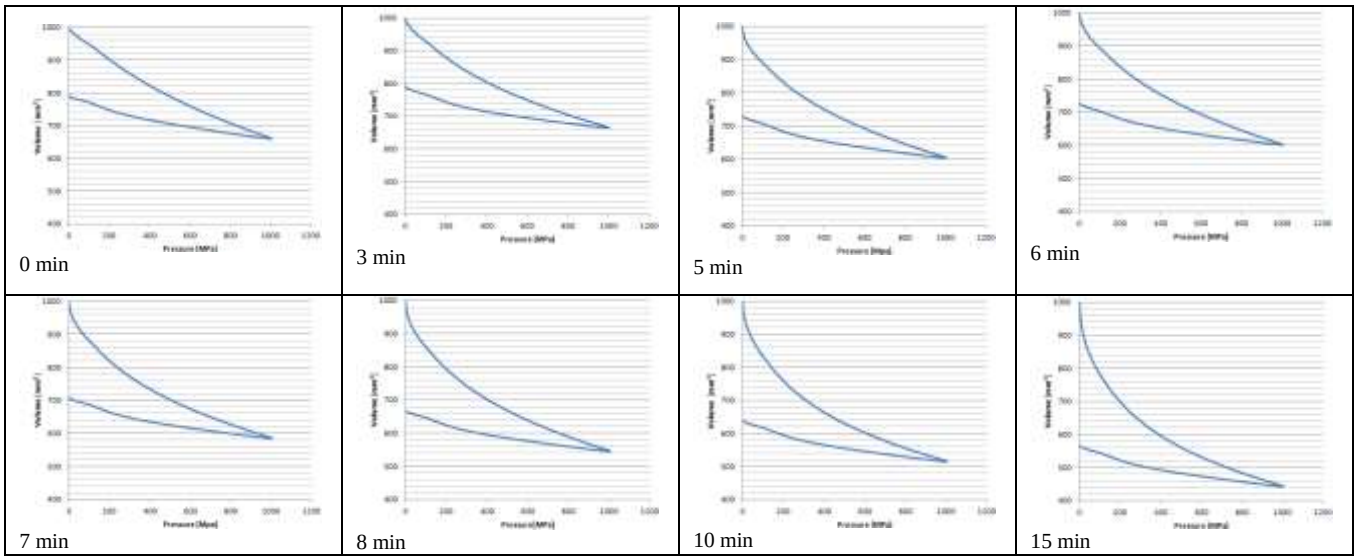

Figure 10 Compression curves

After 8 minutes of milling on frequency 30Hz was able to obtain the compact cylindrical shaped sample, but from the compressibility curves was possible to predict that it would not be possible to compress a complex shape. The more complex ring shaped sample with manipulative strength was possible to compress only after 15 min off milling. For further improvement of properties was powder as received and powder after 15 min milling on frequency 30 Hz annealed. With mechanical milling was obtained the powder with lattice defects and mechanical stresses, therefore it was necessary to recover the material. Microwave annealing technique [3] was used to prevent creation of sintered cake, that is characteristic for annealing in hydrogen in conventional furnaces. It was possible to compress complex ring shaped sample despite that relative compression after annealing was a little bit lower (Fig. 11). This phenomena will be further investigated. Samples of cylindrical, prism and ring shapes (Fig. 12) were consolidated and sintered in conventional furnace.

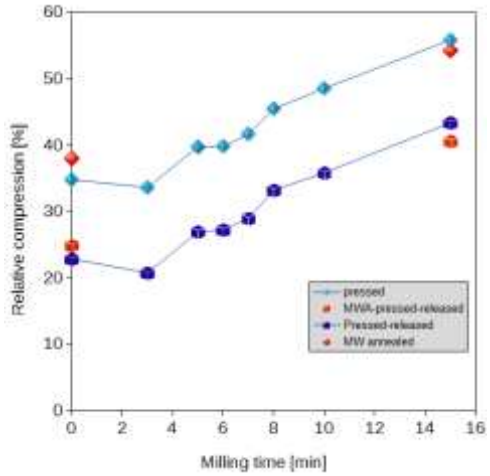

Figure 11 Relative compression to milling time dependence

Figure 12 Samples after sintering

Surface and microstructure of metallographicaly prepared cylindrical sample was observed the with z-focusing on OM. Sample has 3D polygonal large grains and pores of complex shape with rounded corners (Fig. 13 and Fig. 14).

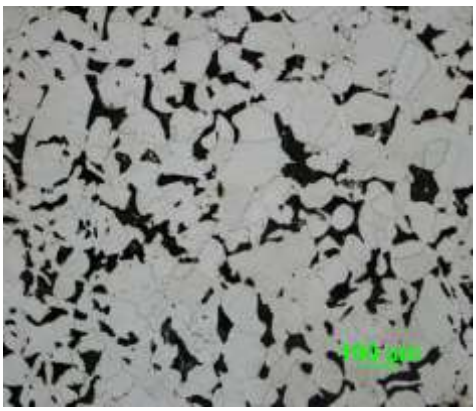

Figure 13 Surface of the sample (10% nital in absolute etylalcohol+ core), OM

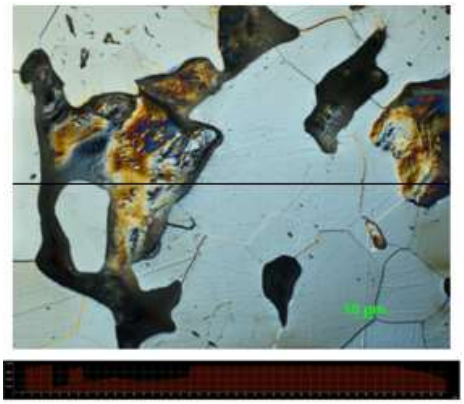

Figure 7 Profile of surface of the sample

Conclusion

Fe6.8Si powder was milled to find the optimal parameters of milling to make it compressible. Whole process was documented by optical and electron microscopes for observing changes of morphology and also the physical properties such as coercive field, density and compressibility was monitored. Based on the optimal change of the morphology of the Fe6,8Si powder, by selecting the optimal parameters of milling, was prepared the compact sample. Optimal parameters of milling were 15min on frequency

30Hz, and were followed by microwave annealing 500°C/20min/Ar. Preparation of consolidation process of silicon steel will be subject of further investigation with the aim to improve its physical properties.

Acknowledgement
This work was supported by the projects VEGA 2/0108/18 and APVV 0115-15.

References

[1] Wu Z. Y. et al., J. Alloys Compd 742 (2018) 90-98
[2] Igarashi N. et al., SEI TECHNICAL REVIEW 80 (2015) 99-103
[3] Bureš R., Fáberová M., Patent proposal No. PP 00057-2016. ÚPV SR, (2016)

Determination of arsenic, iron and hydrogen sulphide in mineral water from the spring "Gajdovka" in Košice

Martina Dudová[1], Alexander Hudák [2]

[1]Institute of Recycling Technologies, Faculty of Materials, Metallurgy and Recycling, Technical University of Košice, Letná 9, 042 00 Košice
[2]Department of chemistry, biochemistry and biophysics, The University of veterinary medicine and pharmacy, Komenského 73, 041 81 Košice

Abstract

In Košice in recreation area Anička, there is a mineral spring that inhabitants call Gajdovka. It is being used with several breaks since the 19th century. Mineral water of this spring is specific by the presence of arsenic the concentration of which often exceeds permitted limit value. This work is focused on the analysis of mineral composition of the spring water. Chemical and microbiological analysis was made in years 2013-2015. In 2014 the mineral water Gajdovka was regularly monitored during the year respecting the concentration of arsenic, iron and hydrogen sulphide. The following average concentrations were determined for arsenic 0.063 mg dm^{-3}; iron 0.275 mg dm^{-3}; and hydrogen sulphide 4.608 mg dm^{-3}.

Introduction

In particular regions there are also less known springs used by local residents. One of these less known springs is mineral spring Anička that inhabitants call "Gajdovka" and is located in the area of Košice in suburban park named Anička, nearby the river Hornád. Mineral water quality monitoring is executed by Regional Public Health Authority based in Košice four times a year. Monitored are the indicators of quality defined in decree of Ministry of Agriculture and Rural Development of the Slovak Republic No. 51 of 15 March 2004 which the 25th chapter of Food Code of the Slovak Republic was issued by. In the Annex No. 1of this material microbiological, biological, physical and chemical indicators, and demand for mineral water are defined [1]. The spring water is also known for the fact that its limit value of arsenic determined by relevant regulation is often exceeded [2]. Arsenic belongs to the most significant contaminants of environment with high potential to harm human health. Arsenic is present in nature in many oxidation states (V, III, 0, -III). In natural waters, it is mostly in form of As^{III} as arsenite anion typical for underground waters with shortage of oxygen. As^{V} dominates in surface waters in form of arsenate anions [3]. Less stable form is As^{III} that easily oxidizes. The activity of microorganisms may contribute to change of inorganic forms of As to volatile or non-volatile organic forms in nature [4]. In some works it is stated that the natural background of arsenic in underground waters is value of 5 μg dm^{-3} [5]. The most significant factors affecting particular forms of arsenic in water environment are pH and oxidation reduction potential of environment (Eh) [6. 7]. Inorganic forms of As are more toxic for humans than organic forms. As^{III} is organically bound and chemically or biochemically oxidizes to As^{V}. As^{V} is more stable in aerobic condition. As^{III} is more toxic. it causes chronic diseases and belongs to inhibitors of biochemical oxidations. Many mammals methylate inorganic arsenic to dimethylarsinic acid. This substance causes organ-specific toxicity and is promoter of genesis of tumours in many organs [8]. Arsenic was classified in 1. class by International Agency for Research on Cancer (I.A.R.C.) as proven carcinogen for humans.

This element has carcinogenic, mutagene and teratogene effects on human body. Long-term exposure can cause severe damage to organism [9]. Due to its chemical structure, it has similar biochemical properties as phosphorus that it can replace in a certain way. It affects perniciously almost at the DNA level, it destroys enzymes and proteins. Many epidemiological studies in the world showed that intake of over-limited values of arsenic into human body causes degenerative changes in optic and acoustic nerve, painful periphery polyneuropathy, encephalopathy, anemia and pernicious tumours mainly of skin, kidneys, liver and lungs, leukaemogenesis and lymphoma [10]. Arsenic is cumulated in bones, hair and nails. Permanent concentration of arsenic of 100 μg dm^{-3} is life-long possibility of tumour disease 1:200 what exceeds

the annual probability of death of tumour disease. Acute toxicity was recorded after drinking water from well with the arsenic content 1.3-20 mg dm^{-3} [11].

There is no expert study in the literature that would give more complex view on the properties of mineral water Gajdovka. Arsenic concentration has been lately sporadically monitored. Moreover, there is no overview of its presence during the year, dependency on season, connection between particular components of mineral water, eventually the dependency on the level of nearby flowing river Hornád. This work is therefore oriented on the detailed characteristics of mineral water "Gajdovka".

Materials and methods

Sampling and sample treatment

In 2014 regular monitoring of concentration of arsenic, iron and hydrogen sulphide in mineral water was made. The sample was taken once per week, always on Wednesdays in the morning. The determination of arsenic and iron through the AAS method was made in accredited laboratory of Regional Authority of Public Health in Košice. In total, 52 samples of mineral water were taken and analysed. All withdrawal vessels designed to sample withdrawals were perfectly washed and dried before use. The sample for determination of arsenic and iron was taken into polyethylene sample tube with volume 250 cm^3 and addition of 1.25 cm^3 of concentrated HNO_3. To determine H_2S it was taken 250 cm^3 of water into glass sample tube with addition of 2.5 cm^3 of cadmium acetate with concentration 100 g dm^{-3} and 1.25 cm^3 of 25-%-solution of NaOH.

Analytical methods

At monitoring of arsenic and iron volume during the year 2014, these elements were determined through the method of atomic absorption spectrometry with electrothermic atomizer (AAS-GTA) using the device SpektrAA 220 (Varian), with Zeeman background correction.

The hydrogen sulphide content in samples was determined through the method of volumetric analysis, i.e. iodometry. The result of determination was defined as average value of titration of three samples.

Statistical Methods

The analysis of Variance (ANOVA) was used for the statistical assessment of the results. The analysis is a parametric statistical method developed for mutual comparison of the groups which total number exceeds 2. The one way ANOVA which compares more groups and answers the question if the statistics differ just in one parameter [12], was used in this paper. The program Excel was used for the calculation. The probability of the mistake of the first kind marked p-value being compared to the selected level of the significance, was calculated using a statistical programme ANOVA. Using this method, the effect of the season of year on observed parameters, namely the concentration of arsenic, iron, sulphate, and level high of Hornád, was observed. Moreover, the correlation among individual parameters was carried out.

Results

In 2014 the all-year monitoring of concentration of arsenic, iron and hydrogen sulphide in mineral water was made. The aim was to determine if it comes to the change of arsenic concentration in mineral water throughout the year respectively to determine the connection between the concentration of arsenic, iron and hydrogen sulphide. The level of river Hornád was monitored as other factor with possible influence on arsenic concentration in mineral water. These data were obtained from Slovak water-management company (Banská Štiavnica) [13]. The water sample was taken once a week and was analysed after the stabilisation and delivery to laboratory. The results are listed in Table 1.

Table 1 *Determination of hydrogen sulphide, arsenic and iron in mineral water in period January – December 2014*

Month	H_2S [mg dm^{-3}]	As [mg dm^{-3}]	Fe [mg dm^{-3}]	Level of river Hornád [cm]
January	5.24	0.078	0.41	105.75
February	5.048	0.071	0.388	122.25
March	5.71	0.067	0.233	109.75
April	5.082	0.051	0.222	110.8
May	5.675	0.059	0.23	168.5
June	2.718	0.054	0.293	110
July	4.30	0.047	0.158	147.5
August	4.278	0.063	0.148	130.25
September	4.38	0.054	0.236	119.6
October	3.774	0.066	0.194	116.4
November	4.61	0.078	0.255	119.75
December	4.96	0.110	0.495	111

Discussion

Using the method of atomic absorption spectrometry with electrothermic atomizer (AAS-GTA) the total arsenic content in mineral water was determined. The average concentrations of total arsenic in the samples of mineral water for individual months (January-December 2014) are shown in Table 1. In the Food Code (Part 3, Chapter 25, Annex No. 1 – Quality indicators for drinking and mineral water) the limit value 0.05 mg dm^{-3} for As^{III} is set. Many analyzes have shown that the amount of As^{III} is 80 to 90% of the total amount of arsenic occuring in groundwater [14]. In order to compare the measured concentrations of arsenic with a limit value the concentration corresponding to 80 % (first row of As^{III} section in the Table 2) and 90% (second row of As^{III} section in the Table 2) of the total arsenic content (Table 2) was calculated.

Table 2 *As^{III} content in mineral water Gajdovka*

Month	1.	2.	3.	4.	5.	6.	7.	8.	9.	10.	11.	12.
As (tot.) (mg dm^{-3})	0.078	0.071	0.067	0.051	0.059	0.054	0.047	0.063	0.054	0.066	0.078	0.110
As^{III}	0.062	0.057	0.054	**0.041**	**0.047**	**0.043**	**0.038**	0.051	**0.043**	0.053	0.062	0.088
(mg dm^{-3})	0.070	0.064	0.060	**0.046**	**0.053**	**0.047**	**0.042**	0.057	**0.049**	0.059	0.070	0.099

The Table 2 shows that the limit value for the As^{III} was not exceeded during 5 months of the year 2014 (mostly during summer months). Under the anaerobic conditions of underground mineral waters, As^{III} dominates (which is a carcinogenic form of arsenic) [15]. Under aerobic conditions As^{III} easily oxidizes to As^{V}. Therefore, the content of the more toxic form of arsenic will be reduced after sampling and handling when in contact with air. As^{III} can also be determined directly using different separation techniques and chromatographic methods. The average iron content in this mineral water during January-December 2014 ranged from 0.148 to 0.495 mg dm^{-3} (Table 1). The highest content of iron was found in samples analyzed during the winter months – January, February and December 2014. The Food Code sets a maximum concentration for the iron content 10.0 mg dm^{-3} in mineral water. The results show that this value was not exceeded during the year 2014. Iron is not a toxic metal, however, should the limit value exceed, it can only negatively affect the sensory properties of mineral water – cloudiness or a yellowish precipitate may occur. It can discourages consumers from using this mineral water. Mineral water Gajdovka has a characteristic smell due to the content of free hydrogen sulphide. The average hydrogen sulphide content in the monitored period was found in the range 2.718 do 5.675 mg dm^{-3} (Table 1). Free hydrogen

sulphide is not listed in the Food Code as a mineral water quality indicator, so there is no limit for it. To some people is the smell of this mineral water unpleasant but this type of water is very popular for some of its healing properties. Hydrogen sulphide in mineral water has regenerative and anti-inflammatory properties, and a positive effect on the skin. It is known to help with a gynecological problems, too [15]. The mineral spring Gajdovka is located very close to the Hornád river. The aim of this paper was to find out the relationship between the height level of the river and the concentration of the monitored indicators. A one-way ANOVA was used for the correlation between the concentrations of As, Fe and H_2S and the height level of the Hornád river. The relationship between these parameters was not confirmed. Furthermore, the impact of the seasons on the above parameters was studied, as well. The analysis results were divided into four groups according to the season, as follows: 1. Winter (January-March), 2. Spring (April-June), 3. Summer (July-September), 4. Autumn (October-December). Based on the statistical analysis, it was found out that a season is statistically significant for the parameter: H_2S ($p < 0.05$), concentration of Fe ($p < 0.001$) and the height level of Hornád river ($p < 0.05$). For arsenic concentration the seasonal variations were not statistically significant. The correlation between the individual parameters has been performed but has not been confirmed.

Conclusion

The mineral water Gajdovka is among the inhabitants of Košice very popular. The most of them are drinking it occasionally during walks in the park. Others, especially the older inhabitants, take the larger amounts of this water and use it for drinking and cooking purposes. Therefore monitoring the quality of this water is very important. The amount of arsenic, which is one of the toxic elements and in a case of regular intake can cause harm to health, is the most important parameter for monitoring. The results of arsenic determination in mineral water throughout the year 2014 confirmed that its concentration changes and often exceeds the limit concentration. The results shows that the limit value for the As^{III} was not exceeded during 5 months of the year 2014 (mostly during summer months). The limit concentration for the iron content which influences the sensory quality of mineral water was not exceeded during the year at all. Based on a statistical analysis of monitored parameters (arsenic, iron and hydrogen sulphide concentration and the height level of Hornád river), it has been found out that the season changes influences the iron and hydrogen sulphide content and the height level of Hornád river and does not affect the arsenic concentration. The correlation between the individual monitored parameters has not been confirmed. Due to the increased arsenic content, the Regional Public Health Office in Košice issued recommendations for the consumption of mineral water Gajdovka. These recommendations are located at the water collection point and indicate the recommended amounts and way of using mineral water.

References

[1] Štátna veterinárna a potravinová správa SR: Potravinový kódex (aktualizovaný k 31.01.2017) – Tretia časť 25. hlava – Príloha č.1 – Ukazovatele kvality stolovej vody. dojčenskej vody a minerálnej vody.: http://www.svssr.sk/legislativa/kodex_03_25_01.asp. (accessed 2017-11-15)

[2] Dietzová Z., Bratská Z.: Odhad zdravotného rizika z konzumácie vody z voľne prístupného prameňa v Košiciach. In: Životné prostredie a a zdravie: Zborník vedeckých prác. Bratislava. 2010, p. 25 – 30 ISBN 978 – 80 – 7159 – 176 – 4

[3] Žemberyová M., Chromá O., Shearman A., Hagarová I.: Špeciácia chrómu a anorganických foriem arzénu vo vodách s využitím extrakcie tuhou fázou a atómovej absorpčnej spektrometrie. Chem. Listy, 2007, 101: 303-309

[4] Ševc J., Čerňanský S.: Microbial methylation as a part of transformation processes and migration of arsenic under natural conditions. Phytopedon (Bratislava), 2003, 2 :60-68

[5] Pitter P.: Hydrochemie, Vydavatelství VŠCHT., Praha, 1999, 568 s. ISBN 80-03-00525-62.

[6] Jurkovič Ľ., Hiller E., Slaninka I., Kordík J., Majzlan J.: Geochemické štúdium kontaminovaných riečnych sedimentov a povrchových vôd a experimentálne hodnotenie mobility As (povodie toku Kyjov a Ondava. odkalisko Poša. východné Slovensko).Workshop BO, 2006
[7] Jurkovič Ľ., Kordik J., Slaninka I.: Geochemical study of arsenic mobility insecondarily influenced Kyjov Brook and Ondava river (Eastern Slovakia). Slovak Geol. Mag., 2006, 12: 31–38
[8] Hughes M. F., Razo L.M., Kenyon N.E.M.: Dose dependent effects on tissue distribution and metabolism of dimethylarsinic acid in the mouse after intravenous administration. Toxicology, 2000, 143 (2): 155-166
[9] IARC – International Agency for Research on Cancer). In IARC Monographs on the Evaluation of the Carcinogenic Risk of Chemicals to Humans. Vol. 20. Some Metals and Metallic Compounds. 1980. pp.39-140. IARC Lyon.
[10] ATSDR- Agency for Toxic Substances and Disease Registry, Toxicological Profile for Arsenic. U.S. Department Of Health And Human Services Public Health Service. Division of Toxicology and Environmental Medicine/Applied Toxicology Branch 1600 Clifton Road NE Mailstop F-32 Atlanta. Georgia 30333, 2007
[11] https://euroclean.sk/slovnik-sk/arsen-ve-vode-jeho-odstraneni/ (accessed 2018 – 2 – 02)
[12] http://statistikapspp.sk/anova/ (accessed 2018 – 4 – 20)
[13] Slovenský vodohospodársky podnik. Merná krivka r.2014 vodočet Hornád-Kysak. Vodné stavy r.2014. 2014
[14] Hegedűsová A., Pavlík V., Hegedűs O.: Výskyt arzénuv artézskych studniach vybraných lokalít. Acta Universitatis Matthiae Belli. Ser. Chem.., 2010, 12:81-86
[15] Gürkan R., Kir U., Altunay N.: Development of a simple. sensitive and inexpensive ion – pairing cloud point extraction approach for the determination of trace inorganic arsenic species in spring water. beverage and rice samples by UV–Vis spectrophotometry. Food Chemistry. doi: 10.1016/j.foodchem.2015.01.142., 2015 (accessed 2018 – 2 – 02).
[16] http://www.putujici.cz/?p=p_354&sName=Prameny-plne-arzenu. (In Czech)(accessed 02.02.18)

Effect of plastic deformation on mechanical properties of austenitic stainless steel under cryogenic condition

Alica Fedoriková

Institute of Materials and Quality Engineering, Faculty of Material, Metallurgy and Recycling, Technical University of Kosice

Abstract

The aim of the work is to describe effect of plastic deformation on mechanical properties of selected metal material – nitrogen-enhanced austenitic stainless steel (SS) 316LN. An improvement of mechanical properties of austenitic SS is possible by cold deformation. The low temperature of deformation would prevent dynamic recovery and stimulate mechanical twinning what enhance the grain refinement effect. Therefore, research is focused on plastic deformation under cryogenic conditions of ferrous and non-ferrous metallic materials.

Introduction

The 316LN steel contains at least 16 wt. % of chromium and 6 wt.% of nickel belongs to the 300 Series stainless steel. Other alloying elements such as titanium or copper improve some of the properties of these steels which are required for high temperature applications. The presence of nickel allows usage of the steel at cryogenic temperatures, what will be discussed later [1].

Austenitic stainless steels have many advantages - e.g. they can be sufficiently soft (strength about 200 MPa), and thus can be machined and moulded by conventional processes, on the other hand by cold forming, their strength properties can be increase above 2000 MPa. Their face-centred austenitic cubic structure is tough and plastic up to the cryogenic temperature range. Otherwise, at elevated temperatures, they do not lose their strength properties as fast as iron-based ferrite materials [2]. The disadvantages of these steels may be that they are less resistant to cyclic oxidation than ferritic types of stainless steels because a higher coefficient of thermal expansion results in a flawed breakdown of the protective oxide layer. Furthermore, it is possible to cause corrosion cracking due to use in an environment where the material is not sufficiently resistant. The fatigue range of these materials is lower compared to ferrites. This fatigue limit in combination with a higher coefficient of thermal expansion is the cause of the heat fatigue susceptibility of austenitic stainless steels [3].

Properties of austenitic stainless steels cannot be altering by heat treatment but only by cold plastic deformation. In the annealed state they are fully non-magnetic, but due to cold deformation, some may become slightly magnetic. The base steel of this group is 304, which is also the most widely used [4].

The cold forming process applied on the steel is usually carried out without preheating at room temperature or at slightly elevated temperatures which causes the deformation heat generated during the deformation process. The reasons for the practical use of cold forming are: - small thickness cannot be achieved by hot rolling, - improvement of accuracy of product dimensions (reduction of dimensional tolerances).

It furthermore enhance surface quality by increase of surface smoothness, eliminate undesirable phenomena resulting from heating and heat treatment such as surface decarburization in the case of high carbon steels. Last but not least, the desirable directional anisotropy of the physical and mechanical properties of the formed and then heat-treated material can be achieved by cold forming. Due to the temperatures at which the cold forming is carried out, there is no substitution diffusion of the atoms in the metal lattice, but only diffusion of interstitially dissolved elements with a very small atomic diameter can occur. Therefore, in contrast to hot forming, cold forming is accompanied by the intensive work-hardening of the formed metal [5].

Temperatures below 273K are generally considered to be low temperatures. Working conditions below the freezing point must be counted in the construction, transport, and power sectors of the pipeline. Steels designed under cryogenic conditions were designed for the transport of flowing gases. Last but not

least, it is important to mention the superconductivity of materials, which is secured by temperature conditions below 273K.

In materials deformed at temperatures below 273K, dynamic recovery processes are fully inhibited and lead to accumulation of dislocations. With increasing density of dislocations, their movement is slowed down and concentration is concentrated. This causes the mechanism of plastic deformation is the slip and mechanical twinning, while the main mechanism of conventional plastic deformation is slid of dislocations. With further increase of tension, it is possible to assume that the grain size is refined to the order of nanometres. The grain size is related to the mechanical properties of the materials, what means that by forming under cryogenic conditions it is possible to achieve an increase in the mechanical properties of selected metallic materials [6].

Material and experimental procedure

In the work modified 316LN austenitic stainless was used. The steel was shaped by hot forging followed by heat treatement at 1050°C for 60min fast cooled to room temperature. Samples for this study were cut from the middle of the slab. Chemical composition of the experimental material is listed in Table 1.

Table 1. *Chemical composition of experimental material (wt. %)*

	C	Cr	Ni	Mn	Mo	Si	P	S	V	Ti	Nb	N	B
316LN	0,06	18,76	13,73	1,5	1,87	0,5	0,007	0,003	0,02	0,004	0,02	0,13	<0,001

Two types of experimental unidirectional rolling at were carried out – at room temperature and under cryogenic conditions. Specimens were rolled by about 10% reduction at each pass, and the total deformation was 10%, 30% and 50%. The cryogenic rolling conditions were secured by immersing the specimens to liquid nitrogenous for 30 min. before rolling and for 10 min. after each pass. Dimension of specimens for experimental rolling are: h0 = 11mm, b0 = 41mm, l0 = 80mm.

Static tensile test was carried out by universal testing machine (ATLAS, load capacity 650kN) at three temperatures ranging from 4,2K to 293K. Cryogenic temperatures were secured by the cryostat system inbuilt in Atlas testing machine filled with liquid helium (4,2K) and liquid nitrogenous (77K).

Results and discussion

The engineering stress-strain curves obtained from static tensile test at three different temperatures are shown in Fig.1. The initial state is represented by black colour in each graph. Testing the 316LN stainless steel at room temperature (293K) in initial state before experimental rolling shows: yield strength (YS) = 325 MPa, ultimate tensile strength (UTS) = 641MPa and total elongation (TE) = 48,7 %. Mechanical characteristics obtained for all tests are listed in Table2. It can be said that yield strength and ultimate tensile strength of modified 316LN increase with deformation and the rolling temperature has impact to the final mechanical properties. On the other hand, the total elongation significantly decreases with deformation what is caused by exhaustion of plasticity and increase of the deformation resistance of material during experimental rolling. Therefore after rolling process, the heat treatment should be done.

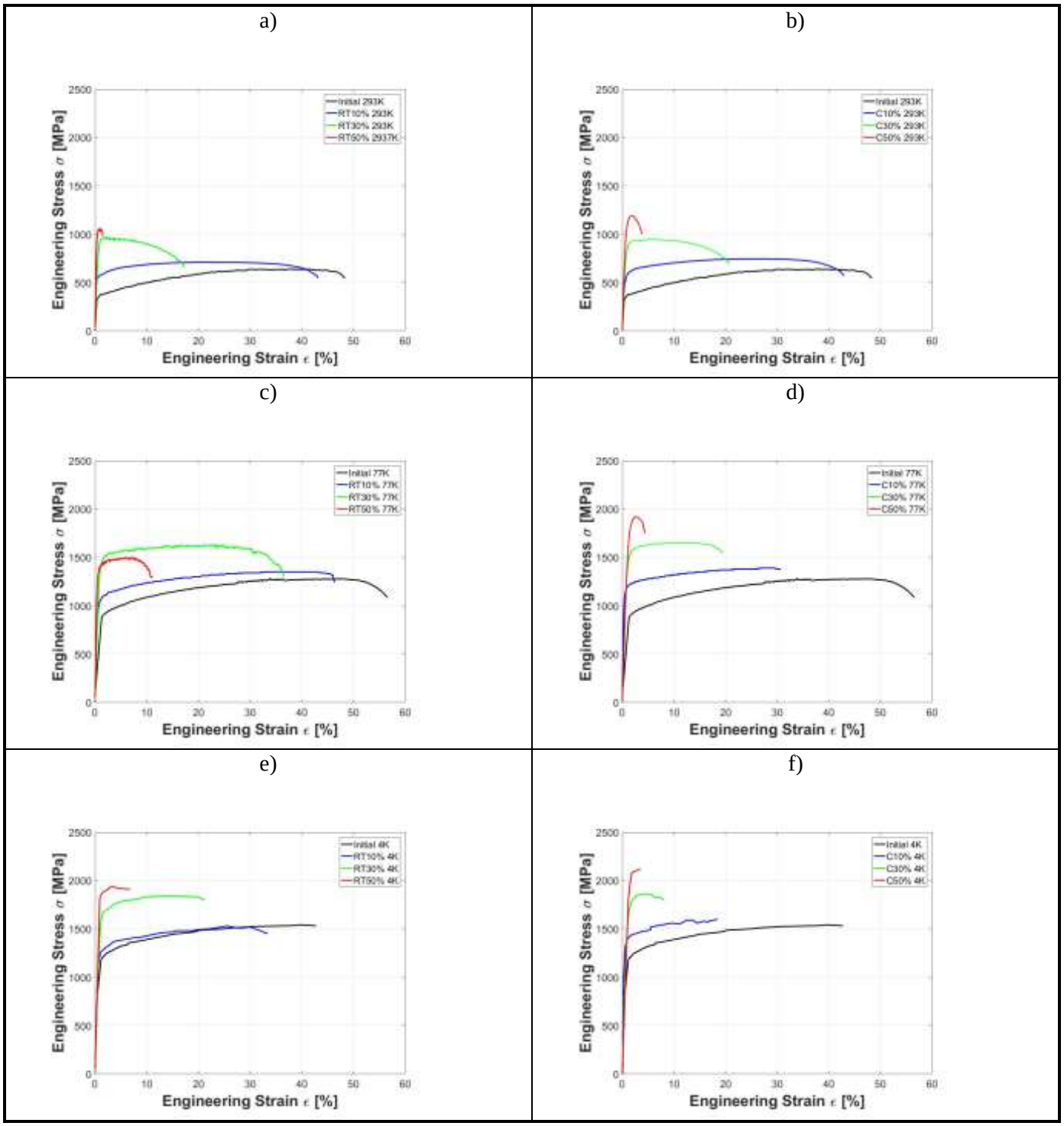

Figure 1 Stress-strain curves – static tensile test of rolled 316LN at different temperature: a) ambiet rolling – tensile test at 293, b) cryorolling – tensile test at 293K, c) ambient rolling – tensile test at 77K, d) cryorolling – tensile test at 77K, e) ambient rolling – tensile test at 4,2K, f) cryorolling – tensile test at 4,2K

The hypothesis that by cryogenic rolling higher mechanical properties will be achieved have not been confirmed. At 77K tensile test showed that after ambient rolling with total deformation 30% the mechanical properties are higher. To understand the reason further investigation is required combining differential scanning calorimetric measurement, microstructure observation, hardness testing, and so on.

Table 2. *Static tensile test results*

Tensile test temperature	RT (room temperature)				CT (cryo temperature)			
	ε [%]	**YS [MPa]**	**UTS [MPa]**	**TE [MPa]**	**ε [%]**	**YS [MPa]**	**UTS [MPa]**	**TE [MPa]**
293K	**0**	325.0	641	48.7	**0**	325	641	48.7
	10	493	701	30.7	**10**	476	749.1	36
	30	823	967.4	11	**30**	773	960	17
	50	1010	1060.4	0.8	**50**	947	1192	3
77K	**0**	790.0	1282	56.6	**0**	790	1282	56.6
	10	993	1300	52	**10**	1052.3	1374.6	30
	30	1349	1627.7	26	**30**	1304	1601	14
	50	1297.1	1507.1	11.2	**50**	1571.3	1880.4	3
4,2K	**0**	1070.0	1543	45.2	**0**	1070	1543	45.2
	10	1195.8	1538.8	34.1	**10**	1319.9	1543.1	10
	30	1453.6	1768.2	12	**30**	1672	1887	7
	50	1755.6	1940.9	7.4	**50**	1804	2081	2.2

Conclusion

On the base of results achieved by the performed experiment, the following conclusions can be formulated:

- With higher deformation and decreasing test temperature, the yield strength and ultimate tensile strength increase, while plasticity is significantly decreases.
- The austenitic stainless steel can be strongly reinforced by plastic deformation under cryogenic conditions.
- In order to preserve plasticity of the final material, additional heat treatment is required. But there are are applications where the high strength is required without any need for plastic properties. Such strong materials can be prepared by rolling under cryogenic conditions.

References

[1] Barna R. et al.: Effect of cryorolling on the microstructure and tensile properties of bulk nano-austenitic stainless steel. Materials Science and Engineering A, Vol. 631, 2015, p. 241-247

[2] Ravi K. et al.: Enhancement of mechanical properties of low stacking energy brass processed by cryorolling followed by short-annealing. Materials and Design, Vol. 67, p.637-643

[3] Mizera J., Wyrzykowski J. W.: An Analysis of the Effect of Twin Boundaries on Mechanical Properties of Austenitic Steel.Materials Science and Engineering A, Vol. 112, 1989, p. 39-42

[4] Yueling Guo et al.: Effects of forging and heat treatments on the microstructure and oxidation behavior of 316LN stainless steel in high temperature water. Journal of Materials Science and Technology, Vol. 31, 2015, p. 403-412

[5] Sas J. el al.: The mechanical and material properties of 316LN austenitic stainless steel for the fusion application in cryogenic temperatures. IOP Conf. Series: Materials Science and Engineering, Vol. 102, 2015

[6] Kvačkaj, T. et. al.: Influence of anealing conditions on structural development of cryo rolled FeSi Steel. Acta physica polonica, Vol. 126

Research and development of new thermoelectric materials

Miloš Fejerčák[1,2], Michaela Šuliková[2], Katarína Šuľová[1,3], Zuzana Molčanová[1], Viktor Puchý[1], Martin Fides[1,3], Ondrej Milkovič[1], Katarína Ďurišinová[1], Peter Baláž[4], Matej Baláž[4], Karel Saksl[1,2]

[1] *Institute of Materials Research, Slovak Academy of Sciences, Košice Slovak republic*
[2] *Faculty of Sciences, Institute of Physics, P.J. Šafárik University, Košice, Slovak Republic*[3] *Faculty of Metallurgy, Materials and Recycling, Technical University of Košice, Košice, Slovak Republic*
[4] *Institute of Geotechnics of Slovak Academy of Sciences, Košice Slovak republic*
milos.fejercak@gmail.com

Introduction

Statistical results show that more than 60% of the energy produced worldwide is largely lost in the form of waste heat. Thermoelectric materials have a remarkable ability to transform heat directly and reversibly into electrical energy [1]. The advantages of thermoelectric devices include the absence of moving parts, reliability, durability, quiet operation and the fact that they do not produce any polluting emissions, so they can be used in a wide range of applications and are also attractive from an environmental point of view. The thermoelectric efficiency of the material denotes a dimensionless variable *ZT* defined as

$$ZT = \frac{\alpha^2 \sigma}{\kappa} T \qquad (1)$$

where α is the Seebeck coefficient, σ the electrical conductivity, T is the absolute temperature (working temperature) and κ the thermal conductivity of the material (Figure 6.). From the equation 1 is clear that for enhancement of *ZT* we must increase Seebeck coefficient and electrical conductivity. On the other hand, we need to lover thermal conductivity. Unfortunately, all three parameters are strongly correlated, dependent on number of free carriers, therefore increase of power factor ($\alpha^2 \sigma$) often leads to simultaneous increase of κ and resulting *ZT* is the same, if not even worse. There are few approaches to overcome this problem nowadays. Most of the research groups are focusing on reduction of the thermal conductivity of the material by effective scattering of the phonons (lattice vibrations). This can be achieved by doping matrix with appropriate elements, alloying or nano-structuring. Also, material preparation method plays an important role [2].

Thermoelectric Effects

There are three major thermoelectric effects: *Seebeck effect*, *Peltier effect* and *Thomson effect*. Seebeck effect is manifest as an electromotive force (EMF) or voltage, *V*, which appears when the junction between two dissimilar conductors (P-type and N-type) is heated. Strictly speaking, the effect depends on the temperature difference, ΔT, between the two junctions that are needed to complete the electrical circuit. The Seebeck coefficient is defined as

$$\alpha = \frac{V}{\Delta T} \qquad (2)$$

Although the effect occurs only when there is a junction between two materials, the schematics of Seebeck effect is shown in Fig. 1. A closely related, reverse, effect was discovered in 1834 by Jean Peltier. Peltier heating or cooling occurs when an electric current, I, flows through the junction between two conductors. The Peltier coefficient, π_{AB}, is defined as

$$\pi_{AB} = \frac{q}{I} \qquad (3)$$

where q is rate of heating or cooling. It is rather more difficult to demonstrate the Peltier effect than the Seebeck effect. If the thermocouple branches are metallic, the reversible Peltier effect is usually overshadowed by irreversible Joule heating. Thus, unless the electric current is very small, the best that can

be done is to show that the overall heating is less for the current flow in one direction rather than the other, what is known as Thomson effect [3].

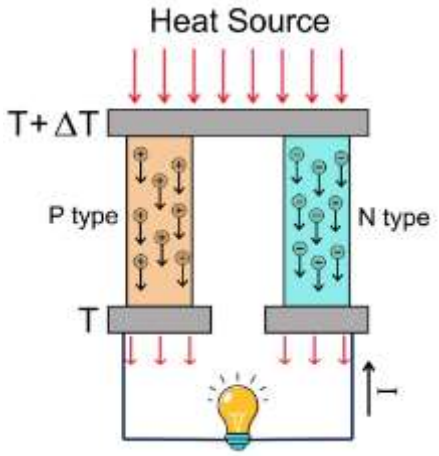

Figure 1 Thermoelectric couple. Demonstration of Seebeck effect

Thermoelectrics of Today

One of the first thermoelectric devices was "Candle radio!" sold around 1990, using iron silicide ($FeSi_2$) thermo-elements produced at KELK Ltd [4]. Since that, thermoelectric research comes through big development. Very known are thermoelectric radioisotope generators (SiGe generators using Po decomposition) powering space probes like Voyager and Pioneer. Because in deep space there is not enough sun light, thermoelectricity is the very last power source. Today are often used Peltier thermoelectric coolers (e.g. TEC 12706 based of BiTe) in applications like refrigerators, temperature stabilizers, or you can simply charge your smartphone with a tea candle. Disadvantage of all these thermoelectric devices is that they are composed of toxic neither radioactive elements, best ZT have at high temperature and are not cheap. Global thermoelectric goal is to produce cheap materials with low working temperature, composed of earth abundant and non-toxic elements. One can simply realize that this is hard to achieve and most of the thermoelectric groups are pursuing highest ZT values by using complicated materials. Fig. 2 a) shows the various materials used in thermoelectric research and development and their individual contribution and 2 b) they comparison with various energy conversion technologies [5].

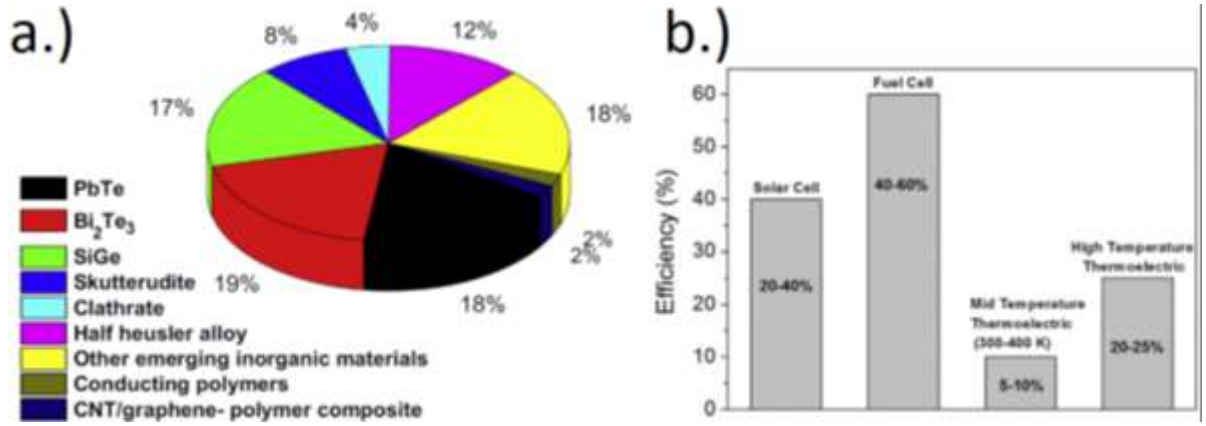

Figure 2 a) Materials used in thermoelectric research and development. **b)** Schematic represents the global energy conversion (in%) by various technologies [5]

It is clear that thermoelectric materials start challenging solar cells and with ZT parameter higher than 2.5 they will be more effective [5].

Preparation Methods

Preparation methods plays a big role in thermoelectric material desing. Researchers often have to chose best preparation method for each material, because one and the same material has different thermoelectric parameters if it is prepared by different method (mostly they are limited by their lab equipment). Fig. 3 a) shows yearly publications related to thermoelectric materials processed by different methods and also rising interest in thermoelectric research in past 15 years related to number of publications [6]. In Fig. 3 b) is demonstrated phonon scattering in thermoelectric material and electronic transport of hot and cold electrons. One can see that phonons are mostly scattered on grain boundaries and nanoparticles. Effective phonon scattering in material leads to decreasing the thermal conductivity κ and therefore to higher ZT. Novel approaches in thermoelectric research in last years shows that, nanostructuring (by e.g. ball milling) and doping wih appropriate materials are best ways for ZT enhancement [7].

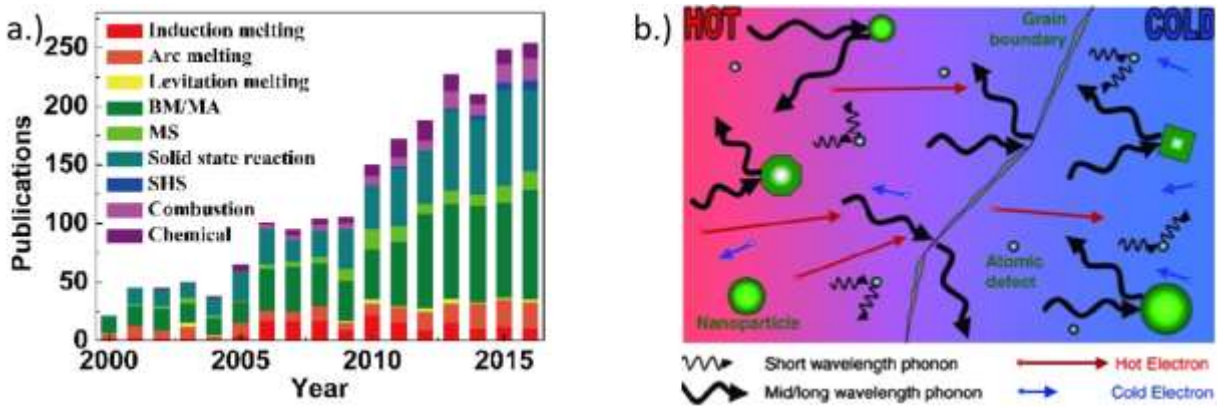

Figure 3 a) Yearly publications related to thermoelectric materials processed by different methods [6]. **b)** Schematic diagram illustrating phonon scattering mechanisms and electronic transport of hot and cold electrons within a thermoelectric material [7]

Experimental

In our research we focus on the Half-Heusler (HH) system $Zr_{0,25}Hf_{0,25}Ti_{0,5}Ni1Sn_{0,998}Sb_{0,002}$ for a first time presented by Sakurada in 2005 [8]. This HH compound exhibit ZT peak 1.5 located at ~400 °C, temperature suitable for low temperature applications. ZT curves of different HHs are shown on the Fig. 4. In order to improve already high ZT parameter of the $Zr_{0,25}Hf_{0,25}Ti_{0,5}Ni1Sn_{0,998}Sb_{0,002}$ compound we have combine it with 2 and 5 wt. % of β-$FeSi_2$ system, which is long known as good thermoelectric material for ambient temperature applications (e.g. thermoelectric radio powered by candle in 1990). We hoped that, small additions of low thermal conductive β-$FeSi_2$ will improve phonon waves dissipation (scattering) leading to further reduction of thermal conductivity in our investigated HH system.

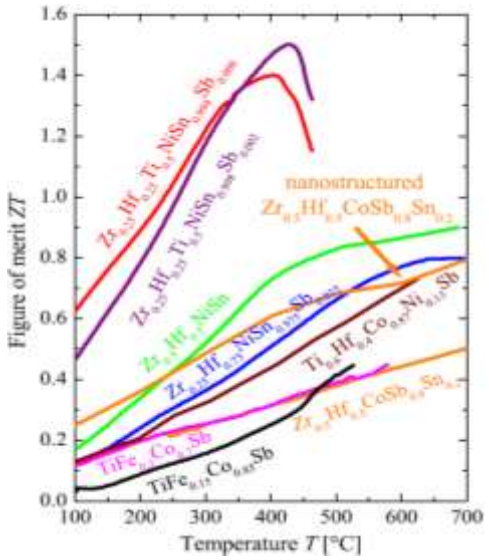

Figure 4 State-of-the-art thermoelectric figure of merit of half-Heusler materials [9]

Sample preparation

The $Zr_{0,25}Hf_{0,25}Ti_{0,5}Ni1Sn_{0,998}Sb_{0,002}$ HH compound was prepared by arc melting of pure elements in the Compact Arc Melter MAM-1 (from Edmund Bühler GmbH). Titanium granules (99.99% from Alfa Aesar), Zirconium lump (99.8% from Alfa Aesar), Hafnium chips (99.8% from MaTecK), Nickel powder (99.999% from Sigma Aldrich), Tin rod (99.9%), and Antimony metal shot (99.999% from Alfa Aesar) were properly weighted and mixed in one charge. Such charge was arc-melted under argon atmosphere (50 kPa). Each charge was remelted at least three times to ensure chemical homogeneity over the whole compound volume. The alloy was milled together with addition of β-$FeSi_2$ to fine powder in planetary mono mill PULVERISETTE 6. Milling parameters were: 2x30 minutes milling at 600 RPM, with 30 minutes break in between to cool tungsten carbide bowl containing charge and tungsten carbide balls. Resulting fine powder was filled in Ar glow bag to 20 mm diameter graphite mold. Sintering of powders was carried at load 16 kN and temperature 1473 K for 10 minutes in spark plasma sintering (SPS) machine, model HP D10-SD under nitrogen atmosphere. Parameters of SPS compaction are shown on Fig. 5a) Compaction was done.

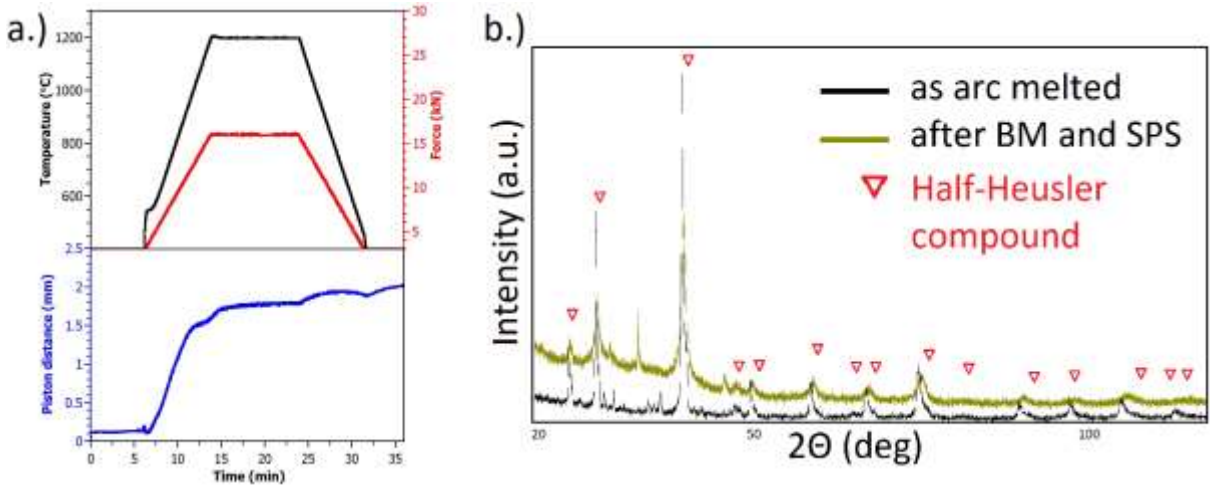

Figure 5 a) SPS curvers of sintering process for nano Half-Heusler Compound + 5 wt β-FeSi2%. **b)** X-ray diffraction patterns of the $Zr_{0,25}Hf_{0,25}Ti_{0,5}Ni1Sn_{0,998}Sb_{0,002}$ (black) and $Zr_{0,25}Hf_{0,25}Ti_{0,5}Ni1Sn_{0,998}Sb_{0,002}$ + 5 wt% β-$FeSi_2$ (brown)

Sample Characterization

Phase composition of the samples was determined by X-ray diffraction using Cu Kα radiation at X-Ray Diffractometer Phillips X´Pert Pro. XRD patterns of arc melted $Zr_{0,25}Hf_{0,25}Ti_{0,5}Ni1Sn_{0,998}Sb_{0,002}$ (black) and the milled (with extra added 5 wt. % of β-$FeSi_2$) (green) are shown together on Figure 5.b.). One can see that sample after milling exhibit significant Bragg's peak broadening. In order to observe microstructure of sintered material, samples were etched for 1 second in diluted 1:3 Kroll etchant followed by rinsing in ethanol. After it sample surface morphology was observed at Light Microscope Olympus GX71, where record good homogeneity and almost no pores. Photos from LM are shown in Fig. 6 a). To confirm chemical composition of our samples we used microanalysis EDX system of the Scanning Electron Microscope, SEM JEOL JSM 7000F. We observed good sample homogeneity, with some cracks (samples were just 0.5 mm thick) and some pores on the edges of the pellets (SPS process is denser in the middle of the compact, where most of Joule temperature is generated). SEM images are shown in Fig. 6 b), c). Element chemical composition is not in good agreement with our origin composition, due the fact, that Hafnium has strong absorption edge L_3 at 9,65 kV, so that means when other elements like: Fe, Ni, Si, have K edges under 9,65 kV, they will be invincible for used e.g. 10 kV accelerating voltage (10 kV is standard voltage for SEM). Micro-hardness of the samples was measured by Wilson Tukon 1102 & 1202 Micro Hardness tester equipped by Vicker indentor. Average microhardness of the alloys is ~1000 HV0.1.

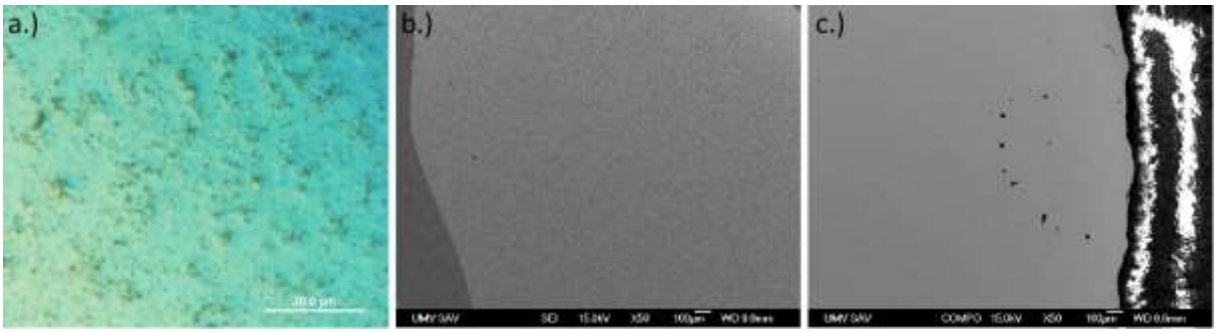

Figure 6 a) Light Microscopy of sample surface, with polarization filter. **b) c)** SEM image of HH sample with extra added 5 wt% β-$FeSi_2$. b.) Sample surface on left edge in SE mode. c.) Sample surface on right edge in BSE mode

Conclusions

In this work we prepared and characterized two Half-Heusler thermoelectric compounds $Zr_{0,25}Hf_{0,25}Ti_{0,5}Ni1Sn_{0,998}Sb_{0,002}$ doped with 2 and 5 wt % β - $FeSi_2$. Both compounds are homogenous, exhibits high microhardness and consists from one Half-Heusler phase. Further research on these alloys will follow.

Acknowledgement

This work was supported by the Slovak Research and Development Agency under the contract No. APVV-15-0202. Miloš Fejerčák and Karel Saksl are grateful to the Scientific Grant Agency of the Ministry of Education, Science, Research and Sport of the Slovak Republic and the Slovak Academy of Sciences (APVV-15-0202). This work was realized within the frame of the project „Research Centre of Advanced Materials and Technologies for Recent and Future Applications „PROMATECH“, ITMS 26220220186, supported by the Operational Program “Research and Development” financed through European Regional Development Fund. Special acknowledgment is to prof Peter Baláž and Matej Baláž from Institute of Geotechnics SAS for using planetary ball mill.

References

[1] Zhang X. and Zhao L. D.: Thermoelectric materials: Energy conversion between heat and electricity. J. Mater., 2015, vol. 1, no. 2, pp. 92–105
[2] Rull-Bravo M. et al.: Skutterudites as thermoelectric materials: revisited. RSC Adv., 2015, vol. 5, no. 52, pp. 41653–41667
[3] Goldsmid H. J.: The Seebeck and Peltier effects. Phys. Thermoelectr. Energy Convers., 2017.
[4] “www.kelk.co.jpenglishusefulnetsuden3.html” .
[5] Gayner C. and Kar K. K.: Recent advances in thermoelectric materials. Prog. Mater. Sci., 2016, vol. 83, pp. 330–382
[6] Li J. F. et al.: Processing of advanced thermoelectric materials. Sci. China Technol. Sci., 2017, vol. 60, no. 9, pp. 1347–1364
[7] Chen Z. G. et al.: Nanostructured thermoelectric materials: Current research and future challenge. Prog. Nat. Sci. Mater. Int., 2012, vol. 22, no. 6, pp. 535–549
[8] Shutoh N. and Sakurada S.: Thermoelectric properties of the TiX(Zr0.5Hf0.5)1 - XNiSn half-Heusler compounds. J. Alloys Compd., 2005, vol. 389, no. 1–2, pp. 204–208
[9] Casper F. et al.: Half-Heusler compounds: Novel materials for energy and spintronic applications. Semicond. Sci. Technol., 2012, vol. 27, no. 6

Molecular identification and data processing in phylogenetic study of extreme acidophiles from metal-rich environments

Lenka Hagarová, Daniel Kupka

Institute of Geotechnics, Slovak Academy of Sciences, Watsonova 45, 040 01 Košice, Slovak Republic, hagarova@saske.sk, dankup@saske.sk

Introduction

Extreme acidophiles belong to the big group of bacteria called acidophilic microorganisms (mostly prokaryotes). These specialized bacteria are able to grow in acidic environments optimally at pH < 3. Acidic environments may occur naturally (vulcanic, geothermal areas) or as a result of human activities, the most important of which is mining of metals and coal. Number of acidophiles cannot be cultivated *in vitro*, however, some of significant microorganisms such as acidophilic iron and sulfur oxidizing chemolitotrophs can be cultivated in synthetic liquid as well as on solid media [1]. Careless handling of specimens may cause contamination of the culture media and for that reason it is necessary to check the purity of maintained bacterial cultures.

Biodiversity of extreme acidophiles can be described and characterized by various traditional techniques (pour plate and spread plate method, Gram's staining, biochemical tests, microscopy-based approaches using light, electron microscopy, phase contrast microscopy), but the disadvantages of these methods are insufficient precision for identification, time-consuming as well as dependence upon many environmental factors [2]. Utilization of molecular techniques has brought a new view on identification and taxonomic classification in environmental microbiology. In general, this article deals with some of the most common DNA-based techniques and data processing for bacterial typing applied to the detection, identification and phylogenetic study of extreme acidophilic microorganisms. The results mentioned in this contribution are obtained from the examination of acidophilic heterotrophic bacteria *Acidiphilium* SJH.

DNA Isolation and Polymerase Chain Reaction (PCR)

The first requirement for work with these techniques is the isolation of pure DNA from bacterial cultures or various environmental matrices. There are many traditional DNA extraction methods e.g. phenol/chloroform/isoamyl alcohol extraction or specialized DNA extraction kits, which use patented inhibitor removal technology for isolation of DNA with highest level of purity. To ensure their effectivity, contaminants and other impurities (e.g. heavy metals, inhibitors), have to be removed from media prior the test.

Discovery of PCR by Mullis and Faloona [3] represents important milestone in biology. PCR is promising technique of rapid detection of bacteria, which allows amplification of nucleic acids, making a huge amount of copies of target sequence using DNA polymerase enzyme and a specific pair of DNA primers (forward and reverse primers, oligonucleotides with a length of usually about 20 nucleotides). The target DNA sequence (usually fewer than 3000 bp) can be amplified (by ca 30 cycles of denaturing, annealing and extension) about a million-fold. The reaction usually takes place in the thermal cycler with the reaction volume of 10–200 μL.

Application of 16S rRNA

The comparison of rRNA sequence is a powerful tool for deducing phylogenetic and evolutionary relationships among prokaryotic and eukaryotic organisms. Different types of rRNA sequences that are stably inherited, informative and easy detectable are used to mark particular genotypes. A molecular marker can be a single gene (e.g. 16S rRNA gene), a group of genes (e.g. number of housekeeping genes), a set of sequence repeats or restriction sites as well as a single nucleotide that exists in several polymorphic states in different bacteria [4]. There are several specific gene markers sufficient for determination of phylogenetic lines of microorganisms like: 16S rRNA, gyrB, rpoA, rpoB, rpoC, rpoD etc. [5]. 16S rRNA

gene is the molecular marker used commonly in modern bacterial identification and taxonomy for number of reasons: a) it can be found in all species of organisms where performs the same function, b) its sequence is sufficiently conserved and contains regions of conserved, variable and hypervariable sequence, c) its size (ca.1500 bp) is sufficient for relatively easy sequencing and contains sufficient information for identification and phylogenetic analysis [6].

DNA sequencing and phylogenetic analysis

DNA sequencing represents a method, by which the exact order of nucleotides in polynucleotide chains can be obtained. These polynucleotide chains contain the information for hereditary and biochemical properties of terrestrial life. One of the traditional techniques of sequencing, which has been still improved and more automated, is Sanger method. Synthesis of complementary DNA strands is ensured by the presence of polymerases, mixture of standard nucleotides as well as terminal labeled nucleotides, whereby the fragments of DNA with different lengths are created. After incorporation of terminal nucleotides into the DNA chain, further elongation of the complementary strand is prevented. Taking into account that this reaction is in progress with a lot of identical templates simultaneously, all possible DNA fragments are arising. The observed DNA chain is determined by ordering of obtained fragments according to their length and pursuant to fluorescent signal from terminal nucleotide.

After sequencing of 16S rDNA gene, the next step is performing of a phylogenetic analysis. The key of bacteria correct classification is the comparison of the obtained gene sequence with other sequences of organisms classified until now. There are plenty of 16S rRNA sequences in available databases such as NCBI (GenBank) and secondary dedicated databases (e.g. EzTaxon, SILVA). At GenBank the basic local alignment searching tool BLAST is used for comparison of a new sequence. If the sequence similarity between two microorganisms is more than 95% they probably belong to the same genus [7]. When the compared gene sequences share ca. 98% of identity it can be said that they probably belong to the same species. The currently accepted definition of species in microbiology requires that the strains share more than 70% global DNA similarity (from DNA-DNA hybridization analysis) and have less than 5% difference at their genomic DNA melting temperatures [8].

For example, after detection of the differences in chromosomal GC content and 16S rRNA gene sequence of isolate *Acidithiobacillus ferrooxidans*, it has been considered that this acidophile contains more than one species. Using the sequences of the 16S-23S intergenic spacers (ITS) the phylogenetic heterogeneity was determined and despite of 98,5% 16S rRNA identity two main groups have been identified - the strain of *Acidithiobacillus ferrooxidans* and the new species *Acidithiobacillus ferrivorans* [9]. *Acidiphilium* SJH (NCIMB 12826) belongs to a group of extreme acidophiles that are widely distributed in metal-rich, acidic environments. This iron reducing bacterium is able to reduce ferric iron Fe(III) to ferrous iron Fe(II) and was isolated from highly acidic mine drainage water in Scotland. The methods mentioned above were applied to the identification and taxonomic assigning of this bacterium.

Materials and methods

The *Acidiphilium* SJH (NCIMB 12826) isolate used in the study was obtained as a gift from Dr. Barrie Johnson (University of Wales, Bangor, UK). The bacterium was grown aerobically in an acidic medium, that contained (per liter) tryptic soy broth (0.25 g), glucosum (1.8 g), $(NH_4)_2SO_4$ (12.5 g), $MgSO_4 \cdot 7H_2O$ (5 g) and solution of trace elements (1 mL). Bacteria obtained from 100 ml of 48 hours culture were collected by centrifugation and then phenol/chloroform/isoamyl alcohol extraction was used for isolation of chromosomal DNA [10]. The isolated DNA was used as a template for amplification of 16S rDNA with universal primers 0028F and 1521R [11]. PCR products were checked by agarose electrophoresis gel and purified PCR amplicons were sequenced. The obtained sequence was compared against GenBank database using local sequence alignment (blastn algorithm) and against EzTaxon database using robust global pairwise sequence alignment process. The 16S sequences showing highest similarity in EzTaxon database were downloaded and multiple sequence alignments were constructed using MEGA software. The phylogenetic relatedness of the sequences was assessed using Neighbor-Joining algorithm implemented in MEGA software.

Results and Discussion

Using procedures described above the DNA with high quality was isolated from the investigated bacterial sample (not shown). Using universal PCR primers nearly full length of 16S rRNA gene was amplified (Fig. 1).

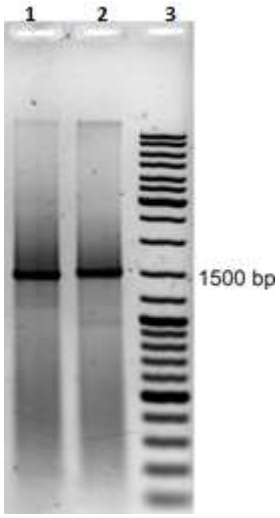

Figure 1 16S rDNA PCR products on 1% agarose gel (1,2-*Acidiphilium* SJH, 3-ladder)

The nucleotide sequences of obtained PCR products were determined by Sanger's dideoxy termination method at the Institute of Microbiology of the ASCR, v.v.i. Obtained nucleotide sequences of 16S rDNA of *Acidiphilium* SJH were compared with nucleotide sequences present in the NCBI database using BLAST® (http://blast.ncbi.nlm.nih.gov/Blast.cgi/). The highest similarity values – over 99% were observed for the group of *Acidiphilium* species (*Acidiphilium multivorum, Acidiphilium cryptum* and *Acidiphilium organovorum*, data not shown). The result of 16S rDNA sequencing was also compared with data from EzTaxon database, which is directly used for identification of prokaryotes pursuant to 16S rRNA (Table 1).

Similar to the GenBank database very high similarity values were observed for the group of *Acidiphilium* species. For *Acidiphilium multivorum* and *Acidiphilium cryptum* 100% identity was observed. Multiple sequence alignment confirmed phylogenetic placement of SJH isolate (Fig. 2).

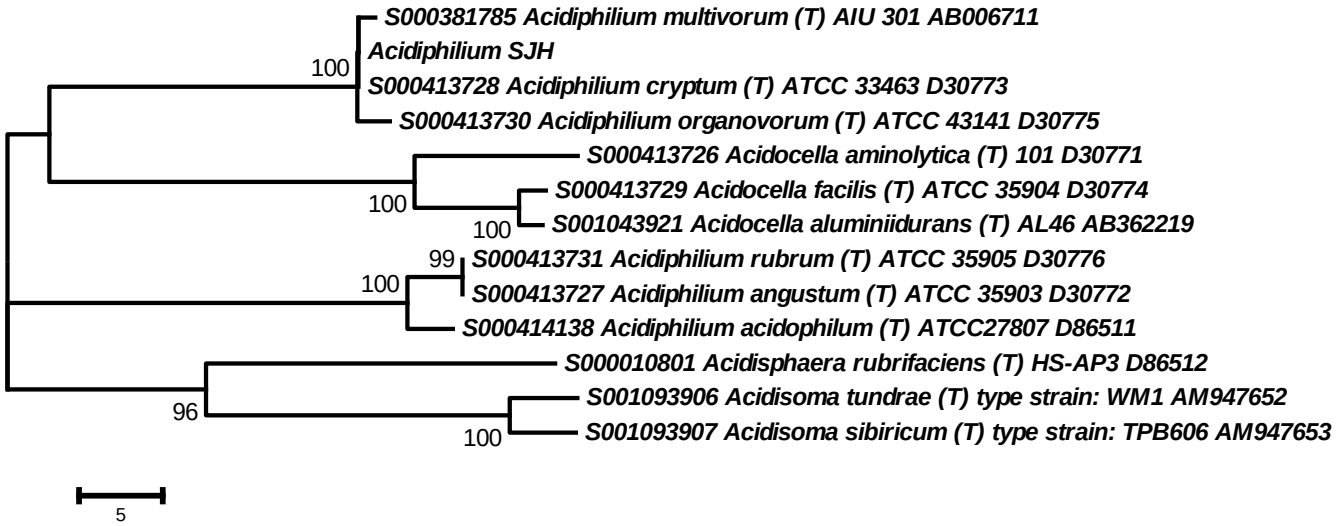

Figure 2 Neighbor-Joining phylogenetic tree showing relationship between *Acidiphilium* SJH and other acidophilic bacteria

Table 2 *Output of 16S rDNA comparison of Acidiphilium SJH with EzTaxon database*

Rank	Name	Strain	Authors	Taxonomy	Accession	Pairwise Similarity (%)	Diff/Total nt	Completeness (%)
1	Acidiphilium multivorum	AIU301(T)	Wakao et al. 1995	Bacteria; Proteobacteria; Alphaproteobacteria; Rhodospirillales; Acetobacteraceae; Acidiphilium	AP012035	100.00	0/870	100
2	Acidiphilium cryptum	ATCC 33463(T)	Harrison 1981	Bacteria; Proteobacteria; Alphaproteobacteria; Rhodospirillales; Acetobacteraceae; Acidiphilium	D30773	100.00	0/870	100
3	Acidiphilium organovorum	ATCC 43141(T)	Lobos et al. 1986	Bacteria; Proteobacteria; Alphaproteobacteria; Rhodospirillales; Acetobacteraceae; Acidiphilium	D30775	99.77	2/870	100

All phylogenetic comparisons indicated that the 16S rRNA sequence of *Acidiphilium* SJH shows considerable homology with other three species of *Acidiphilium* genus, particularly *Acidiphilium cryptum*, *Acidiphilium multivorum a Acidiphilium organovorum*. Although the SJH isolate falls into this *"Acidiphilium cryptum* cluster" [12] its true phylogenetic placement cannot be established, as this group of species cannot be distinguished using 16S rRNA sequences and for the differentiation of species other molecular markers are used.

Acidiphilium is a genus of acidophilic dissimilatory iron-reducing proteobacteria, which are frequently detected in a variety of "extreme" low-pH and heavy-metal contaminated habitats where Fe(III) reduction is taking place, and may represent a significant proportion of metal-transforming organisms in these environments. These bacteria are found worldwide. While *A.* SJH isolate was isolated from an abandoned pyrite mine in North Wales [13], iron-respiring bacteria *A. cryptum* was found directly in coal refuse as well as like contaminant in cultures of *A. ferrooxidans* isolated from coal mine drainage and from a copper ore leaching site [14]. Isolation of ferric iron reducing bacteria *A. organovorum* was firstly performed from *Thiobacillus ferrooxidans* culture [15] and at least but not last *A. multivorum* was detected in acid mine drainage from abandoned Matsuo sulphur-pyrite mine area in Iwate Prefecture [16].

Conclusions

Reliable identification of microorganisms requires the use of modern molecular techniques based on DNA sequencing. The resolution possible from comparative analysis of 16S rRNA gene sequences is to the species level, providing in many case the phylogenetic neighborhood and only tentative identification. Sequencing of the other gene regions or whole genome is often necessary. *A.* SJH isolate was identified as a member of *A. cryptum* group. However, for detailed classification of *A.* SJH isolate another analysis has to be performed as members of *A. cryptum* group cannot be distinguished using 16S rRNA sequences.

Aknowledgement

The authors would like to thank to the Slovak Grant Agency VEGA, project No 2/0145/15, and the Operational Programme Research and Development through the project: Centre of Excellence for Integrated Research of the Earth's Geosphere (ITMS: 26220120064).

References

[1] Johnson D. B., Okibe N., Hallberg, K. B.: Differentiation and identification of iron-oxidizing acidophilic bacteria using cultivation techniques and amplified ribosomal DNA restriction enzyme analysis. Journal of Microbiological methods, 60, 2005, 299-313

[2] Rawlings D. E., Johnson D. B.: Biomining. Heidelberg: Springer-Verlag, 2007, 314 pp

[3] Mullis K. B., Faloona F. A.: Specific synthesis of DNA in vitro via a polymerase-catalyzed chain reaction. Meth Enzymol., 155, 1987, 335-350

[4] Nunez H. et. al.: Detection, identification and typing of Acidithiobacillus species and strains: a review. Research in Microbiology, 167, 2016, 555-567

[5] Glazunova O. O., Raould D., Roux V.: Partial sequence comparison of the rpoB, soda, groEL and gyrB genes within the genus Streptococcus. Int. J. Syst. Evol. Microbiol., 59, 2009, 2317-2322

[6] Clarridge III, J. E.: Impact of 16S rRNA gene sequence analysis for identification of bacteria on clinical microbiology and infectious diseases. Clin. Microbiol. Rev., 17, 2004, 840-862

[7] Stackebrandt E., Goebel B. M.: Taxonomic Note: A Place for DNA-DNA Reassociation and 16S rRNA Sequence Analysis in the Present Species Definition in Bacteriology. Int. J. Syst. Bacteriol., 44, 1994, 846-849

[8] Goris J. et al.: DNA-DNA hybridization values and their relationship to whole-genome sequence similarities. Int J Syst Evol Microbiol, 57, 2007, 81-91

[9] Hallberg K. B. et al.: Physiological and phylogenetic heterogeneity among iron-oxidizing Acidithiobacillus spp., and characteristics of novel species Acidithiobacillus ferrivorans. Advanced Materials Research., 71-73, 2009, 167-170

[10] Sambrook J., Russell D. W.: Molecular cloning: a laboratory manual. Cold Spring Harbor, New York: Cold Spring Harbor Laboratory Press. 2001

[11] Zeng X. et al.: Isolation, characterization and extraction of mer gene of Hg^{2+} resisting strain D_2. Trans. Nonferrous Met. Soc. China., 20, 2010, 507-512

[12] Johnson D. B., McGinness S.: Ferric iron reduction by acidophilic heterotrophic bacteria. Applied and Environmental Microbiology., 57, 1991, 207-211

[13] Bridge T. A. M., Johnson D. B.: Reductive dissolution of ferric iron minerals by Acidiphilium SJH. Geomicrobiology Journal, 17, 2000, 193-206

[14] Harrison A. P. J.: The acidophilic thiobacilli and other acidophilic bacteria that share their habitat. Annu. Rev. Micro-biol. 38, 265–292

[15] Lobos J. H. et al.: Acidiphilium organovorum sp. Nov., an Acidophilic Heterotroph Isolated from a Thiobacillus ferrooxidans Culture. Int. J. Syst. Bacteriol., 36, 1986, 139-144

[16] Wakao N et. al.: Acidiphilium miltivorum sp. Nov., an acidophilic chemoorganotrophic bacterium from pyritic acid mine drainage. J. Gen. Appl. Microbiol., 40, 1994, 143-159

Preparation and characterization of GdBCO bulk superconductors

Petra Hajdová, Pavel Diko

Institute of Experimental Physics, Slovak Academy of Sciences, Watsonova 47, 040 01 Košice, Slovakia
hajdova@saske.sk, dikos@saske.sk

Abstract

In this study, we prepared $GdBa_2Cu_3O_{7-\delta}$ single-grain bulks with addition of silver via the top-seeded melt growth method in air with different temperature profile and only the best sample was analyzed. The particles morphology was observed by the scanning electron microscope. The magnetic measurements of superconducting properties (critical temperature, T_c and critical current density, J_c) were performed by a vibrating sample magnetometer. T_c and J_c measurements were carried out on the specimens taken from two different locations of the same crystal plane.

Introduction

High-temperature LRE-Ba-Cu-O superconductors, where LRE is a light rare earth element such as Nd, Sm, Eu, Gd, fabricated in the form of large single-grain have significant potential for high-field industrial applications due to their high critical current density (J_c) and critical temperature (T_c) [1]. Unfortunately, REBCO bulk superconductors are known to have relatively poor mechanical properties, therefore silver is an established additive for improving these properties through suppression of the crack formation [2]. Moreover, magnetic properties (such as J_c) are strongly dependent on the microstructure of the sample. The important microstructural components of these superconductors are particles of RE_2BaCuO_5 (RE211) phase [3]. It had been found that CeO_2 and Pt dopants refine the size of RE211 particles trapped in the RE123 phase matrix, which act as an effective flux pinning centres [4, 5].
The growth of large LREBCO single-grains in air with homogenous superconducting properties is difficult for LRE-Ba substitution, where the LRE element substitutes on the Ba-site ($LRE_xBa_{2-x}Cu_3O_{7-\delta}$) [6]. LRE-Ba substitution lowers T_c value and broaders the transition to the superconducting state, but it can be suppressed by addition of barium-rich compounds (e.g. BaO_2) or crystal growth under reduced partial pressure.

Experimental materials and methods

Commercially available powders were used to fabricate of Gd-123 bulk single-grains with Ag addition. Nominal composition of prepared precursor powder was *1 mol.* $GdBa_2Cu_3O_{7-\delta}$ (Gd123)+ *½ mol.* Gd_2BaCuO_5 (Gd211) + *20 wt. %* Ag_2O + *0.2 wt. %* $PtO_2{\cdot}H_2O$. Precursor powder together with the seed was uniaxially pressed into the 50 gram cylindrical pellets of 32 mm in diameter. The thin film seed consists of NdBCO of thickness 700 nm deposited on a single crystal MgO-substrate.

The top-seeded melt growth method with different temperature profiles was used to fabricate the bulk single-grain crystals in air. The pellets were heated up to melting temperature 1060 °C and held at this level for 1 h to allow the precursor pellet to decompose. The samples were undercooled to a different temperatures (1005, 1010, 1015, 1020, 1025 °C) by a rate of 100 °C/h. Single-grains started to grow during the slow cooling at the rate of 0.2 °C/h, which ended up at the temperature 30 °C lower than selected one. Subsequently, the furnace with the samples was cooled down to a room temperature.

The sample, produced by optimized process (Fig. 1), was then cut in two halves. One half was polished for microstructural observation by the scanning electron microscope (SEM). The other one was prepared for measurement of magnetic properties (J_c and T_c). The specimens of size approximately 1.5 mm × 1.5 mm × 0.5 mm were cut systematically from one plane (Fig. 2). Subsequently, cut specimens were oxygenated at temperature 410 °C for 10 days in a flowing oxygen atmosphere, to drive the non-superconducting tetragonal Gd123 phase to the desired orthorhombic superconducting phase.

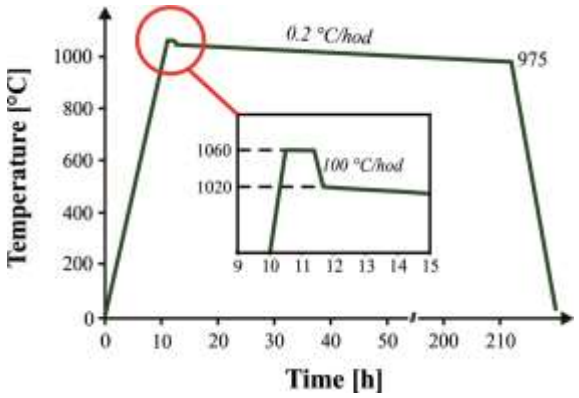

Figure 1 Schematic illustration of the optimized time-temperature profile of the melt growth process

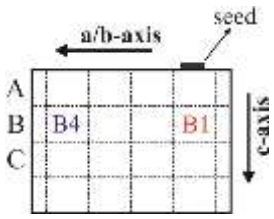

Figure 2 Schematic illustration of specimen positions of single GdBCO grain for measurement of T_c and J_c

The magnetic measurements were performed by a vibrating sample magnetometer (VSM) in a cryogen free high field measurement system. The temperature dependent magnetization was measured in zero field cooled regime at constant external magnetic field. A field of 2 mT that was applied parallel to the c-axis of specimens. The transition widths (ΔT) were determined from magnetic transition curves as the T_c(90%)-T_c(10%). J_c was calculated using the extended Bean model form the measured *M-B* hysteresis loops at 77 K [7].

Results and Discussion

It is important to find a temperature window for growth of RE123 single-grain below the temperature of heterogeneous nucleation of the used seed and above the temperature of self-nucleation of RE123 phase. This window is usually narrow and also the quality of the grown sample depends on the position in this window [8]. Based on several experiments, we have found this window for our system. Top surface photographs of all produced GdBCO bulk grains are documented in Fig. 3. As can be seen, in the samples that have started to grow at a lower temperature after undercooling the crystal did not grow throughout the all sample (Gd007-009). On the contrary, the seed was dissolved at the highest used temperature (Gd016).

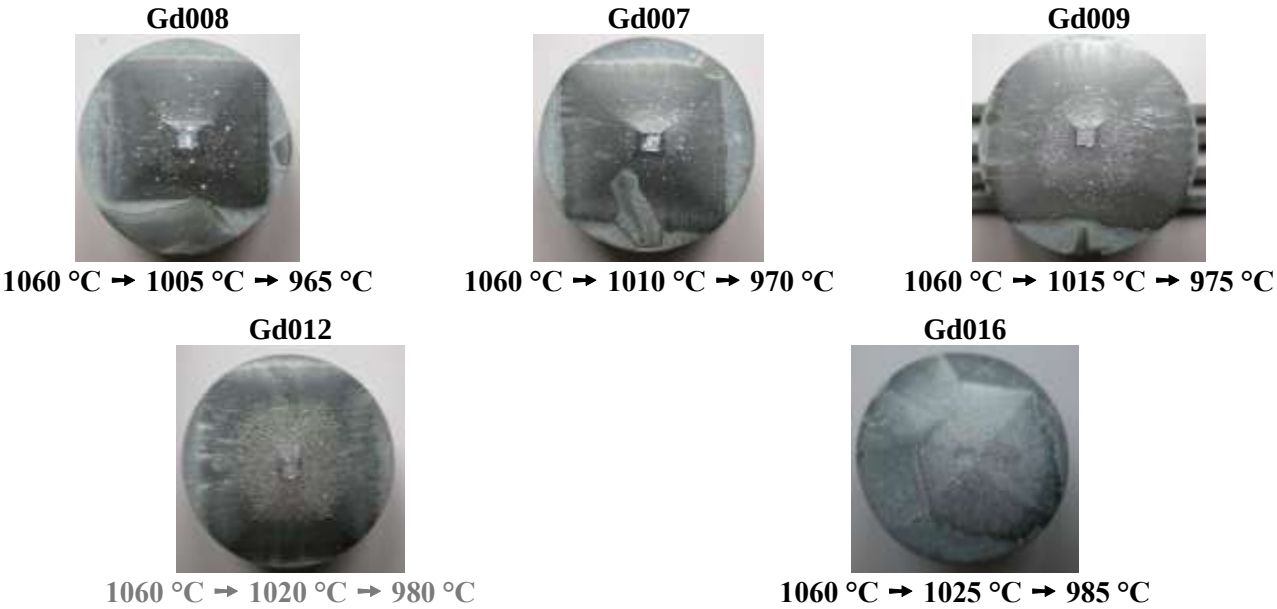

Figure 3 Photographs of the top surfaces of GdBCO bulk grains growned at different temperature profiles

The microstructure of REBCO superconductors is significantly influenced by the growth of RE123 monocrystal in growth sectors (GS). They are separated from each other by grown sector boundaries (GSB), which represent the trajectory of the crystal corners during growth. The particle concentration of the RE211phases in the GS is non-homogeneous due to pushing of these particles by the crystallizing

front. From a certain critical dimension, the particle is not pushed by a front and instead it is trapped by the growing crystal. The REBCO superconductors prepared by the TSMG method consisted of five growth sectors, which were four a-GS and one c-GS.

Photographs of microstructures are presented in Fig. 4. The Ag particles are elongated in the growth direction and therefore the boundary between GSs are better highlighted. Sometimes these particles create beautiful shapes.

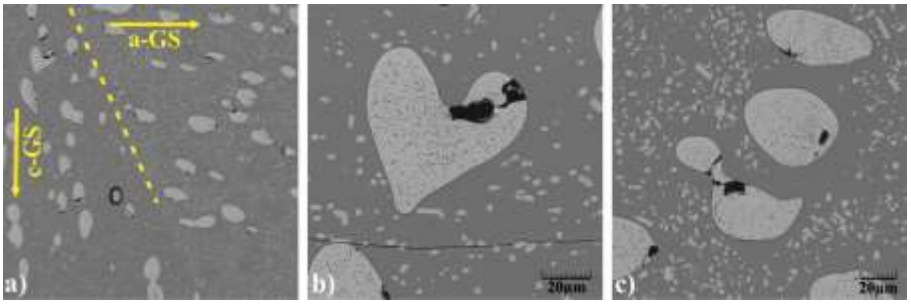

Figure 4 Gd211 and Ag particles seen in SEM **a)** Ag particles elongated in the growth direction **b-c)** examples of Ag (bigger) and Gd211 (smaller) particles

Gd211 particles at the beginning and at the end of GSs are presented in Fig. 5. It can be seen that the volume fraction of Gd211 particles is increasing with the distance from the seed in both GSs. Observed behaviour is typical for bulk single-grain REBCO samples growth by TSMG proces.The inhomogeneities of 211 particles can be explained by anisotropic pushing of little particles, caused by growth of RE123 crystal is more intense in c-GS and therefore there is higher 211 particle concentration, which is clearly visible in a-GS.

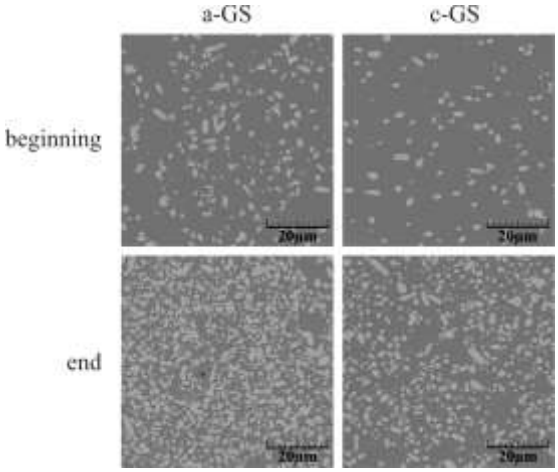

Figure 5 Gd211 particles at the beginning and at the end of a- and c-GS

Magnetization measurements of the specimens separated from the cut sample, as shown schematically in Fig. 2, are depicted in Fig. 6. They exhibit differences in transition to the superconducting state but also in the field dependences of criticall current density. Crystal area that grew first (specimen B1) has the highest middle transition temperature $T_{c,m}$, narrower transition to the superconducting state and reaches higher values of J_c. Additionally, secondary peak was observed in this field dependence, what can be caused by partial substitution of Ba by Gd.

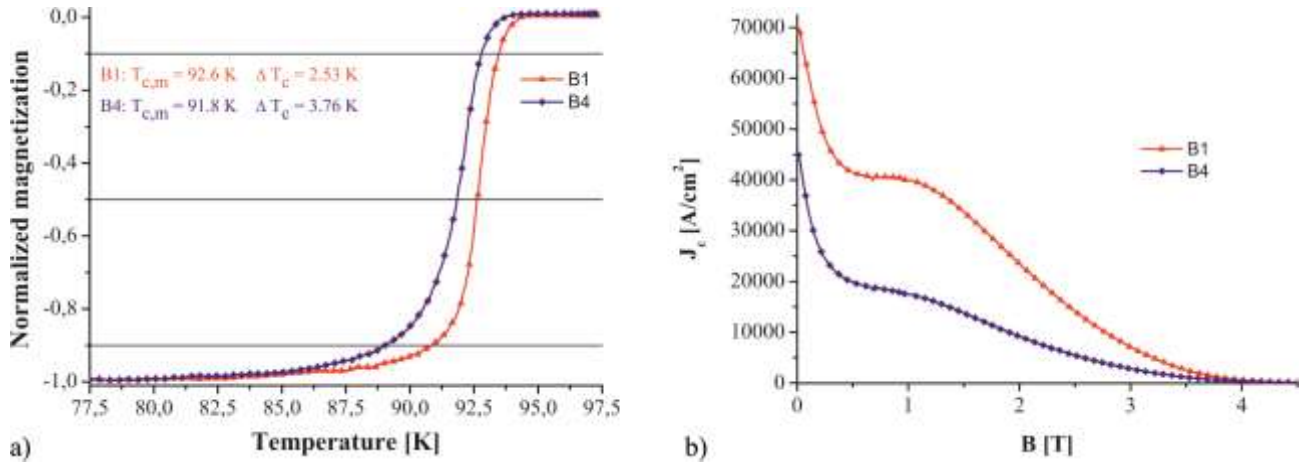

Figure 6 a) temperature dependences of the magnetization of the specimens
b) critical current density for the GdBCO specimens at 77 K

Conclusion

We have successfully fabricated bulk single-grain GdBCO sample with *1 mol. $GdBa_2Cu_3O_{7-\delta}$ + ½ mol. Gd_2BaCuO_5 + 20 wt. % Ag_2O + 0.2 wt. % $PtO_2 \cdot H_2O$* composition, prepared by TSMG method in air. The experiments showed that the magnetic properties (critical temperature T_c and critical current density J_c) are decreasing with the cut distance from the seed. This may have origin in the higher substitution of Ba by Gd at lower temperatures of GdBCO crystal growth.

Acknowledgment

This work was realised within the framework of the projects: New Materials and Technologies for Energetic (ITMS 26220220061), Research and Development of Second Generation YBCO Bulk Superconductors (ITMS 26220220041), APVV No. 0330-12, VEGA No. 2/0121/16.

References

[1] Werfel F. N. et al.: Technical Progress in HTS Magnetic Bulk Application Development. IEEE Transactions on Applied Superconductivity, vol. 25, no 3, 2015
[2] Sakai N. et al.: Mechanical properties of RE-Ba-Cu-O superconductors", Physica C, vol.335, 2000, pp. 107-111
[3] Cloots R.: From RE-211 to RE-123. How to control the final microstructure of superconducting single-domains. Supercond. Sci. Technol., vol. 18, no 3, 2005, pp. R9-R23
[4] Diko P. et al.: The influence of starting $YBa_2Cu_3O_{7-x}$ particle size and Pt/Ce addition on the microstructure of $YBa_2Cu_3O_{7-x}$-Y_2BaCuO_5 melt processed bulks", Supercond. Sci. Technol., vol. 11, no 1, 1998, pp. 49-53
[5] Zhao W. et al.: Comparison of the effects of platinum and CeO_2 on the properties of single grain, Sm-Ba-Cu-O bulk superconductors. Supercond. Sci. Technol., vol.29, no. 12, 2016, art. no 125002 (11pp)
[6] Murakami M. et al.: Melt-processed light rare earth element-Ba-Cu-O, "Supercond. Sci. Technol., vol. 9, no 12, 1996, pp. 1015-1032
[7] Bean C. P. : Magnetization of Hard Superconductors. Phys.Rev. Lett., vol. 8, no 6, 1962, pp. 250-253
[8] Diko P.: Growth-related microstructure of melt-grown $REBa_2Cu_3O_y$ bulk superconductors. Supercond. Sci. Technol., vol. 13, no 8, 2000, pp. 1202-121
[9] Diko P.: Microstructure of melt-grown $REBa_2Cu_3O_{7-x}$ superconductors. In: Microstructural Studies of High T_C Superconductors and More on Quaternary Borocarbides" (Studies of high temperature superconductors). Nova Science Publishers, 1999, 287 Pages. ISBN 1-56072-685-7

Regeneration of solution from alkaline leaching of EAF dust

Ján Jaščišák, Silvia Ružičková, Vladislava Mičková

Technical University of Košice, Faculty of Materials, Metallurgy and Recycling, Institute of Recycling Technologies, Letná 9, 042 00 Košice, Slovakia
jan.jascisak@tuke.sk

Abstract

In the process of alkaline leaching of the electric arc furnace (EAF) dust, the leachate, is subjected to thickening and crystallisation in a vacuum apparatus. In this process, liquid condensate with high ammonia content is produced. The work aims to regenerate ammonia into the product, e.g. $(NH_4)_2CO_3$, which is reusable in the leaching process. In this sense, the influence of various factors (temperature, time, CO_2 flow-rate) on the efficiency of precipitation $(NH_4)_2CO_3$ from condensate was studied. This work was supported by the Slovak Research and Development Agency under the contract No. APVV-14-0591.

Introduction

In solving the research task within the frame of APVV-14-0591 project, which is focused on the hydrometallurgical technology development of waste containing zinc processing, there was a need to regenerate a high ammonia condensate into a suitable product. The condensate is formed in the process of thickening and crystallization of the leachate in the vacuum equipment, after dust leaching from the electric arc furnace (EAF) in the basic branch. This liquid waste (condensate), due to its high ammonia content, would be appropriate to evaluate. It saves operating costs and work environment (Slovak Government Regulation No. 355/2006 Coll.) as well as the environment (Decree No. 55/2004 Coll.).

Experimental

Leaching agent regeneration

The most appropriate approach to redundant ammonia regeneration is its return to leaching process in the form of leaching agent – $(NH_4)_2CO_3$ solution. Following reactions can be suppose in NH_3-CO_2-H_2O system (1-6) [1, 2].

Table 1. *Supposed reactions*

	ΔG^0_{293} [kJ/mol]	ΔG^0_{353} [kJ/mol]	
$CO_2(g) + 2NH_3(g) + H_2O(g) = (NH_4)_2CO_3$	-33.822	3.958	(1)
$CO_2(g) + NH_3(g) + H_2O(g) = NH_4HCO_3$	-31.941	-2.966	(2)
$O_2(g) + 2NH_3(a) + H_2O(l) = (NH_4)_2CO_3$	-3.300	17.936	(3)
$CO_2(g) + NH_3(a) + H_2O(l) = NH_4HCO_3$	-12.102	5.134	(4)
$2NH_3(a) + CO_2(a) + H_2O(l) = (NH_4)_2CO_3$	-13.678	2.350	(5)
$NH_3(a) + H_2CO_3(a) = (NH_4)_2CO_3$	-13.616	1.157	(6)

In accordance with the Gibbs free energy values it can be assumed that increased temperature in reactor will slow down progress of the reactions. Increasing of the temperature causes reduced NH_3 and CO_2 solubility in water (Fig. 1).

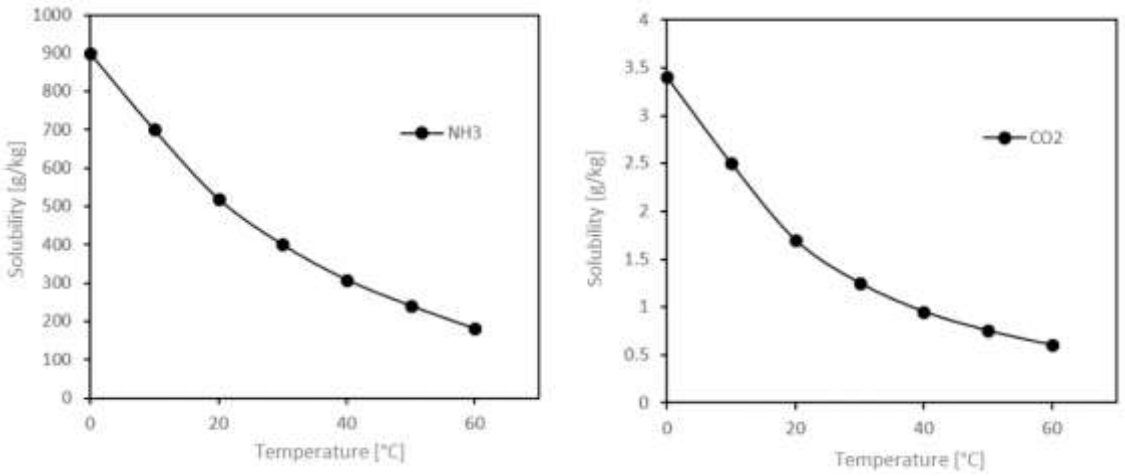

Figure 1 NH_3 and CO_2 solubility in water [3]

Material and methods

The apparatus shown in Fig. 2 was used for the experiment. It consists of reactor, containing 200 ml of condensate, into which gaseous CO_2 flowed for precipitation through a glass frit covering the bottom of reactor. Agitation of the solution was realised by gas flow, which was controled by flow meter. In dependence of CO_2 flow rate the efficiency of precipitation was studied. The output form the reactor was at atmospheric pressure. Because of expected exothermic reaction, it was necessary to ensure constant temperature in reactor using thermally adjustable water bath. As known from literature, $(NH_4)_2CO_3$ precipitation is strongly affected by temperature. Therefore, reaction temperature control in reactor was needed as well as temperature influence on effectiveness of product precipitation.

Samples (10 ml) were taken from reaction mixture at different times (5, 10, 15, 20, 30 and 60 minutes). The concentration of NH_3 was determined using multiparameter UV-VIS photometer HI 83200. For the phase analysis of solid crystalization product, X-ray diffractometer PANalytical X'pert PRO MPD was used.

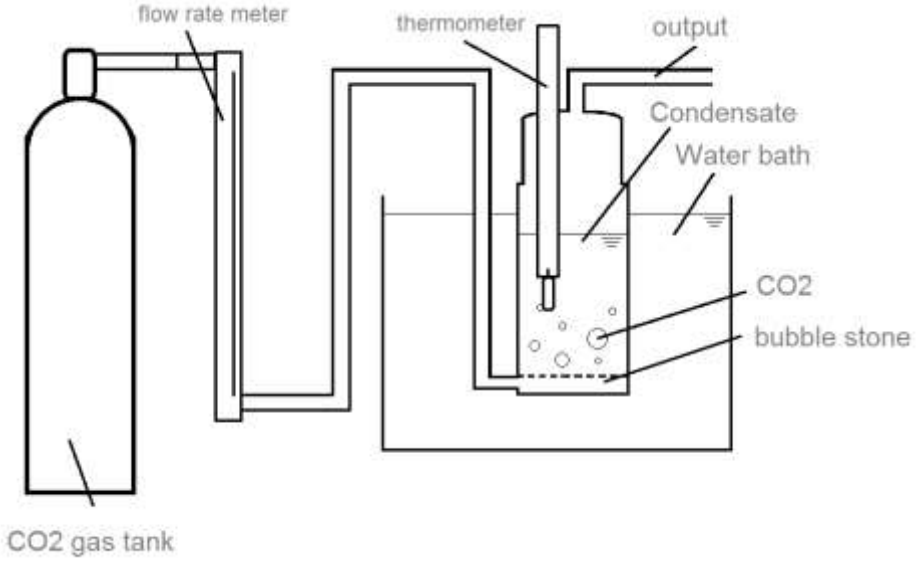

Figure 2 Scheme of the apparatus

Results and discussion

Experimental work was focused on the monitoring of NH_3 concentration reduction in the $(NH_4)_2CO_3$ precipitation process. On the base of this information, the efficiency depending on temperature, CO_2 flow and reaction time was calculated.

Fig. 3 shows the temperature influence of the reaction medium on the NH_3 precipitation efficiency from the solution. From the results in 60 minutes (CO_2 flow rate 70 l/h) seems, that the most suitable temperature for the process is 20 °C. At this temperature, series of experiments, aimed at precipitation efficiency monitoring at different precipitating gas flow rates, was performed (Fig. 4).

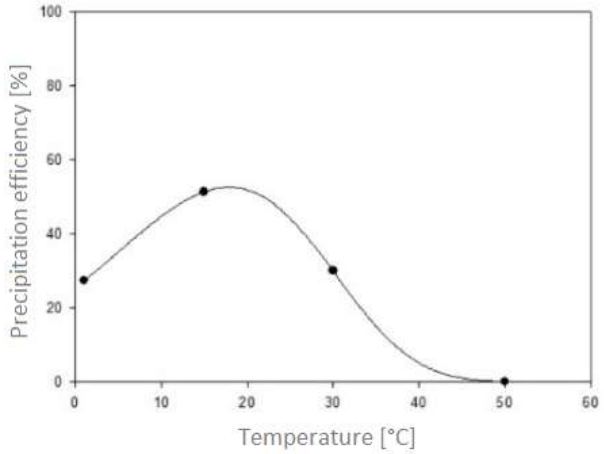

Figure 3 Dependence of precipitation efficiency on reactor temperature (after 60 minutes)

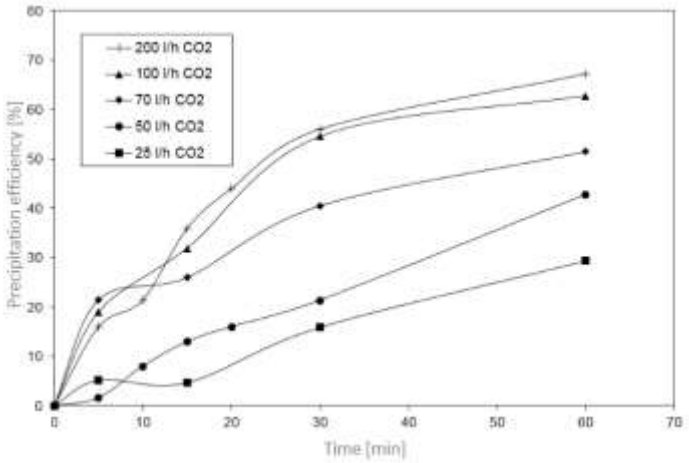

Figure 4 Time dependence of precipitation efficiency at different CO_2 flow rates

From the time dependencies (Fig. 4), a slowdown of the precipitation process can be observed between 5 and 15 minutes at CO_2 flow rate of 25, 50, 70, 100, and 200 l/ h. This phenomenon can be explained by a sudden temperature increase inside the reactor due to an exothermic reaction (1-6). The increase in temperature temporarily slowed the process, but gradually (up to 30 min) the solution temperature was again the same as the temperature of the water bath (20 °C). Graphically, this phenomenon is depicted in Fig. 5, which shows a temperature change in the reactor over time at CO_2 flow rate of 200 l/h.

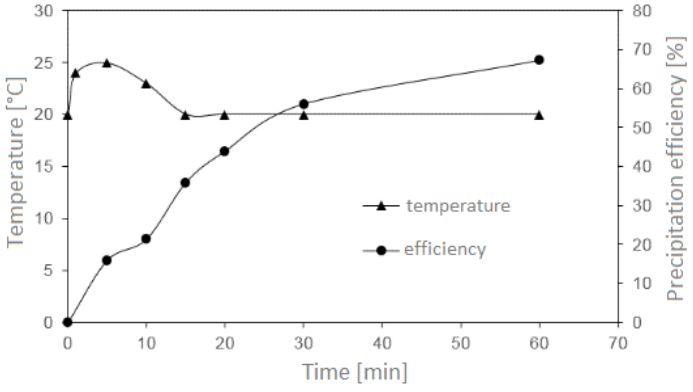

Figure 5 The influence of temperature change in the reactor on the efficiency of precipitation over time

The highest precipitation efficiency (67 %) was achieved after 60 minutes at CO_2 flow rate 200 l/h and reaction medium temperature of 20 °C. In term of the potential application of the process in practice it is essential, that 62 % efficiency was already achieved at CO_2 flow rate of 100 l/h. Dependence of precipitation efficiency after 60 minutes on the flow rate illustrates Fig. 6.

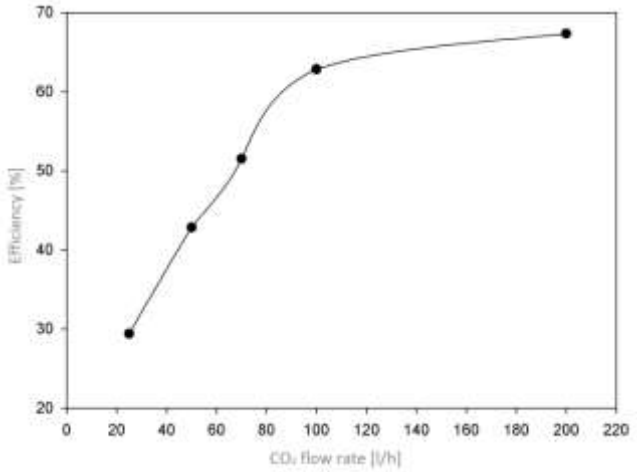

Figure 6 Dependence of precipitation efficiency on the flow rate of precipitating gas (60 minutes)

The precipitation product was white crystalline precipitate, which was after filtration subjected to the XRD analysis (Fig. 7). The record confirmed, that it is ammonium bicarbonate, produced by spontaneous decomposition of precipitated ammonium carbonate. This product can be re-use again as a leaching agent in the basic leaching of EAF dust.

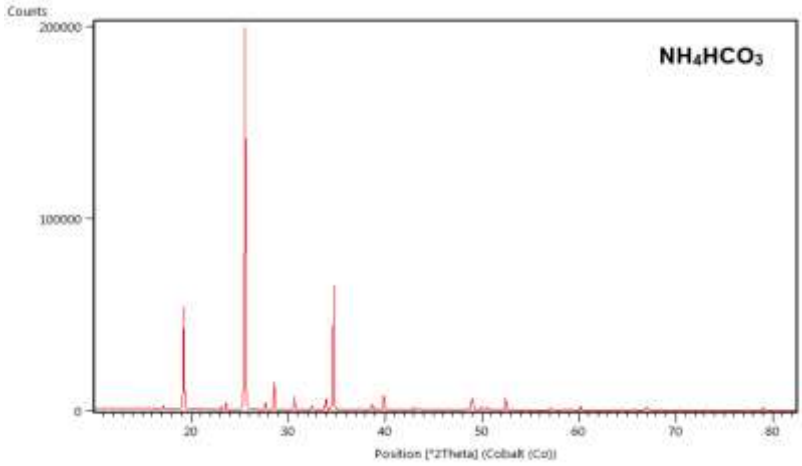

Figure 7 Diffractogram of the precipitate after 60 minutes at CO_2 flow rate 200 l/h

Acknowledgement: This work was supported by APVV project No. 14-0591 and VEGA project No. 1/0631/17.

References

[1] Min-Hao Y. et al.: Removal of ammonia from wastewater by air stripping process in laboratory and pilot scales using a rotating packed bed at ambient temperature. Journal of the Taiwan Institute of Chemical Engineers, Vol. 60, 2016, p. 488-495

[2] Meng Lingyu: Development of an Analytical Method for Distinguishing Ammonium Bicarbonate from the Products of an Aqueous Ammonia Co2 Scrubber and the Characterization of Ammonium Bicarbonate (2004). Masters Theses & Specialist Projects. Paper 243. http://digitalcommons.wku.edu/theses/243

[3] Solubility of Gases in Water, https://www.engineeringtoolbox.com

Measurements and Data Processing in Short Run Small Batch Mixed Production Statistical Process Control

Darina Juhászová[1], *Miroslav Čička*[2]

[1]*Technical University of Košice, Faculty of Materials, Metallurgy and Recycling, Institute of Materials and Quality Engineering, Rademaker Slovakia, s.r.o.*
[2]*Technical University of Košice, Faculty of Materials, Metallurgy and Recycling, Institute of Materials and Quality Engineering*

Abstract

The publication aims to present the current state of knowledge in the field of measurements and data processing in short, small batch mixed production SPC and its application to a specific case of the organisation. It is focused on procedures that allow determining the normality of data and the homogeneity of variance, prior to perform the statistical process control itself. There are several different ways to verify the normality of the data. In this paper is described the way of choosing the right test for the verification of data normality, and also how to verify the consistency of variances by applying Hartley's F_{max} test.

Introduction

Statistical Process Control can be described as a feedback system, which unlike the detection system, helps to prevent non-production mismatches and not just to record them [1]. The attention is focused on where the quality fluctuates and can be influenced in the process. An appropriate quality management system should ensure that the product is produced in the required quality by the first time [2]. To indicate a statistical approach to process management, the Statistical Process Control (SPC) abbreviation is used. The process control system is closely related to the capability and performance of the process. Process capability is determined by fluctuations induced by random causes, while both internal and external customers are more focused on process performance, i.e. the total output from the process and how this output corresponds to their requirements defined by the technical specification regardless of the process variation.

Data Normality Verification

The basic information according to which is the type of control charts chosen, is the information about consistency of variability of all products we want to follow in one common control chart.
Before proceeding to testing the homogeneity of variances, it is necessary to verify the normality of the data, i.e. to verify whether the monitored variable has a normal distribution. There are several different ways to verify the normality of data [3 - 5]:

- Kolmogorov-Smirnov test for any distribution;
- Lilliefors test is a modification of Kolmogorov-Smirnov test for normal distribution;
- Chi-squared goodness of fit test for measured data at intervals with the appropriate frequency;
- Shapiro-Wilk test.

A suitable test can also be selected according to the range (n) of the selection file:

$n > 100$	Chi-squared goodness of fit test;
$30 \leq n \leq 100$	D´Agostino test;
$7 \leq n < 30$	Shapiro-Wilk test.

At the output of the statistical test, *p*-value is in addition to the tested statistics. If *p*-value < α, the tested hypothesis is rejected at the level of significance – α.

Level of significance of the result obtained from the sample is the probability, that the observed dependence (the difference between the variables in the selection file) is random, and that in the whole production from which the sample was obtained, this dependence does not exist there.
The higher is the level of significance, the less can be the detected dependence (gained from the selection file) expected on the whole production. For a truly significant dependence is considered such a result if *p*-value is less than *0.05*.

The base file in the application example is 150 measured values of the diameter of the shaft from the production process of 3 different types of stainless steel cylinders (400; 600; 800) which differ in shaft length and tube length. Their common indicator is identical shaft diameter ∅50 mm. The selection file (*n*) consists of 50 values. Considering the range of selection file *n=50*, Shapiro-Wilk's normality test is applied at the significance level of *p=0.05*. Shapiro-Wilk's test leads to the computation of the *W* statistics, which is compared with the defined critical values [6].

Shapiro-Wilk Normality Test

Originally, Shapiro-Wilk´s test (1965) was not intended for a sample with number of values less than 50. This test was the first one capable of detecting deviations from normality, towards skewness and kurtosis. Shapiro-Wilk's normality test is related to the model of dependence of ascending and measured values $\bar{x}_i$ on the corresponding quantiles of standardized normal distribution. The test result indicates whether the sample data distribution is significantly different from normal distribution or not [7]. The *W* value lies between *0* and *1*. Low *W* values lead to the rejection of normality, while the value of *1* indicates the normal distribution.

Step 1: From the base file of 150 measured values of the shaft diameter for cylinder types 400, 600 and 800 is the average value of the character $\bar{X}_i$ for each subgroup calculated.
Step 2: Selection file *n* = 50 values for X_1 to X_{50} is specified from calculations.
Step 3: Values are ranked from the lowest to the highest value (y_i) and squared (y_i^2).
Step 4: The average of values y_1 to y_{50} and $\bar{y}$ is calculated. Subsequently, this value is subtracted from the mean value $y_i - \bar{y}$.
Step 5: Listed values a_i are Shapiro-Wilk test values for *n* = 50 and (25).
Step 6: Values Y_i are sorted into two columns with the same amount of data, as follows:
Y_i = *for i=1 to 25*
Y_i = *for i=50 to 26.*
Step 7: $a_i * y_i$ is calculated as the basis for calculating statistics *W*.
Step 8: Formula is used to calculate *W* value according to formula (1):

$$W \frac{\sum_{i=1}^{n} a_i y_i}{\sum_{i=1}^{n} (y_i - \bar{y})^2} \qquad (1)$$

Step 9: *W* value for *p = 0.05* according to Shapiro-Wilk test table is 0.947.
Step 10: The data are normally distributed at *p < 0.05*.

There is no breach of the assumption of normal distribution according to Shapiro-Wilk´s chart of normality for (*n* = 50).

The Homogeneity of Variances

In statistical regulation by measurement, a stood intra-group variability is a precondition for interpreting control chart for the means. Standing variability is verified by either *R* or *S* diagram. However, for short cycle production processes, when to compare the variability in M groups is needed, are tests for the homogeneity of variances applied.
Among the best known are:

- Bartlett test (not suitable for small observation groups),
- Cochran Q test (compares the largest variance with the average of variances),

- Hartley´s F_{max} test (compares the largest variance with the smallest variance).

These tests are based on intragroup variances, they assume a normal distribution of the monitored character and the use of a statistical program.

The following tests:

- Leven´s test,
- O´Brian´s test,
- Brown-Forsythe test,

are based on the absolute deviations of the measured values from the mean or median in the group, and ANOVA [3] can be applied to these deviations. All three tests are relatively robust against deviations from normal distribution, while for the most robust may be considered Brown-Forsythe test.

If the results are implemented in the statistical program (e.g. SigmaZone Quantum XL, 2016), it decides through a *p*-value. The hypothesis is rejected at a *p*-value of less than 0,05 formula (2) [8]:

$$H_0: \sigma_1^2 = \sigma_1^2 = \cdots \sigma_M^2. \qquad (2)$$

The hypothesis test is focused on verification of zero hypothesis H_0. When deciding on the validity or invalidity of the zero hypothesis, the *p*-value is used. It can be defined as the smallest level of significance of the test, in which the hypothesis on the given data is still rejected.

The principle is that the lower the *p*-value of the test is, the lesser the test indicates the likelihood that the zero hypothesis applies. In other words, when evaluating a statistical test and the *p*-value is close to zero it means, that our zero hypothesis has a very little support in the observed data and we can reject it.

The decision about validity or invalidity of the zero hypothesis is performed by comparing the resulting *p*-value of the test with chosen level of significance *α:*

- if $p < \alpha$ zero hypothesis is rejected;
- if $p < 0.05$ the difference is demonstrated;
- if $p < 0.01$ the difference is highly demonstrated.

Hartley´s F_{MAX} Test of Homogeneity of Variances

Conformity of variances (consistency of variability) means, that the variance in products is not significantly different. When verifying this precondition, there is a range of tests to verify the homogeneity of variances. An important prerequisite for an efficient application of the control chart is to define consistent product groups, that will have a common control chart, and which are called – product family. These groups should be as homogeneous as possible in terms of the process conditions.

Once normal production conditions are in place, it is possible to start process monitoring, i.e. to take subgroups in range of *n=3* or higher (usually ranging from 3 to 5 values). The number of subgroups should be at least 20. The total number of values should be at least 100. Some sources report a minimum of 125 values [9].

In practice, a process of manufacturing three types of stainless steel cylinders was monitored (Table 1). Cylinders differ in shaft length and pipe length. Their common indicator is an identical shaft diameter Ø50 mm:

Table 1 *Types of monitored cylinders*

Cylinder type	**Shaft length** [mm]	**Shaft diameter** Ø [mm]	**Tube length** [mm]
400	941	50	404
600	1,141	50	604
800	1,341	50	804

After verifying the normality of the data (Shapiro-Wilk test of normality), it is possible to proceed to test the homogeneity of variances.

For testing, a **Hartley´s F_{max} test** was selected. This test is suitable to use if all selection files have same ranges, i.e. the abundance of all groups is the same. In this case the range of selection files is *n=3*.

Hartley´s F_{max} test is based on the test criterion formula (3):

$$F_{max} = \frac{S^2_{max}}{S^2_{min}} \tag{3}$$

whereabouts:
S^2_{max} is the largest from variances of groups,
S^2_{min} is the smallest from variances of groups.

If the calculated value of the F_{max} test criterion is less than the critical value for the Hartley´s test $F_{max,\alpha}(k, v)$ we accept the zero hypothesis of variances compliance, whereabouts: *k* is the number of compared variances, *v = n -1* are the degrees of freedom, *α* is the level of significance.

The zero hypothesis assumes that there is no statistically significant difference between the variables, thus the hypothesis will be tested at 5% level of significance.

First, from the base file is by random selection a file of *n=10* values of variances selected, and these will be used for testing the homogeneity of variances (Table 2):

Table 2 *Table of selection file of variances*

Selection file of variances (n=10)		
Order	**Reference number of variance**	**Value [mm]**
1	s_{44}^2	0.0000036
2	s_{28}^2	0.0001109
3	s_{10}^2	0.0000087
4	s_{35}^2	0.0000009
5	s_{50}^2	0.0000180
6	s_{39}^2	0.0000727
7	s_{34}^2	0.0000762
8	s_{48}^2	0.0000620
9	s_{4}^2	0.0001316
10	s_{10}^2	0.0000087

From the selection file, the following values have been calculated:

$S^2_{max} = 0.0000009$
$S^2_{min} = 0.0001316$

The following characteristics were subsequently identified (Table 3):

Table 3 *Table of calculated characteristics for Hartley´s Fmax test*

K	10
N	3
v = (n-1) (df – degrees of freedom)	2
A	0,05
F_{max}	148,00
$F_{max,\ \alpha}$ (k, v)	549,80

The $F_{max,\ \alpha}$ value is obtained through a coefficient table for the Hartley´s F_{max} test. In the coefficient table, the calculated value F_{max} is not bigger than the value $F_{max,\ \alpha}$. The zero hypothesis is accepted at significance level α. The result of the test leads to the conclusion that there is no significant

difference between variances, i.e. the data demonstrate homogeneity of variances and the variability of the exact diameter turning process can be considered as consistent. It is possible to apply the Q-diagram.

Conclusion

In practice, statistical process control appears quite often. A simple and effective tool such as a control chart helps to understand the process through small samples taken during production, and thus prevent the occurrence of quality problems. With the onset of production in small batches with a high variability, there is also a problem with the application of classic control charts. The reason for this is the insufficient number of measurements. Statistical assumptions for the correct use of Shewhart Control Charts by measurement are data normality and independence of data. And, variance homogeneity tests are applied. Both are presented in this article.

The role of further research within the dissertation will be based on case studies:

- To present an extensive overview and select a suitable type of control chart. And to assess whether the process is statistically controlled and regulable.
- To identify the process capability, the number and duration of feedback control interventions in specific small batch production.

Acknowledgement

This article was created under the project VEGA 1/0904/16 "The utilization of processes capability and performance and products dimensional tolerances in the management of material consumption and related economic, energy and environmental consequences (MINIMAX-3E)" supported by the Ministry of Education, Science, Research and Sports of Slovak Republic.

References

[1] Plura J.: Plánovaní a neustále zlepšování jakosti, Brno: Computer Press, 2001
[2] Nenadál J. et al.: Moderní řizení jakosti, Praha: Management Press, 2008
[3] Tošenovský J., Noskievičová D.: Statistické metody pro zlepšování jakosti, Ostrava: Montanex a.s. Vydavatelství, 2000
[4] Turisová R., Pačaiová H.: Inžinierstvo kvality produkcie, Košice: Technická univerzita v Košiciach, 2017
[5] Zgodavová K. et al.: Profesionál kvality, Košice: Technická univerzita v Košiciach, 2003
[6] Shapiro S.S., Wilk M.B.: An analysis of variance test for normality (complete samples), Biometrika, 52 (1), pp. 591–611, 1965
[7] Tošenovský F.: Process Capability and Data Contamination, Quality Innovation Prosperity, 21 (1) pp. 50-61, 2017
[8] Jarošová E., Noskievičová D.: Pokročilejší metody statistické regulace procesu, Praha: Grada Publishing, a.s., Praha, 2015
[9] Keppel G., Wickens T. Design and analysis (4th ed.), Englewood Cliffs, NJ: Prentice-Hall, 2004

Treatment of anode furnace dust in sulfuric acid

Dušan Klein, Dušan Oráč

Institute of Recycling Technologies, Faculty of Materials, Metallurgy and Recycling, Technical University of Košice, Letná 9, 042 00, Košice, Slovensko
dusan.klein@tuke.sk,

Abstract

Copper is a very desirable metal, because of its properties. Its production produces a number of waste, which is also a potential source of raw materials. One of these wastes is the anode furnace dust, which is interesting for the high content of zinc. This dust was subjected to a series of experiments - leaching in sulfuric acid under various conditions. In all cases the yield of zinc was very similar, ranging from 70 % to 80 %.

Introduction

Modern times are demanding for material consumption, but at the same time the trend of saving resources increases. This opens the way for recycling. Industrial waste is a rich source of raw materials. Often richer than primary sources, but more heterogeneous, making their processing more difficult.

In pyrometallurgical copper production several types of waste arise. One of the resulting wastes is a dust of pyrometallurgical refining. The purpose of pyrometallurgical refining in anode furnace is to remove elements with higher affinity to oxygen than copper, for example sulfur, zinc, iron. By blowing air into the molten copper, oxides are formed to pass into the slag or dust. Reaction of impurities with oxygen generates oxides that form predominantly slag, but also dust. For a high zinc content around 30%, it is an interesting secondary raw material [1][2].

In 2017, 19.7 million tons of copper were produced in the world. Copper has a variety of uses. Almost half of the copper produced is used in construction. Approximately a quarter is used in electrical and electronic devices. The following are vehicles, consumer products and industrial machinery and equipment [3][4].

The aim of the work is to verify the possibility of hydrometallurgical treatment of the dust from pyrometallurgical refining copper by leaching in sulfuric acid solution.

Experimental part

Material

In the experiments were used the anode furnace dust from the production of copper anodes. To determine the content of interest metals, the material was subjected to chemical analysis by AAS - atomic absorption spectrometry. The determined metals contents are listed in Table1.

Table 1. *The content of the metals in the sample*

Element	Zn	Cu	Sn	Fe	Pb
Contents [%]	32,99	7,57	1,67	0,607	10,94

Methods

The dust was subjected to leaching in sulfuric acid at a concentration of 0.5 M and 1 M. The leaching took place in the glass reactors which were placed in the thermostatically controlled water bath to ensure the selected temperature. The leaching was realized at the temperatures 20, 60 and 80 °C. The weight of sample was 10 g in all cases and the volume of the leaching reagent was 400 ml. The leaching time was 60 minutes. Liquid samples (5 ml) were collected at 5, 10, 15, 30 and 60 minutes of leaching. The AAS method determined the Zn, Cu, Sn and Fe concentration in the solution.

Results and discussions

Zinc

Fig. 1 to 3 illustrate the leaching curves of Zn at different temperatures. First experiments were performed at 20 °C (Fig. 1). After an hour of leaching at 20 °C in solution 0.5 M H_2SO_4, a yield of 73.74% Zn was obtained. Using 1 M H_2SO_4, yield increased by approximately 3% to 76.8% Zn. After one hour of leaching at 60 °C, and using a solution 0.5 H_2SO_4, 77.14% Zn was passed into the solution and, using a solution 1 M H_2SO_4, a yield of 80.53% Zn was obtained. The curves of the leaching at 60 °C are shown in Fig. 2. As shown in Fig. 3 at 80 °C and using the solution 0.5 M H_2SO_4, the extraction of 77,53 % Zn was achieved after one hour of the leaching. Using the solution 1 M H_2SO_4, 82.09% Zn was obtained in the solution.

In Fig. 4 is a comparison of yields of Zn at different temperatures. The influence of temperature was linear at both concentrations, but not very significant. By leaching in a solution 0.5 M H_2SO_4, increasing the temperature from 20 °C to 80° C increased extraction from 73.74% Zn to 77.57% Zn. By leaching in 1 M H_2SO_4, an increase in temperature from 20 °C to 80 °C increased the extraction from 76.8% Zn to 82.09% Zn. Further temperature rise would inefficient in terms of time and energy demands.

Copper, tin and iron

The copper yield at 20 °C and the concentration of H_2SO_4 of 0.5 M reached 96.96%. Using the 1 M solution of H_2SO_4, the yield increased to 98.26% Cu. At temperatures of 60 °C and 80 °C, was passed into the solution of almost 100%.

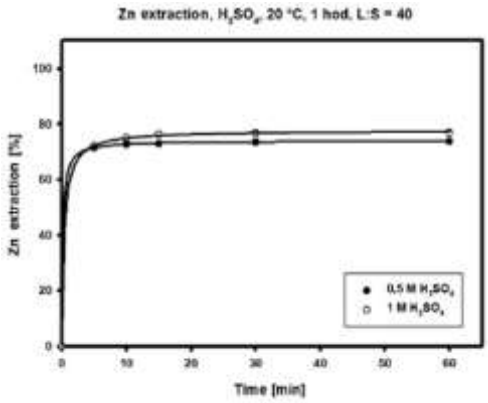

Figure 1 Extraction curves, 20°C, H_2SO_4

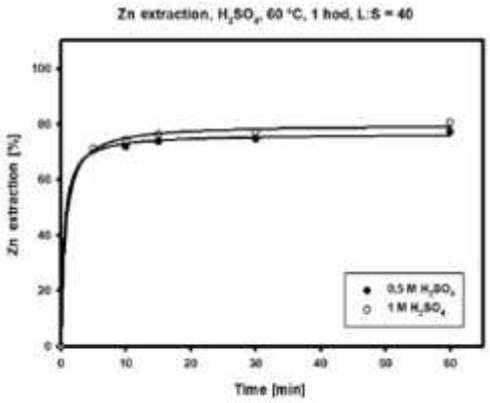

Figure 2 Extraction curves, 60°C, H_2SO_4

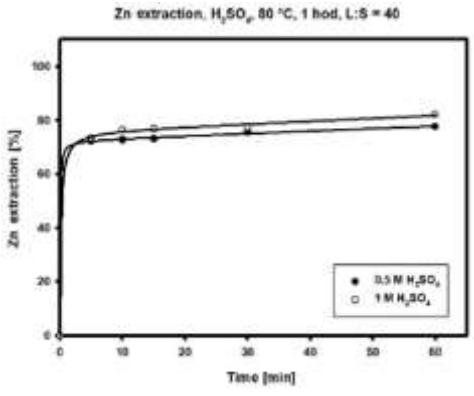

Figure 3 Extraction curves, 80°C, H_2SO_4

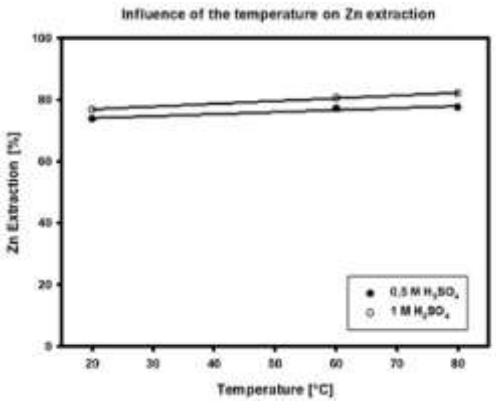

Figure 4 Influence of temperature on the Zn extraction

The extraction of tin with increasing concentration and temperature increased significantly. When dust was leached in the solution 0.5M H_2SO_4 at 20 °C, the extraction of tin was 26.07% after one hour, when was leaching in solution 1 M H_2SO_4 at 80 °C it was almost 100% Sn.

At the temperature of 20 °C and 1M leaching reagent concentration the lowest yield of iron 33% was achieved. On the other hand, most of iron passed into the solution at 80 °C and a concentration of 1M. The yields of Cu, Sn and Fe at all temperatures and concentrations of the leaching reagent are shown in Fig. 5.

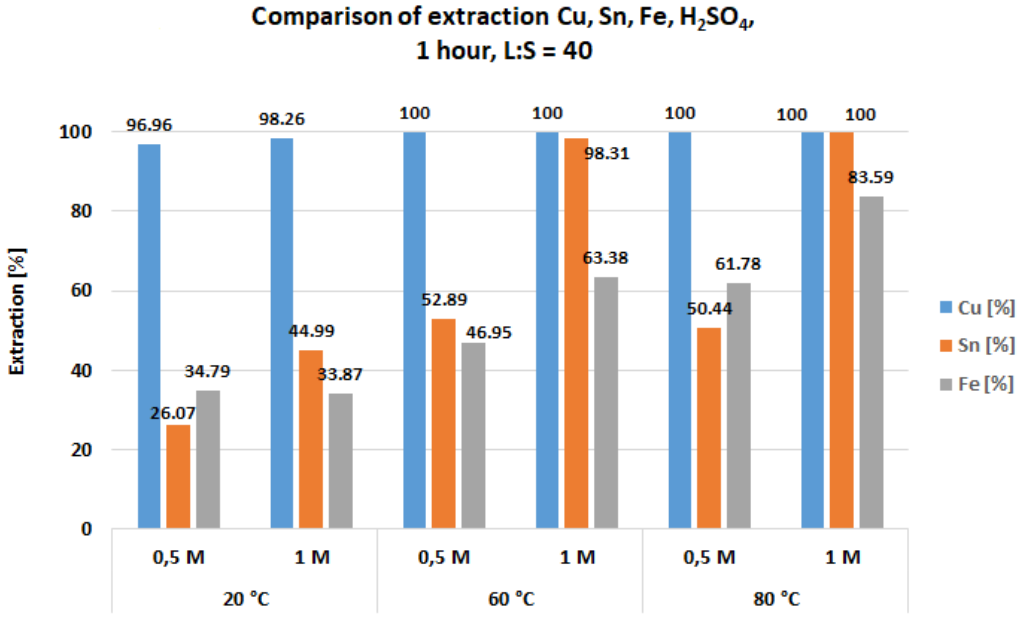

Figure 5 Comparison of extraction Cu, Sn, Fe

The solid residue after leaching was washed, dried and subsequently subjected to XRD analysis. In the insoluble residue a phase of $PbSO_4$ was detected.

Conclusion

The dust was subjected to hydrometallurgical treatment to leach out Zn. The experiments were carried out at temperatures 20 °C, 60 °C and 80 °C. Sulfuric acid was used as the leaching reagent at two concentrations 0.5 M and 1 M. The best yield, 82.09 % Zn, was achieved at 80 °C using solution 1M H_2SO_4.

The input sample also contained 7.57% of Cu, which, at 60 °C and 80 °C in 0,5M and 1M H_2SO_4, was passed into the solution with the efficiency of almost 100%. By zinc cementation, copper could be obtained from the solution. After removing impurities from the solution, zinc could be obtained by electrolysis.

Acknowledgements

This work was supported by the Slovak Research and Development Agency under the contract No. APVV-14-0591. This work was supported by Ministry of Education of the Slovak Republic under grant VEGA MŠ SR 1/0724/17.

References

[1] Trpčevská, J.: Neželezné kovy, Košice TU, 2017, ISBN: 978-80-553-3140-9
[2] Pirošková J., Laubertová M., Miškufová A., Oráč D.: Hydrometallurgical Treatment of Copper Shaft Furnace Dust for Lead Recovery In: World of Metallurgy - Erzmetall. Vol. 71, no. 1, 2018, p. 37-40
[3] Top copper producton by country, Website. 2018: https://investingnews.com/daily/resource-investing/base-metals-investing/copper-investing/copper-production-country/
[4] Facts about copper, Website: https://geology.com/usgs/uses-of-copper/

Lithium battery recycling and analysis of the slag formed by pyrometallurgical treatment of lithium batteries

Jakub Klimko, Dušan Oráč

Institute of Recycling Technologies, Faculty of Materials, Metallurgy and Recycling, Technical University of Košice

Abstract

More than 200,000 tonnes of portable batteries and accumulators are placed on the market annually in the EU countries and more than 20 wt. % of them are lithium ones. Except lithium they contain rare and for EU important metal – cobalt, which price has been raised by 67% over the past year. There are currently many scientific studies dealing with hydrometallurgical treatment of active mass. Because of the increased price of cobalt, waste with lower contents of this metal are becoming also suitable for recycling. The aim of this work is to analyze the chemical composition of the slag, which was created as a by-product of pyrometallurgical Li and Li-ion battery processing and determine the possibilities of applying these existing methods to mentioned waste type. Compared to the active mass, the slag differs in its increased content of slag-forming additives that can influence further hydrometallurgical processes. The AAS results confirm that approximately 13% of cobalt is present in the slag, which makes it an interesting secondary raw material. Except cobalt there are other interesting metals such as lithium, nickel, copper and others.

Introduction

The production of metals from primary raw materials already faces several problems, such as the high costs of mining, the loss of raw materials, low content of metals in the primary raw materials, their problematic processing, the production of large quantities of waste and others. These problems can be partially or completely eliminated in the case of the recovery of metals from secondary raw materials. In 2017, 61 materials (or groups of materials) were judged by the European Commission, resulting in a list of 27 Critical Raw Materials (CRMs). The results show that there is a risk of supplying EU with lithium, but economic importance is not significant to the EU. However, in the case of cobalt, its economic importance and supply risk are above threshold values and is therefore classified as CRM. These 2 metals are also represent in waste of portable lithium batteries. Their recycling can partially secure the needs of these metals in the EU and reduce the risk of supply [1].

The average annual quantities of lithium mined from primary raw materials ranged from 30000 to 35000 tonnes per year between 2010 and 2016 [2]. The consumption of lithium in the form of $LiCO_3$ increased from 100,000 metric tons per year in 2010 to 212,000 metric tons per year in 2016 [3]. Converted into pure lithium, consumption is 20,000 tons per year. Global lithium reserves are estimated at 14 million tons, while the largest reserves of countries have Chile, China, Argentina and Australia. EU countries do not have significant stocks or deposits and therefore it is necessary to rely on import and recycling. Approximately 35% of the world's lithium production is consumed to produce lithium batteries. Lithium also used for the production of Ceramics and Glass (32%), lubricating greases (9%), continuous casting (5%), air pollution treatment (5%) polymers (4%) and other (11%) [4]. Li price is currently at 18 000$/t [5]. Despite the fact that lithium is not CRM and the content in Li batteries is the same as in the primary raw material (2-5%), the recycling of this element is still economically and environmentally appropriate.

Cobalt is an important part of lithium accumulators. In 2016 approximately 60% of cobalt mined was as a by-product of copper, 38% as a by-product of nickel, and the remaining 2% from primary cobalt mines [6]. Approximately 51% of annual world cobalt production is consumed for the production of Li-ION batteries. Cobalt is also used to make super alloys (20%), hard materials (8%), ceramics and pigments (8%) and others [6]. Cobalt price has raised from 55000$/t to 92000 $/t in only 1 year [7] While the content of cobalt in ores is very low, 0.06 - 0.7%, its content in Li-ion accumulators is up to 20%. The increasing demand for cobalt and the limited supply, which is also confirmed by its rising price, are the reasons for obtaining these resources from secondary raw materials. Such appropriate secondary source

are also waste of portable Li batteries not just because of the cobalt content, but also other present metals like copper aluminum, nickel and lithium.

The aim of this work is to describe types of lithium batteries and accumulators, analyze numbers of these batteries placed on the market and collected in EU countries and analyze input material – Li battery slag for further metal recovery.

Types of portable lithium batteries

Lithium batteries can be distinguished from other types of batteries according to their shape. Most coin and button cell anodes of batteries are made of lithium metals or from their alloys. In most cases, these batteries are non-rechargeable. On the other hand, the most common type of rechargeable Li-ion batteries are cylindrical shape, used inside notebooks, basic electronic devices and electric vehicles. Another common Li-ion battery type is prismatic shape. These are used in small devices like smartphones, tablets etc. [8]. There are also Pouch, button, coin rechargeable batteries as well. Lithium batteries have high electrochemical potential per cell due to the presence of lithium which has a high negative standard electrode potential E^0 (E^0 redox pair Li^+ / Li = -3.04 V) and is highly reactive. Lithium batteries are as well as other types of batteries designed as electrolytic cells containing anode, cathode, electrolyte and sometimes also a separator. The difference between rechargeable and non-rechargeable lithium batteries is in the form of lithium used. After the load is attached to non-rechargeable battery, the metal lithium anode is slowly oxidized to Li^+ with the release of the electrons (1).

$$Li \xrightarrow[discharge]{} Li^+ + e^- \qquad (1)$$

$$Cathode: \quad LiCO_2 \underset{Discharge\ Charge}{\longleftrightarrow} Li_{1-x}CO_2 + xLi^+ \qquad (2)$$

$$Anode: \quad C + xLi^+ \underset{Discharge\ Charge}{\longleftrightarrow} Li_xC \qquad (3)$$

The advantages of the lithium cells include the high voltage compared to other types of batteries which have a voltage of 1.2-1.5 V, high specific energy and energy density, high current density, long life and low battery weight because lithium is the lightest of all metals. After oxidation of lithium occur, it is not possible to reverse the process and the battery becomes waste. In the case of the rechargeable lithium batteries, the lithium is in a different form and recharging is possible (2) and (3). The cathode is composed of chemical compounds such as $LiCoO_2$, $LiNiO_2$, $LiMn_2O_4$, $LiFePO_4$ and others. Materials used in anodes are graphite, fine carbon or hard carbon. Between those electrodes there is pure electrolyte and separator preventing short circuit and only small positively charged ions can pass this separator. The electrolyte is a low viscosity organic solvent in which the lithium conductive salts are dissolved. Cathode, anode and electrolyte is also called active or black mass. The phase composition of batteries is shown in Table 1.

Table 3 *comparison of the composition of lithium rechargeable and non-rechargeable batteries [9, 10]*

MSDS of Non-rechargeable Li coin batteries		**MSDS of Rechargeable Li-ion batteries**	
Chemical Name	**Percentage of total weight**	**Chemical Name**	**Percentage of total weight**
Lithium or Lithium Alloy	1 to 5	**Lithium Cobalt Oxide**	25 to 35
Manganese Dioxide	15 to 40	**Carbon, various forms**	10 – 30
Propylene Carbonate	2 to 6	**Copper**	1 – 15
1,2-Dimethoxyethane	1 to 5	**Aluminum**	1 – 10
Lithium Perchlorate	0 to 1.5	**Biphenyl**	0.1 - 0.3
Graphite	1 to 4	**Organic Carbonates**	5 – 10
		Lithium Salts	1 – 6

Portable battery waste collection

In 2015, 222,000 tonnes of portable batteries were reported to have been placed on the market of EU countries plus Switzerland in 2015, while 91,000 tonnes of waste portable batteries were reported as collected. This corresponds to a collection rate on a current year basis of 41%, up from 25% in 2010. Single use lithium batteries represent 2% of total batteries placed on the market (POM) per weight and rechargeable Li-ion accumulators represent 19% of all batteries POM per weight [11]. According to the statistics of Institute of Recycling Technologies, which collects portable battery waste at campus of Technical University of Košice, share of the li-ion battery in the collecting tanks increases. In 2009, lithium batteries represented 1.2 wt. % of collected batteries. The average share of lithium batteries collected is above 5 wt. % since 2016. This number is significantly lower than 19% POM. The main reason is that these batteries are often collected together with the WEEE in which they were originally used (mobile phones, notebooks, and other electronic equipment). The ratio of collected and POM batteries in the EU countries is shown in Table 3. Since year 2012, Slovakia is achieving 45% ratio of collected/POM which was target until year 2015.

Table 4 *EEA + Switzerland, portable battery POM and collection 2010 – 2015[11]*

Portable Batteries EEA + Switzerland	Grams per capita[18]						Units per capita					
	2010	2011	2012	2013	2014	2015	2010	2011	2012	2013	2014	2015
POM	436	426	422	409	415	425	18.9	18.8	18.9	18.5	19.6	20.2
Collection	107	141	152	156	165	174	2.3	3.0	3.2	3.3	3.5	3.7
Collection / POM	25%	33%	36%	38%	40%	41%	12%	16%	17%	18%	18%	18%

Processing of waste batteries

Used portable lithium batteries and accumulators can be processed mechanically, pyrometallurgicaly, hydrometallurgically or by combining some of these methods. ***Mechanical*** processing is often the first of the processing steps. This includes crushing, milling and sizing and is carried out in order to separate individual components. In the case of mechanical pre-treatment, the battery should be discharged in order to avoid short-circuiting and subsequent fire of the material. ***Pyrometalurgical*** methods are a processes of obtaining metals at high melting temperatures or methods for thermal pre-treatment of inputs for leaching processes. Mechanical pre-treatment is not necessary, and careful battery sorting is not always required but it may negatively affect product quality and purity of products. The smelting product is an alloy of interest metals, and a slag, which may also contain metals suitable for further recovery. ***Hydrometalurgy*** is a series of metal-recovery processes where the principle is to transfer the metal to the leachate and then selectively recover it from the leachate. Leaching, metal transfer to the leachate, may be acidic or basic, oxidative or non-oxidative, pressure or atmospheric. The leaching is most often carried out at temperatures of 25-100 ° C, in cases of high pressure leaching up to 250 ° C. The metals are obtained from the leachate by methods such as precipitation, cementation, ion exchange, liquid extraction, electrolysis and its combinations to obtain metals, their salts or other chemical compounds. Battery processing deals with a great deal of research work, and there are also many technologies already existing.

Material

Sample of lithium batteries slag was obtained by smelting of battery active mass containing Li and Co with a slag-forming additives such as Fe_2O_3, CaO and SiO_2. Melting products were metal with high Cobalt content and mentioned slag. The aim of this work is to analyze this material and to propose a processing procedure for material recycling Co and Li or other metals present. Separated slag was mechanically treated bygrinding and milling. Subsequently, 5 representative samples were taken from the material. The chemical composition of input was determined by AAS method on Varian spectrophotometer AA20+ shown in table 3. Optical microscope observations were performed on the Dino-Lite MZK 1701 digital microscope at 50x and 230x magnifications. Sample images at 50x and 230x magnifications are shown in Fig 2. EDX (Energy-dispersive X-ray spectroscopy) was performed at Shimadzu's EDX-7000 (Measurement range: $_{11}$Na to $_{92}$U).

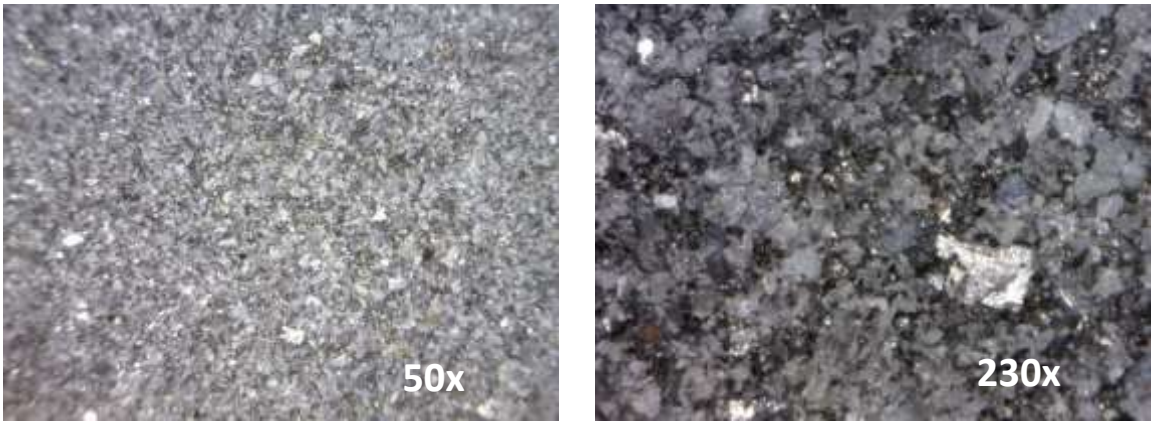

Figure 1 Sample observed with Dino-Lite MZK 1701 optical microscope (Magnification 50x and 230x)

Table 5 *Chemical analysis of lithium batteries slag*

Sample	Co	Li	Mn	Ni	Fe	Ca	Al	Cu	Ti	Si
1	13.54	3.31	1.83	1.89	8.55	3.56	6.88	2.33	0	13.76
2	12.62	2.68	1.79	2.05	9.25	4.48	7.28	2.28	0	14.08
3	12.34	2.62	2.05	1.95	9.25	4.26	8.24	2.21	0	15.2
4	12.26	2.65	1.78	1.87	8.6	3.84	8.54	2.18	0	14.83
5	14.76	2.5	2.38	2.08	9.8	3.76	8.62	2.21	0	12.87
Average	**13.10**	**2.75**	**1.96**	**1.96**	**9.09**	**3.99**	**7.91**	**2.24**	**0**	**14.14**

Table 6 *EDX (Measurement range: $_{11}$Na to $_{92}$U) analysis of lithium batteries slag*

Element	Ca	Si	Al	Fe	Co	Mn	Cu	Ni	S	La	K	Ce	Zr	Pr
Result [%]	27.791	21.999	17.227	13.669	9.743	3.831	2.28	1.581	0.715	0.255	0.206	0.184	0.172	0.137

Conclusion

The importance of material recycling of portable lithium batteries waste was confirmed in this work due to an increase in lithium and mainly cobalt consumption. The increases are related to the increasing production of electronic devices requiring rechargeable batteries such as electric cars, domestic electrical energy storage, small portable electrical equipment, electric bicycles and scooters and many other electronic devices. While lithium reserves are sufficient, there is a lack of cobalt, which has been reflected in a substantial increase in its market value. The work also confirmed the high amount of cobalt (13.1%) in slag produced by melting of the lithium battery active mass.

The differences between the results of AAS and EDX analysis could be influenced by the fact that EDX is a semi-quantitative analysis that cannot identify all the metals present. Due to the relatively simple existing Li and Co leaching methods, but more complicated possibilities of obtaining individual metals from solutions, the following objective will be to investigate and experimentally verify selective leaching reagents and leaching conditions, optimize processes, test methods for obtaining metals from solutions and apply those finding directly on lithium battery slag.

References

[1] Report of EU Critical Raw Materials 2017 - [Date: 15.4.2018.] <http://ec.europa.eu/growth/sectors/raw-materials/specific-interest/critical_en >

[2] Major countries in worldwide lithium mine production from 2012 to 2017 [Date: 15.4.2018.] <https://www.statista.com/statistics/268789/countries-with-the-largest-production-output-of-lithium/ >

[3] Total global consumption of lithium from 2008 to 2016 [Date: 15.4.2018.] <https://www.statista.com/statistics/451999/global-total-consumption-of-lithium/>

[4] U.S. Geological Survey – Lithium; Mineral Commodity Summaries, January 2016[Date: 15.4.2018.], < https://minerals.usgs.gov/minerals/pubs/commodity/lithium/mcs-2016-lithi.pdf >
[5] Lithium price [Date: 15.4.2018.] <https://www.metalary.com/lithium-price/>
[6] Cobalt: world demand [Date: 15.4.2018.] <https://www.globalenergymetals.com/cobalt/cobalt-demand/>
[7] Cobalt price [Date: 15.4.2018.]< http://www.infomine.com/investment/metal-prices/cobalt/1-year >
[8] Types of Battery Cells [Date:15.4.2018.], < http://batteryuniversity.com/ learn/article/types_of_battery_cells/>
[9] Disposal Li battery MSDS: [Date: 15.4.2018.] < http://www.gpbmindustry.com/public/downloads /batteries/sds/gp-cr-coin-en.pdf/>
[10] Rechargeable Li-ion battery MSDS [Date: 15.4.2018.] <http://www.bipowerusa.com/documents/ BP-MSDS-Li-ion.pdf/>
[11] The collection of waste portable batteries in Europe in view of the achievability of the collection targets set by Batteries. [Date: 15.4.2018.] <https://www.epbaeurope.net/wp-content/uploads/2017/03/Report-on-the-portable-batterycollection-rates-Update-Dec-16-full-version-FINAL.pdf >

Tribological properties of soft magnetic Fe/MgO composite

Pavel Kurek, Radovan Bureš

Institute of Materials Research of SAS, Watsonova 47, 040 01 Košice Slovakia,
pkurek@saske.sk

Introduction

Soft magnetic composites (SMC) can be describe like, a composition of soft magnetic metal particles electrically insulated each other. The aim of SMC is to minimize eddy current losses, and retain the permeability at same level in higher frequencies [1]. Application of the SMC's are in the field of static and rotating structural part of electrical devices. For potential industrial application can be important to characterize the wear resistant of the SMC's especially in case of fast moving structural parts [2].

Experimental

As experimental material were chosen ASC 100.29 (Fe) produced by Höganäs and MgO produced by MTI. Fe is technically pure iron with chemical composition 99 % of Fe, 0,02 % of C, 0,08 % of O and mean particle size 98 μm. MgO particles has polyhedral morphology, particle size is 20-40 nm, purity 99 % and true density is 3,58 g/cm^3. MgO was dry admixed in Fe by resonant acoustic mixer LabRAM. Mixing of mixtures was made in proportions of 1; 2; 3; 5; 10; 13,85 wt.% of MgO in Fe. Compaction of samples was made by uniaxial cold pressing at pressure 600 MPa using press machine Labtest 5.600 Zl. Dimension of cylindrical samples were 3,5 mm in high and 16 mm in diameter. Samples were sintered at 600 °C in furnace with conventional heating (CS), single-mode microwave furnace (MWS-S) and multi-mode microwave furnace (MWS-M). In CS process was dwell time 1 hour. In both microwave processes dwell time was 15 min. Vickers hardness were measured by LECO LM700AT with a load 10 N. Tribological properties were measured in accordance of standard ISO 20808: 2004 (E). Standard describe the tribological method "ball on disc" as it is visible in Fig 1-2. As a tribological pair was used a ball made of WC with diameter 6 mm. The Ball passed distance 200 m under load 50 N with sliding speed was 0,1 m/s. Coefficient of friction (COF) was measured during dry sliding of the ball on the rotated disc by universal tribometer Bruker UMT (tribo) in air. After the tests were measured cross sections areas of wear tracks by profilometer confocal microscop SENSOFAR (CM). The cross section areas were used in further calculation of wear volume and specific wear rate by equation 1, 2 and 3 [2]. Where $S_{1\text{-}4}$ are cross sections areas, R is radius of a track, V_{disc} wear volume F_p is load during a test, $W_{S(Disc)}$ is specific wear rate (W_S), L is distance passed by a ball, F_f is friction force and μ is COF.

$$V_{Disc} = \frac{\pi x R(S_1+S_2+S_3+S_4)}{2}[m^3] \quad (1)$$

$$W_{s(disc)} = \frac{V_{disc}}{F_p x L}[m^2 N^{-1}] \quad (2)$$

$$\mu = \frac{\overline{Ff}}{Fp} \quad (3)$$

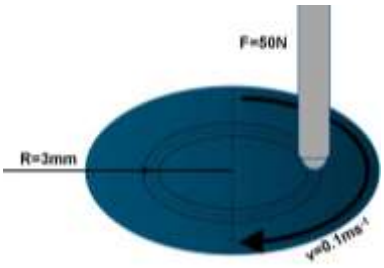

Figure 1 Schema of tribology test

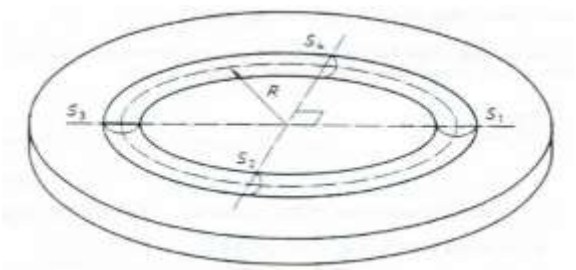

Figure 2 Schema of wear track regions for measuring cross sections areas

Results and discussion

Cross section areas measured by CM, in Fig. 3-8, were used in calculation of wear volume and specific wear rate using equation (1), (2) and (3). In Figure 9, dependence of the specific wear rate on MgO addition indicate increase of W_s above 10 wt.% of secondary phase in the composite. The most significant increase of W_s values were observed in case of MWS-S samples. Sintering based on conventional heating led to much more lower volume of removed material in comparison with microwave sintered samples at the same (10 and 13,85 wt.%) MgO content ratio. Value of the COF, in Fig.10 was lower in comparison to sintered ASC100.29 as reference material [3], regardless of used sintering technology. Changes of COF in dependence on MgO content indicate changes in wear mechanism.

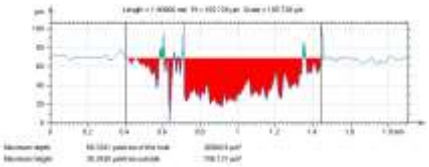

Figure 3 Cross section area 1 wt%MgO CS CM

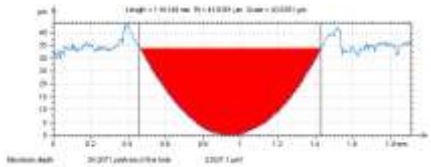

Figure 4 Cross section area 1 wt%MgO MWS-M CM

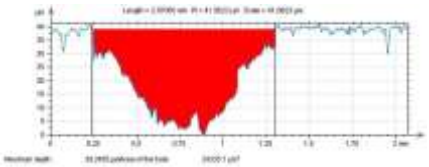

Figure 5 Cross section area 1 wt%MgO MWS-S CM

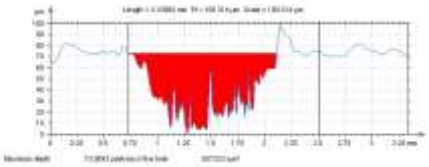

Figure 6 Cross section area 10 wt%MgO CS CM

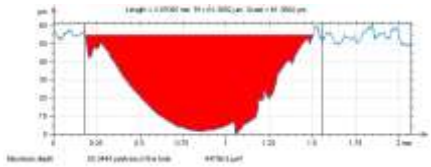

Figure 7 Cross section area 10 wt%MgO MWS-M CM

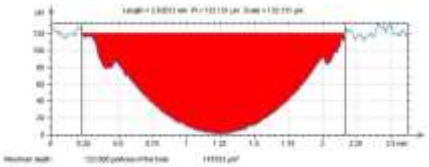

Figure 8 Cross section area 10 wt%MgO MWS-S CM

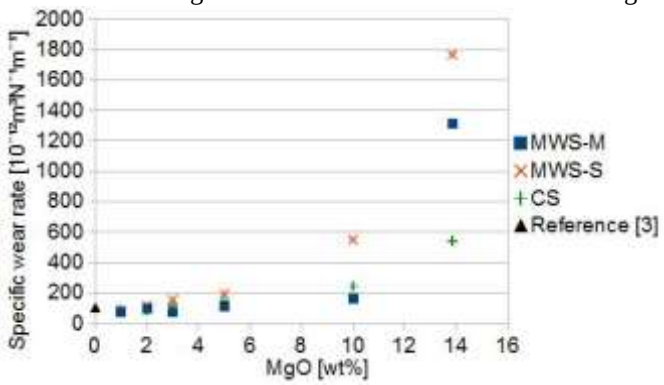

Figure 9 Specific wear rate in dependence on MgO content

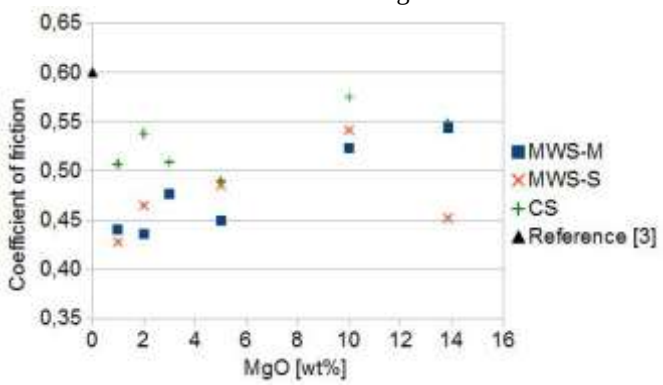

Figure 10 Dependence of COF on content MgO

Wear track of the Fe1MgO and Fe10MgO composites were investigated by OM using polarized light (pl) as it is shown in Fig.11. and 14. Detail of the boundary between untreated sintered surface and wear track was documented by OM-pl using differential interference contrast technique (dic). Topographical profile at the selected region is presented in Fig.13 and 16. together with Z-focused OM-pl-dic images. Textures of the surface of sintered composites are shown in Fig.12. and 15. From the previously work is known that in samples with content higher than 5 wt% MgO increasing the content of unreacted MgO that causes lower mechanical properties as mentioned in the [4].

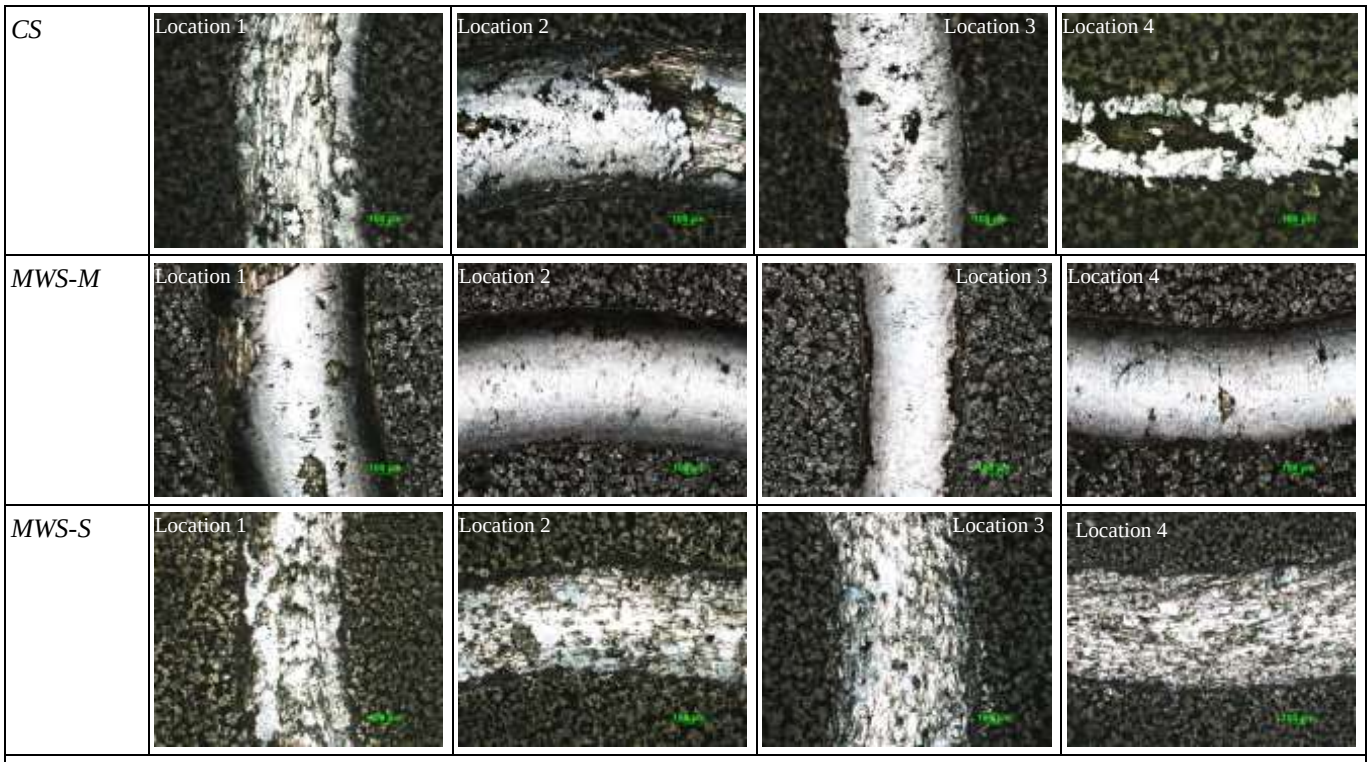

Figure 11 Wear tracks of samples Fe+1% wt MgO, OM-pl

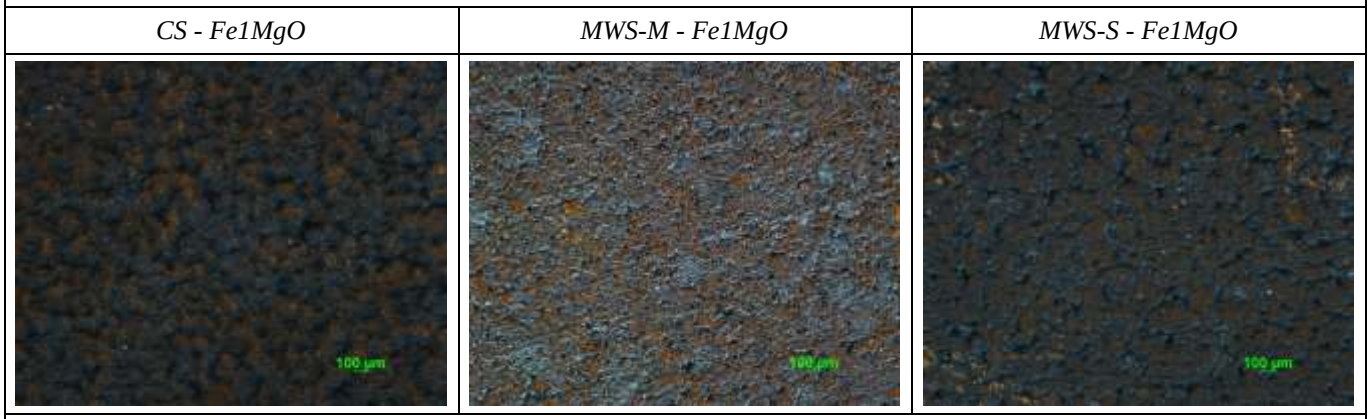

Figure 12 Texture of sintered surface, OM-pl

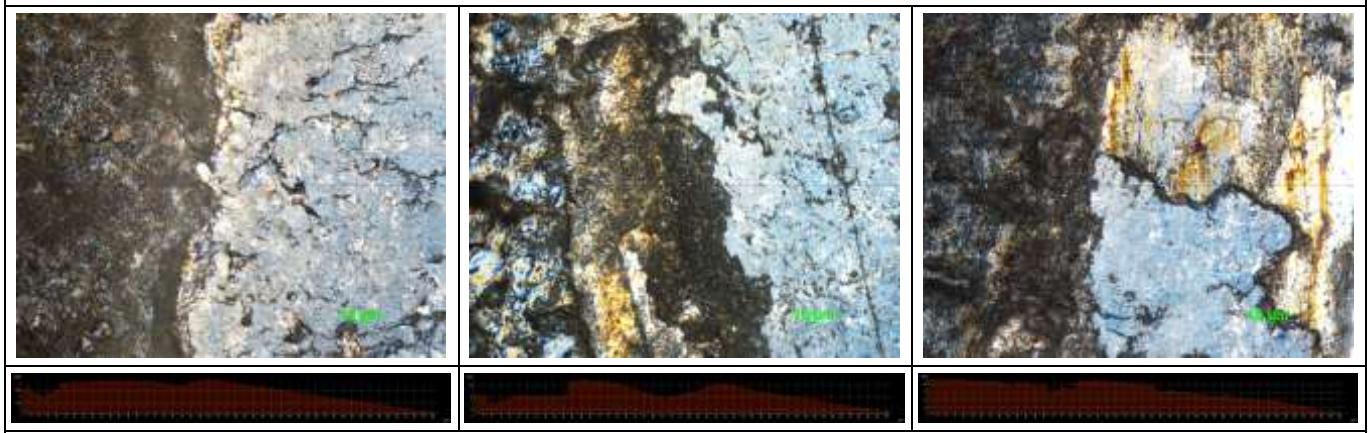

Figure 13 Boundary of surface – track OM-pl-dic, Z-profile in signed region (blue line)

Increasing MgO ratio influence on change of wear mechanism of the composite. Low content ratio 1 or 2 wt.% of MgO lead to fatigue failure of the primary iron phase. The result is tumble out of single iron particles especially at the boundary of wear track and origin sintered surface as it is shown in Fig.11. and 13.

Increasing MgO content ratio in the composite changed a texture of the surface of sintered composite as it is documented in comparison of Fig.12 and 15. High content of secondary phase change this mechanism to combination of the abrasion and decohesion in interphase region of primary and secondary phase.

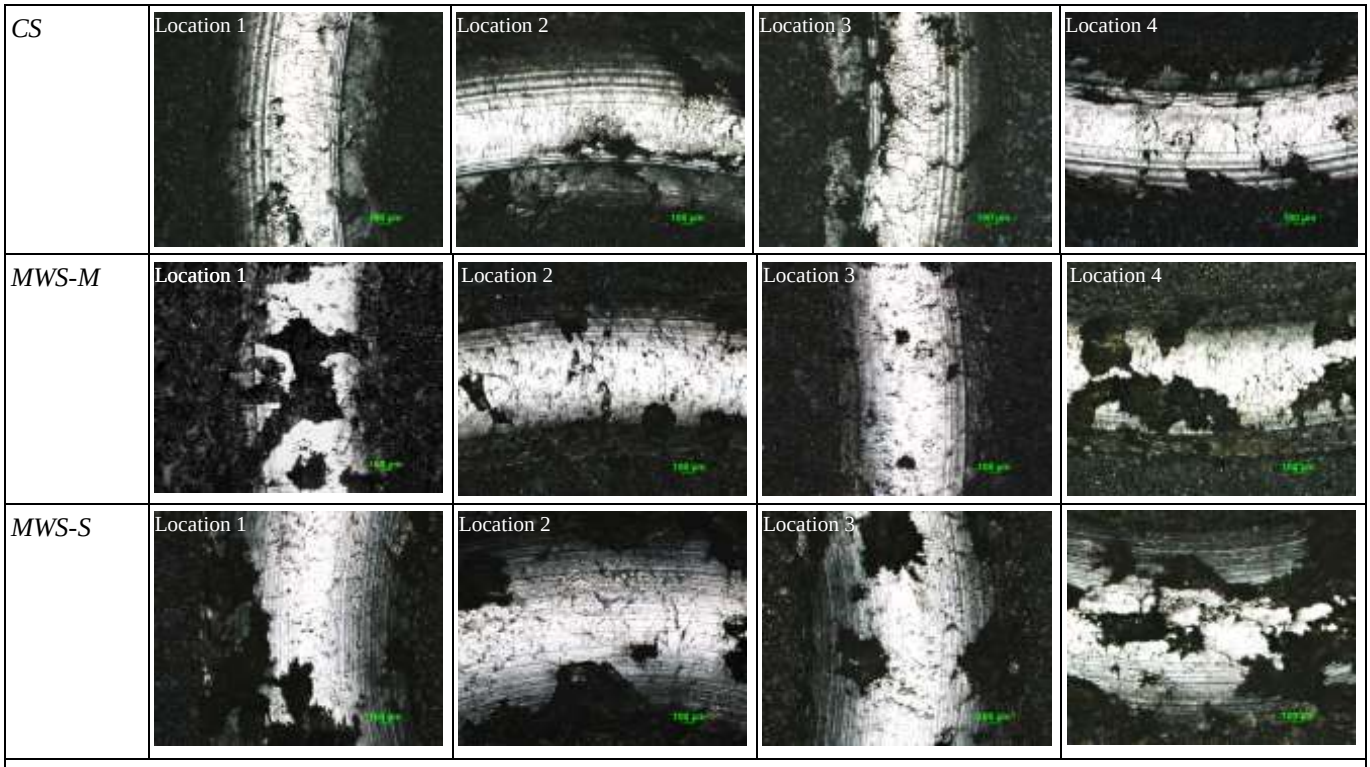

Figure 14 Wear tracks of samples Fe+10% wt. MgO, OM-pl

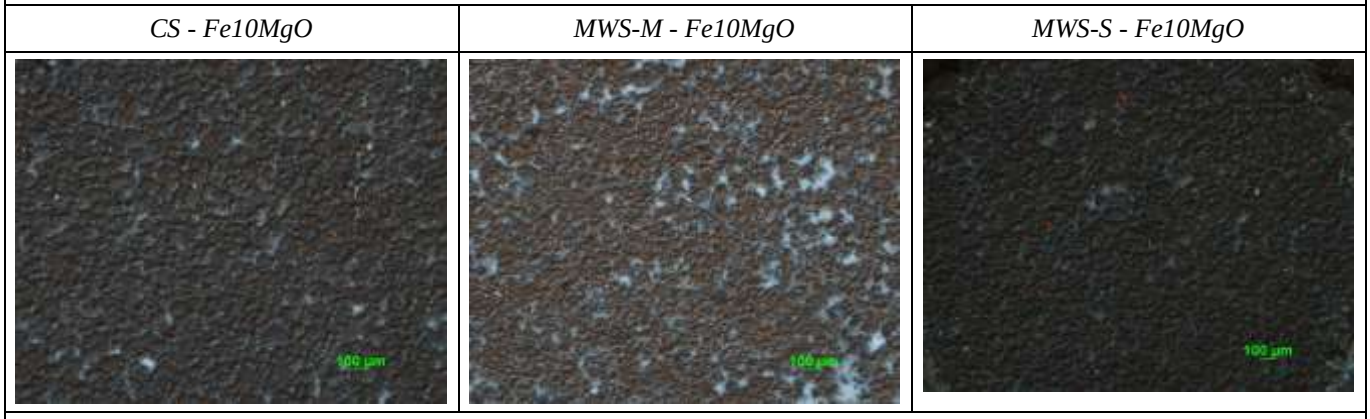

Figure 15 Texture of sintered surface, OM-pl

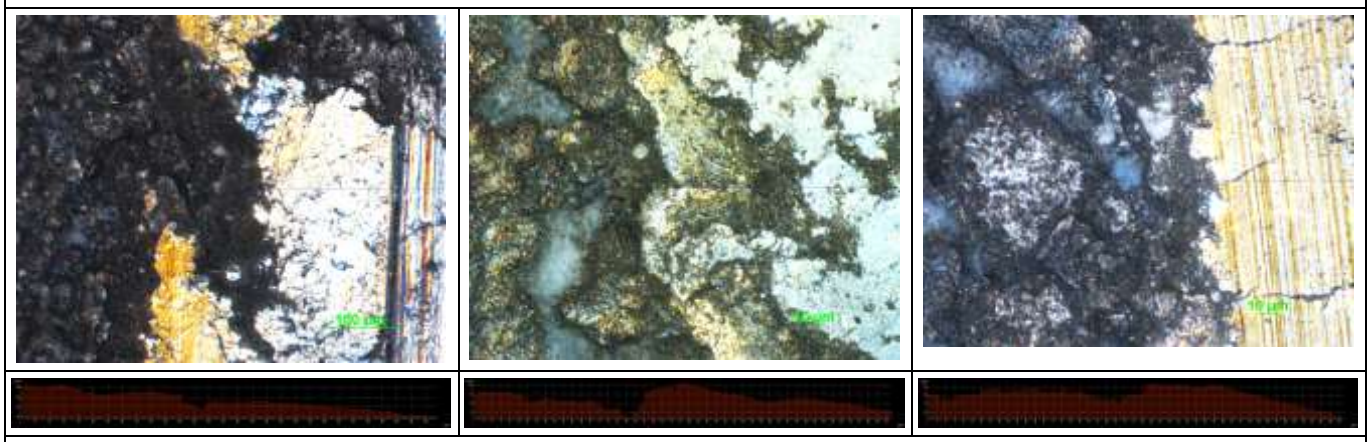

Figure 16 Boundary of surface – track OM-pl-dic, Z-profile in signed region (blue line)

The result of this combining mechanism was peel off observed in the wear track as it is shown in Fig.14 and 16. Low content of secondary phase increase of wear resistance and decrease of friction coefficient at the same time. Higher secondary phase content decrease wear resistance. MW-S sintering cause creation of hard phases which cause rapid secondary phase decohesion. MW-M sintering led to similar wear resistance as CS, but sintering time is 4 time shorter in comparison with CS. In Table 1 are Vickers hardness values of the primary and secondary phase in dependence on MgO addition in the composite. Hardness values of the secondary phase of MWS samples above 5 wt.% of MgO are divided to two groups, where first group is created based on the residual MgO and second group is based on interphase of Fe and MgO. The composition of the interphase is based on non-stoichiometric Mg ferrite as it was presented in [4].

Table 1 *Hardness of primary and secondary phase of CS and MWS samples*

	CS		MWS		
wt.% MgO	Primary phase	Secondary phase	Primary phase	Secondary phase	
1	162±6	255±10	188±1	438±6	
2	164±6	255±6	185±5	446±6	
3	162±6	249±19	196±7	480±51	
5	163±3	256±11	194±4	535±32	116±3
10	163±4	298±9	194±4	591±26	114±4

Proposed wear mechanism is consistent with our previous observation of the mechanical properties of these composites [5]. However, clear interpretation of the wear mechanism requires more detail microstructural observation and analysis.

Conclusions

Tribological properties of the Fe/MgO composites were investigated in dependence on MgO content ratio from 1 to 13.85 wt.%. Analysis of the tribological characteristics and microstructure observation of the wear track led to following results:

- increasing MgO content from in the range from 0 to 3 wt.% can improve the wear resistance of the Fe/MgO composite
- higher content ratio above 10 wt.% of MgO has no positive effect to tribological properties of the Fe/MgO composite
- microwave sintering regardless of regime of microwave cavity have strong influence on the surface texture and wear track microstructure as well as tribological characteristics of the sintered composites
- multi-mode microwave sintering provide close similar tribological properties of the composite, but sintering time is 4 time shorter in comparison to sintering using conventional heating

Acknowledgement

This work was supported by the projects VEGA 2/0108/18 and APVV 0115-15.

References

[1] Shokrollahi H., Janghorban K.: Soft magnetic composite materials (SMCs). In *JMPT* (2007) 1–12. ISSN 09240136

[2] Koji K., Adachi K.: Wear Mechanisms. Modern Tribology Handbook 1 (2001) 273–300

[3] Liersch A., Danninger H., Ratzi R.: The Role of Admixed Hexagonal Boron Nitride in Sintered Steels 2 . Effect on Sliding Wear and Machinability. In *PMP 7 (*2007) 2

[4] Deraz N.M., Abd-Elkader O.H.: International Journal of Electrochemical Science 8 (2013) 8632-8644

[5] Kurek P., Bureš B., Faberová M.: Microstructure and mechanical properties of Fe/MgO micro- nanocomposite. In: DFPM (2017) 74. ISBN 978-80-89782-07-9

Preliminary Experiment on Hydrometallurgical Treatment of Slag with Ozone

Patrik Kuruc, Andrea Miškufová

Technical University of Košice, Faculty of Materials, Metallurgy and Recycling, Institute of Recycling Technologies, Letná 9, 042 00, Košice, Slovakia
patrik.kurucuke.sk

Abstract

Despite the fact that some types of slags contain interesting amounts of deficient metals and represent a valuable secondary source of metals, often this increased content of some heavy and toxic metals (Cr, Ni, V) is the key factor for their application. It is necessary to study potential possibilities of recycling and material recovery of these secondary resources in order to prevent wasting of primary and non-renewable resources. This paper and corresponding research is conducted as a part of the project funded by HORIZON 2020 Research and Innovation program under Grant Agreement No.730 471 with acronym CHROMIC. This project aims to develop new recovery processes for critical and economically valuable metals (Cr, Nb, Mo, V) from secondary recources, mainly slags. The chemical composition of the slag depends on a number of factors, particularly the batch (the type of steel required), the method of production and the technological process, which also affects the usability of the alloying ingredients. Within the scope of the CHROMIC project, there are three types of studied slags. Slag from electric arc furnace, slag from FeCr production and slag from stainless steel production. In this paper, issues with slag recycling and preliminary results from treatment of one of the studied slags are presented.

Introduction

Steel slag is a solid waste that is produced as a by-product of steel production. Depending on the aggregate in which steel slag is formed, the slags are divided into two groups: EAF slag (slag from electric arc furnace) and BOF slags (basic oxygen furnace). Another commonly used classification of slags is according to the product with which they are produced, such as slag from the production of stainless steel or ferrous slag. The chemical, mineralogical and morphological properties of the slags are determined by process conditions in which they are produced. Not only groups of slags differ from each other, but also slags from one aggregate produced in different batches may have different properties. If the slag contains sufficient amount of iron, it is returned to the production of iron or steel as feedstock. If it does not meet required properties for such use, slag is landfilled or demetallized and used in civil engineering. Approximately 35% of slags produced worldwide are landfilled [1]. In dependence on mechanical properties and methods of slag treatment, it can be used for landscaping, backfilling, road maintenance, as additives in concrete and other applications in construction. Treating slags by this approach, the natural resources and aggregates that would be otherwise used are preserved but the potential of slag as the secondary raw material is not fully exploited. Following chapter describes some studies on hydrometallurgical treatment of slags for the purpose of metal (mainly Cr) extraction.

Studies on Hydrometallurgical Processing of Slags

In the study of Wang et al. [2], leaching of steel slag in sulphuric acid without enhancing the process was conducted. It was found that high recovery of Cr can be achieved, but also other metals as Fe and Ca are dissolved. This effect is unwanted due to followed extractions of Cr from solution. Zydorczak et al. [3] studied leaching of chromium from powdered Cr (technical grade) in sodium hydroxide under standard conditions. Even after 75 days the leaching process did not reached maximum recovery and thus, this process is not suitable for slag treatment. Intensifying the leaching in sodium hydroxide by pressure leaching showed higher recovery rates, but achieved results (46% Cr recovery) are not sufficient for such a costly process [4]. Pre-treatment of slag by roasting followed by leaching in water showed the highest effectivity [5-7]. Different additives and conditions of roasting were studied and in some cases,

the efficiency of leaching of treated slag in water achieved 100 % recovery of Cr. Additional advantage of this process is that the matrix material of slag remain intact, or only a fraction of metals as Fe or Ca are leached. On the other hand, roasting larger quantities of material can produce unwanted gaseous byproducts. Roasting itself can also consume high amount of energy. Use of ozone as an oxidant in leaching process can be considered as environmentally and economically more acceptable process. Leaching by use of ozone, no byproducts are produced. Whereas oxygen is only product of ozone decomposition, the leaching solution is not contaminated. On the other hand, there is still a lack of research on subject of ozone leaching of slags. Thus, this paper and research on this subject is conducted as a part of CHROMIC project.

Experimental Part

Material Analysis

For the purpose of the project, three types of slags were used and characterized. The samples of slags are shown on Fig.1. EAF slag comes from the production of carbon steel in electric arc furnace, FeCr slag is from the production of ferro-chromium, and SS slag is from stainless steel slag production. Slag samples were subjected to chemical analysis and mineralogical analysis.

a) **b)** **c)**

Figure 8 Studied slags: EAF slag (a), FeCr slag (b) and SS slag (c)

The results of the partial chemical analysis of the slags are shown in Tab. 1. The analysis was primarily oriented to the content of chromium, vanadium, iron, aluminum and calcium. The samples differ mainly in the matrix material composition. While EAF contains a significant amount of iron, FeCr and SS slags have almost no iron, but on the other hand they contain more calcium.

Tab. 7 *Chemical composition of studied slags*

	wt.%					mg.g^{-1}
Type of slag	**Fe**	**Al**	**Ca**	**Mg**	**Cr**	**V**
EAF	30,7	4,78	27,29	2,24	2,25	0,976
FeCr	0,35	2,7	33,03	5,57	2,5	0,288
SS	0,31	0,96	38,66	3,95	1,6	0,58

From XRD patterns it was observed that in EAF slag, dominant phases are: ferrous oxide (FeO), calcium alumina-silicate (gehlenite), calcium silicate (Ca_2SiO_4), magnetite (Fe_3O_4) and magnesioferrite ($Mg_8Fe_{16}O_{32}$). Chrome was identified as chromite ($FeCr_2O_4$). Sample also contained calcium in the form of calcium carbonate ($CaCO_3$) and calcium aluminate ($CaAl_2O_4$). Sample from FeCr production contained more magnesium, thus more Mg based phases were found by XRD analysis, such as merwinite, bredigit, periclase, ghelenite, hercynite, spinels, etc. Chrome was identified in complex spinel phase with Mg, Al. Other possible phase is also. In third sample, slag from stainless steel production, except from calcium/magnesium alumina-silicates, also maghemite (Fe_2O_3) and compound based on Ca, Mn

was found. Chrome was indentified as dopant in akermanite mineral and in complex compounds as $Ca_2Al_3CrO_8$ and $NaK_3(CrO_4)_2$.

Methodology and Used Apparatus

For leaching experiments, the equipment shown on Fig. 2 was used. Apparatus consists of pressure cylinder as oxygen supply for ozone production, ozone generator, ozone measuring instrument, flow rate meter and reaction vessel with magnetic stirrer.

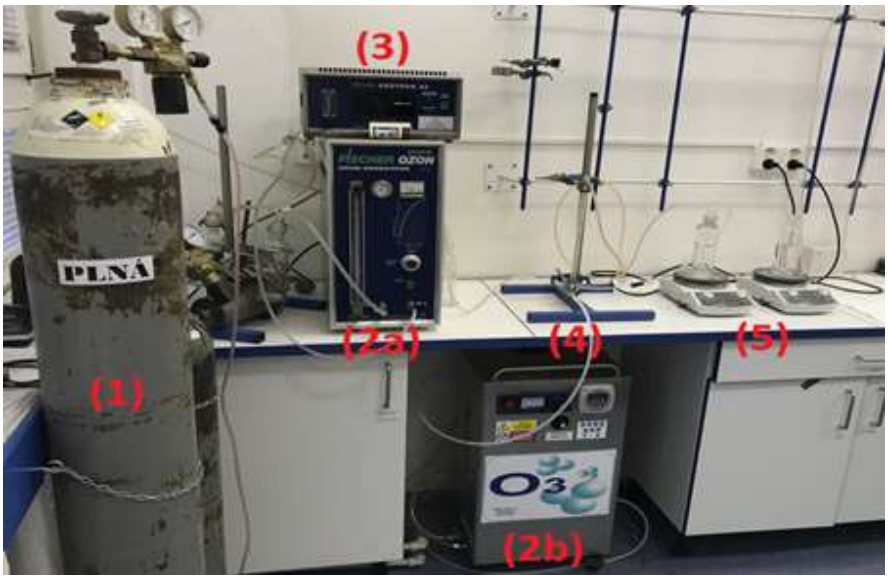

Figure 9 Experiment setup: 1) pressure cylinder (O_2), 2) ozone generators, 3) ozone analyzer, 4) flow rate meter and 5) reaction vessel

In preliminary experiments, 10 grams of slag sample was leached in 200 ml of alkaline solutions with addition of gaseous ozone bubbled through the frit. Sodium carbonate, sodium hydroxide and potassium hydroxide were used as leaching solutions with 2 M concentrations. Experiments were conducted under normal conditions for temperature and pressure (20°C and 101 325 Pa). The flow rate of gas was maintained at around 250 $l.hod^{-1}$. Under this conditions, ozone concentration on entry in vessel was around 33 $g.m^{-3}$, which is equal to 8,25 grams of ozone produced per hour.

Before leaching experiment, slag samples were grinded in vibration mill (VM4) for different time, in dependence of character of material. Material was then sieved and fraction between 90 and 125 µm. EAF slag was stiffer and after 5 minute of grinding, large amount of material was in the fraction over 125 µm. So this fraction was grinded again for 2 minutes. For FeCr slag, 5 minute of grinding was sufficient. Slag from stainless steel production was soft and adhesive, so only 30 second of grinding was applied and after sieving, fraction over 125 µm was grinded for another 20 sec.

Results and Discussion

After 1 hour of leaching, barely 3% recovery of chromium to solution was achieved. However process of leaching did not seem to reach the highest yields for chosen conditions, because the concentration of Cr in solution continued to increase after 1 hour. Experiments with longer duration should be carried to acquire higher yields under studied conditions. Other possibilities of improving the leachability of chromium are to be examined. One potential option is to raise temperature; however when using ozone as oxidant, the higher temperature may negate the effect of O_3. Most likely, pretreatment of samples will be carried. This can be done by mechanical activation of slags by grinding o lowest grain size possible or by roasting it with additives, then proceed to leaching in water or solutions of hydroxide with addition of ozone as oxidant.

Acknowledgement
The CHROMIC project received funding from the European Union's Horizon 2020 Research and Innovation program under Grant Agreement n° 730471. This work was also supported by the Slovak Research and Development Agency under the contract No. APVV-14 0591.

References

[1] The European Slag Association: Position paper on the satus of ferrous slag [online]. The European Slag Association, 0/2012. [cit. 2016-10-30]. Dostupné na internete: http://www.euroslag.org/fileadmin/_media/images/Status_of_slag/Position_Pa per_April_2012.pdf Asd
[2] Wang et al.: A novel technology for vanadium and chromium recovery from V-Cr-bearing reducing slag. Hydrometallurgy. Volume 171 (2017), 116-122
[3] Zydorczak et al.: Dissolution of $Cr_2O_{3(s)}$ and the Behavior of chromium in concentrated NaOH solutions. Industrial & Engineering Chemistry Research (2012) 51 (51), 16537-16543
[4] Kim et al.: Valorization of stainless steel slag by selective chromium recovery and subsequent carbonation of the matrix material. Journal of Cleaner Production. Volume 117 (2016), 221-228
[5] Jun et al.: Characteristics and treatment technologies of stainless steel slag. Advanced Materials Research. Vols. 225-226 (4/2011), 812 – 815
[6] Kim et al.: Selective recovery of Cr from stainless steel slag by alkaline roasting followed by water leaching. Hydrometallurgy. Volume 158 (12/2015), 139 – 148
[7] Yilong et al.: Mechanisms Involved in the Roasting of Pellets Composed of Stainless Steel Slag and Sodium Hydroxide to Extract Chromium. ISIJ International. Vol. 56 (2016), No. 10, 1751 – 1757

A kinetic study of the acid leaching of magnesite for preparation of pure magnesium salts.

Maryna Kyslytsyna, Pavel Raschman

Technical university of Kosice, Faculty of materials, metallurgy and recycling, Institute of metallurgy, Letna 9, 042 00 Kosice, Slovak Republic
maryna.kyslytsyna@tuke.sk

Introduction

Magnesium plays an important role in the production of magnesia, magnesium metal and magnesium compounds. These products are widely used in many industries: from metallurgy to pharmaceuticals, agriculture and environmental protection. Slovak deposits of crystalline magnesite belong to the largest and most important in the world. Due to the decrease in consumption of refractory materials in recent years, the development of non-traditional ways of using magnesite is of interest.

The hydrometallurgical processing of magnesite usually begins with the leaching using solutions of inorganic or organic acids, or hydrolysable salts. Inorganic acids show a higher rate of leaching, but a lower selectivity than organic ones. Also, the limiting factor for organic acids is a relatively low boiling point, resp. their decomposition [1].

Theoretical

Analysis of the published results of the experimental study of the leaching of natural magnesite by solutions of inorganic or organic acids [1-9] showed an interesting phenomenon: the rate of dissolution increased with increasing acid concentration only up to a certain maximum - with further increase of concentration decreased [4, 8, 9] or remained almost constant [7].

In the literature [1, 3, 4] the authors give two reasons for the existence of this maximum:

- If the acid concentration is too high, the water content in the solution is decreased and the activity of hydrogen ions is decreased, as well.
- The reaction products form a poorly soluble film around the solid particles, thereby the transfer of the reactants to the reaction surface and products from the reaction surface is slowed down.

Akselrud and Molchanov [8,9] studied the leaching process, when the rate-controlling step was the external diffusion. They proposed a methodology for estimating the value of the total mass transfer coefficient, which includes the effect of mixing the solution with a stirrer and at the same time with bubbles of releasing gas. However, the values of apparent activation energy published in the works of other authors [1, 4, 7] indicate that the rate-controlling step of the leaching of magnesite can also be the chemical reaction. For this case, the effect of CO_2 releasing from the solid surface on the overall process has not been deeper analyzed yet.

Experimental

Material and method

In the experiments, the magnesite from Jelšava was used. The material was washed, dried and subsequently divided into fractions by sieving. For the leaching tests the fraction of 80-125 μm was used - the chemical (elemental) analysis (AAS method) is in table 1. The leaching of magnesite was realized in a glass mixed batch reactor with a defined liquid-to-solid weight ratio at different temperatures and concentrations of hydrochloric acid. High excess of the acid was used in all experiments. In the first set of experiments, the slurry was mixed with a turbine stirrer and in the second set of experiments with magnetic stirrer. The mixing speed varied from 500 rpm to 800 rpm. Changing the nature of the mixer did not influence the leaching process. At defined reaction times, samples of 20 ml were taken from the reaction suspension. The concentrations of metals dissolved were determined by the complexometric method.

Table 8 *Chemical composition of magnesite*

Al %	Si %	Ca %	Mg %	Fe %	Mn %	s.ž. %
0.16	0.6	3.5	27.6	3.26	0.3	49.92

Results and discussions

Figures 1 and 2 show the time dependence of the conversion of magnesite on the concentration of HCl and temperature. The effect of temperature was significant and increased with increase of temperature. An increase in the acid concentration led to an increase in the leaching rate to a certain maximum (about 2 M HCl). The initial dissolution rates observed for the higher acid concentration were already lower than that for 2 M HCl. The effect of acid concentration on the dissolution rate is shown in Figure 3 for leaching at 70°C and 100°C. At 100°C, the effect of concentration was more visible. From the experimental data, we calculated the initial dissolution rate, *r* (in $mol.m^{-2}.s^{-1}$), using the following equation:

$$r = \frac{w_{Mg}}{M_{Mg} s_G} * \frac{dx}{dt}\Big|_{x=0,1} = k * \frac{dx}{dt}\Big|_{x=0,1} \qquad (1)$$

where x is the degree of conversion of $MgCO_3$, t – reaction time (s), w_{Mg} – the weight fraction of Mg in $MgCO_3$ from the chemical analysis, M_{Mg} – the molar mass of Mg ($g.mol^{-1}$), s_G – geometric surface (≈0.02 $m^2.g^{-1}$).

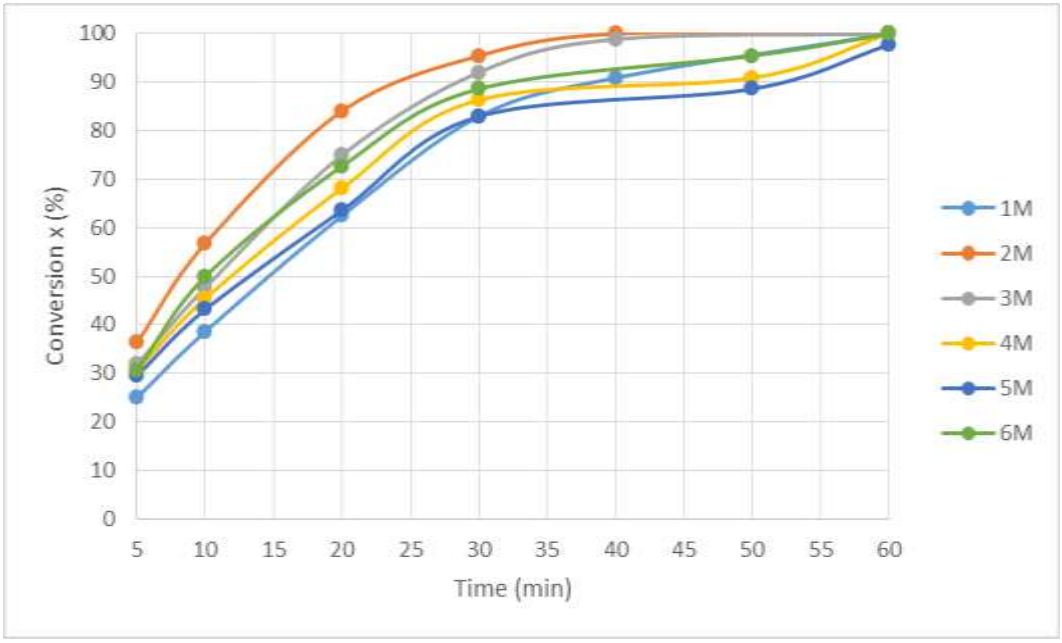

Figure 7 The effect of HCl concentration on the conversion of magnesite (at 100°C)

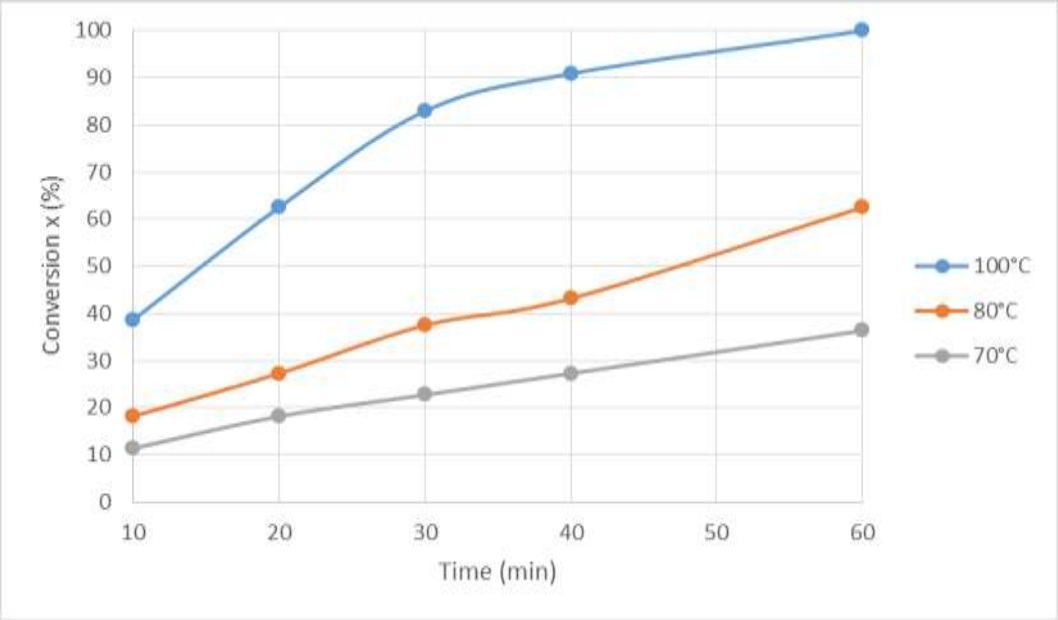

Figure 8 The effect of the temperature on the conversion of magnesite (in 1M HCl)

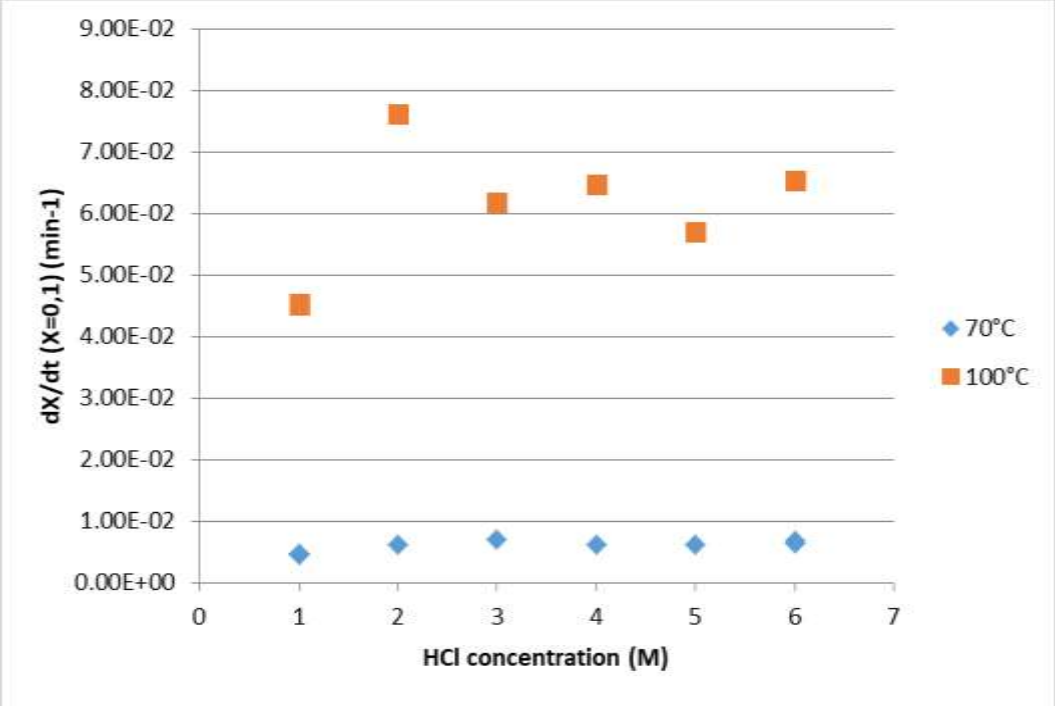

Figure 9 The curves of Mg dissolution: dx/dt (x=0,1) (min^{-1}) – HCl concentration (M); 70°C, 100°C

The values of apparent activation energy calculated from the results presented were 51.0 $kJ.mol^{-1}$ for 3M HCl and 63.2 $kJ.mol^{-1}$ for 1M HCl. They indicate that the leaching process was controlled by the surface chemical reaction. Therefore, the influence of the gaseous product on the magnesite leaching rate in the processes controlled by chemical reaction is still an interesting topic for further research.

Conclusion

Experiments were carried out to study the kinetics of leaching of magnesite in hydrochloric acid. In the leaching tests, different temperatures and different concentrations of hydrochloric acid were used. It was confirmed that the temperature has a significant effect on the dissolution rate of magnesite.

However, it was observed that the dissolution of the crystalline Slovak magnesite is much slower than the dissolution of Turkish (microcrystalline) magnesite or dolomite at the same temperature and HCl concentration, as reported by other authors. It can be assumed that this is due to the crystalline structure of the Slovak magnesite. The highest initial dissolution rate was measured in 2 M HCl. This indicated the existence of a maximum in the dependence of the dissolution rate on the acid concentration. The values of the activation energy presented by other authors are comparable with those calculated on the basis of the results of our experiments. They show that the rate of leaching of magnesite was controlled by the chemical reaction, that is, the chemical reaction was the slowest step of the overall process of leaching. This was a different situation than that analyzed by Akselrud and Molchanov. The influence of gaseous CO_2 on the leaching rate under reaction-control conditions has not been systematically studied yet, so it will be the subject of our following research.

Acknowledgements: This work was supported by the Scientific Grant Agency of the Ministry of Education of the Slovak Republic and by the Slovak Academy of Sciences (grant 1/0592/17).

References

[1] Lacin O., Dönmez B., Demir F.: Dissolution kinetics of natural magnesite in acetic acid solutions. In: Int. J. Miner. Process. 75 (2005) 91– 99
[2] Köse T. E.: Dissolution of magnesium from natural magnesite ore by nitric acid leaching. In: Journal of Engineering and Architecture Faculty of Eskişehir Osmangazi University, Vol : XXV, No: 2, 2012
[3] Bayrak B., Lacin O., Bakan F., Sarac H.: Investigation of dissolution kinetics of natural magnesite in gluconic acid solutions. In: Chemical Engineering Journal 117 (2006) 109-115
[4] Bakan F., Lacin O., Bayrak B., Sarac H.: Dissolution kinetics of natural magnesite in lactic acid solutions. In: Int. J. Miner. Process. 80 (2006) 27–34
[5] Özdemir M., Çakir D., Kipcak İ.: Magnesium recovery from magnesite tailings by acid leaching and production of magnesium chloride hexahydrate from leaching solution by evaporation. In: Int. J. Miner. Process. 93 (2009) 209–212
[6] Hosgün H. L., Kurama H.: Dissolution Kinetics of Magnesite Waste in HCl Solution. In: Ind. Eng. Chem. Res. 2012, 51, 1087−1092
[7] Özbek H. et al.: Dissolution kinetics of magnesite mineral in water saturated by chlorine gas. In: Hydrometallurgy 51 1999. 173–185
[8] Akselrud G.A.: Massoobmen v sisteme tvjordoje telo—židkosť. Lv. Univ., 1970. p. 186
[9] Akselrud G.A., Molchanov A.D.: Rasstvorenije tverdych veščestv. Chimija, Moskva, 1977

High Pressure Die Casting Defects Overview Vol. 1

Dávid Mahút, Peter Futáš

Faculty of Materials, Metallurgy and Recycling, Techical University of Kosice, Letna 9, 042 00 Kosice, Slovak Republic

Abstract

High pressure die casting is a progressive technology able to produce large amounts of high quality dimesionally equal and complex castings. The most commonly used material in high pressure die casting technology are aluminium alloys called silumins. These materials are characterized by low mass and high strength. That makes silumines an ideal material for production of automotive industry components but also other industrial segments. In spite of all the benefits of this technology, foundry defects, which occur during casting production by this method, occur. These defects negatively influence mechanical properties of final castings and thus have an adverse effect on their quality. That is why a considerable effort is made to determine the cause of foundry defects occurence and consequently decrease their occurence during production as much as possible.

Introduction

Technology of high pressure die casting of metals has a significant place in the field of casting production from non-ferrous metals. Castings produced using this technology are characterized by high surface finish quality and dimensional unity and accuracy [1,2]. This technology is characterized by replacing gravitational metallostatic pressure by effect of plunger pressing the liquid metal in filling chamber of die casting machine. The plunger pushes the metal, in speeds in magnitude of several meters per second, into the mold cavity through inlets where metal flows at speeds of tens of meters per second. These infromation shows that cavity filling is measured in milliseconds.This, also in conjunction with mechanization and automatisation of the casting process, with high production rate are reasons of decisive share of high pressure casting technology in production of comlex shaped castings from non-ferrous metals and their alloys[3].

Problem introduction

High pressure casting must satisfy a wide spectrum of requirements, from cosmetic to structural, and performance depends on chemical composition properties of alloy from which the casting is made from [4]. Occurrence of foundry defects in high pressure die casting is influenced by various factors. Base technological parameters influencing the final quality of casting include pressing speed, specific pressure applied to liquid metal during casting cycle, mold cavity filling time, metal casting temperature, mold temperature [5-7].These factors influence each other and thus create complex of intertwining connections. Excluding technological parameters, occurrence of foundry defects is influenced by other factors, such as type of die casting machine, type of cast alloy and its metallurgical processing, correct mold construction, intake system, degassing system, cooling system and working cycle of the machine. Optimal setting of these factors is a prerequisite of high quality casting production [8, 9].

Blister

From morphologic point of view, blisters consist of small amount of material which expands in relation to surrounding surface. On a smooth component, cast under high pressure, local change of surface in range of several hundreds of a millimetre is enough to evaluate the component as aesthetically and functionally inapplicable.

In general, creation of blister during thermal cycles of the casting can occur after its extraction from the mould. It can also occur when the layer containing gas close to surface is heated to a high temperature. The pressure at high temperature gains such force that plastic deformation of surface

layer can occur. This phenomenon is occurring mainly in parts of casting which are prone to turbulent flow of metal. Turbulent flow of metal causes air entrapment in these parts of castings [10]. Visual representation of a blister is shown on fig. 1.

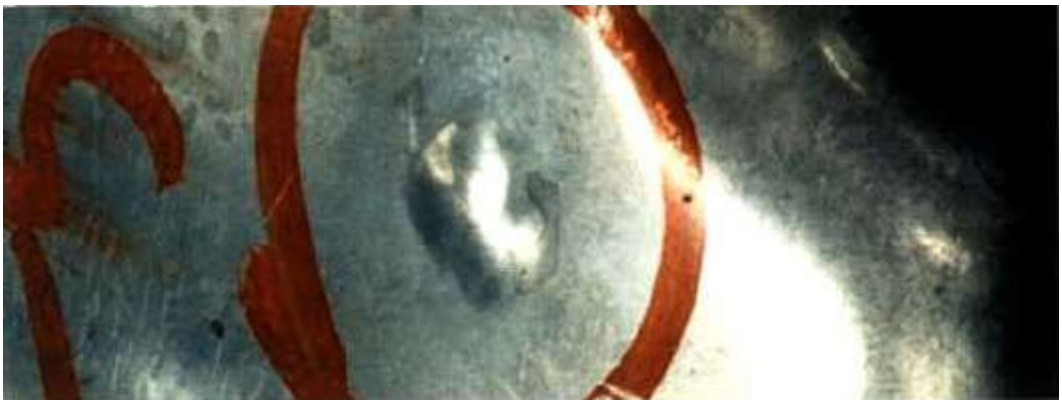

Figure 10 Blister shown on a casting surface [Nemak Slovakia s.r.o.]

Porosity

Porosity is a casting defect under which we characterize holes, or voids in castings produced in high pressure casting process. The exact cause of this defect may vary, depending on cast material, aluminium, zinc or magnesium. Porosity is usually caused by gas entrapment.

Porosity is a problem at every project of high pressure die casting. It cannot be entirely eliminated, however it is possible to control it to some degree by careful design, process control and finishing operations.

Gas porosity

The term porosity has two sub-groups. Surrounding air can be trapped in the mould and has to be extracted by means of degassing canals. It is possible, that some amount of air will be trapped in the alloy (Figure 2.). This process is called entraining. Correct mould design can, to a large extent, prevent air entraining by eliminating sharp edges and deep pockets.

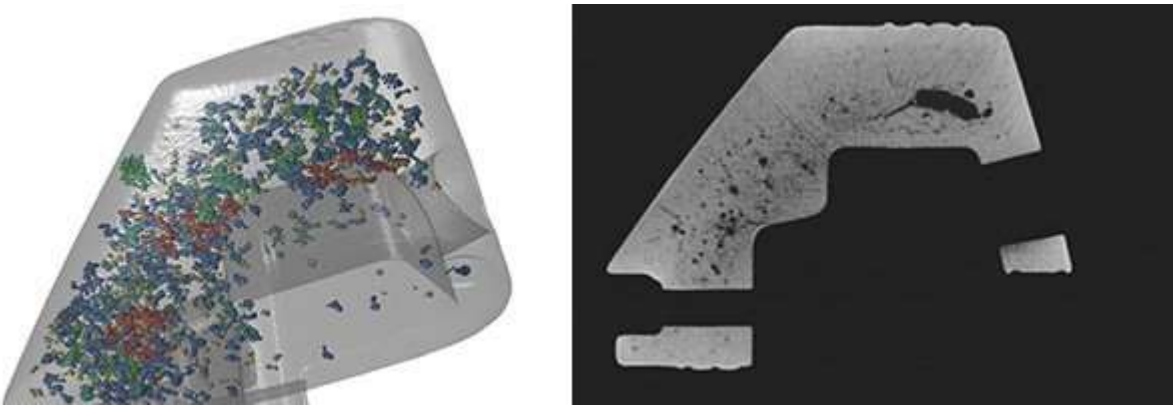

Figure 11 Simulation result and X-ray tomography scan of an aluminium die casting [https://www.starrapid.com/blog/porosity-in-pressure-die-casting-and-how-to-control-it/]

The second sub-group of porosity is gas microporosity, which occurs in deeper parts of the casting. On the surface, the metal cools quickly, and solidifies to a fine grain texture. Deeper under the surface, the liquid metal cools slower. Solidification takes more time and during that the metal shrinks. This internal shrinkage creates small voids. Into these voids gasses migrate, such as hydrogen molecules, especially in aluminium alloys, and change their state to gas. Thus creating gas filled voids in the solid metal [11-13].

Hot Tearing

One of the main foundry defects is hot tearing or hot cracking. This phenomenon represents a formation of irreversible failure (tear) in still semi-solid casting (Figure 3.). The main tearing and spreading from it many smaller tears usually occur on intergranular spaces and the surface of the defect unveils a dendritic morphology. As soon as the tear occurs, it is necessary to repair or discard, which results in increased financial losses. Hot tearing is a complex phenomenon which lies on an interface of thermal flow, liquid flow and flow of matter. Several factors influence the occurrence of hot tearing. The factors are alloy composition, mould properties, process parameters and casting design. Fine grain structure and casting process control mitigate hot tearing. It is widely accepted that hot tearing occurs because of shrinkage creation during solidification and thermal deformation during solidification. However, it is not entirely certain if the deciding factor is thermal stress, thermal strain or strain rate.

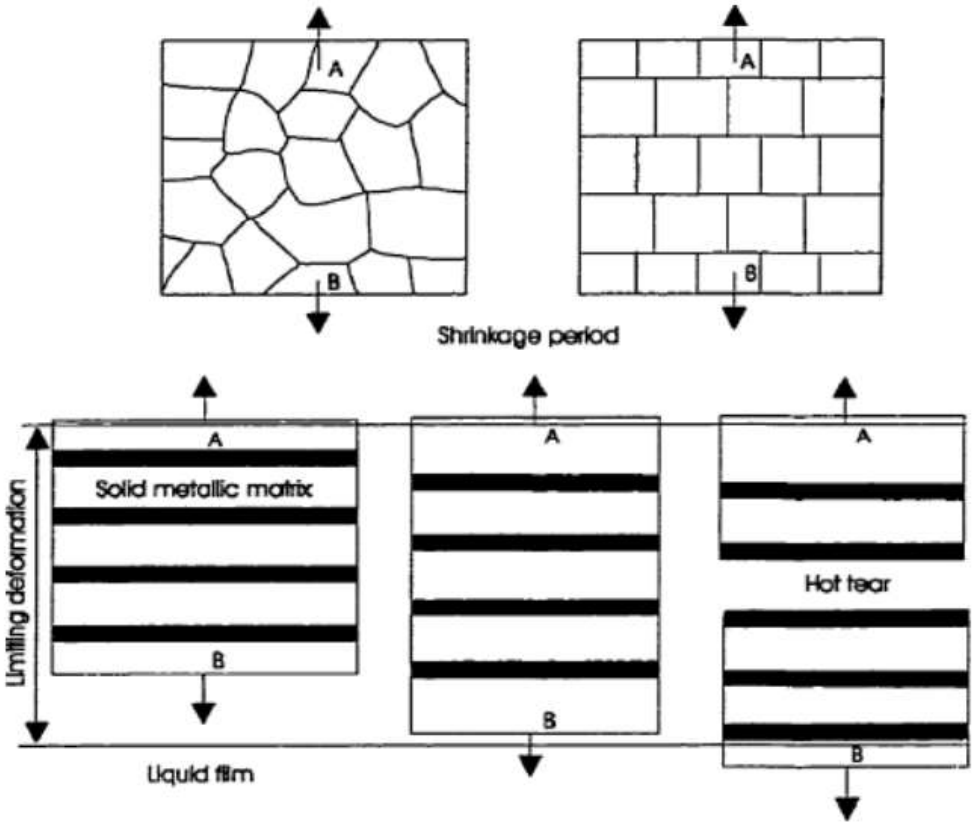

Figure 12 Hot tearing formation based on an interdendritic liquid film concept LI, S.(2010). [Hot Tearing in Cast Aluminium Alloys: Measures and Effects of Process Variables. Worcester Polytechnic Institute]

Hot tearing can be theoretically summarized into two groups:

- The first group of theories is based on stress, strain and strain rate, and these are related to thermos mechanical properties of the alloy.
- The second group of theories is based on a liquid film and insufficient filling, which are connected to metallurgical factors.

That means that hot tearing is a complex phenomenon which combines metallurgical and thermos-mechanical interactions. And even though that all of the base parameters of hot tearing formation are clear, there still isn´t a definitive consensus on the deciding factors which influence creation of this defect [14,15].

Figure 13 Photographic illustration of hot tearing on cast surface, [Nemak Slovakia s.r.o.]

Conclusion

These several casting defects mentioned above, are a part of a large technological issue which is present in die casting industry. High pressure casting defects are a ongoing problem which is tackled by optimization of casting parameters, theoretical simulations, casting, proces and mold modifications. Optimization of casting proces is a prerequisite to achievement of fine tuned production process of high quality castings for every type of industry. Description and explanation of other casting defects occuring in high pressure die casting proces, which were not mentioned in this article will be carried out in next volume of this paper.

Acknowledgements

This work was supported by the Scientific Grant Agency of The Ministry of Education of the Slovak republic VEGA1/0073/17.

References

[1] Ragan E. et al., (2007). Liatie pod tlakom, 392p., FVT Prešov
[2] Valecký J., (1963). Lití kovu pod tlakem, 450p., STNL Praha
[3] Malik J., (2013). Technológia tlakového liatia zliatin hliníka, 274p., HF TU Košice
[4] Andresen W., (2005). Die casting engineering, 400p., New York
[5] Pastirčák R., (2014). Effect of low pressure application during solidification on microstructure of AlSi alloy. In.: Manufacturing Technology. Vol. 14, No.3.(2014),. 397-402
[6] Nová I., Machuta J. (2013). Squeeze casting results of aluminium alloys. In.: Manufacturing Technology. Vol. 13, No. 1, p, 73-79
[7] Michina Š., Nová I. (2008) Technológia a spracovanie kovových materiálov. Adin, s.r.o. Prešov
[8] Bolibruchová D. (2010). Casting technology. GEORG Žilina
[9] Žmindak M. et al.,(2014). Finite element analysis of crack growth in pipelines. In.: Manufacturing Technology. Vol. 14, No. 1
[10] Ozhoga-Maslovskaja O. et.al.,(2015). Conditions for blister formation during thermal cycles of Al-Si-Cu-Fe alloys for high pressure die-casting. Politecnico di Milano
[11] https://www.starrapid.com/blog/porosity-in-pressure-die-casting-and-how-to-control-it/
[12] Quang-Cherng H. et.al.,(2013). Minimum Porosity Formation in Pressure Die Casting by Taguchi Method. National Kaohsiung University of Applied Sciences
[13] Ferencz. et.al.,(2011). Analyze of The Possible Causes of Porosity Type Defects in Aluminium High Pressure Diecast Parts, Scientific Bulleting of the Petru Maior University of Targu Mures
[14] https://www.totalmateria.com/page.aspx?ID=CheckArticle&LN=ES&site=ktn&NM=204
[15] Li, S.(2010). Hot Tearing in Cast Aluminium Alloys: Measures and Effects of Process Variables. Worcester Polytechnic Institute

Viscosity and electrical conductivity of direct-to-blister slags

Piotr Palimąka, Stanisław Pietrzyk

AGH-University of Science and Technology, Faculty of Non-Ferrous Metals, Department of Physical Chemistry and Metallurgy of Non-Ferrous Metals

Abstract

In this work, the effect of temperature on the electrical conductivity and viscosity of slags coming from a flash smelting furnace and electric furnace was examined. The slags contained 14 and 0.5 wt.% of copper, respectively. Based on the obtained results, it was found that the electrical conductivity of both slags increases with the increase of temperature. The effect of temperature on the viscosity is quite opposite to the effect on conductivity – the viscosity decreases with the increasing temperature. It was also found that at 1360 ^{o}C the slag containing 14 wt% Cu has almost 2.5 times higher electrical conductivity than the slag containing 0.5 wt.% Cu. In turn, at the same temperature, the viscosity of decopperised slag is about 3.5 times higher compared to slag before cleaning.

Introduction

Copper production technologies almost entirely use the technology of copper matte smelting and in the next stage its converting into the copper blister. The direct-to-blister technology, based on the OUTOKUMPU license, allows obtaining the metallic copper in one stage in a flash smelting furnace. This type of process is used in three places in the world - in Poland (Głogów), in Australia (Olympic Dam) and in Zambia [1]. The technology diagram is shown in Figure 1.

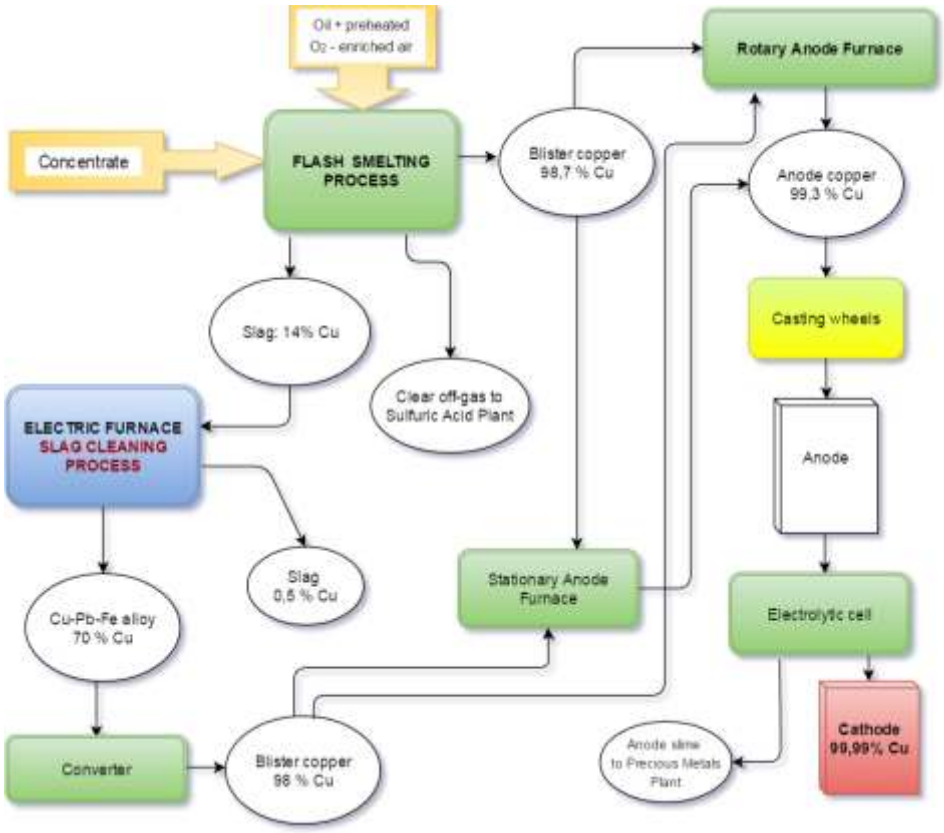

Figure 1 Diagram of the Outokumpu's Flash Smelting Process (Direct-to-blister) showing a single-step process from concentrate to end product [2]

The ditect-to-blister technology used in the KGHM Głogów Copper Smelter (Poland) consists of the following steps [3]:

- preparation of concentrate,
- copper smelting in a flash furnace (FS process),
- slag cleaning in an electric furnace (EF process),
- converting of Cu-Pb-Fe alloy,
- refining of blister copper in rotary and stationary anode furnace,
- anode copper electrorefinning.

The most serious disadvantage of the technology is the formation of slag, in which the copper content can be up to 15 wt%. Thus, the next step, i.e. the slag cleaning process, is necessary. It is carried out in electric furnace and requires significant energy expenditure. During this process, the copper oxides are reduced and the metallic phase falls down through the slag layer towards the liquid phase. The products of slag cleaning process are [3]:

- Cu-Pb-Fe alloy (70-80 wt.% Cu, 15-25 wt.% Pb),
- slag containing 0.4-0.5 wt.% Cu,
- dusts containing ~ 30 wt.% Pb and 15 wt.% Zn used for lead and zinc production,
- gases (CO, CO_2, N_2,O_2).

The Cu-Pb-Fe alloy is converted to blister copper and then refined in anode furnaces together with copper blister from FS.

In the electric furnace, the heat necessary for smelting is generated by the resistance of the slag to the passage of current (Joule heating) between Soderberg electrodes immersed in the slag. The slag should have a low viscosity to allow adequate separation and settling of liquid metal towards the metallic phase (Cu-Pb-Fe). Thus, the viscosity and electrical conductivity are among the most important properties of the slag. Additionally, knowledge about the electrical conductivity and viscosity of molten slags as a function of their composition and temperature is very important in the design of new furnaces or modification of the existing ones.

Experimental

Electrical conductivity

In this work, the CVCC (Continuously Varying Cell Constant) was used for measurements of electrical conductivity. This is the technique with a moving electrode in a relatively large diameter capillary (tube-type) conductivity cell. The principle of the CVCC technique is based on the continuously varying cell constant, measuring at the same time the real component of the circuit, R_m, at a fixed high frequency [4]. Because of the linearity of R_m versus the cell constant, the electrical conductivity of the electrolyte can be obtained from equation (1).

$$\kappa = \frac{1}{A(\frac{dRm}{dL}]} \qquad (1)$$

where: κ - electrical conductivity, S/cm, A - inner cross - sectional area of capillary, cm^2, dR_m/dL - slope of the resistance of the measuring circuit versus the cell length.

The scheme of the cell for electrical conductivity measurement is shown in Figure 2. High density alumina was used as a capillary and crucible material. Both electrodes were made of stainless steel. The crucible with about 150 g slag sample was placed in a vertical furnace with controlled atmosphere (argon) and heated up to the required temperature. Within a run, the measurements were carried out at different temperatures (1210-1360 ^oC at every 30 ^oC). The AUTOLAB with FRA (Frequency Response Analyzer) module was used for the measurement of the cell impedance. The amplitude was 10 mV, the frequency was varied from 1-100 kHz, and 10 readings were taken within this range.

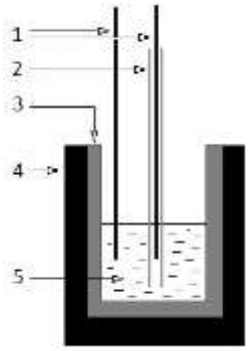

Figure 2 Electrical conductivity cell for slag: 1-stainless steel rod, 2-alumina tube, 3-alumina crucible, 4-graphite crucible, 5-slag

Viscosity

The viscosity measurements were carried out using a high-temperature, rotary viscometer with DV-III Ultra (Brookfield) measuring head. The measuring principle was based on the system of coaxial cylinders. One of them (spindle) rotates at a predetermined speed in the tested molten slag, which is placed in the second cylinder. Shear stress formed in the liquid layer causes a change of torque, which is indirectly correlated with the viscosity of the liquid. Figure 3 shows schematically a crucible filled with the tested molten slag and spindle (coaxial cylinders method).

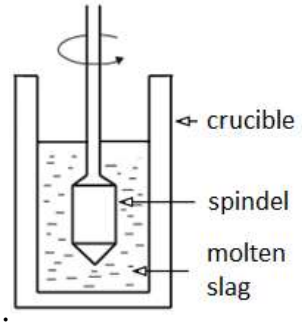

Figure 3 Schematic principle of the viscosity measurement by using coaxial cylinders method

The tested slags were placed in an alumina crucible between the three special rods. Molybdenum penetrator was suspended on a steel rod and a silver chain. The system was moved down into the furnace and purged with argon for 12h. After that, the furnace was heated to the required temperature and the penetrator was immersed into the molten slag (each time at the same depth). Measurements were made in the temperature range of 1210 – 1360°C at every 30°C.

Materials

The tested materials were taken from a flash smelting furnace operating in a direct-to-blister technology (slag before purification) and from an electric furnace (slag after cleaning). The chemical compositions of both slags are given in Table 1.

Table 1 *Chemical composition of slags*

Slags composition (main components), [wt. %]						
Component	SiO_2	FeO	CaO	Al_2O_3	MgO	Cu
Before cleaning	33,6	16,2	16,5	8,9	8,6	14,0
After cleaning	38,2	16,5	22,0	11,3	9,2	0,5

Results and discussion

The obtained results of impedance measurements shown in Figure 4a for slag before cleaning at 1360°C indicate that the real parts of impedance are practically independent on frequency. Therefore, all the measured real parts of impedance were averaged. Then, the relationship R_m=f(L) was plotted (Fig. 4b), and the slope dR_m/dL as well as the electrical conductivity were calculated. This procedure was used for all temperature. The results of the calculations are presented in Figure 5a. In turn, the results of viscosity measurements, which were obtained based on the calibration of the system with standard calibration liquids, are shown in Figure 5b. In Figures 6a and 6b, the viscosity and conductivity are presented, to show the inverse temperature effect.

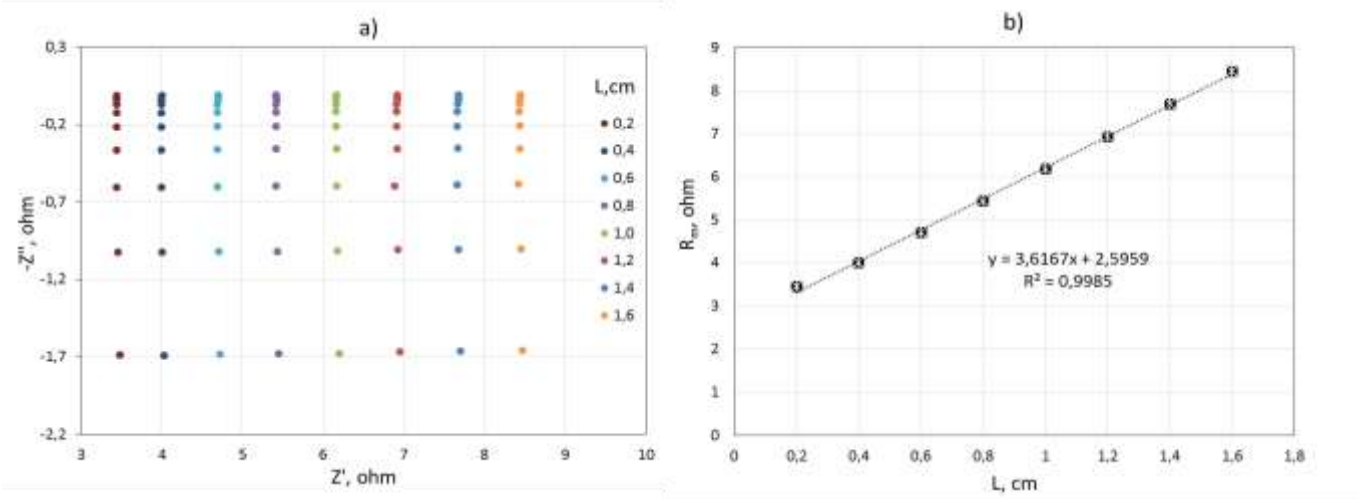

Figure 4 Nyquist plot (a) and measured resistivity versus distance between electrodes (b) for direct-to blister slag at 1360 °C

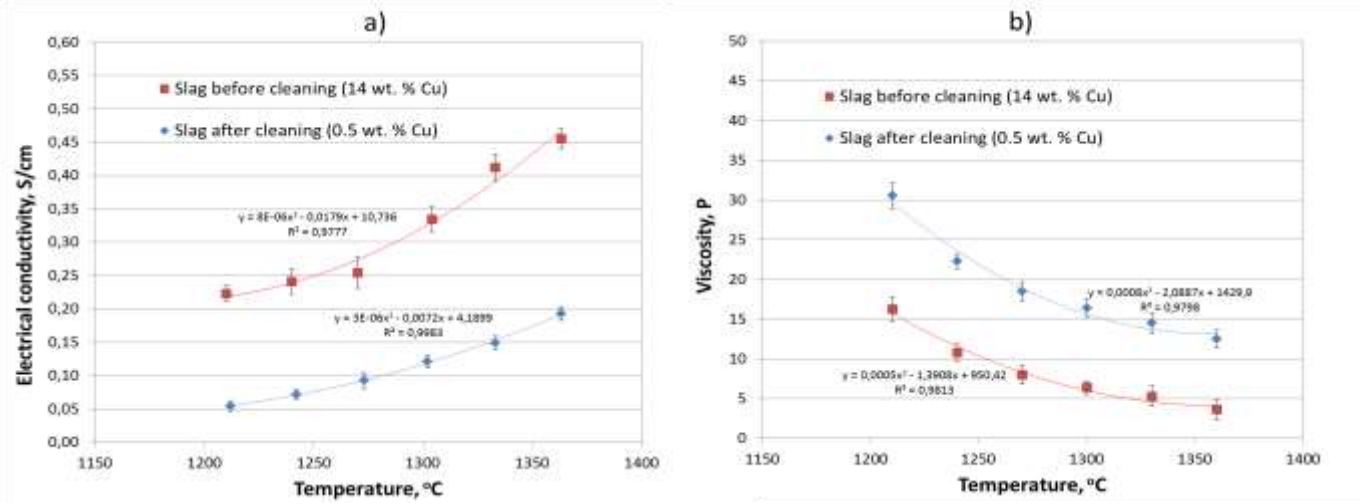

Figure 5 The electrical conductivity (a) and viscosity (b) of slags before and after cleaning (points: measured data, lines: fit)

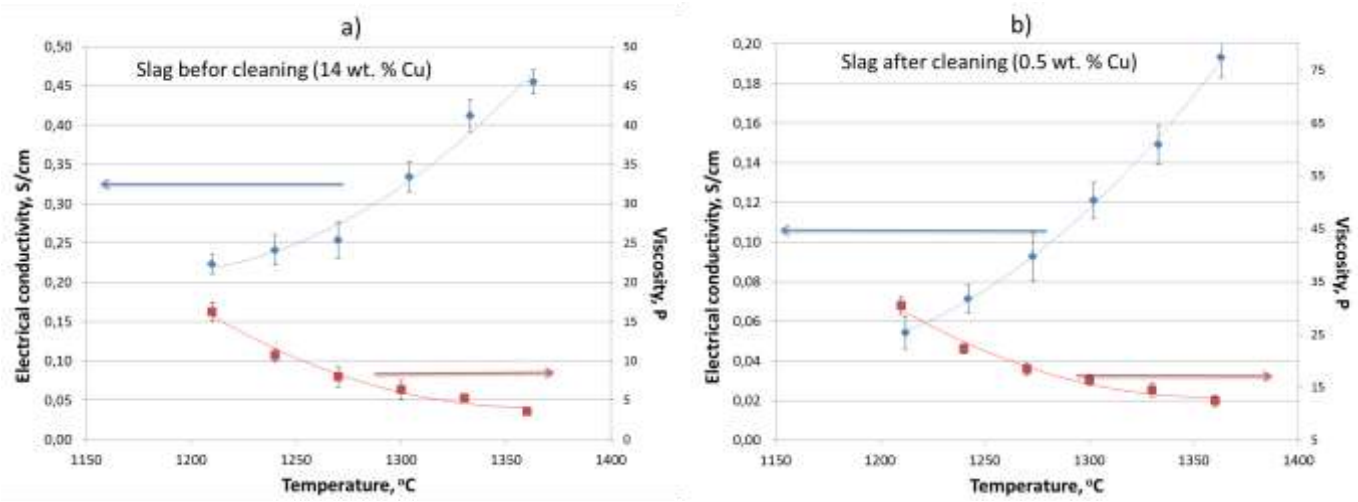

Figure 6 Electrical conductivity and viscosity of slags before (a) and after (b) cleaning (points: measured data, lines: fit)

The results of electrical conductivity measurements indicate that the slag containing 14% Cu has a much higher electrical conductivity than the slag after decopperisation. This is important, because during the slag cleaning process in EF, the concentration of copper in the slag gradually decreases, and thus the conductivity of the slag will also decrease with an imminent risk of disturbances in the electric furnace operation. In turn, the viscosity of the slag increases along with the time of the process in EF.

The viscosity measured in this work indicates that at a temperature close to the temperature in an electric furnace (1360 ^{o}C), the slag with 0,5 wt.% Cu has over three times higher viscosity than the slag containing 14 wt.% Cu. This indicates that settling of Cu-Pb-Fe alloy droplets through the slag layer will be more and more difficult along with the duration of the cleaning process.

The results obtained in this work are only extreme values for the slag that enters and leaves the electric furnace. It would be important to study the impact of the most important slag components on both the electrical conductivity and viscosity, as it would allow predicting the phenomena that occur in the furnace and guiding the process so as to maximize the recovery of copper from the slag and minimize energy consumption.

References

[1] Kojo I.V., Storch H.: Copper Production With Outokumpu Flash Smelting: an Update; Sohn International Symposium Advanced processing of metals and materials, International Symposium on Sulfide Smelting 2006, Edited by F. Kongoli and R.G. Reddy TMS, 2006

[2] Palimąka P. et al.: Inclusions of metallic copper in slag from direct-to-blister process, before and after cleaning, Proceedings of Copper 2016 International Conference, Kobe, Japan, 2016

[3] CzerneckiJ. Et al.: Copper metallurgy at KGHM Polska Miedz S.A – present state and perspectives, Proceedings of Copper 99 – Cobre 99 International Conference, Volume V – Smelting Operations and Advences, 1999

[4] Wang X., Peterson R. D., Tabereaux A. T.: Electrical conductivity of cryolitic melts, Light Metals, 199

Evaluation of porous morphology in alloys based on titanium and cobalt-chromium produced by addive manufacturing

Patrik Petroušek

Institute of Materials, Faculty of Materials, Metallurgy and Recycling, Technical University of Košice, 042 00 Košice, Slovakia

Abstract

The goal of the present work is to evaluate the mechanical properties and porosity of materials produced by Selective Laser Melting (SLM). The investigated materials are Ti6Al4V (90% Ti, 6% Al and 4% V) and CoCrW (60,5% Co, 28% Cr and 9% W). The samples for the static tensile test were made according to MPIF Standard 10. The static tensile test after heat treatment (Ti6Al4V: T = 820°C, t = 90 min, Ar; CoCrW: T = 1150°C, t = 60 min, Ar) was carried out. Porosity evaluation was performed by two methods - Archimedes method and the stereological investigation of images taken from optical microscopy. The results show the significant inhomogeneity of the morphology and pores size in the investigated materials. The porosity of the alloy Ti6Al4V was about 5% and CoCrW about 2,8%.

Introduction

Engineering reach a new era of design disruption controlled by the new technologies, led by additive manufacturing, and it has a huge potential to disrupt current manufacturing process paradigms. This paradigm can be seen as a part of emerging Third Industrial Revolution which is combining physical and digital processes into new ways. Main progress in Additive Manufacturing (AM), is to take care of a forum demonstrating the depth and breadth of the research and development activities through manufacturing technology which most describes that goal [1-3].

The field of additive manufacturing production has resulted in significant growth over the last 25 years in areas moved to a higher number of machines sold to the number of parts produced, with the same increase in research and development activities in the form of publications and patents. The potential of AM is fully realized by substantial research and development efforts, especially for complex metal components. The main reason of success is the industrial implementation of additive technology in the aerospace industry, which opens the way for wider applications in other industries such as biomedical and automotive industries [4-7].

Materials and methods

As experimental materials, the powder Ti6Al4V and CoCrW were used. The chemical compositions are shown in Table 1 and Table 2.

Table 1 *Chemical composition of Ti6Al4V material*

Components	Ti	Al	V
	90 wt. %	6 wt. %	4 wt. %
Other elements < 1% wt.: N, C, H, Fe, O			

Table 2 *Chemical composition of CoCrW material*

Components	Co	Cr	W	Si
	60,5 wt. %	28 wt. %	9 wt. %	1,5 wt. %
Other elements < 1% wt.: Mn, N, Nb, Fe (Ni, Be a Ga free form)				

The samples were prepared by the Mlab Cursing R (Concept Laser, Germany), which works by Selective Laser Melting (SLM) technology. The workspace for sample preparation is 90x90x80 mm^3 (x, y, z). The device is equipped with a 100 Watt laser. The dimensions of the samples according to the MPIF Standard Test Methods Edition 2007 are shown in Fig.1. The thickness of samples was 2,67 mm. All samples were produced in one batch.

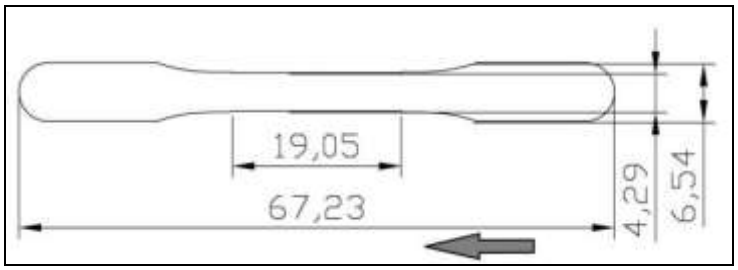

Figure 1 Dimension of sample for static tensile test prepared by SLM technology

The specimens for microstructural analyze were taken from the area in the center of the sample along the length. Evaluation of porosity was realized on non-etched samples using by optical microscope Zeiss Axiovert A1 equipped with an image analyzer. Characterization was carried out at 100x magnification on the minimum seven different image fields for specimens prepared by AM technology. The pores were evaluated by Image pro plus software. Quantitative image analysis of investigated material treats pores as isolated objects in the two-dimensional plane in order to describe the dimensional and morphological porosity characteristics. The dimensional characteristic D_{circle} (representing the diameter of the equivalent circle showing the same area as the metallographic cross-section of the pore) and aspect ratio A (representing the ratio between major axis and minor axis of ellipse equivalent to pore; according to [8,9], the aspect ratio considers the stress and strain situation in the process of AM). The evaluation procedure described in more detail is at work [9]. From other studies, it is known that nanopores do not affect on the mechanism of fracture formation. Therefore, only pores of a size greater than 1 μm were investigated.

Results and discussion

Microstructural and porosity analysis

The investigated non-etched microstructures of Ti6Al4V and CoCrW alloys are shown in Fig. 2 and Fig. 3. In these figures are highlighted pores witch had critical dimensions, respectively morphology. The pores in the Ti6Al4V alloy showed homogeneous distribution without significant large pores. In the CoCrW alloy were pores of 2-4 μm which were present as well as pores with a size above 90 μm.

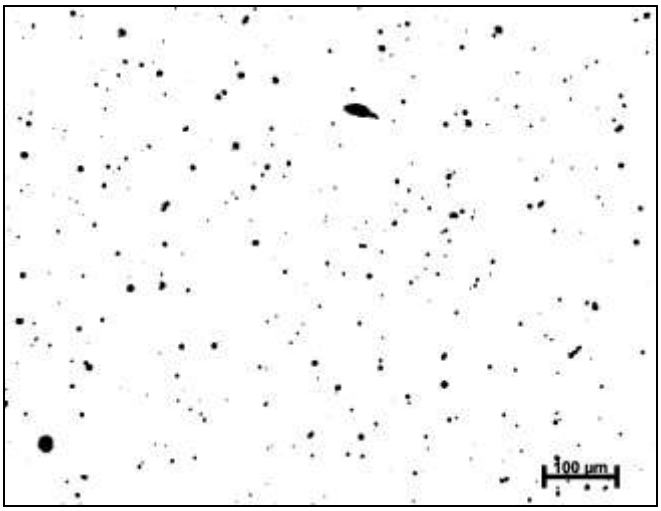

Figure 2 Porosity analysis of Ti6Al4V

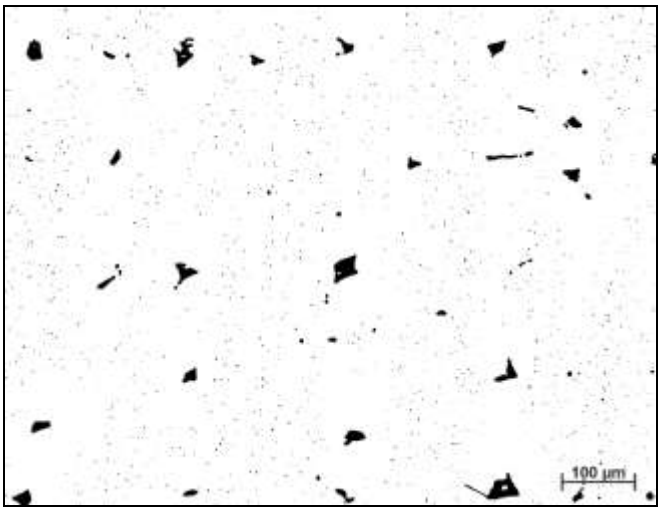

Figure 3 Porosity analysis of CoCrW

In the Fig. 4 is a macroscope view. In the picture, it is possible to see that the pores created the lineage of pores in the same lines along the sample. Some authors define it as pores [10] others like Si-rich inclusions [11]. Distribution of inclusions is line spaced also. Fig. 5 shows the detail of the edge of the sample. Such linearity is very inappropriate in attempting to achieve high mechanical properties. In the static tensile test, these pores were associated to units and formed extensive crack concentrators. This fact is also related to the fact that the deformation was not localized to the central part of the sample but also to the places which were ticker than the central part of the sample (under the headers).

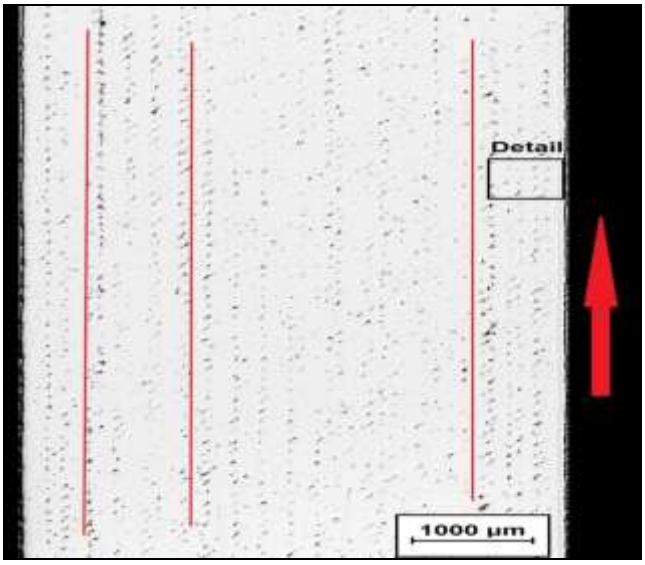

Figure 4 The macroscope view of Ti6Al4V

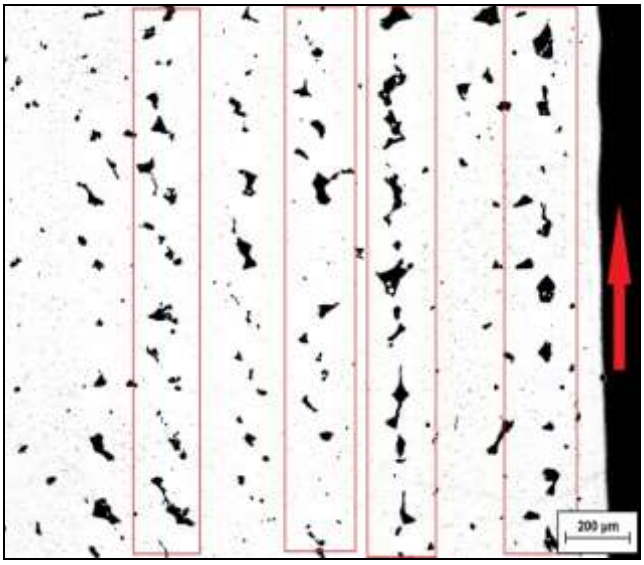

Figure 5 Detail of the edge of the sample from macroscope

The porosity results obtained by the Image pro plus software are shown in Fig. 6 and Fig. 7. In the Figs. 6, 7 is dependence between D_{circle} and Aspect. This dependency indicates the shape of the pores in relation to the size.

One of the possibilities for the evaluation of the pore size is a mathematical description. A two-stage method, based on local polynomial fitting for a non-linear regression model of porosity behavior, was used (Eqs. 1, 2) corresponding to Figs. 6, 7, respectively.

$$y = 0.0002 . x^2 - 0.0006 . x + 1.2416 \quad (1)$$

$$y = -0.0003 . x^2 - 0.0418 . x + 1.5041 \quad (2)$$

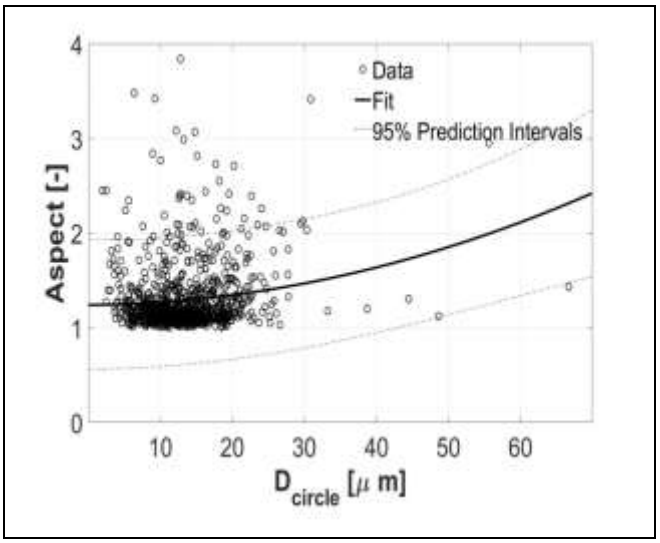

Figure 6 The dependence between D_{circle} and Aspect of Ti6Al4V

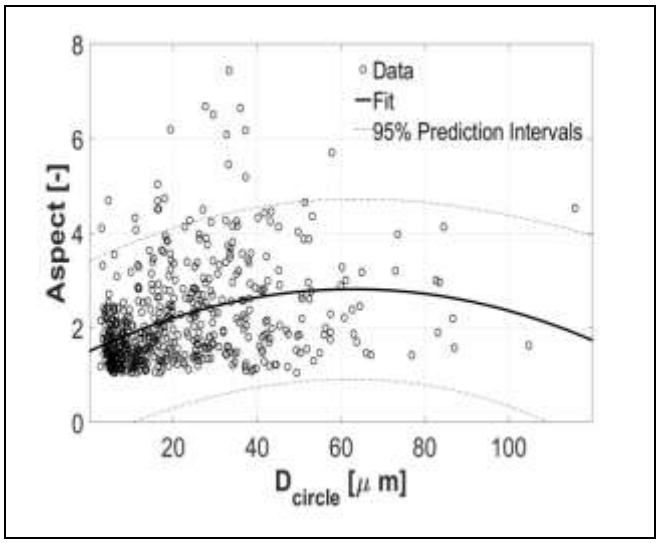

Figure 7 The dependence between D_{circle} and Aspect of CoCrW

Pores, present within the proposed maps, act as crack initiators and due to their presence distribution of stress due to heat treatment after AM processing is inhomogeneous across the cross section and leads to a reduction of the effective load bearing area. Moreover, in specimens processed by AM, the mean stress is responsible for the radial growth rate of pores and for equivalent stress, which correlates more closely with changes in pore shape and has a stronger effect on the elliptic pores. The shear component of the applied stress causes particle rearrangement and the collapse of large pores. The particle rearrangement and macroscopic deformation of pores increase the number of particle contacts, meaning a better overall bonding in the component.

Conclusion

A significant disadvantage of the PM processing methods is the presence of porosity, as well as (in general) the highly inhomogeneous microstructures. Most of the properties of PM materials are strongly related to porosity.

Both the morphology and distribution of pores have a significant effect on the mechanical behavior of PM materials.

References

[1] Herderick E. D.: Additive Manufacturing in the Minerals, Metals, and Materials Community: Past, Present, and Exciting Future. The Minerals, Metals & Materials Society, Vol. 68, 2016, No. 3, p. 721-723, DOI: 10.1007/s11837-015-1799-4

[2] Frazier W. E.: Metal Additive Manufacturing: A Review. Journal of Materials Engineering and Performance, Vol. 23, 2014, p. 1917-1928, DOI: 10.1007/s11665-014-0958-z

[3] Fedorikova A. et al.: Mechanical properties of powder CoCrW-alloy prepared by am technology. MM Science Journal, Vol. 2016, no. 2016, p. 1586-1589, DOI: 10.17973/MMSJ.2016_12_2016189
[4] Aversa A. et al: A study of the microstructure and the mechanical properties of an Alsingle bondSisingle bondNi alloy produced via selective laser melting. Journal of Alloys and Compounds, Vol. 695, 2017, p. 1470-1478, DOI: 10.1016/j.jallcom.2016.10.285
[5] Kvačkaj T. et al.: Analysis of metallic materials for iter with the emphasis on copper alloys. Acta Metallurgica Slovaca, Vol. 20, 2014, No. 4, p. 397-404, DOI 10.12776/ams.v20i4.438
[6] Petroušek P. et al.: Evaluation of formability of thin sheets based on Al-Mg-Si for automotive industry. Acta Metallurgica Slovaca, Vol. 21, 2015, No. 3, p. 176-183, DOI 10.12776/ams.v21i3.615
[7] Španielka J., Škrobian M., Bidulský R.: Extrusion of short aluminium billets - simulation and semi-pilot test. Acta Metallurgica Slovaca, Vol. 21, 2015, No. 2, p. 164-170, DOI 10.12776/ams.v21i2.583
[8] Petroušek P. et al.: Mechanical properties and porosity of Ti-6Al-4V alloy prepared by AM technology. MM Science Journal, Vol. 2017, no. 2017, p. 1752-1755, DOI: 10.17973/MMSJ.2017_02_2016190
[9] Bidulska J. et al: Identification of the critical pore sizes in sintered ECAPed aluminium 6xxx alloy. Archives of metallurgy and materials, Vol.58, 2013, No.2, p. 371-375, DOI: 10.2478/amm-2013-0002
[10] Slotwinski J.A.: Porosity Measurements and analysis for metal additive manufacturing process control. Journal of Research of the National Institute of Standards and Technology, Vol.119, 2014, p. 494–528, DOI: 10.6028/jres.119.019
[11] Kim H.R.: Microstructures and mechanical properties of Co-Cr dental alloy fabricated by three CAD/CAM-based processing techniques. Materials, Vol.9, 2016, No.7, p. 596–610, DOI: 10.3390/MA9070596

Electrodeposited metallic coatings inspired by nature

Ewa Rudnik, Karolina Chat

Faculty of Non-Ferrous Metals, AGH University of Science and Technology
Al. Mickiewicza 30; 30-059 Cracow, Poland
erudnik@agh.edu.pl

Abstract:

Electroplated metallic layers of a special surface morphology and chemistry represent novel type of functional coatings. Their hierarchical surface roughness in micro- and nanoscale results in superhydrophobic behavior, i.e. unusual high repellence of water. Development of superhydrophobic metallic materials was motivated by a wide range of potential practical applications like anticorrosion protection, self-cleaning, anti-icing, reduced fluid drag etc. However, commercialization of laboratory work requires good understanding principles of fabrication and specific surface properties of the coatings, including morphology, roughness, surface chemistry, surface wetting and long-term stability.

This paper presents short overview of the latest achievements on the superhydrophobic galvanic coatings, electrolysis conditions, methods of surface chemical modification as well as some properties of the final layers.

Introduction

For last ten years, there is growing interest in the electrodeposition of novel functional metallic coatings characterizing by self-cleaning, anti-icing, anti-fouling, anti-corrosion, reduced fluid drag, enhanced heat transfer etc. [1-3]. Development of special superhydrophobic layers was inspired by work of German botanists [4, 5] who explained self-cleaning effect of leaves of lotus *Nelumbo* and permanent retention of air under water by floating ferns of genus *Salvinia*. It was found that superhydrophobicity of many plant species results from hierarchical surface structures formed by convex to papillose epidermal cells and a very dense arrangement of three-dimensional epicuticular waxes of different shapes.

Superhydrophobic surfaces characterize with low energy, water contact angle higher than 150^{o} and slide (rolling) angle below 5^{o} [6]. As it was shown for many natural surfaces like leaves of nasturtium, tulip or ramee, rose petals, fruits, herbaceous stems, wings of cicada or butterfly, mosquito compound eye, water strider's legs, shark skin, duck feather etc. (Fig.1), two essential features are necessary for superhydrophobicity of technical materials: a combination of surface structure in a micro- and nanoscale and a nonpolar surface chemistry. Both factors help trapping a large amount of the air in the surface cavities while material is exposed to the air atmosphere, thus reducing attractive interactions between the solid surface and the liquid (Fig.2). The latter is especially important for anti-corrosion protection of metallic structures with electroplated metallic coatings [11]. Hence, the aim of this paper was to show some applications of electrochemical method for production of metallic layers with special surface microstructure and unusual low wettability.

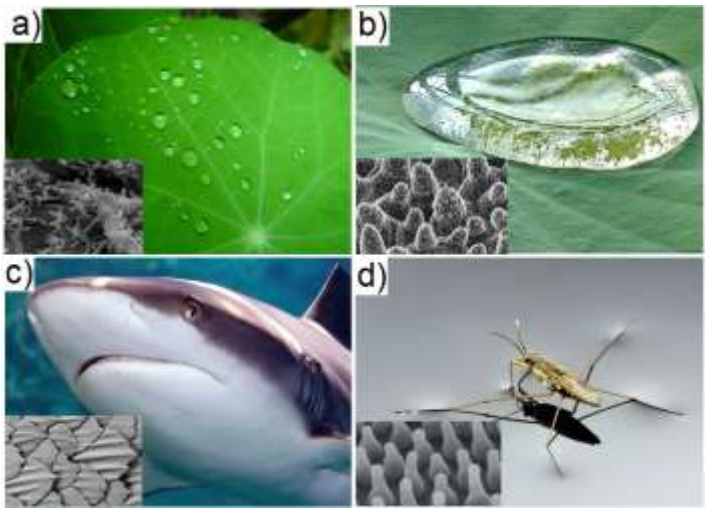

Figure 1 Superhydrophobic natural surfaces: a) nasturtium leaf [7], b) lotus leaf [8], c) shark skin [9], d) water strider leg [10]

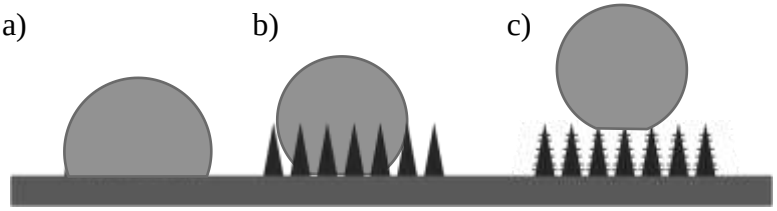

Figure 2 Influence of roughness on wettability of solid surface: a) flat surface, b) rough surface, c) hierarchical roughness of surface

Electrodeposition modes

Artificial fabrication of superhydrophobic metallic materials involves development of special hierarchical roughness of the surface, chemical modification of a rough surface with hydrophobic material or incorporation of hydrophobic particles into the bulk of the material (composite). Figure 3 shows typical modes of electrolysis in aqueous solutions combined sometimes with further modification of surface chemistry.

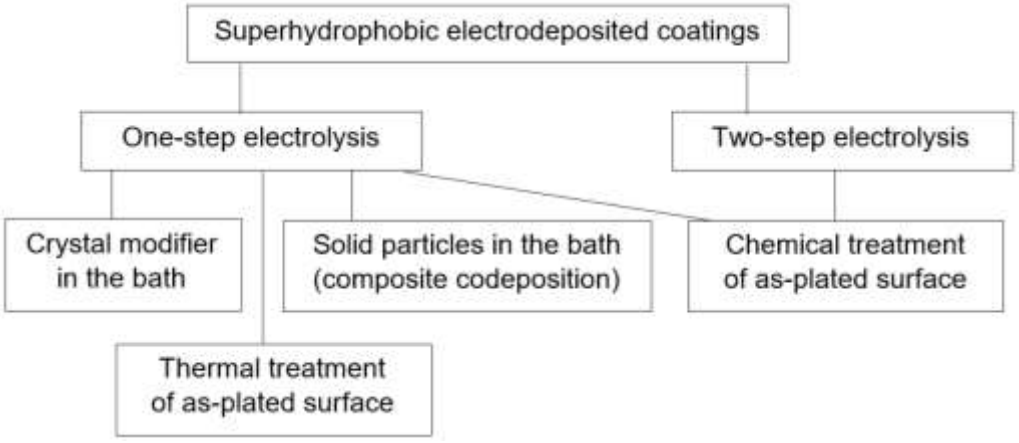

Figure 3 Fabrication modes of superhydrophobic electrodeposited metallic coatings

Traditional electrodeposition setup consists of a cathode being substrate to be coated and soluble or insoluble anode immersed in the electrolytic baths. Electrolysis can be carried out in galvanostatic or potentiostatic conditions. Usually, surface morphology of the deposited metal is controlled by addition of special additives to the electrolyte and/or by current/potential parameters.

Application of proper composition of the bath is the simplest way to change roughness of the coatings. For example, ethylenediammonium dichloride [12] or ammonium chloride [13] were used as crystal modifiers to produce nickel coatings of micro- and nanocone array surface microstructures. For optimal electrolysis parameters, the water contact angles (WCA) were 151-156^{o}. Investigations of corrosion resistivity in neutral NaCl solution revealed that superhydrophobicity can considerably increase corrosion resistance of the nickel coatings, but after 24 h immersion, polarization resistance of the superhydrophobic surface decreased due to the decline of the hydrophobicity [13]. This showed that initial surface properties of the coating can be changed in quite unexpected way during practical usage.

Potential/current conditions seriously affect roughness of the metallic surfaces. Characteristic biomimetic layers can be produced by copper [14], nickel [15], gold [16] (cauliflower like), cobalt (six-petal flowers) [17], silver (branches) [18], palladium (cabbage leafs) [19], tin (tremella fungi) [20], zinc (branches, willow leaf) [21, 22] etc. Development of hierarchical roughness in micro- and nanoscale is enhanced during two-stage electrolysis. It consist in the application of low current density or low cathode overpotential in the first stage and higher current or higher overpotential in the second one. It allows to produce much smaller growths on the previously deposited structures. Such mode of electrolysis results in the formation of metallic arrangements similar to pinecone (nickel) [23], globe-shaped hierarchical structures (copper) [24] etc.

As-deposited layers are often hydrophilic in nature, therefore they are further modified by immersion or spraying with solutions of non-polar organic compounds to obtain superhydrophobocity. Chemical treatment with alcoholic solutions of myristic acid [15], stearic acid [21], n-dodecanethiol [18, 19], various organic fluorocompounds [16] is used most often, but annealing at higher temperature in air atmosphere was also found as effective method for decreasing wettability of the metallic surfaces [20, 22].

Electrochemical synthesis of composite coatings is another relatively simple way for producing metal-based layers of high hydrophobic properties. It involves incorporation of inert nanoparticles into the growing metal matrix to produce hierarchical surface microstructure followed by surface modification (e.g. TiO_2) or codeposition of hydrophobic particles (e.g. PTFE, WC, WS_2) [25-27]. Codeposition of hydrophobic particles does not require further surface modifications with materials of low surface energy, but unusually proper surfactant in the suspension is necessary to disperse the particle's in the bulk of the bath.

Conclusions

Electrodeposition is a relatively simple and inexpensive method for production of superhydrophobic functional coatings. Such layers can be applied for anticorrosion purposes in automotive industry or for protection of marine structures. However, commercialization of the novel coatings still requires deeper research on scale-up of the laboratory experiments and investigations of the long-term stability of the superhydrophobic surface properties under actual usage conditions. Some problems related to methodology of the characterization of the superhydrophobic materials still require standardization. It applies mainly to proper measurement of contact angles and different fitting modes of the static contact angle giving inconsistent data for the same system of water droplet-substrate. Further challenges are related to total understanding the basics for designing procedures of the electroplating to obtain coatings of desired morphology and properties. Finally, faster progress in this scientific field should be motivated by simpler and cost-effective production procedures of durable and environmentally friendly superhydrophobic galvanic coatings.

References

[1] Bhushan B., Jung Y. C., Prog. Mater. Sci., 56(1) (2011), 1-108
[2] Bhattacharyya R., Nov. Int. J. Anal. Innov., 2(4) (2013), 1-9
[3] Tian X., Verho T., Ras R.H. A., Sci., 352 (6282) (2016), 142-143
[4] Barthlott, W., Neinhuis C., Planta, 202 (1997), 1–8
[5] Barthlott W. et al., Adv. Mater., 22(21) (2010), 2325–2328

[6] Crawford R. J.,. Ivanova E. P.: Superhydrophobic surfaces, Elsevier, Amsterdam-Boston-Heidelberg-London-New York-Oxford-Paris-San Diego-San Francisco- Singapore -Sydney-Tokyo, 2015
[7] www.nisenet.org
[8] www.beilstein-journals.org/bjnano/articles/2/19
[9] www.ocean.si.edu
[10] Guo H-Y. et al., RSC Adv., 5 (2015), 66901-66926
[11] Zhan-Fang C. et al., Metall. Res. Technol., 114 (2017), 203 (1-11)
[12] Farzaneh A., Asl S.K., and Hosseini M.G., Prot. Met. Phys.. Chem. Surf., 53(1) 2017, 88–93
[13] Hashemzadeh M., Raeissi K., Ashrafizadeh F., Khorsand S., Surf. Coat. Technol., 283 (2015), 318-328
[14] Haghdoost A, Pitchumani R., Self-cleaning superhydrophobic metallic coatings, Proceedings Annual Meeting of Adhesion Society, Daytona Beach, Florida, USA 3-6.03.2013, (2013) 126-128
[15] Rudnik E., Madej M., Rudy Metale, 62(3), (2017) 13-18
[16] Ren H.X. et al, J. Coll. Inter. Sci., 334 (2009) 103–107.
[17] Qiu R. et al, J., Coll. Surf. A: Phys. Eng. Asp., 377(1-3), (2011) 144–149
[18] Gu C., Zhang T., Langmuir, 24(20), (2008) 12010–12016
[19] Jeong H., Kim J., ACS Appl. Mater. Inter., 7(13), (2015) 7129–7135
[20] He G. et al., Surf. Coat. Technol., 309 (2017) 590-599
[21] Jain R., Pitchumani R., Surf. Coat. Technol., 337 (2018) 223–231
[22] He G. et al., Phys. Chem. Chem. Phys., 17 (2015) 10871–10880
[23] Khorsand S., Raeissi K., Ashrafizadeh F., Appl. Surf. Sci., 305 (2014), 498-505
[24] Wang S. et al., ChemPhysChem, 6 (2005), 1475–1478
[25] Aruna S.T. Muniprakash M., Grips V.K.W., J. Appl. Electrochem., 43 (2013) 805-815
[26] Zhao G.et al., RSC Adv., 7 (2017) 44896-44903
[27] Iacovetta D., Tam J., Erb U., Surf. Coat. Technol., 279 (2015)134-141

Possibilities of Biodegradation of Phenol by Sulphate-Reducing Bacteria from Model Solutions

Dominika Rudzanová

Institute of Geotechnics, Slovak Academy of Sciences,
Watsonova 45, 043 53 Kosice, Slovak Republic,
rudzanova@saske.sk

Abstract

In the present study, anaerobic biodegradation of phenol by sulphate-reducing bacteria (SRB) from model solutions was investigated. SRB culture was enriched from natural mineral water Gajdovka. Batch anaerobic studies were conducted with phenol (10 $mg.l^{-1}$). After 21 days of incubation, from 22.6% to 38.2% of phenol was degraded under sulphate-reducing conditions.

Introduction

Phenol is known as one of the most common environmental contaminants. High solubility of phenol in water leads to widespread contamination of natural aquatic environments [1]. Because of its teratogenic, mutagenic and carcinogenic effects, it has been listed in the 129 priority pollutants [2]. Phenol has been reported in industrial wastewaters from metallurgical industry (coal gasification, coke oven batteries), petrochemical plants, agricultural industry (production of herbicides and pesticides), in pulp and paper wastewaters or in wastewaters from chemical industry, etc. [3**]**. Concentration of phenol, in industrial wastewaters may ranging from several hundred to up to 10 000 $mg.l^{-1}$ [4].

Sulphate-reducing bacteria (SRB) represent a morphologically and metabolically highly diverse group of chemoorganotrophic and strictly anaerobic microorganisms present in most anaerobic environments, containing sulphates and organic compounds, for instance, soils, marine sediments, crude oil areas [5]. These bacteria are responsible for the process called as anaerobic respiration of sulphate or microbial anaerobic sulphate reduction. In this process, SRB do not use oxygen as the electron acceptor in their metabolism [6], but they use or „respire“ sulphates as the final electron acceptor in the breathing chain, and gain energy or carbon source from oxidation of great variety of organic compounds or molecular hydrogen [7]. As a result, they produce considerable quantity of gaseous hydrogen sulphide [8]. At present, about 125 kinds of organic compounds used by SRB are known and their number continues to grow [5].

Considering the inorganic or organic character of energy source of these bacteria, they are known to grow both autotrophically, using H_2 as the electron donor, and heterotrophically using organic molecules (lactate, furmarate, pyruvate, alcohols, hydrocarbons, etc.). Depending on the final product of organic substrate oxidation we know: incomplete heterotrophic oxidation of organic substrate, in which the final product is acetate and complete heterotrophic oxidation of organic substrate in which the final products are CO_2 and H_2O [9].

Microbial sulphate reduction is part of the natural cycle of sulphur in nature and it has been studied and applied in environmental protection and cleaning methods. In recent years, several bioremediation processes based on the use of SRB have been developed for the treatment of acid mine drainage or sulphate rich effluents [10]. Because of the ability of SRB to metabolize variable organic compounds (more than 125 kinds), there is a great area for utilization of SRB in treatment of effluents with high load of organic compounds [5].

The aim of the present study is to investigate the possibility of degradation of phenol as the one of the significant organic pollutant in the environment by SRB from model solutions.

Material and methods

Microorganism and Growth Medium

SRB utilized in these experiments were obtained from potable mineral water (Gajdovka spring, located in Kosice, Slovakia). The SRB were grown and maintained in modified Postgate’s medium C [11].

Isolation and cultivation of SRB

Isolation and cultivation was performed under strictly anaerobic conditions. The medium was prepared in 1200 ml glass bottle with 1000 ml volume of medium and bubbled with nitrogen gas, for adherence to anaerobic conditions. The pH was finally set at 7.5. 180 ml of medium was transferred into four 250 ml flasks. 20 ml of bacterial inoculum (natural mineral water Gajdovka) was added into the each of four 250 ml flask containing 180 ml of medium. The bottles were scaled with butyl rubber stoppers and incubated in a temperature controlled chamber at 30°C, in dark, without shaking, for 2 weeks. Periodically, each two weeks in next 2 months, 20 ml of bacterial culture was transferred into fresh cultivation medium under the same conditions.

Batch phenol biodegradation study

Batch experiments were designed to examine the ability of the SRB in the degradation of phenol. The Postgate's medium C was modified for the biodegradation experiments. The modified medium was prepared in 1200 ml glass bottle with 1000 ml of medium, as usual (bubbled with nitrogen gas for adherence to anaerobic conditions), but without addition of lactate. Lactate was not delivered into the medium, as the carbon and energy source. As the carbon and energy source for SRB, a stock solution of phenol (concentration 10 $mg.l^{-1}$) was used. 10 ml of sulphate heptahydrate was used as a sulphate source.

2 biotic sets of biodegradation experiments were carried out simultaneously, including one set with previously cultivated SRB culture and one set with mineral natural water Gajdovka, containing SRB.

In the biotic experiments, 20 ml of the cultivated SRB (10% v/v), was inoculated into the 250 flasks containing 180 ml of modified medium (without lactate) and 2 ml of stock phenol solution (concentration of phenol 10 $mg.l^{-1}$) with pH 7.5. To ensure anaerobic conditions, bottles were replaced with nitrogen and, immediately, after added bacterial culture, sealed with butyl rubber stoppers.

The second biotic set was prepared with samples of natural mineral water Gajdovka. 500 ml of natural mineral water was filtered onto 0.2 μm nucleopore polycarbonate filter under vacuum pressure. Then the filter was added into the 250 ml flask containing 200 ml of modified medium (without lactate) and 2 ml of stock phenol solution (concentration of phenol 10 $mg.l^{-1}$). The pH of the medium was modified with NaOH to final pH value 7.5. To ensure anaerobic conditions, bottles were replaced with nitrogen and, immediately, after added bacterial culture, sealed with butyl rubber stoppers.

All experimental samples were incubated in the temperature controlled chamber at 30°C, in dark, without shaking, for 21 days. Samples were collected at 0, 7, 14 and 21 day to measure the sulphate concentration and phenol concentration. A 2 ml of samples were collected, centrifuged at 10 000 rpm for 10 minute, and then taken for determination of sulphate concentration and phenol concentration.

Samples were analyzed for concentration of sulphates by ion chromatography using Dionex ICS 5000 instrument (Sunnyvale, CA, USA), equipped with an IonPac AS11-HC anion column and suppressed conductivity detector. Phenol was determined by liquid chromatography-HPLC.

Results and discussion

Sulphate reduction

In these biodegradation experiments by SRB, sulphate is utilized as a final electron acceptor and the consumption of sulphate throughout the experiment reflects the performance of the system. The experimental results showed that sulphate reduction was observed in the biotic samples. The sulphate reduction with phenol as carbon source is shown in Fig. 1. Results from the sulphate reduction were recorded in Tab.1. Results implied that phenol was biotransformed concurrently while sulphate was reduced in the biotic experiments. In biotic experiments with previously cultivated SRB, concentration of sulphates decreases from 1650 $mg.l^{-1}$ to 1564 $mg.l^{-1}$ (sample F1-1) and 1583 $mg.l^{-1}$ to 1576 $mg.l^{-1}$ (sample F1-2), when phenol was added into the biotic system, during 21 days.

Table 1 *Sulphate reduction by SRB*

Sulphate reduction [mg.l^{-1}]			
Sample / **Time[day]**	**F1-1**	**F1-2**	**F1-G**
0	1650	1583	1532
7	1594	1572	1580
14	1586	1596	1561
21	1564	1576	1536

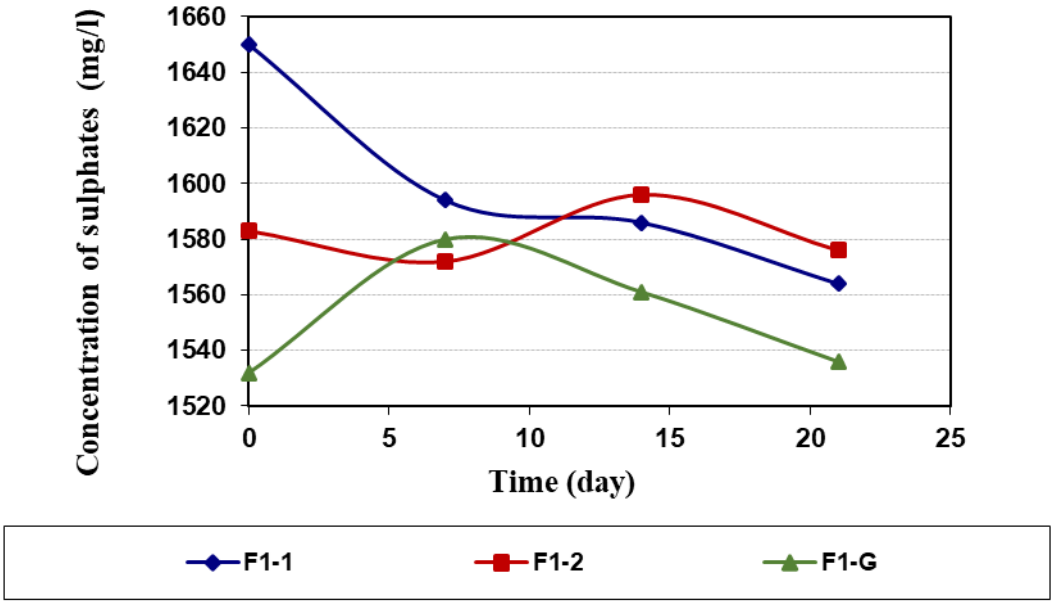

Figure 1 *Reduction of sulphates during 21 days of cultivation, in addition of phenol to cultivation medium. F1-1: biotic sample with previously cultivated SRB with phenol, F1-2: biotic sample with previously cultivated SRB with phenol, parallel to F1-1, F1-G: biotic sample with phenol and pure natural mineral water Gajdovka with SRB*

Phenol biodegradation

During the biodegradation experiments of phenol by SRB, phenol was utilized as a final electron donor and source of carbon and energy for SRB. The degradation of phenol as carbon source is shown in Fig. 2. Results of degradation of phenol were recorded in Tab.2. In first 14 days of experimental part, decrease of phenol was observed. In biotic experiments with previously cultivated SRB, concentration of phenol decreased from 10 mg.l^{-1} to 4.53 mg.l^{-1} (removed 54.7%) in sample F1-1 and from 10 mg.l^{-1} to 4.20 mg.l^{-1} (58% removal) for sample F1-2, respectively. In case of samples with mineral water Gajdovka, concentration of phenol decreased from 10 mg.l^{-1} to 2.49 mg.l^{-1} (75,1% removal), when phenol was added into the biotic system. However, on 21 day, increase of phenol concentration was observed. After 21 days of incubation, phenol concentration decreased from 10 mg.l^{-1} to 6.61 mg.l^{-1} (33,9% removal) in sample F1-G, from 10 mg.l^{-1} to 7.74 mg.l^{-1} (22,6% removal) in sample F1-2, and from 10 mg.l^{-1} to 6.18 mg.l^{-1} (38,2% removal) in sample F1-1, respectively. This increase may be augmented by formation of another immediates or metabolites, which can be produced during the biodegradation process with very similar composition as phenol.

Table 2 *Biodegradation of phenol during 21 days by SRB*

Biodegradation of phenol [mg.l^{-1}]			
Sample / **Time[day]**	**F1-1**	**F1-2**	**F1-G**
0	9.42	4.84	3.94
7	8.34	3.25	3.68
14	4.53	4.20	2.49
21	6.18	7.74	6.61

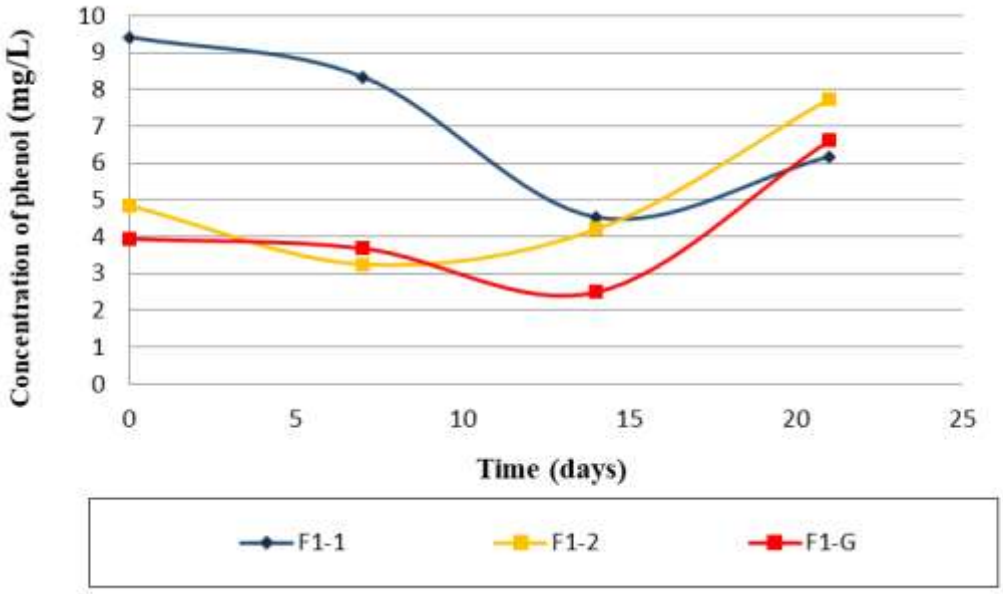

Figure 2 Biodegradation of phenol during 21 days of cultivation, in addition of phenol to system. F1-1: biotic sample with previously cultivated SRB with phenol, F1-2: biotic sample with previously cultivated SRB with phenol, parallel to F1-1, F1-G: biotic sample with phenol and pure natural mineral water Gajdovka with SRB

Conclusion

In the present study, a bacterial culture was enriched that has the ability to degrade phenol under sulphate-reducing conditions. Experimental results demonstrate that, it is possible use phenol as a source of carbon for SRB, during the anaerobic sulphate reduction. Indigenous microbial culture have been shown to has the ability to grow with phenol as the sole source of carbon and has the potential for biodegradation of phenol. The best results were obtained after 14 days of cultivation of SRB on phenol (75.1%, 54.7% and 58% removal). After 21 days of incubation, phenol concentration decreased to 33.9%, 22.6% and 38.2% removal. This increase may be augmented by formation of another immediates and metabolites, which have similar composition as phenol. Results obtained provide bases for further study and understanding processes performed by SRB.

Acknowledgements

This work has been supported by the project VEGA 2/0145/15 and Slovak R&D Agency project No APVV-10-0252-WATRIP.

References

[1] Ahn Y.B. et al.: Degradation of Phenol via Phenylphosphate and Carboxylation to 4-Hydroxybenzoate by a New Isolated strain of the Sulfate-Reducing Bacterium Desulfobacterium anilini. In: Applied and Environmental Microbiology Vol. 75, No. 13, 2009, p. 4248-4253

[2] Si, L. et al.: Study on Treatment Methods of Phenol in industrial Wastewaters. In: International Journal of Scientific and Engineering Research, Vol. 4, 5, 2013, p. 230-232
[3] Fang H.H.P. et al.: Anaerobic degradation of phenol in wastewater at ambient temperature. In: Water Science and Technology, Vol, 49, No. 1, 2004, p. 95-102
[4] M. Van Schie, P., Young, L.Y.: Biodegradation of Phenol: Mechanisms and Applications. In: Bioremediation journal 4 (1), 2000, p. 1-18
[5] Wolicka D., Borowski A.: The Geomicro biological Role of Sulphate-Reducing Bacteria in Environments contaminated by petroleum Products. In. Geomicro biology journal, 24, 2007, p. 599-607
[6] Baumgartner, L.K. et al.: Sulfate reducing bacteria in microbial maths: changing paradigms, new discoveries. In: Sedimentary Geology 185, 2006, p. 131-145
[7] Brioukhanov A., Pleulle L., Dolla A.: Antioxidative defense systems of anaerobic sulfate-reducing microorganism. In.: Current Research, Technology and Education topics in Applied Microbiology and Microbial Biotechnology, 2010, p. 148-159
[8] Luptáková A.: Importance of sulphate-reducing bacteria in environment. In.: Nova Biotechnologica VII-I, 2007, p. 17-22
[9] Nagpal S. et al.: Ethanol Utilization by Sulfate-Reducing Bacteria: An Experimental and Modeling Study. In.: Biotechnology and Bioengineering, Vol. 70, NO. 5, 2000, p. 533-543
[10] Wawrzak D.: Microbiological reduction of sulphates to sulphides used in Dairy Wastewater treatment. In. Inżynieria Mineralna, 2013, p. 109-114
[11] Postgate J.R.: The sulphate-reducing bacteria, 2nd edition. Cambridge University Press,1984, p. 208

Analysis and utilization of steelmaking secondary products

Jana Šoltész Matulová, Jaroslav Legemza

Technical University of Košice, Faculty of Materials, Metallurgy and Recycling, Institute of Metallurgy,Park Komenského 14, 042 00 Košice, Slovac Republic,
jana.soltesz.matulova@tuke.sk

Abstract

Secondary products and waste arising from metallurgical production are very difficult to recycle directly for a number of reasons. One of the problems that prevents such recycling is the fact that in many cases they contain hazardous chemicals such as heavy metals Pb, Cd, Zn. It is for this reason that they are classified as hazardous waste or substances posing a potential risk. Zinc has a specific role in this issue because it represents a valuable element and its concentrations in secondary products often exceed the concentrations in primary raw materials. One reason for this phenomenon is the fact that galvanized steel scrap is increasingly being used for reuse in batch. The objective of the legislation adopted in the form of REACH is to protect the environment to the extent that it meets the conditions that are required in the EU. Improving the safety of the use of chemicals and mixtures throughout the chain - manufacturer, supplier, consumer.

Introduction

By-products of industrial production are increasingly perceived as materials with great potential for further use. This trend is strongly supported by the ever stricter and more complex legislation dealing with environmental protection, waste management and disposal. The further driving force behind these changes is also the great economic pressure to make production more efficient and reduce the cost of input raw materials, materials and energy. Metallurgical production, of course, is no exception. Huge quantities of waste, respectively. by-products of iron and steel production are sufficient incentives for a detailed examination of their properties and the possibility of their re-use in production. Steelmaking dust and sludge are a byproduct of production that has its specific properties. It is these properties that need to be monitored and analyzed in order to find the most effective solution to the problem of their re-use in metallurgical production. The most important properties include chemical composition and mineralogical composition. This is a key factor deciding on the possibilities and ways of further utilization of steelmaking dust and sludge. On the one hand, they represent a source of raw material rich in the content of the metals obtained and, on the other hand, they are the fastest and most effective way of eliminating the environmental burden of the deposited materials. Thorough and accurate chemical analysis of such materials is a further step towards their better knowledge and at the same time determines the way they are used and handled further. Their use therefore offers solutions to two problems at the same time.

Material analysis as part of REACH

Currently, the REACH Regulations dealing with potentially hazardous and hazardous substances and their handling, hazard and toxicity are assessed, in particular because of the content of hazardous chemical elements (Zn, Pb). These regulations are currently one of the most extensive and the most comprehensive tools for monitoring, categorizing and assessing all chemicals and products that are the outputs of industrial production. The specificity with which steelmaking dust and sludge is applied derives precisely from their chemical composition. It is the result of the presence of several chemicals that pose a potential risk in certain concentrations. It is for this reason that it is important to precisely determine and define what chemical properties or the chemical composition of secondary products of metallurgical production can be considered dangerous or inappropriate for further processing. Together with this trend, there is also a need for efficient recycling and recovery of these secondary raw materials. REACH completely changes the way and requirements for controlling chemicals. It deals with

metallurgical byproducts for several reasons. One of them is the huge quantities in which they are produced, the other is minimal reuse. For these reasons, it was decided that secondary products from metallurgical production would be considered preferentially. The evaluation is conducted in four main steps (Figure 1), valid for all companies.

Figure 1 Main steps for the evaluation of chemicals

An important part of the application and documentation is the CSR (Chemical Safety Report), a chemical safety report that must include the results, analysis and chemical safety assessment from testing. Individual substances are thus considered in several respects as shown in Figure 2.

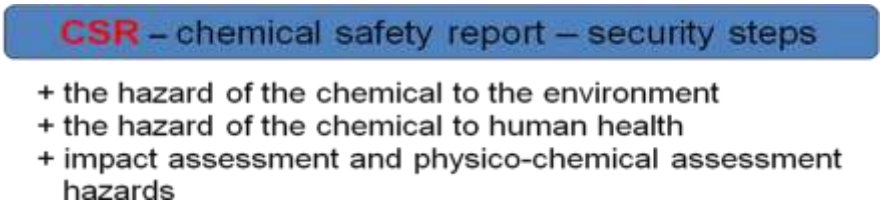

Figure 2 Security Steps in the CSR Report

Potential risk is associated with their chemical nature, as these elements are mobile and travel in environmental compartments. The large quantities in which these substances are still deposited at landfills again represent an environmental burden of considerable size.

In this paper, we focused on chemical analysis, but also on methods of investigation of mineralogical properties of steelmaking dusts and sludge. It is important to recognize that these characteristics are closely related and interrelated. To achieve a thorough evaluation of samples of steelmaking dust and sludge from the metallurgical plant, the following methodologies are used:

- determining the moisture content of the test samples,
- granulometric composition - ie identification of size fractions according to the analyzed sample and percentage of fractions,
- chemical elemental analysis - the chemical composition of the output byproducts (steelmaking dust and sludge - waste products) was carried out by the apparatus - the Nitin XL3 Gold mobile spectrometer,
- mineralogical composition - Analysis of the output test samples on the X-ray diffraction spectrometer using the special PDF2 datasets and AutoQuant (using the Rietveld method) determined the proportions of the individual mineral phases.

Table 1 *Particular parts of analyzed samples and sample humidity*

Steelmaking dust	Steelmaking sludge
1 part – fine dust – gas cleaner 1 part – fine dust - silo 1 part – coarse dust – fabric filter	2 parts – fine sludge –sludge bed 1 part – coarse sludge sedimentation tank -
Humidity (weight. %)	
4,32	25,46

Various granulometric classes and particle distribution in the sample have a relatively large impact on their potential for further potential use on higher added value products.These materials contain a high proportion of iron but also other components that are reusable in the metallurgical process. Specific orientation grain grades in the analyzed samples are shown in Table 2.

Table 2 *Granulometric composition of the analyzed samples*

Particle size range classification	<20 µm	20-47 µm	47-63 µm	>63 µm
steelmaking dust (%)	59.6	6.8	4.9	28.7
steelmaking sludge (%)	16.3	18.3	22.8	42.6

In Table no. 3 shows the specific values of these substances found in the analysis of samples of steel dust and sludge in different chemical compounds.

Table 3 *Chemical composition of steel dust and sludge*

Sample / %	Fe	Mn	Pb	Zn	Mg	CaO	MgO	Al2O3	SiO2	P2O5	K2O
Steelmaking dust	55,444	0,747	0,215	5,175	1,319	8,323	2,188	1,022	1,053	0,394	0,479
Steelmaking sludge	52,014	0,756	0,361	6,214	2,12	8,799	3,519	0,747	0,895	0,428	0,202

Mineralogical composition is another very important feature, especially because twosamples with approximately the same chemical composition may differ in their properties due to the different mineralogical composition (species and amount of individual minerals) that may be present there. In the samples analyzed, the proportions of each phase were determined using the special PDF2 and AutoQuant (using the Rietveld method) as shown in the diagram. In the dust sample, the phases as shown in FIG. no. 3

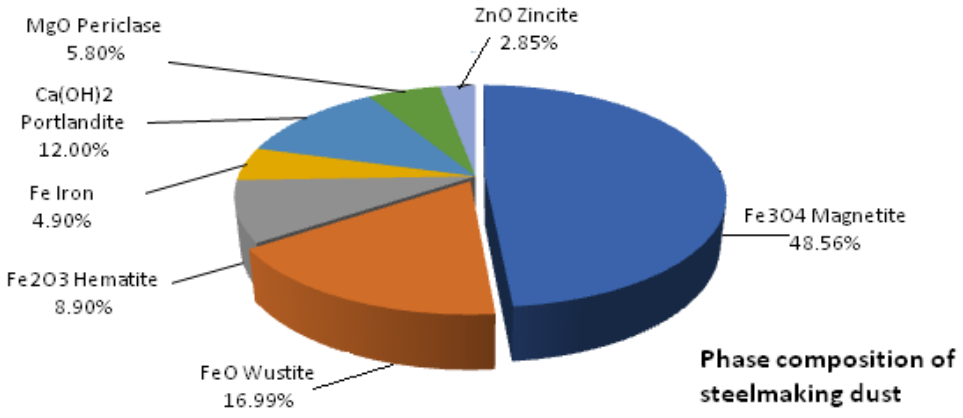

Figure 3 Mineralogical phase composition of the steelmaking dust sample with percentages by weight

In the analyzed sample of the steelmaking sludge, the mineralogical composition shown in Figure 4 was found.

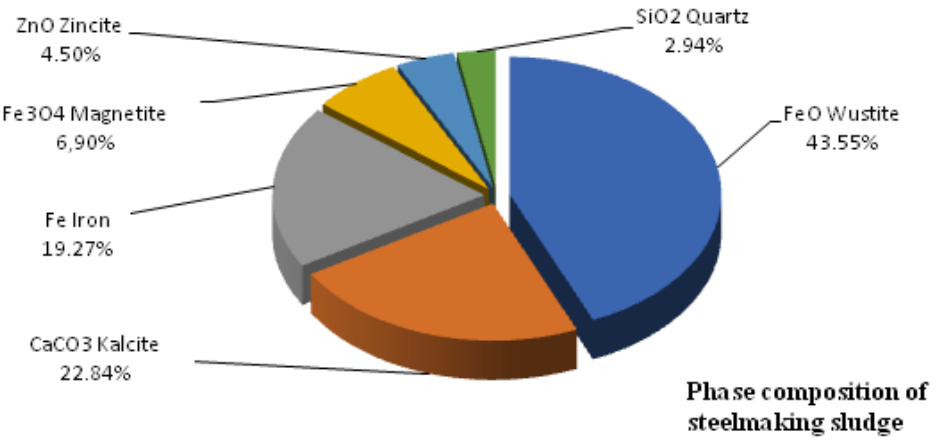

Figure 4 Mineralogical phase composition of the steelmaking sludge sample with percentages by weight

This material research have in the analyzed samples detected some of the same phase, such as magnetite, Wüstit, but also zinc, however in different representations. Examined samples had different representation of majority phases.

Conclusion and discussion

Increasingly, efforts are being made to find the most appropriate way of utilizing steelmaking dusts and sludges, which are constantly dumped in large quantities and form virtually heaps of high-content material such as Fe, but also Zn, which is also reusable. At present handling of these continuously generated materials according to current trends is inadequate to the requirements and conditions of the REACH regulations. The ideal state is a wasteless economy. The zero production of waste materials in the production of iron and steel undoubtedly leads to a long and complicated journey. Whether it is possible to achieve this far-reaching goal seems to be time. Research suggests that several possible solutions to the problem of efficient processing of such materials are several, and some of them are currently being used in real-time or semi-operational mode. For processing of ferrous secondary raw materials, the following technological processes are currently commercially used: Waelz Kiln, Rotary Heart, Ausmelt, Primus, OxyFines, OxyCup, Plasmared. Such solutions appear to be mutually advantageous. However, despite all efforts, this material is insufficiently eco-evaluated and recycled only in small quantities. From analyzes of the tested samples we can confirm that the content of the steel dust sample is the major component of Fe - 55,444%. Also, in the next sample of steel sludge, the major component of the Fe 52,014% is again. Zn is also analyzed in both samples - Zn-5,175% steel powder, Zn-6,214% steel sludge. The moisture content of the samples was 4.32% by weight of the steel dust sample, but the steel slurry sample was 25.46% by weight. %. The mineralogical phase composition of the analyzed steelmaking dust sample formed the iron oxide major phase. In the presence of magnetite Fe_3O_4 - 48.56%, wustite - 16.99% and hematite 8.90%. In casting steel, the major component was wustite - 43.55%, but also iron metal - 19.27%, together with calcite - 22.84%. Both samples contained zinc ZnO - steelmaking dust - 2.85% and the steelmaking sludge sample contained ZnO - 4.50%. Analyzed zinc oxide is a better and more easily processable form than ferrite zinc. The aim is therefore to develop methods and procedures that could be used to the greatest extent possible to eliminate secondary materials and to prevent them from landfilling. Groups of test chemicals and mixtures manufactured or produced annually in quantities of less than 100 tonnes per year or less than 1 tonne per year currently have all evaluated and received information on the nature and assessment of compliance with the REACH Regulation and will then be closed in June this year 2018.

Literature

[1] Center for Chemicals and Preparations. [Online]. [cit 2018-04-02].
Available on the Internet: http: // www.cchlp.sk
[2] ECHA - European chemical agency. [Online]. [cit 2018-04-10].
Available at: http: //echa.Euro pa.eu/
[3] Key terms under REACH and CLP. [Online]. [Cit. 2017-12-30].
Available at: http: // www.cchlp.sk/pages/harmonogram.pdf
[4] REACH / CLP / BPD / SDS. [Online]. [cited 2018-04-13].
Available on the Internet: http: // www. siad.com
[5] Internal Materials of U.S.S. Steel Košice, s.r.o., UGM for Enviroment, UGMVV and REACH,
U.S.S. Steel Entrance Complex, Košice

Ti-Si intermetallics alloys for orthopedic applications

Michaela Šuliková[1], Karel Saksl[1,2]

[1] Faculty of Science, Institute of Physics, Pavol Jozef Šafárik University in Košice, Košice, Slovak Republic
[2] Institute of Materials Research, Slovak Academy of Sciences, Košice, Slovak Republic
michaela.sulikova1@student.upjs.sk

Abstract

Orthopaedic surgery has immeasurably improved the lives of millions of people, restoring their mobility, bringing pain relief and ultimately giving them a better quality of life. The main orthopaedic implants currently in use are prostheses for replacing arthritic joints and devices for fixing fractures and stabilizing the spine. However, they commonly contain elements like aluminium, vanadium, chromium, cobalt, manganese etc., which ions cause damage human tissues. We decided to develop a low-density alloy with a high hardness that will be biocompatible and cost-effective.

Titanium and Silicon are biocompatible elements. Silicon support bone calcification. We prepared and characterized five Ti-Si binary alloys. One of the five is monophase system, containing single hexagonal Ti_5Si_3. Microstructure was examined by synchrotron X-rays diffraction and high-resolution transmission electron microscopy. This alloy is almost 300% harder compared the implants used, today. Mass density of the alloy is 4.27 g/cm^3, while modulus of elasticity is 187 GPa. All the Ti-Si alloys are biocompatible asertaineded with respect to MC3T3E1 mouse preosteoblastic cells.

Introduction

Metallic materials are often used as biomaterials to replace or repair structural components of the human body. Due to their high mechanical strength and fracture toughness they are more suitable for load-bearing orthopedic implants applications than polymeric or ceramics materials [1-5]. Metallic biomaterials are used in orthopedics for two types of implants: I. as substitutes for bone and joints, and II. implants for the fixation of fractured bones [6, 7].

Currently, titanium and its alloys e. g. Ti-6Al-4V constitute the most favoured implant materials in the field of trauma and orthopedic surgery. There are problems of safety and long-term durability in the human body, resulting in repeat to surgical operations [1-5]. One of the major problems is the typical mode of degradation in implants through a corrosion process. We need implants which consist of the useful elements for the human body. In this work we focus on preparation and characterization of Ti-Si binary alloys. Both Ti and Si are biocompatible elements while Si is helpful in process of bone calcification.

Experimental section

Apparatus and equipment

We prepared alloys from high purity elements Ti (99.99 wt.%) and Si (99.9999 wt.%). First the elements were weighted by the analytical balance Kern ABT 120 - 4M. Secondly, the dose was arc-melted using the Mini Arc Melting System MAM-1. All meltings were done in under argon (99.999%) atmosphere. The samples were prepared in form of buttons. From each type alloys two arc melted buttons were prepared. One of it was heat treated (annealed to 700°C) in resistance furnace LAC under nitrogen. Density of the alloys was determined by Archimedes principle. Measurements were realized by analytical balance Kern ABT 120-4M with special density determination kit ABT-A01. Phase composition of the samples was ascertained by X-ray diffraction utilizing synchrotron radiation of photon energy of 79.74 keV (λ= 0.15548 Å) at the beamline I12 at the Diamond Light Source. Microstructure of single phase alloy Ti_5Si_3 was examined by high resolution transmission electron microscope JEOL JEM 2100F UHR operating at the accelerating voltage 200 keV. Microhardness was determined by hardness

tester Wilson-Wolper Tukon 1102 equipped with Wicker indentor. For indentation we used load 300g applied for 10s. Modulus of elasticity was determined from nanoindentation tests using the Nanoindenter Agilent G200 with Berkovich diamond indentor. Each sample was measured in CSM mode (indentor has taken the same depth of penetration, 2 000 nm). On the each sample was measured 16 injection points ordered in matrix 4 x 4 (distance between each point was 100 µm). On all samples in-vitro cytotoxicity testing of extracts and live-dead staining of MC3T3E1 cells were performed. For in vitro cytotoxicity tests of extracts were used samples in form cylinders (7 mm in diameter and 2 mm in height). The samples were exposed to the solution kept in the incubator at 37 °C for 24 h. After 24 h of soaking, the samples were removed from the tube and the extracts were tested for cytotoxicity according to *ISO 10993-5: 2009*.

All experiments were carried out in triplicate. The extract from titanium was considered as a negative control. After 24 h of culturing, the extracts were discarded and replaced with by fresh culture medium and the *in-vitro* cytotoxicity was evaluated by the MTS proliferation test assay (cell titer 96 aqueous one solution cell proliferation assay, Promega, USA). The absorbance of formazan (the product of mitochondrial enzymatic activity) after 4 h of cultivation was determined by a UV VIS spectrophotometer (Shimadzu 1800 UV) and compared with negative control. Live-dead staining of MC3T3E1 cells on tested alloys. The polished (abrasive paper nr.) cylindric samples (Ø 6 mm, height 1-2 mm) after cleaning in ethanol and sterilization in oven (170 °C for 1 hour) were placed into the wells of 96 pure Grade microplate containing osteoblasts in 200 µl of complete culture medium (EMEM with 10 % FBS, 1 % ATB-ATM). After 48 hours, the fluorescent images of cells (live-dead staining) on samples were recorded. The density, distribution and morphology of MC3T3E1 cells on the surfaces of tested samples were evaluated by an inverted optical fluorescence microscope (Leica DM IL LED, blue filter). Live-dead staining was based on fluorescein diacetate (FDA)/propidium iodide (PI) mixture.

Results and discussion

We have prepared alloys which have two times higher mass density than cortical bone. Microhardness HV0.3 in the some alloys is 300% higher than actually using implants. In the fig. 1 one can see dependence of microhardness on mass density where currently used implants (blue squares) our alloys arc-melted (red squares) and after the heat treatment (purple circles).

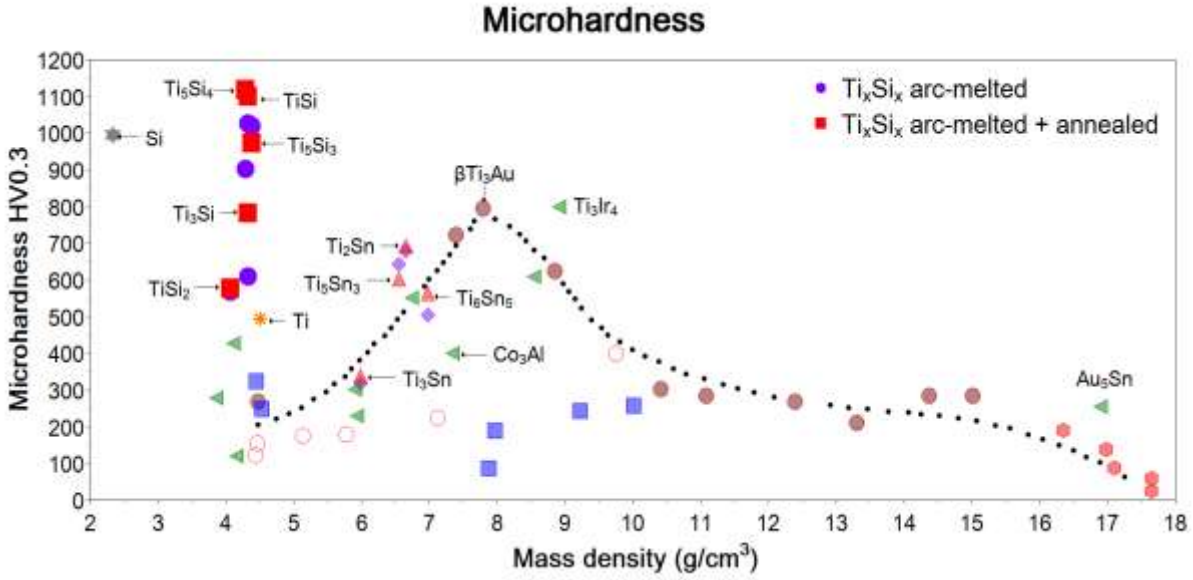

Figure 1 Dependence of microhardness on mass density, actually using implants and our samples

Microstructure of alloys was examined by synchrotron radiation. The results prove the only one monophase alloy is Ti_5Si_3. This phase is hexagonal. Structural parameters from XRD patterns were determined by Rietveld refinement using the program GSAS-II. Lettice parameters of the phase are a= 0.746 nm and c= 0.516 nm. Structural parameter of Ti_5Si_3 basal plane has been compared

to interference pattern obtained by high-resolution transmission electron microscopy (HR-TEM) in the fig. 2. Distance between interference maxima are 0.743 nm what is in very good agreement with the XRD obtained data.

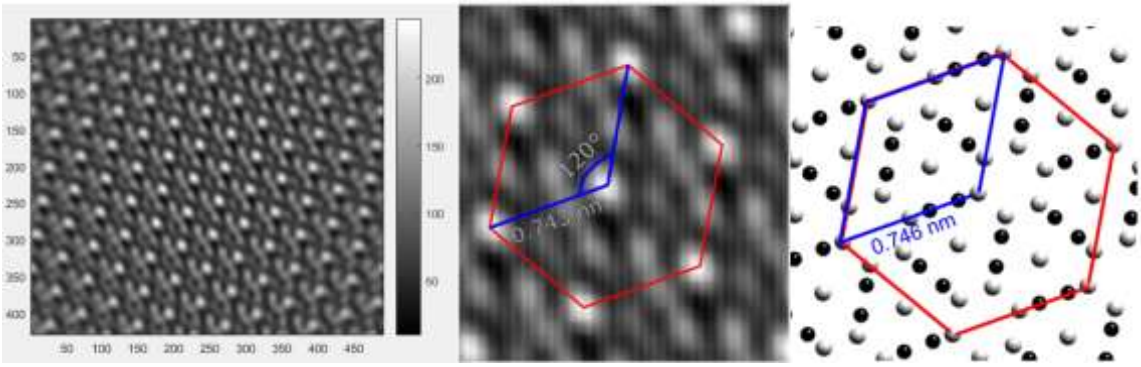

Figure 2 View on the basal plane (0001) by transmission electron microscopy JEOL 2100F

In the tab. 1 are listed modulus of elasticity which for all the alloys are approximately ten times higher than modulus of elasticity human bone (20.1 ± 5.4 GPa).

Table 1 *Value of modulus of elasticity for the Ti_xSi_x alloys*

Alloys	Modulus of elasticity (GPa)
Ti_5Si_4	180
TiSi	216
Ti_5Si_3	187
Ti_3Si	175
$TiSi_2$	210

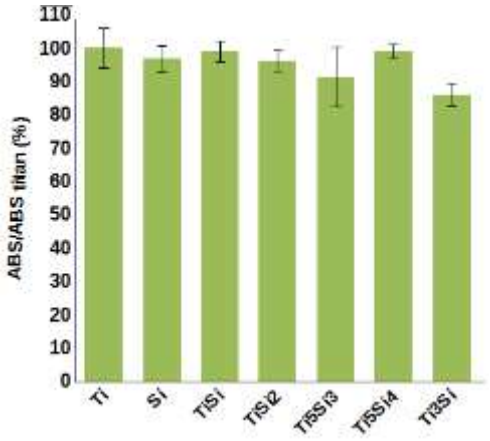

Figure 3 Relative proliferation of MC3T3E1 cells (%) in sample extracts after 24 hours of cultivation

Figure 3 shows the relative viabilities (mean ± standard deviation) of osteoblasts cultured in 100 % extracts from Ti alloys in relation to negative control (pure titanium). From cytotoxicity testing and measured relative proliferations of osteoblasts cultured in sample extracts resulted that extracts had a very low cytotoxicity potential (significantly different ($p<0.02$) from 70 % level of cell viability represents limits of the potential cytotoxicity of sample (*STN ISO 10993-5*). The morphology and distribution of the osteoblasts seeded on surfaces of tested alloys and cultured for 48 h in medium are shown in fig. 4. The similar density and morphology of well spreaded live cells with developed filopodia were found on the surface of samples based on TiSi as compared with Ti control. A lower density of cells

was observed on Si sample. Note that a more accurate statistical evaluation of live-dead cell fractions was not possible because of a weak adherence of osteoblasts (especially dead osteoblasts) to sample surfaces.

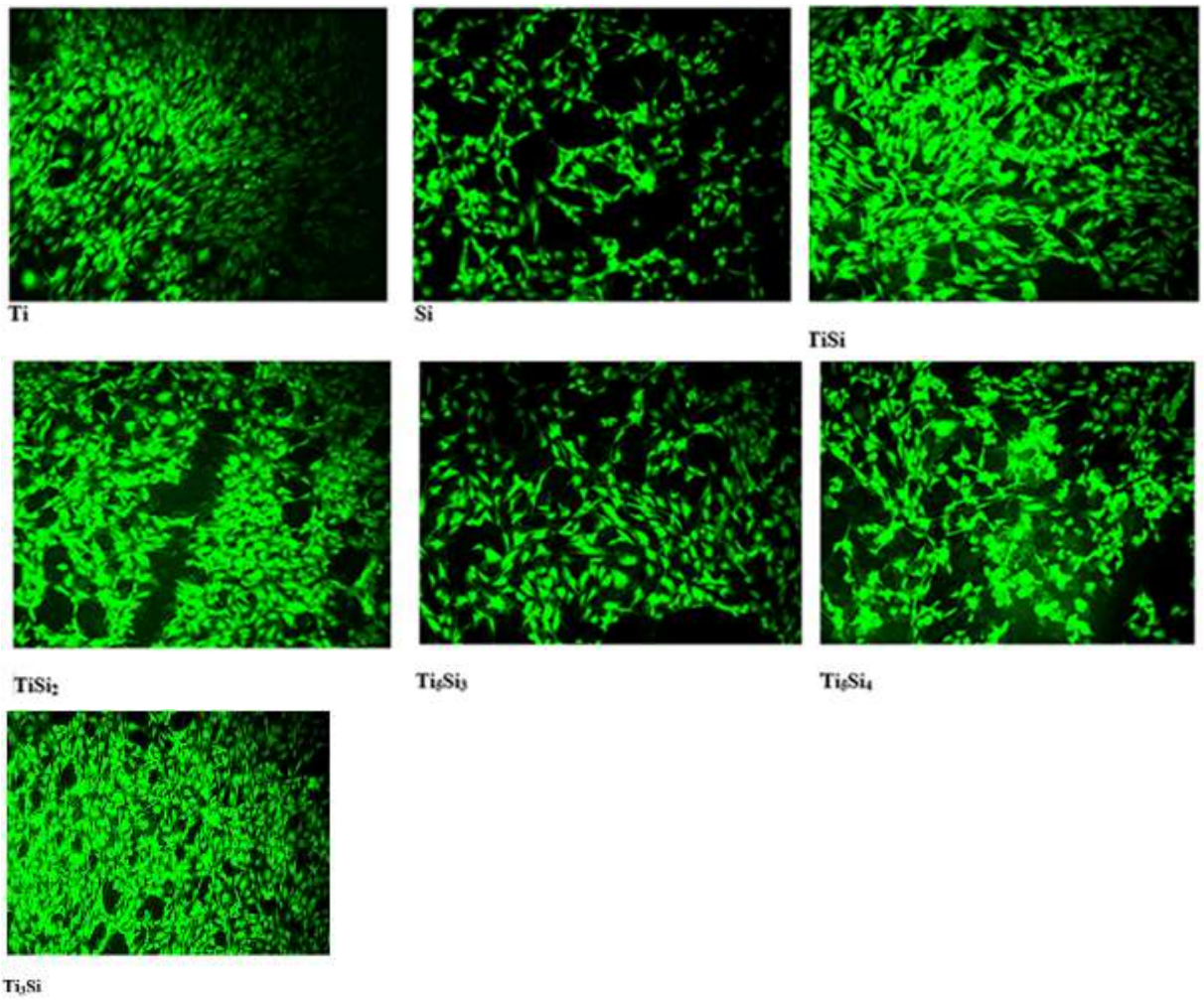

Figure 4 Osteoblasts cells seeded on surfaces of the alloys, cultured for 48 hours in medium

Conclusions

We prepared five binary Ti-Si intermetallic alloys. However, only one alloy was single-phase system, consisting of sole hcp Ti_5Si_3 phase. This fact was confirmed by XRD measurement performed at the Diamond Light Source as well as by HR-TEM. Mass density of alloys is two times higher than of human bone. Modulus of elasticity alloys is approximately ten times higher compared a human bone. Microhardness of the Ti-Si is 300% higher than of currently used implants. Alloys based on elements Ti and Si are biocompatible in respect to the MC3T3E1 cells. Cytotoxicity test and relative proliferations of osteoblasts cultured in the samples extracts indicates that extracts had a very low cytotoxicity potential. We prepared material which is biocompatible, harder but modulus of elasticity is higher to compare with actually using implants.

Acknowledgement

This work was supported by the Slovak Research and Development Agency under contract No. APVV-15-0202. Katarína Šuľová, Karel Saksl, Michaela Šuliková are grateful to the Scientific Grant Agency of the Ministry of Education, Science, Research and Sport of the Slovak Republic and the Slovak Academy of Sciences (VEGA project No. 2/0021/16). This work was realized within the framework of the project „Research Centre of Advanced Materials and Technologies for Recent and Future

Applications „PROMATECH“, ITMS 26220220186, supported by the Operational Program “Research and Development” financed through the European Regional Development Fund.

References

[1] Ninomi M., 2010. Metals for Biomedical Devices, CRC Press, 2010, 405 s. ISBN 978-1-84569-434-0
[2] Leyens, M., Peters, M., 2003, Titanium and Titanium Alloys: Fundamentals and Applications, Wiley-VCH Verlag GmbH & Co. KGaA, Weinheim, 2003, 523 s. ISBN 9783527602117
[3] Basu B., Katti D., Kumar A. 2009, Advanced Biomaterials — Fundamentals, Processing, and Applications, 2009, Johny Wiley & Sons, Inc., Hoboken, New Jersey, 2009, 707 s. ISBN: 978-0-470-19340-2
[4] Geetha M et al.: 2009, Ti based biomaterials, the ultimate choice for orthopaedic implants**.** Progress in Materials Science. 54, 397-425
[5] Long M., Rack H.J.: 1998, Titanium alloys in total joint replacement—a materials science perspective. Biomaterials 19, 1621–1639
[6] Frosch K.-H., Stürmer K.M.: 2006, Metallic biomaterials in skeletal repair. Eur. J. Trauma 32, 149–159
[7] Disegni J.A.: 2000, Titanium alloys for fracture fixation implants. Injury 31, D14–D17

Microstructural analyses and hydrogen storage capacity of $Mg_{(70-x)}$ Ni_{20} Ce_{10} Cu_x (x=0,5,10,15) metallic glasses

Katarína Šuľová [1,2], Karel Saksl [2,3]

[1] Faculty of Materials, metallurgy and recycling, Technical University of Košice, Letná 9, 042 00 Košice, Slovak Republic.
[2] Institute of Materials Research, Slovak Academy of Sciences, Watsonova 47, 04001Košice, Slovak Republic.
[3]Faculty of Science, Institute of Physics, Pavol Jozef Šafárik University in Košice, Košice 041 80, Slovak Republic.
ksulova@saske.sk

Abstract

Interest in energy sustainability exponentially increases with the development of new technologies. Hydrogen energy is one of the potential sources for long-term sustainable energy development. The important challenge of the technology is to provide the storage of energy in form of hydrogen with aspect to the cyclic stability and reversibility of this medium. Mg-based hydrides stand as promising candidate for competitive hydrogen storage with reversible hydrogen capacity up to 7.6 wt.% for on-board applications [2].

Our recent study on metallic glass system $Mg_{(70-x)}$ Ni_{20} Ce_{10} Cu_x (x=0,5,10,15) have been inspired by recent work of Lin et. al [1] and Zhang et. al [2]. Their study of glass- to-glass transition in the $Mg_{80}Ce_{10}Ni_{10}$ at.% metallic glass induced by an amount of hydrogen contained in metalhydride structure. In our work we focus on development and characterization of Mg based amorphous alloys in which magnesium was substituted by copper with the aim to lower hydrogen absorption/desorption temperature. The alloys were prepared by rapid melt quenching technique (melt-spinning capable to cool down the melt with a rate up to 10^6 $K.s^{-1}$) combined with the alloys surface activation by ball-milling process. The aim of our study is to characterize structure of the $Mg_{(70-x)}$ Ni_{20} Ce_{10} Cu_x (x=0,5,10,15) at.% metallic glasses by hard X-ray diffraction techniques and compare their hydrogen storage capacities. We determine capacity of bonded hydrogen in structure of metalhydrides via termogravimetric measurements.

Introduction

World's energy management mainly depends on non-renewable resources, such as petroleum, natural gas and coal [3]. With higher population growth increasing demand of energy dependence on global scale and the non-renewable energy resources can't infinitely cover the world's energies requirements. Despite the simplicity of the exploitation carbon sources, increasing amount of world pollution and limited access to energy resources [4] are the main drive engine for interchange to renewable and sustainable resources.

Direct consumption from renewable energetic sources is accompanied with high wasting of unused energy from over-producing and the storage of produced energy is needed. The hydrogen storage research represents the most promising alternative to fossil fuel energy. As is known from [5] and [6], annealing or melt-spinning technique are effective techniques for preparing materials with flatness plateau regions important for their practical hydrogen storage applications [7]. Mg-metallic systems are very promising and highly absorbing alloys with hydrogen absorption capacity up to 7,6 wt.%. However, further research of MgH_2 alloy have confirmed their low kinetic properties [8], this leads on research and development of new alloys with improved hydrogen storage kinetics.

This paper compares hydrogen (deuterium) storage capacities and present structural characterization of amorphous alloys $Mg_{70}Ni_{20}Ce_{10}$, $Mg_{65}Ni_{20}Ce_{10}Cu_5$, $Mg_{60}Ni_{20}Ce_{10}Cu_{10}$ and $Mg_{55}Ni_{20}Ce_{10}Cu_{15}$ at.%, prepared by rapid solidification combined with alloys surface activation by ball-milling.

Experimental

The $Mg_{70}Ni_{20}Ce_{10}$, $Mg_{65}Ni_{20}Ce_{10}Cu_5$, $Mg_{60}Ni_{20}Ce_{10}Cu_{10}$ and $Mg_{55}Ni_{20}Ce_{10}Cu_{15}$ metallic glasses were designed, prepared and tested based on idea and the work of Lin et. al. [1] done on model $Mg_{80}Ni_{10}Ce_{10}$ alloy. The samples for hydrogen storage were prepared in three steps.

1. Pre-alloy preparation: Ni, Cu and Ce elements of purity ≥ 99.9% were arc melted and 3 times re-melted under protective Ar atmosphere.

2. The pre-alloy together with stochiometric amount of matrix magnesium (of purity ≥ 99.9%) was placed to a quartz ampoule and re-melt again by induction melting. The melt at temperature ~1300 K was pour on rotating wheel of surface velocity ~ 62.8 $m.s^{-1}$ under high vacuum condition (< 3.0×10^{-3} Pa). Thicknesses of the final ribbons are 40 μm and their surface morphologies are shown on Figure 1.

3. The last preparation step was ball-milling of the ribbons in order to activate surface enhancing hydrogenation/dehydrogenation processes. Ball-milling was realized in Fritsch P7 planetary ball mill under Ar (99.999%) atmosphere at rotation speed of 200 rpm for 1 hour. Temperature of milling process was kept under crystallization temperature of individual alloys. To protect on surface of powder against oxidization, all manipulations with the powder were carried under Ar in glove bag.

Chemical composition of the studied amorphous ribbons was examined by the scanning electron microscopy Jeol JSM 7000F equipped by EDX spectrometer. Density was determined by Archimedes principle using analytical balance Kern ABT 120-4M with special density determination kit ABT-A01.

Measurements were performed on air and in pure ethylalcohol with a density equal 0.788 $g.cm^{-3}$. Phase composition was determined by using hard X-ray diffraction performed at the I12 – JEEP (Joint Engineering, Environmental and Processing) beamline at the Diamond Light Source. Experimental conditions of the measurement were the following: Energy of a monochromatic high-photon energy beam was 80.113 keV (λ=0.15476 Å), beam cross-section on the sample was ~ 0,4 mm × 0,4 mm. The samples in powder form were filled to quartz capillaries of diameter of 1 mm which under X-ray illumination were rotated. The measured diffraction data were recorded by summing of 40 images each recorded for 4 s.

Deuteration of the alloys was performed in steel vessel (reaction chamber) with an internal volume of 14 cm^3 filled by sample up to 80 vol.% under the pressure of H 4,5 MPa. The amount of deuterium stored by the alloy was probed during desorption cycle, via thermogravimetric measurement in temperature range from 303 K to 773 K at the heating rate 30 $K.min^{-1}$ in Jupiter STA 449-F1 Netsch.

Results and discussion

Chemical and phase composition

Chemical compositions of all the prepared alloys together with the alloys densities are listed in Table 1.

Table 1 *EDS results of chemical compositions for each sample prepared by melt-spinning technique.*

Sample / Atoms	$Mg_{70}Ni_{20}Ce_{10}$ (at.%)	$Mg_{65}Ni_{20}Ce_{10}Cu_5$ (at.%)	$Mg_{60}Ni_{20}Ce_{10}Cu_{10}$ (at.%)	$Mg_{55}Ni_{20}Ce_{10}Cu_{15}$ (at.%)
Mg	72	63	58	52
Ni	18	20	20	21
Ce	10	11	11	11
Cu		6	11	16
Density ($g.cm^{-3}$)	**2.99**	**3.29**	**3.75**	**4.16**

The XRD patterns from hard X-ray energy beamline confirmed amorphous nature of all the prepared alloys. The predicted XRD patterns should contain, in fully-absorbed state, signals from the hydrides generated in the amorphous matrix of the material. Figure 10 shows the as-prepared alloy patterns (left) and alloys in state fully absorbed by hydrogen (right). As we can observe from the XRD curves, a crystalline phase has created and this confirms the expected assumption.

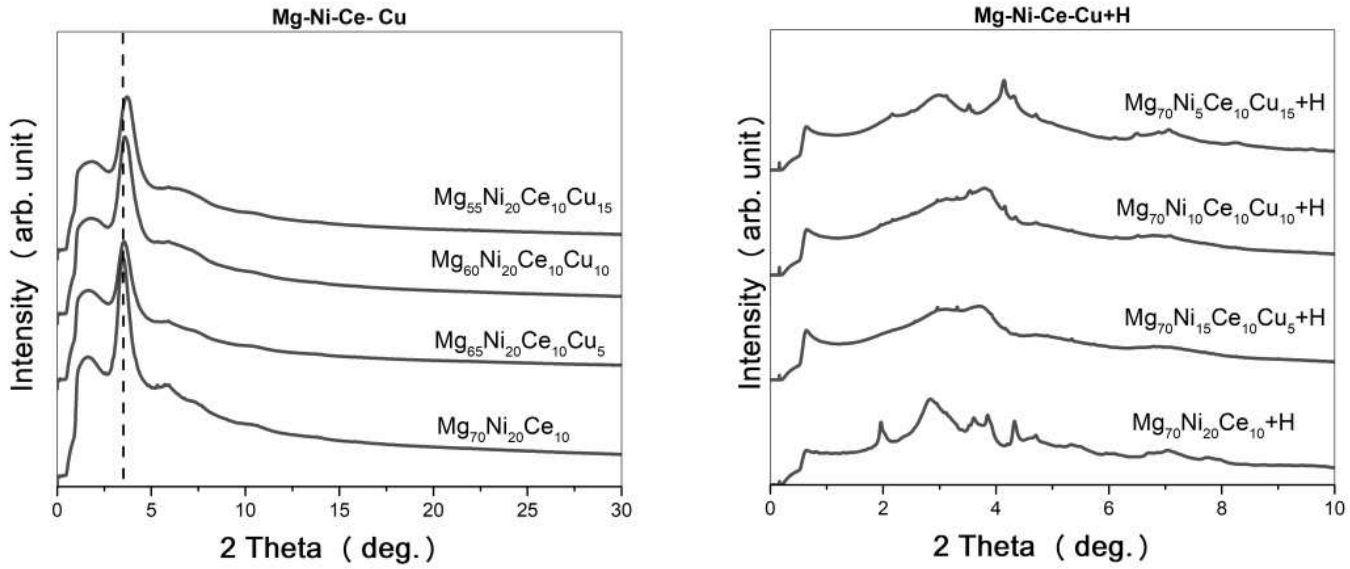

Figure 10 XRD patterns of the $Mg_{(70-x)}$ Ni_{20} Ce_{10} Cu_x (x=0,5,10,15) at.% amorphous alloys (left) , and XRD patterns of the $Mg_{(70-x)}$ Ni_{20} Ce_{10} Cu_x (x=0,5,10,15) +H at.% in fully absorbed state (right)

Hydrogen storage characteristics

It´s very common than wide range of materials, need activation of structure before hydrogenation process in repetition of high temperatures absorption and desorption cycles. The MgNiCe+Cu system is specific with hydrogen capacity absorption without previous activation. Figure 2 shows STA signals: DSC (differential scanning calorimetry) curves – in blue colour and thermogravimetric (TG) green curves measured in temperature range 25°C - 500°C.

The storage capacities of hydrogen in our samples were determined: $Mg_{70}Ni_{20}Ce_{10}$ = 3.95 wt.%, $Mg_{65}Ni_{20}Ce_{10}Cu_5$ = 3.06 wt.%, $Mg_{60}Ni_{20}Ce_{10}Cu_{10}$ = 3.93 wt.%, $Mg_{55}Ni_{20}Ce_{10}Cu_{15}$ = 1.77 wt.%. From TG curves with combining information from DSC curves can be observed the dehydrogenation kinetics which increased near the temperatures below the temperature of glass transition. The maximal hydrogen desorption offtake with increasing temperature is shown in temperature of crystallization for amorphous material.

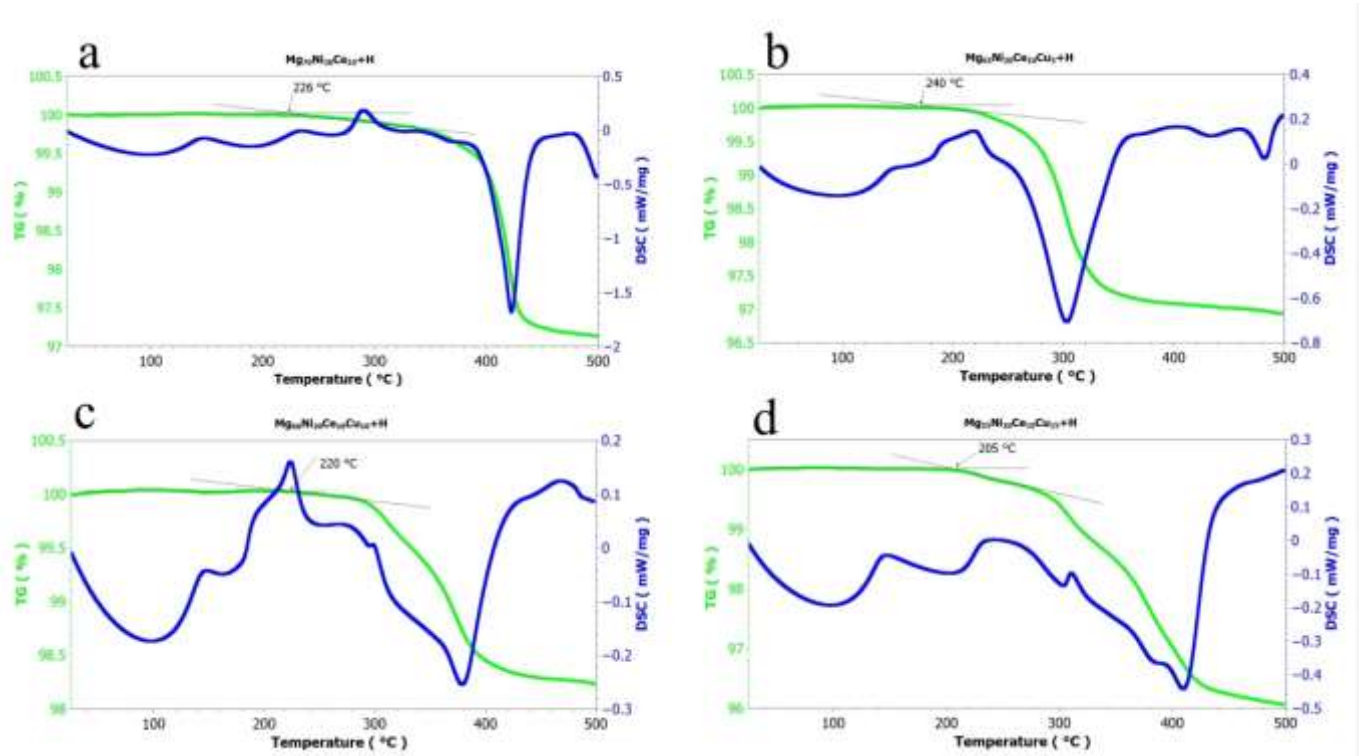

Figure 11 DSC a TG curves of prepared materials in process of dehyd,rogenation a)$Mg_{70}Ni_{20}Ce_{10}$, b)$Mg_{65}Ni_{20}Ce_{10}Cu_5$, c)$Mg_{60}Ni_{20}Ce_{10}Cu_{10}$, d)$Mg_{55}Ni_{20}Ce_{10}Cu_{15}$

Conclusions

We prepared and have characterized four Mg $_{(70-x)}$ Ni_{20} Ce_{10} Cu_x (x=0,5,10,15) at.% amorphous metallic glasses, designed as materials for hydrogen storage. All alloys are amorphous. The highest amount of hydrogen ≈ 3,9 wt.% contain $Mg_{70}Ni_{20}Ce_{10}$ and $Mg_{60}Ni_{20}Ce_{10}Cu_{10}$ alloys. Further research on these alloys will follow.

Acknowledgement

This work was supported by the Slovak Research and Development Agency under the contract No. APVV-15-0202. Katarína Šuľová, Miloš Fejerčák, Michaela Šuliková, Zuzana Molčanová and Karel Saksl are grateful to the Scientific Grant Agency of the Ministry of Education, Science, Research and Sport of the Slovak Republic and the Slovak Academy of Sciences (APVV-15-0202).

This work was realized within the frame of the project „Research Centre of Advanced Materials and Technologies for Recent and Future Applications „PROMATECH“, ITMS 26220220186, supported by the Operational Program “Research and Development” financed through European Regional Development Fund.

References

[1] Lin H. J. et al., “Towards easily tunable hydrogen storage via a hydrogen-induced glass-to-glass transition in Mg-based metallic glasses,” Acta Mater., vol. 120, pp. 68–74, 2016

[2] Zhang C. et al., “Progress in Natural Science : Materials International E ff ect of Cu on dehydrogenation and thermal stability of amorphous Mg-Ce-Ni-Cu alloys,” Prog. Nat. Sci. Mater. Int., vol. 27, no. 5, pp. 622–626, 2017

[3] Zacharia R. and Rather S.U., “Review of solid state hydrogen storage methods adopting different kinds of novel materials,” J. Nanomater., vol. 2015, 2015

[4] Amirante R. et al., “Overview on recent developments in energy storage: Mechanical, electrochemical and hydrogen technologies,” Energy Convers. Manag., vol. 132, pp. 372–387, 2017

[5] Chemie P. et al., “Thermopower Study of Local Hydrogen Content in Rapidly Quenched Zr — Ni Ribbons *,” vol. 372, 1989
[6] Nakamura Y. et al., “Homogenizing behaviour in a hydrogen-absorbing LaNi4.55Al0.45alloy through annealing and rapid quenching,” J. Alloys Compd., vol. 210, no. 1–2, pp. 299–303, 1994
[7] Han X. B. et al., “Effect of Preparation Technique on Microstructure and Hydrogen Storage Properties of LaNi3.8Al1.0Mn0.2Alloys,” J. Mater. Sci. Technol., vol. 32, no. 12, pp. 1332–1338, 2016
[8] Wu D. et al., “Phase transition and hydrogen storage properties of Mg – Ga alloy,” J. Alloys Compd., vol. 642, pp. 180–184, 2015

Mechanochemical reduction of natural and synthetic sulphidic copper-bearing minerals in an industrial scale

Matej Tešinský, Matej Baláž

Institute of Geotechnics of SAS, Department of Mechanochemistry, Watsonova 45, 04353 Košice, Slovak Republic

Abstract

In this paper the mechanical mechanochemical reductions of two binary sulfides chalcocite (Cu_2S) and covellite (CuS) and a ternary sulfide chalcopyrite ($CuFeS_2$) by elemental iron were investigated. The composition and properties of nano-powders prepared by high-energy milling were analyzed by X-ray diffraction and magnetic measurements. The results show that in case of chalcocite Cu_2S the reaction takes place until 120 minutes, as no elemental iron was present, could be identified. In case of covellite CuS, after 480 minutes of mechanochemical reduction, traces of non-reacted elemental iron could still be observed. Mechanochemical reduction of chalcopyrite $CuFeS_2$ was performed for 600 min, however only troilite peaks could be surely identified. The investigation of magnetic properties reveals significant decreasing of saturation magnetization as a result of milling. Unlike the conventional high-temperature reductions of chalcopyrite, chalcocite and covellite, the mechanochemical reduction is fast and ambient temperature and atmospheric pressure are sufficient for its propagation.

Introduction

Mechanochemistry is a branch of science referring to the chemical and physicochemical reactions of substances due to the influence of mechanical force [1]. Mechanochemical pretreatment by intensive grinding is an innovative procedure that improves the efficiency of mineral processing via several factors, most importantly due to the formation of new surfaces and the creation of lattice defects [2-4]. The process is also called mechanochemical processing or mechanical activation. Its benefits include lower reaction temperatures, increased rate and amount of solubility and the formation of water soluble compounds. As a consequence, further processing can be performed in simpler and less expensive reactors during shorter reaction times [5-8, 9, 10]. In a typical technological process, the solid raw materials are transformed by liquid and/or gas phase reactions at high temperatures and pressures. The final products are then separated from the by-products, from the remaining starting materials and/or from the solvent. Very often, the final product is solid again [11, 12]. Mechanochemical processing may offer the possibility to simplify the entire technological flowchart by avoiding operations in the gaseous and liquid states and to design the process according to the flowchart [13, 14]:

Raw materials → Solid state reaction → Desired product

High-energy milling of sulphides with a reactive metal in so-called mechanochemical reduction mode can lead to products in nano-range and to composition which simplifies the following metallurgical processing. Chalcopyrite $CuFeS_2$, a ternary semiconductor with antiferromagnetic properties represents promising candidate as an advanced material for use in inexpensive nano-electronics (solar cells, magnetic materials) [15]. Chalcocite and covellite are binary sulphides of copper which contains the highest amount of copper from sulphide copper bearing minerals. In addition to their unique properties (conductivity, utilization in biomedicine), they are sources of copper in ores for metallurgical operations [15]. In this work, the process of mechanochemical reduction of chalcopyrite, chalcocite and covellite with elemental iron in industrial scale conditions according to reactions (1,2,3) were studied

$$2CuFeS_2 + Fe \rightarrow Cu_2S + 3FeS \qquad (1.1)$$

$$Cu_2S + Fe \rightarrow 2Cu + FeS \qquad (1.2)$$

$$Cu_2S + Fe \rightarrow 2Cu + FeS \quad (2)$$
$$CuS + Fe \rightarrow Cu + FeS \quad (3)$$

The aim of this paper is to illustrate effectiveness of so called process mechanochemical reduction in an industrial scale by industrial eccentric vibration mill (Fig.1) of two binary and one ternary sulphide with elemental iron which leaded to production of nanocomposite of Cu/FeS as an only product. Big advantage of using an industrial eccentric vibration mill in comparison to laboratory high energy milling is in the first place amount of obtained product.

Figure 12 Eccentric vibratory mill with attached closed satellite (left), open satellite filled with balls (right)

Material and methods

Materials

For mechanochemical synthesis of covellite and chacocite copper (99% Merck, Germany) and sulfur (99% CG-Chemikalien, Germany) powders were used as elemental precursors. For mechanochemical reduction, natural chalcopyrite $CuFeS_2$ (98%, deposit Zhezkazgan, Kazakhstan, JCPDS 00-035-0752) or mechanochemically synthesized copper sulfide covellite CuS (JCPDS 00-006-0464) or chalcocite Cu_2S (JCPDS 72-1071) and elemental iron Fe (99% Winlab, Germany)) were used as precursors. Iron was used as a reduction reagent.

Mechanochemical synthesis and reduction

Mechanochemical solid state reductions were performed in an industrial eccentric vibratory ball mill ESM 656−0.5 ks (Siebtechnik, Germany) working under the following conditions: 5 L steel satellite milling chamber attached to the main corpus of the mill, tungsten carbide balls with a diameter of 35 mm with a total mass of 30 kg, 80% ball filling, amplitude of the mill = 20 mm, rotational speed of the eccenter = 960 min^{-1}, argon atmosphere, 100 g of feed. The milling was performed for various times (t_M). In the case of mechanochemical synthesis of CuS and Cu_2S precursors, milling for 40 and 60 min, respectively, has been applied. In case of mechanochemical reduction of chalcocite Cu_2S and covellite CuS according to reactions (2) and (3), respectively, t_M 480 min has been applied. In mechanochemical reduction of natural chalcopyrite $CuFeS_2$, according to reaction (1.1, 1.2), total t_M was set up to 840 min.

Characterization Techniques

The identification of phase composition was performed by XRD method with an X'Pert PW 3040 MPD diffractometer (Phillips, Germany) and D8 Advance diffractometer (Bruker Germany), both working in the 2θ geometry with Cu K_α (40kV, 40 mA) radiation.

In order to obtain information on magnetic properties of the studied samples, mass magnetization was measured. The measurements were performed by using vibrating sample magnetometer (VSM) installed on a cryogen free superconducting magnet (Cryogenic Limited). The samples were measured in powder form packed in a specialized capsule. After the measurements, the magnetic moment values were divided by the sample mass, yielding the mass magnetization.

Results and discussion

In Fig. 2 A and B, XRD patterns of two systems (Cu_2S+Fe) and (CuS+Fe) are shown, respectively. In both cases the main peak corresponding to copper is overlapping with the troilite one. Therefore, the progress of the reaction can be traced mainly by observing the decrease of the intensity of main iron peak located at 2θ ~ 44 °. For Cu_2S+Fe system, iron peak is no longer visible after t_M 360 min, suggesting the completion of the reaction. At the t_M 480 min, there is still small trace of main iron peak visible, therefore we can conclude that reaction is still not completed.

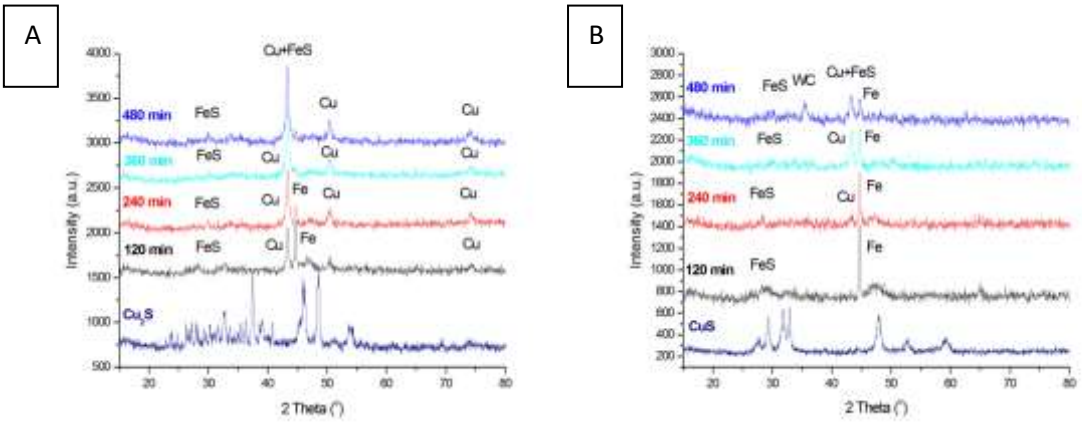

Figure 13 XRD patterns recorded during mechanochemical reaction of mechanochemically synthesed covellite (Cu_2S) (A) and chalcocite (CuS) (B) with iron powder. The XRD of starting Cu_2S and CuS are also provided

The XRD patterns for system ($CuFeS_2$+Fe) are shown at Fig.3. The decrease in the intensity of the main peak of chalcopyrite (2θ ~ 28 °) can be observed. Also the intensity of the main iron (Fe) peak is decreasing during the reaction. Decreasing the intensity of the chalcopyrite ($CuFeS_2$) and iron (Fe) peaks as a consequence of crystalline phase decrease and increase in lattice strain results from the mechanical activation of both reactants, however reaction (1.1) has most probably not taken place yet. From t_M 240 min, the peak of troilite (FeS) at 2θ ~ 43 ° can be observed. At t_M 360 min, further decrease in the intensity of chalcopyrite peak due to formation of the product of troilite (FeS) can be observed. Further, an increase in the intensity of the troilite peak (FeS), which was visible after t_M 240 min can be seen. At t_M 600 to 840 min, the formation of nano-copper (Cu) could be possible, however, its main peak overlaps with troilite peak. Elemental iron (Fe) and chalcopyrite ($CuFeS_2$) are no longer visible in XRD patterns, so it is possible that the reaction is completed. The methodological problem is that Cu_2S, which occurs in the reaction (1.1), cannot be certainly identified, due to the overlapping of its main reflection with those of FeS. Moreover, as a result of amorphisation, diffraction peaks are very broad.

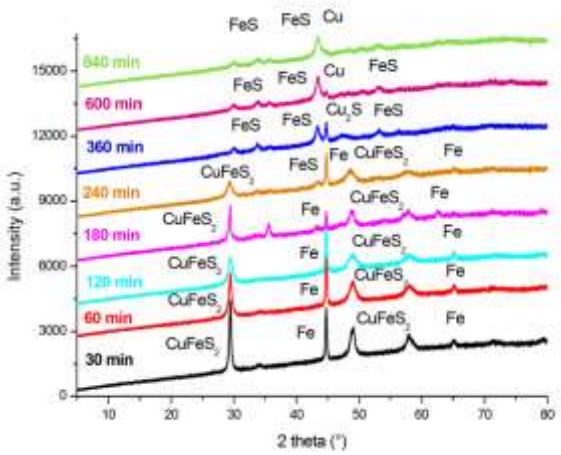

Figure 3 XRD patterns recorded during mechanochemical reaction of natural chalcopyrite with iron powder

In Fig.4, the dependence of saturation magnetization on t_M for all studied systems is given. Regarding the starting mixtures, the highest magnetization value was evidenced for CuS+Fe system and the lowest for $CuFeS_2$+Fe. In all cases, magnetization decrease with t_M, which correlates with the consumption of Fe in reactions. In the case of Cu_2S+Fe system (reaction 2), the magnetization value after t_M 360 min and 480 min is around 10 Am^2/kg, which confirms the observation from XRD that the reaction is almost completed already after t_M 360 min.

In comparison with mechanochemical synthesized samples of Cu_2S+Fe and CuS+Fe systems, the lowest value of saturation magnetization is observed in case of chalcocite Cu_2S, t_M 480 min, which correlates with Fig.2 (A). According to the reaction (3) (covellite CuS reduction), the final value of saturation magnetization is higher, as the reaction did not proceed totally. This fact correlates with Fig.2 (B) where after t_M 480 min, elemental iron (Fe) is still observed. The lowest saturation magnetization is observed in third system of ($CuFeS_2$ + Fe) at 840 min of t_M also suggesting complete consumption of iron.

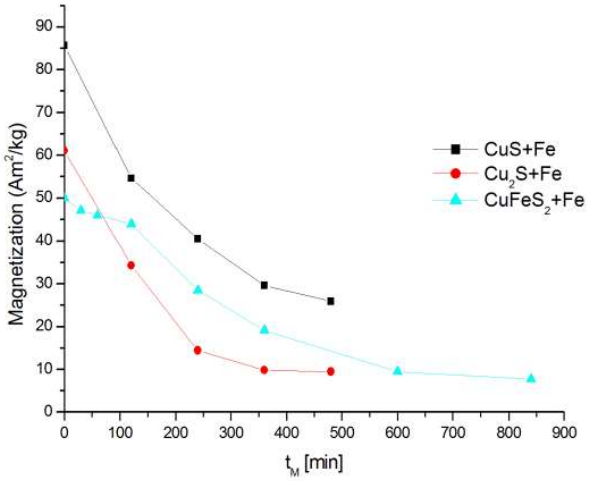

Figure 4 Magnetization vs. tM for $CuFeS_2$ (deposit Zhezkazgan) according to reaction (1.1, 1.2) (blue - triangle), chalcocite Cu_2S according to reaction (2) (red - circles), and covellite CuS according to reaction (3) (black - squares**)**

Conclusion

The mechanochemical reduction of chalcocite Cu_2S, covellite CuS and chalcopyrite $CuFeS_2$ with the application of elemental iron as the reducing element was studied in this article. From the results we can conclude that mechanochemical reduction of all three systems is possible. Therefore, there is a possibility to make chemical reduction without requirement of any high energy consuming processes such as in pyrometallurgy. This fact makes mechanochemical processing more environmental and energy effective way for the treating of minerals in the partial production steps.

Acknowledgements

The authors are grateful for the support of the Slovak Research and Development Agency (project APVV-14-0103) and Slovak Grant Agency (project VEGA 2/0044/18).

References

[1] Baláž P., 2008. Mechanochemistry in Nanoscience and Mineral Engineering. Springer, Berlin
[2] Tkáčová K., 1989. Mechanical Activation of Minerals. Elsevier, Amsterdam
[3] Baláž P., 2000a. Extractive Metallurgy of Activated Minerals. Elsevier, Amsterdam
[4] Baláž P., 2000b. Mechanical activation in technology of metals extraction. Metall. 54, 190– 195
[5] Welham N.J., 1996. A parametric study of the mechanically activated carbothermic reduction of ilmenite. Miner. Eng. 9, 1189– 1200
[6] Welham N.J., 2001a. Enhanced dissolution of tantalite, columbite following milling. Int. J. Miner. Process. 61, 145– 154
[7] Welham N.J., 2001b. Enhancing zircon (ZrSiO4) dissolution by ambient temperature processing. Proc.-Australas. Inst. Min. Metall. 305, 1 –3
[8] Welham N.J., Chapman P.G., 2000. Mechanical activation of coal. Fuel Process. Technol. 68, 75– 82
[9] Aylmore M.G., Lincoln F.J., 2000. Mechanochemical millinginduced reactions between gases and sulfide minerals: I. Reaction of SO2 with arsenopyrite, pyrrhotite and pyrite. J. Alloys Compd. 309, 61– 74
[10] Aylmore M.G., Lincoln F.J., 2001. Mechanochemical millinginduced reactions between gases and sulfide minerals: II. Reactions of CO2 with arsenopyrite, pyrrhotite and pyrite. J. Alloys Compd. 314, 103–113.
[11] Boldyrev V.V., 1998. Mechanical activation and its application in technology. Mat. Sci. Forum 269–272, 227– 234
[12] Boldyrev V.V., Tkáčová K., 2000. Mechanochemistry of solids: past, present, and prospects. J. Mater. Synth. Process. 8, 121–132
[13] Boldyrev V.V., 1996a. Mechanochemistry and mechanical activation. Mat. Sci. Forum 225–227, 511 –520
[14] Boldyrev V.V., 1996b. Reactivity of solids and new technologies. In: Boldyrev, V. (Ed.), Reactivity of Solids: Past, Present and Future. Blackwell Science, Oxford, Great Britain, pp. 267– 286
[15] Baláž P., et al. Mechanochemical reduction of copper sulphide. Materials Science Forum 386-388, 257-262

Determination of the PAH in Soil Contaminated with Coal Tar

Jana Tomčová, Daniel Kupka, Eva Mačingová, Dávid Jáger, Miroslava Václavíková

Institute of Geotechnics, Slovak Academy of Sciences, Watsonova 45, 04001 Košice, Slovakia
vaclavik@saske.sk

Abstract

Polycyclic aromatic hydrocarbons (PAHs) are persistent contaminants with two or more fused aromatic rings. They are ubiquitous pollutants that have been identified in various matrices, such as sediment, water, soil or dust particles. The presence of PAHs in ecosystem is a common environmental concern. They are the result of incomplete combustion of organic material such as coal, oil and wood. Risk assessment soil contaminated with polyaromatic hydrocarbons require accurate analysis of the concentration of each PAH in the soil. In this work, Soxhlet extraction, solid phase extraction clean-up and high performance liquid chromatography equipped with a diode array detector and mass spectrometer was used to determine the initial concentration of 16 PAHs in soil.

Introduction

Polycyclic aromatic hydrocarbons (PAHs) represent a potential hazard to the human health due to their toxicity, mutagenicity and carcinogenicity. The main natural sources include forest fires and volcanic eruptions. The major anthropogenic sources of environmental PAHs contamination are vehicular emissions, waste incineration or production of coal tar. Due to their carcinogenicity, teratogenicity and mutagenicity, 16 PAHs have been listed by the US Environmental Protection Agency (EPA) as priority pollutants. These are naphthalene, acenaphthene, acenaphthylene, fluorene, phenanthrene, anthracene, fluoranthene, pyrene, benzo[a]anthracne, chrysene, benzo[b]fluoranthene, benzo[k]fluoranthene, benzo[a]-pyrene, dibenz[a,h]anthracene, benzo[g,h,i]perylene and indeno[1,2,3-cd]pyrene [1].

The effective monitoring of PAHs content has a great importance from the point of view of both environmental and human safety [2]. The determination of PAHs in soils generally includes several consecutive steps, i.e. separation (extraction), clean-up (fractionation) and final determination (identification and quantification) [3]. PAHs are lipophilic compounds that show high affinity for organic matter and their determination in soil always requires powerful extraction techniques to release strongly adsorbed contaminants from the soil material [4]. Soxhlet and/or ultrasonic extraction are the most common ones. For any extraction methods, clean-up of the extract is a necessary step prior the analysis. Without clean-up the analytical column can be loaded with impurities leading to a loss of column efficiency and a decrease in the lifetime of the LC column. The most frequently used analytical techniques for the determination of PAHs in soil are gas chromatography coupled with mass spectrometric detection (GC–MS) and high performance liquid chromatography with fluorescence (FL) and UV detection.

The objective of this study was the determination of the initial PAH concentration in soil sample contaminated with coal tar. PAH extraction was carried out by Soxhlet extraction; petroleumether was used as a solvent. Clean-up was done by means of solid phase extraction. HPLC with a diode array detector and mass spectrometer was used for PAH identification and quantification.

Experimental

Soil sample was collected from contaminated site with wood-treatment activities, and asphalt mixing plant where PAHs containing products such as creosote, coal tar, asphalt, petroleum and other bituminous materials were extensively used. The air dried soil sample was ground, mixed thoroughly and passed through a 2-mm sieve to remove gravel and debris, individually. 10 g portion of soil was mixed with 10 g of anhydrous sodium sulfate and transferred into pre-extracted extraction thimble inserted into Soxhlet extractor. The extractions were performed with 300 ml of petroleum ether for 20 h. After extraction, the extracts were concentrated under reduced pressure at 40 °C water bath using a rotary evaporator

to volume approximately 150 ml. SPE clean-up of the soil extracts was carried out using by Chromabond CN/SiOH columns (6 ml, 500/1000 mg). The samples were evaporated and dried with a gentle N_2current and vacuum in the sand bath with temperature up to 40°C. Separation of the 16 PAHs was performed with a column 250 x 3 mm Nucleosil 100-5 C18 PAH.

Results and discussion

The mobile phase was made of acetonitrile and water in different ratios, and the gradient elution program was featured by changing ratios of acetonitrile and water (Table 1). Elution was carried out with mobile phase flow rate of 0.5 ml/min with total run time of 32 min per sample extract injection and at a controlled oven temperature of 25ºC. The sample injection volume was 10 µl. The wavelength of the detector was set to 254 nm, as all aromatic compounds have high absorbance at this wavelength.

Table 1 *Mobile phase gradient programme*

Time (min)	Total flow rate (ml/min)	Acetonitrile (%)	Water (%)
0	0.5	65	35
2	0.5	65	35
18	0.5	0	100
32	0.5	0	100

The time for a chromatographic cycle of the full separation for the 16 PAHs was 42 min including 10 min for the equilibration of the column. This time was suitable for economic and routine analysis of the 16 PAHs. The peaks identification was based on thein retention times after separation by HPLC Q-TOF MS. Given that molecular mass of some PAH compounds is same, single standards were used for their identification. The quantification of the PAHs was done by calibration curve. The linearity was evaluated at different concentrations using peak areas. They showed a good linearity since the values of the correlation coefficients ranged from 0.998 to 0.999 for all the 16 PAHs investigated in this study.

Visual comparison of chromatograms of mixed standard and soil extracts is shown in Figure 1. The 16 PAH standard mixture contains 1 - acenaphthene, 2 - naphthalene, 3 - acenaphthylene, , 4 - fluorene, 5 - phenanthrene, 6 - anthracene, 7 - fluoranthene, 8 - pyrene, 9 - benzo[*a*]anthracene, 10 - chrysene, 11 - benzo[*b*]fluoranthene, 12 - benzo[*k*]fluoranthene, 13 - benzo[*a*]pyrene, 14 - dibenzo[*a,h*]anthracene, 15 - benzo[*ghi*]perylene and 16 - indeno[*1,2,3-cd*]pyren.

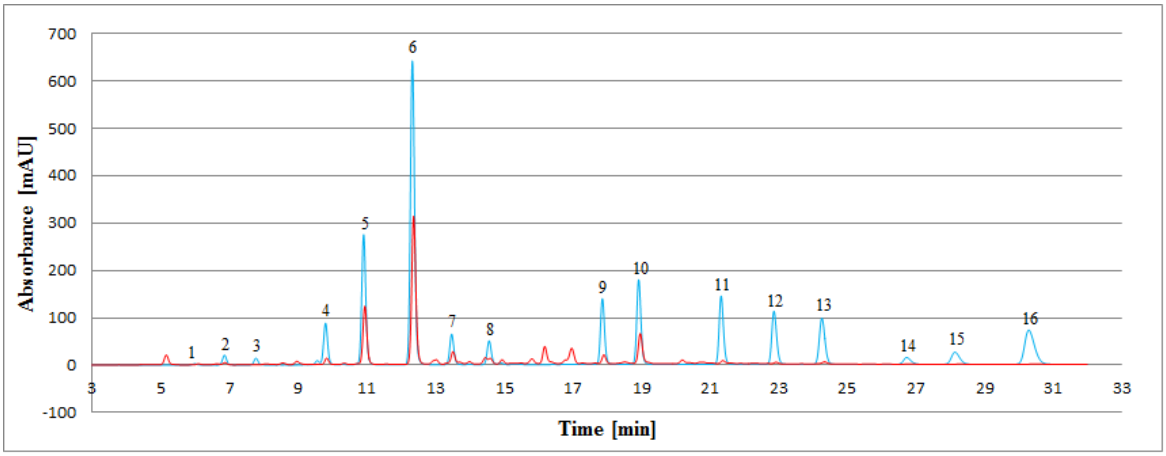

Figure 1 Comparison of chromatograms of real sample extracts and mixed standard: 1 - acenaphthene, 2 - naphthalene 3 - acenaphthylene, 4 - fluorene, 5 - phenanthrene, 6 - anthracene, 7 - fluoranthene, 8 - pyrene, 9 - benzo[*a*]anthracene, 10 - chrysene, 11 - benzo[*b*]fluoranthene, 12 - benzo[*k*]fluoranthene, 13 - benzo[*a*]pyrene, 14 - dibenzo[*a,h*]anthracene, 15 - benzo[*ghi*]perylene and 16 - indeno[*1,2,3-cd*]pyren, (real sample extract – red peaks, standard – blue peaks)

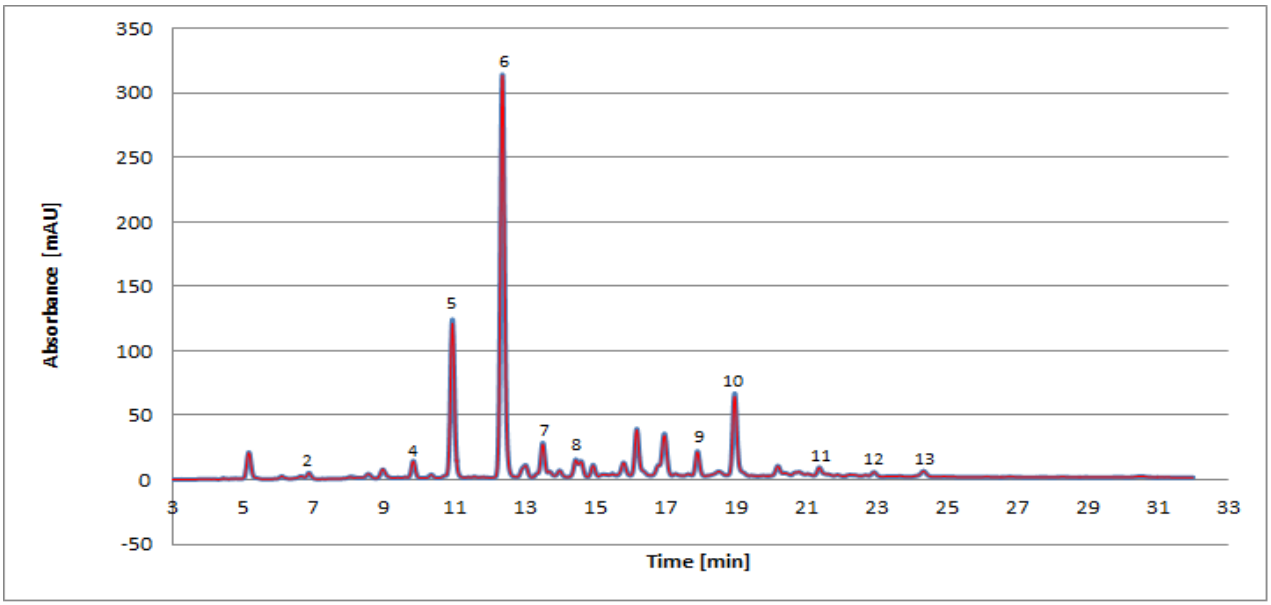

Figure 2 Comparison of chromatograms of two parallel real soil extracts

Comparison of chromatograms of two parallel real samples is shown in Figure 2. They were almost identical. It can be concluded that the soxhlet extraction procedure had a good reproducibility. The presence of 13 priority PAHs has been confirmed in the real soil sample. Quantities of individual PAHs ranged from 5.96 to 405.03 µg/ml. Acenaphthene, dibenzo[a,h]anthracene, benzo[ghi]perylene were not present in the sample. However several unknown peaks were observed in chromatogram, thus their identification will be the objective of future research.

Conclusions

The first step in the analytical determination of priority pollutants, PAHs, in environmental matrices includes separation (extraction) of the fraction concerned. The analytical methods described in this study were shown to be reliable for the determination of the 16 US EPA PAHs in solid samples from the soil. UV detector can be used for the determination of PAHs. UV detectors are often used at 254 nm with no wavelength programming. This provides adequate sensitivity for the PAHs. But more sensitivity and selectivity can be achieved with fluorescence detectors when using wavelength programming. A fluorescence detector in series with a UV detector will provide the best sensitivity and selectivity.

Acknowledgement

This work has been supported by the MarieCurieProgramme FP7-People-2013-IAAP-WaSClean project No 612250, VEGA-2/0158/15 and ERDF GeoCex project No ITMS 26220120064 – Centre of Excellence for Integrated Research of the Earth's Geosphere.

.

Citations

[1] Huang Y. et al.: Determination of low levels of polycyclic aromatic hydrocarbons in soil by high performance liquid chromatography with tandem fluorescence and diode-array detectors. Chemosphere, 2013. 92(8): p. 1010-1016

[2] Włóka D. and M. Smol: Evaluation of extraction methods of polycyclic aromatic hydrocarbons (PAHs) from soil and sewage sludge matrix. Inżynieria i Ochrona Środowiska, 2014. 17

[3] Joa K. et al.: Determination of polycyclic aromatic hydrocarbons (PAHs) in oil shale processing wastes: current practice and new trends. Oil Shale, 2009. 26(1): p. 59-73

[4] Khan Z., Troquet J., and Vachelard C.: Sample preparation and analytical techniques for determination of polyaromatic hydrocarbons in soils. International Journal of Environmental Science & Technology, 2005. 2(3): p. 275-286

Hydrometallurgical treatment of tin sludge in aqueous solutions of sulfuric and acetic acid

Ivana Urban Kobialková, Tomáš Havlík

Technical University of Košice, Faculty of Materials, Metallurgy and Recycling,
Institute of Recycling Technologies
ivana.urban.kobialkova@tuke.sk

Abstract

The paper studies methods of tin leaching from the tin sludge in different solutions. Sulfuric acid and acetic acid as leaching reagent for these experiments were used. The aim of the experiments was to investigate the effect of temperature on the extraction of tin and iron into solution. The results show that the tin and iron extraction into solution is not effective.

Introduction

The amount of waste produced is naturally increasing. The main reason is the continuous development of new technology in the present society and continuously increasing industrialisation [1]. In 2016 the Slovak Republic produced 10.1 million tons of waste [2]. Fees for depositing waste at dumps increased. This is why society is forced to seek new alternative options for utilising waste as a secondary raw material [3]. Recycling is also one such option, which saves natural resources (primary raw materials), energy and last but not least, it minimises the amount of waste deposited at landfills. Demand for metals is increasing worldwide for its use in various industries. The demand for metal is increasing worldwide due to its use in various industries. Replacing metal with other materials is usually problematic.

The main problem is that every metal has its own specific properties. The paper [4] states that from the total amount of metal used in industry, as many as 62 metals cannot be replaced with materials which would meet 100% of the required properties. Tin, one of irrecoverable metal, is contained in industrial waste are dust, slag and sludge from the treatment of industrial waste from the tinning process. Dust treatment was studied by Guldorf et al. [5] and processing the slag by Soewarno et al. [6]. Moreover, most of these articles have older date of publication and this indicate the importance of dealing with this type of waste.

Experimental part

Materials and methods

The input material used for the experiments was tin sludge generated by electrolytic tinning process. The tin sludge is formed during process by the reaction between the molten metal and the MSA acid on the bottom of bath. The material was dried due to its high humidity. Drying was performed to constant weight at 105°C. Loss of drying was from 9.6% to 20,9 %. The content of physically water in the samples was different because of different batches.

Chemical analysis

Chemical analysis was performed using atomic absorption spectometry (AAS) Varian Spctrophotometer AA20+, Tab. 1 and EDX analysis, Tab. 2. Magnification during EDX analysis was 1500x. From the results of analysis, a high tin content is evident. Tin is main metal contained in tin sludge.

Table 1 *Chemical analysis input sample (AAS method)*

Metal	**Sn [%]**	**Fe [%]**	**Cu [%]**	**Sb [%]**	**Mg [%]**	**Zn [%]**	**Ni [%]**
Content	*59.64*	*0.642*	*0.072*	*0.77*	*0.02*	*0*	*0*

EDX analysis confirmed chemical analysis that tin is main metal in tin sludge. EDX shows that tin sludge contains S and Sb, excluded content Fe. However, it is possible that the iron phase did not appear in the analyzed part of the sample. Sample contains also oxygen, confirming the assumption that Sn is present in the sample in the form of oxides or in the form of oxygen compounds.

Table 2 *EDX analysis input sample*

Element Line	*Net Counts*	*Net Counts Error*	*Weight %*	*Weight % Error*	*Atom %*	*Atom % Error*	*Formula*	*Compnd %*	*# Cations*
O K	257	+/- 16	13.49	+/- 0.84	50.56	+/- 3.15	O	13.49	---
S K	1523	+/- 52	4.21	+/- 0.14	7.88	+/- 0.27	S	4.21	---
Sn L	14940	+/- 182	80.27	+/- 0.98	40.56	+/- 0.49	Sn	80.27	---
Sb L	369	+/- 185	2.02	+/- 1.01	1.00	+/- 0.50	Sb	2.02	---
Total			100.00		100.00			100.00	0.000

Mineralogical analysis

XRD analysis was performed by X-ray diffractometer PANalytical X'pert PRO MPD. Fig. 1 shows XRD pattern of input sample and sample after annealing at 600°C and 1000°C.

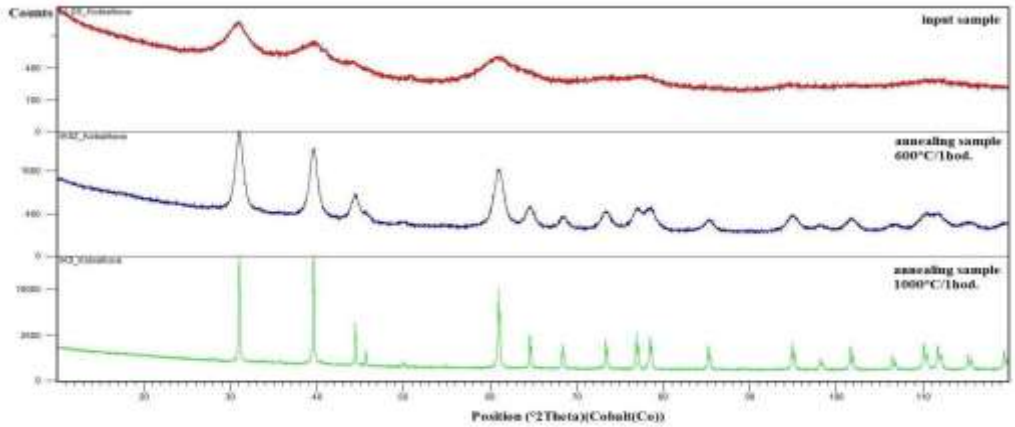

Figure 1 The XRD pattern of input sample and sample after annealing

Fig. 1 shows that input sample is amorphous. After sequentially annealing sample crystallized and the SnO_2 phase was detected. From the results this part of the experimental work it is possible to assume that the sample consists SnO_2 phase as well as chemically and physically bound water.

Morphological analysis

Optical microscope observation were performed on the Dino-Lite MZK 1701 digital microscope at 60x and 195x magnifications. Sample images at 60x and 195x magnifications are shown in Fig. 2.

Leaching

The leaching experiments were carried out in glass reactor with the volume of 800 ml, dipped into water bath at the temperature 20, 50 and 90°C. The aqueous solution of H_2SO_4 at concentration 2M and solution 2M $C_2H_4O_2$ was used as a leaching reagent. The volume of the leaching reagent was 400 ml. The sample weight 20 g was used for the leaching which represent liquid to solid ratio L:S=20. The total experiment time was 300 minutes. The samples of 10 ml were taken at 1, 5, 10, 15, 30 and 60, 120, 240 and 300 min. from the solution. The samples were analysed for tin and iron content.

The aim of this work was to compare leaching of tin sludge in sulfuric acid and acetic acid. The influence of temperature on the amount of leached tin was investigated.

Figure 2 Sample observed with Dino – Lite MZK 1701 optical microscope (magnification 60x and 195x)

Results and discussion

H_2SO_4 leaching

The leaching of sludge was carried out in aqueous solutions of 2M sulfuric acid. Fig. 3 shows kinetics curves of tin leaching in 2M H_2SO_4 and ratio L:S=20. From the graph it results that tin and iron extraction at low concentration is dull. The highest tin extraction (13.8%) at 90°C was achieved in 60 minute of leaching. During these conditions the extraction of iron into solution is about 1%. Increasing temperature and concentration has not significant influence to tin and iron extraction into solution.

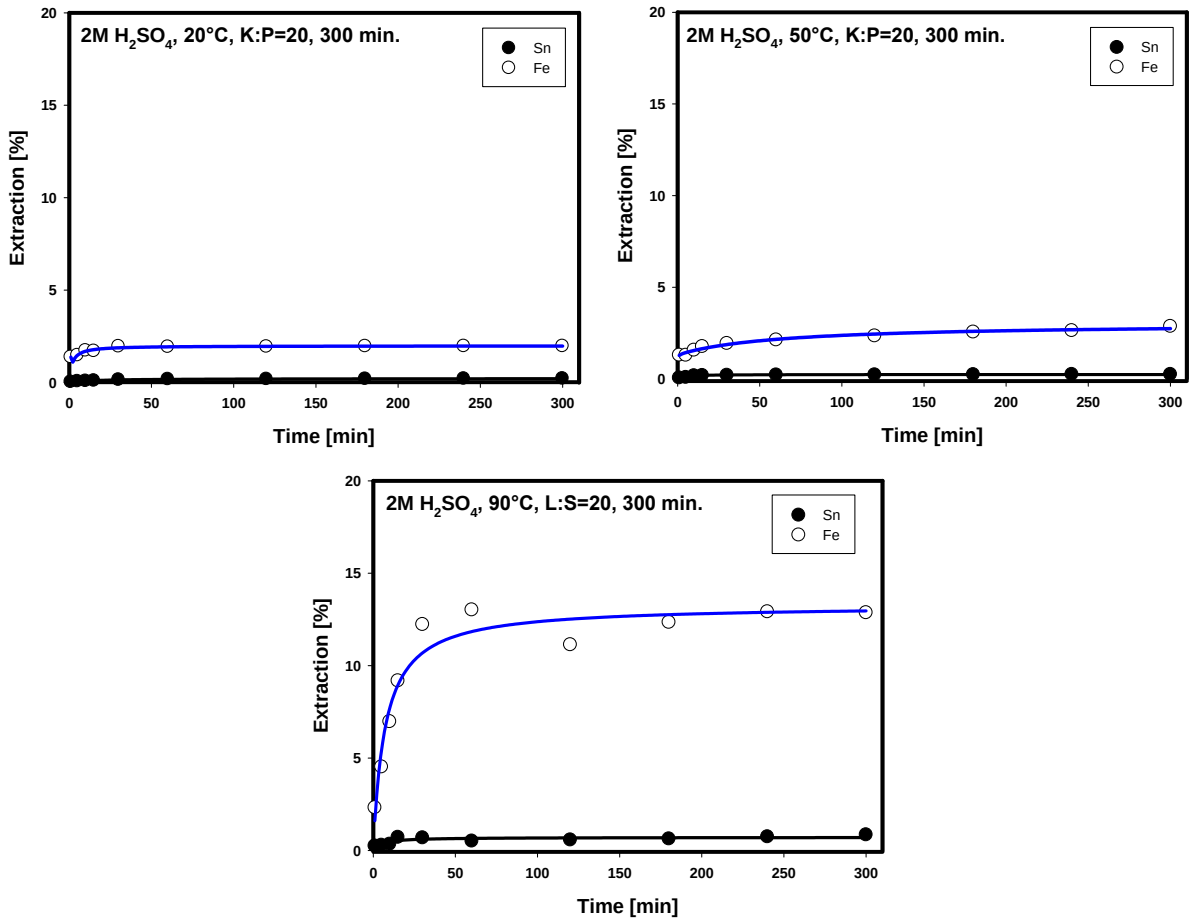

Figure 3 Leaching efficiency of tin and iron from tin sludge in 2M H2SO4 at 20, 50 a 90°C for 300 min.

$C_2H_4O_2$ leaching

Leaching was carried in 2M acetic acid ($C_2H_4O_2$**)** at 20, 50 a 90°C for 300 min. However, the results show that the leaching in acetic acid is not effective, because no tin was passed to the solution in $C_2H_4O_2$ (resp. tin extraction into the solution was below the limit of proof of the AAS analytical method). Iron extraction was low, the highest extraction was achieved by leaching at 20°C in the first minute of leaching (1.82 μg/ml). For these reasons, the leaching of other molarities of acetic acid was not performed as it seems ineffective.

Leaching tin sludge in sulfuric and acetic acid is not effective. Extraction of tin and iron in sulfuric acid was too low, max. 13,8% of tin and 1% of iron.

Conclusion

In this paper, leaching of tin from tin sludge was investigated. The amount of tin makes this sludge interesting secondary raw material. Experiments have shown that the present form of tin in the sample is insoluble. Iron and tin extraction into solution was minimum. The maximum tin extraction achieved in the solution was about 13% and the iron about 1%. The extraction of tin into the solution could be achieved by using an oxidizing agent or by using another leaching medium. Another goal will be to determine the mineralogical composition of the sample because it is not entirely clear how tin is in the sample present. It would be necessary to execute further analyzes of input sample and determine the accurate mineralogical composition of the sample.

Acknowledgement

This work was supported by Ministry of Education of the Slovak Republic under grant MŠ SR VEGA 1/0724/17. This work was supported by the Slovak Research and Development Agency under the contract No. APVV-14-0591.

References

[1] http://epp.eurostat.ec.europa.eu/statistics_explained/index.php/Waste_statistics, [15.01.2017],
[2] http://ec.europa.eu/eurostat/statistics-explained/index.php?title=File:Waste_generation_by_economic_activities_and_households,_2014_YB17.png, [09.04.2018],
[3] Zákon NR SR č. 17/2004 Z. z. zo 4. decembra 2003. (novelizovaný 1. januára 2014) o poplatkoch za uloženie odpadov
[4] Graedel, Harper, Nassar, Barbara: On the Materials Basis of Modern Society, New haven, 2015
[5] Gudorf M., Lazarova Z., Schiigerl K.: Removal of tin from metal-containg industrial dusts, Hydrometallurgy 42, 1996, p. 125-130
[6] Soewarno N. et al.: Tin extraction from slags used hydrochloric acid, IPTEK, Journal of Engineering, Vol. 1, No. 1, 2014, p. 19-21

Performance improvement of the production process of surgical drill controllers

Andrea Vasilňaková, Pavol Palfy

Technical University of Košice, Letná 9, 040 01 Košice
Faculty of Materials, Metallurgy and Recycling, Institute of Materials and Quality Engineering
Department of Integrated Management Systems
andrea.vasilnakova@tuke.sk

Abstract

The paper deals with increasing the performance of the process of surgical drills manufacturing in the AISA Elektric s.r.o. micro-enterprise, which aims to reduce the number of non-conforming products and increase process productivity. We have used the 5S method to reorganize the workplace. We have used the QPR software to visualize the process. By applying the methodology to the problem, we have achieved an improvement in the process of regulators manufacturing. The proportion of non-compliant products declined from 13.3% to 1.66%. The total production time of the regulator was reduced from 60.5 min to 52.5 min.

Introduction

Due to ever-increasing customer demands, businesses are now forced to improve their operations and strive to make their processes as effective as possible, and therefore pay great attention to optimization methods [1]. Even small improvements in the production process are of great importance for businesses. Not only do they increase productivity but also create a competitive advantage [2].

Micro-enterprise Aisa Elektric, s.r.o. deals with hardware and software development, automation, and production line control. Depending on customer requirements, the micro-enterprise is also involved in small series production. One of the serially produced products is the regulator for surgical drills. The process of the regulators manufacturing exhibited a high degree of non-conforming products, i.e., 13.3%. Such a situation is unsustainable in the long run and corrective action had to be taken.

The aim of this study was to reduce the percentage of non-conforming products, optimize the process of regulators production, and at the same time reorganize the workplace.

We have identified a problem that was caused by a high percentage of non-conforming products. The problem was caused by the design of the controllers, when two printed circuit boards (PCBs) had to be connected and, in the case of repairs, they had to be disconnected first, then repaired and then reconnected and checked again. This stressed the contact conducting surfaces of PCBs, which were unnecessarily overheated by soldering and deformed. For these reasons, two PCBs were reduced to one, thereby innovating the final product. In connection with this problem, other shortcomings have also been identified, such as time losses caused by the inefficient arrangement and designation of components necessary for manufacture. 5S method was used to eliminate the deficiencies. The original process was carried out at one workplace. For improvement the process was divided into four workplaces, Fig. 1a.

Methodology and experiment

In the first phase of increasing the process performance, we have modeled the original process of manufacturing in the QPR software, which enables to better visualize the individual steps of the process, Fig. 1b [3]. We have searched for innovative solutions using interviews and questionnaires filled in by employees to identify bottlenecks in the process. We have identified several types of waste, such as time losses and unnecessary movements, Fig. 2. These types of waste reduce productivity while affecting the quality of the product.

In the second phase, we have used the 5S method to eliminate waste and reorganize the workplace. The study also includes product innovation, which consists in reducing the number of PCBs from two to one, Fig. 3.

Regulators for surgical drills are manufactured in a series of 30 pieces. In the original manufacturing process, in the first step, the power transistors are mounted on all 30 pieces in series, and then checked. In the second step, miniature electronic components suitable for surface mount technology (SMD) are installed in all 30 items. In the third step, the attached PCBs are joined. We have eliminated this step in the innovated process. We have found that reducing the number of PCBs from two pieces to one will save the material and time spent on joining them, thereby reducing the scrap. In the fourth step, control and power cables are installed. In the fifth step, the regulators are cleaned using an ultrasonic cleaner, the technical alcohol being used as the cleaning medium. The cleaning process takes 8 minutes, and the cleaner enables cleaning up to 15 units at the same time. The penultimate step is to check the functionality of the controller. The test device can only control one controller and the testing process takes 13 minutes. The last step is to identify and store conforming and non-conforming products according to ISO 9001 [4]. At each step in both the original and the innovated process, the production time of 30 pieces of controllers was measured. The operation times of the individual steps are shown in Tab. 1. Each step of the process is visually inspected by the operator.

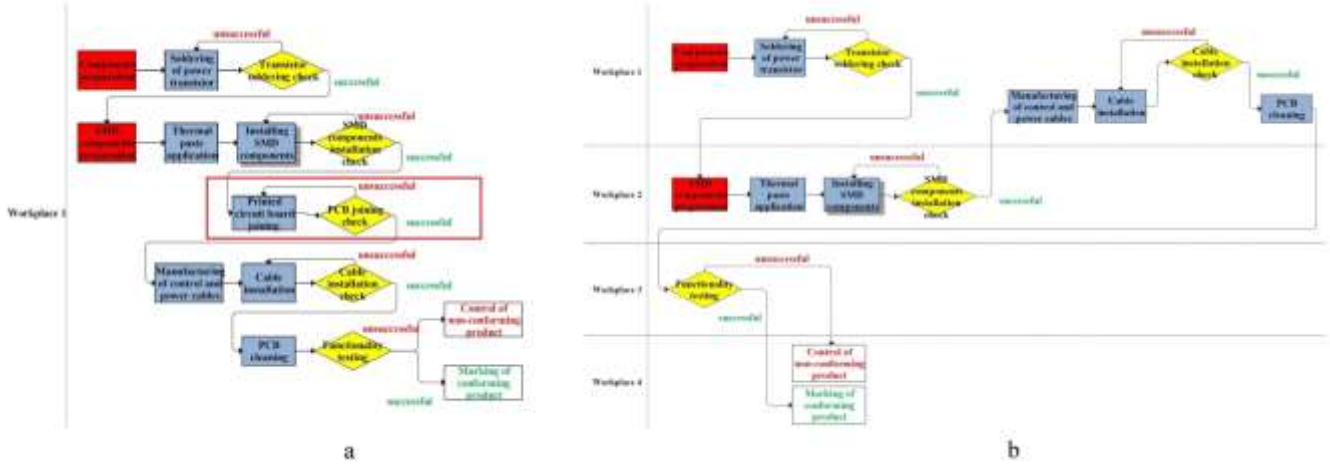

Figure 14a Original Process, **1b** Innovated Process

Table 2 *Operation times of the individual steps in the process*

Step in the process	Operation time (min)			
	The original process		The innovated process	
	Human cycle	Machine cycle	Human cycle	Machine cycle
Component preparation	6		3	
Soldering of power transistor + checking	2,9		2,9	
Paste application + Fitting SMD + Checking	33,3		33,9	
PCB joining + checking	5			
Cable production + installation + checking	13,3		12,8	
Testing and marking 1 pc	-	13		13
PCB cleaning 30 pcs	-	16		16
Sum	60,5	29	52,5	29
Share of non-conforming products	**13,3 %**		**1,66 %**	

Step	Type of waste	Possible Cause	Proposed solutions
Component preparation	time losses caused by searching, useless movements	poor distinguishability of parts, distance to part storage	assign colors to individual categories of parts and keep them closer; separate necessary from unnecessary
Soldering of power transistors	equipment preparation time losses	too much equipment at the workplace	separate necessary equipment from unnecessary
SMD components preparation	time losses caused by searching, useless movements	poor distinguishability of parts, distance to part storage	assign colors to individual categories of parts and keep them closer; separate necessary from unnecessary
Paste application			
Fitting SMD component and check	time losses caused by searching for part	poor distinguishability on PCB	assign colors to intividual parts categories on the layout
PCB joining and checking	time losses due to separation of PCBs in the case of repair, contact overheating	problematic realization	separate necessary equipment from unnecessary; establish several workplaces
Cable production	useless movements	distance to the cable storage; too much equipment	keep cables closer; establish several workplaces
Cable installation and check	time losses uncluttering workspace		separate necessary equipment from unnecessary; establish several workplaces
Cleaning PCB 30 pcs			
Functionality check			

Figure 15 Information from the questionnaire survey

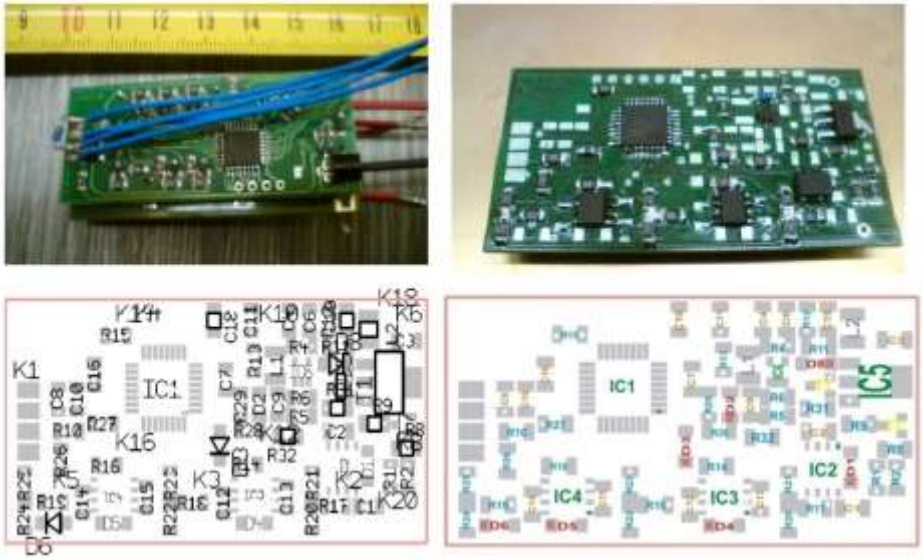

Figure 16 Original and innovated parts layout

Results

The shortcomings identified from the evaluated questionnaires were eliminated using the 5S method. Using the method, organizational changes were implemented at the workplace. The work activity was divided into four workplaces. The components required for manufacture were arranged into individual boxes, color-coded to ensure clarity, Fig. 4. This reduces time losses in pre-production. At the same time, the parts torage scheme is more transparent (it is color-matched with the component bins). The innovated product contains 61 parts divided into 6 groups and each component type is color-coded:

- Integrated circuits (green color)
- Resistors (blue color)
- Capacitors (orange color)
- Transistors (yellow color)
- Coils (gray color)
- Diodes (red color)

Table 1. shows the times for the individual steps of the original and the innovated process. Using 5S method we have saved 3 minutes in the "parts preparation" step, eliminating the "PCB + check" step was saved another 5 minutes. The longest step is thermal paste application and SMD components fitting. This step requires the most inputs and resources. In this step occured a time lag, due to the poor visualization of the parts in the trays and on the layout scheme. The overall process innovation, in particular by removing one PCB, reduced the percentage of non-conforming products from 13.3% to 1.66%.

Figure 17 Reorganization of the workplace

Discussion and conclusion

The manufacturing process time for surgical drill controllers was reduced by 8 minutes. Resistors (2 contacts) and transistors (3 contacts) have been replaced by integrated circuits (8 contacts). The number of parts decreased, but the number of contacts to solder increased, so the time has not been saved due to innovation, rather slightly increased but there was created room for installing parts on 1 PCB.

This new design has improved quality control and repair options. By reorganizing the workplace, the time needed to prepare the parts and the production itself was saved. The workplace has a more tidy structure, the individual parts are easier to access and more clearly labeled. Time losses were eliminated and the standard of the workplace was set up, which should be observed when working at the workplace. The goal was to reduce the number of non-conforming products and to increase the productivity. The proportion of non-conforming products declined from 13.3% to 1.66%. The total production time of the controller was reduced from 60.5 min. to 52.5 min.

References

[1] Řepa V. Podnikové procesy. 2. ed. Praha: Grada Publishing, a.s., 2007. p.288 ISBN 978-80-247-2252-8

[2] Šatanová A., Figuli L., Sedliačiková M.: Optimization of Production Process through Selected. Procedia Economics and Finance, Prague, 2015, n. 23, p. 959 – 963. ISSN doi: 10.1016/S2212-5671(15)00494-3

[3] PROCESSGUIDE - QPR, Processes, Results. [online]. Available: <http://www.wb-bc.at/processguide-brochure.pdf>. [cit 2018-10-04]

[4] STN EN ISO 9001, Systém Manažérstva kvality 2015

ISBN: 978-80-553-2971-0